VOLUME 78 MAY 9, 1974 NUMBER 10

JPCHAx

THE JOURNAL OF PHYSICAL CHEMISTRY

PUBLISHED BIWEEKLY BY THE AMERICAN CHEMICAL SOCIETY

THE JOURNAL OF

PHYSICAL CHEMISTRY

AMERICAN CHEMICAL SOCIETY, *1155 Sixteenth St., N.W., Washington, D. C. 20036*

Books and Journals Division

JOHN K CRUM *Director*
RUTH REYNARD *Assistant to the Director*

CHARLES R. BERTSCH *Head, Editorial Processing Department*
D. H. MICHAEL BOWEN *Head, Journals Department*
BACIL GUILEY *Head, Graphics and Production Department*
SELDON W. TERRANT *Head, Research and Development Department*

 Published biweekly by the American Chemical Society at 20th and Northampton Sts., Easton, Pa. 18042. Second-class postage paid at Washington, D. C., and at additional mailing offices.

All manuscripts should be sent to *The Journal of Physical Chemistry*, Department of Chemistry, University of Minnesota, Minneapolis, Minn. 55455.

Additions and Corrections are published once yearly in the final issue. See Volume 77, Number 26 for the proper form.

Extensive or unusual alterations in an article after it has been set in type are made at the author's expense, and it is understood that by requesting such alterations the author agrees to defray the cost thereof.

The American Chemical Society and the Editor of *The Journal of Physical Chemistry* assume no responsibility for the statements and opinions advanced by contributors.

Correspondence regarding accepted copy, proofs, and reprints should be directed to Editorial Processing Department, American Chemical Society, 20th and Northampton Sts., Easton, Pa. 18042. Head: CHARLES R. BERTSCH. Editorial Assistant: JOSEPH E. YURVATI.

Advertising Office: Centcom, Ltd., 50 W. State St., Westport, Conn. 06880.

Business and Subscription Information

Send all new and renewal subscriptions *with payment* to: Office of the Controller, 1155 16th Street, N.W., Washington, D. C. 20036. Subscriptions should be renewed promptly to avoid a break in your series. All correspondence and telephone calls regarding changes of address, claims for missing issues, subscription service, the status of records, and accounts should be directed to Manager, Membership and Subscription Services, American Chemical Society, P.O. Box 3337, Columbus, Ohio 43210. Telephone (614) 421-7230.

On changes of address, include both old and new addresses with ZIP code numbers, accompanied by mailing label from a recent issue. Allow four weeks for change to become effective.

Claims for missing numbers will not be allowed (1) if loss was due to failure of notice of change in address to be received before the date specified, (2) if received more than sixty days from date of issue plus time normally required for postal delivery of journal and claim, or (3) if the reason for the claim is "issue missing from files."

Subscription rates (1974): members of the American Chemical Society, $20.00 for 1 year; to nonmembers, $60.00 for 1 year. Those interested in becoming members should write to the Admissions Department, American Chemical Society, 1155 Sixteenth St., N.W., Washington, D. C. 20036. Postage to Canada and countries in the Pan-American Union, $5.00; all other countries, $6.00. Air freight rates available on request. Single copies for current year: $3.00. Rates for back issues from Volume 56 to date are available from the Special Issues Sales Department, 1155 Sixteenth St., N.W., Washington, D. C. 20036.

Subscriptions to this and the other ACS periodical publications are available on microfilm. Supplementary material not printed in this journal is now available in microfiche form on a current subscription basis. For information on microfilm or microfiche subscriptions, write Special Issues Sales Department at the address above.

Notice to Authors last printed in the issue of December 6, 1973

THE JOURNAL OF

PHYSICAL CHEMISTRY

Volume 78, Number 10 May 9, 1974

JPCHAx 78 (10) 951–1042 (1974)
ISSN 0022-3654

COMMUNICATIONS TO THE EDITOR

There is no supplementary material for this issue.

* In papers with more than one author, the asterisk indicates the name of the author to whom inquiries about the paper should be addressed.

AUTHOR INDEX

ANNOUNCEMENT

On the last two pages of this issue you will find reproduced the table of contents of the April 1974 issue of the Journal of Chemical and Engineering Data.

THE JOURNAL OF
PHYSICAL CHEMISTRY

VOLUME 78, NUMBER 10 MAY 9, 1974

The Role of CF_3· Radicals in the Photochemical Iodine Laser

R. Srinivasan* and J. R. Lankard

IBM Thomas J. Watson Research Center, Yorktown Heights, New York 10598 *(Received April 6, 1973; Revised Manuscript Received February 8, 1974)*

Publication costs assisted by The International Business Machines Corporation

The energy and time dependence of the $I_{1/2} \rightarrow I_{3/2}$ laser emission during the flash photolysis of CF_3I was strongly influenced by the addition of CF_3NNCF_3, its effect being related to the total pressure in the system and the ratio of the reactants.

Introduction

The elementary reactions which occur in the photochemical iodine laser have been discussed by numerous workers.[1] With the exception of the dissociation (1) and laser emission (2) steps, there seems to be little agreement on the other reactions in this system.

$$CF_3I + h\nu \longrightarrow CF_3\cdot + I_{1/2} \quad (1)$$

$$I_{1/2} \longrightarrow I_{3/2} + h\nu_{laser} \quad (2)$$

We wish to report here the results of a study in which the effects of a deliberate introduction of CF_3· radicals in this system was investigated. In order to understand these data, the effects of hexafluorocyclobutene (C_4F_6) and octafluorocyclobutane (C_4F_8) on the iodine laser were also measured.

Experimental Section

CF_3I, C_4F_6, and C_4F_8 (PCR Inc., Gainesville, Fla.) and hexafluoroazomethane (Merck Sharpe and Dohme, Montreal) were degassed at liquid nitrogen temperature before use. Two different apparatus were employed. For experiments which involved analytical measurements on CF_3I in the presence and absence of C_4F_6 or C_4F_8, a short (19.5 cm long, 1.2 cm o.d. with flat quartz windows) quartz laser tube which was enclosed with the flashlamp (pumped with a total energy of 430 J) in a polished ellipse was used. A 100% reflecting plane mirror was placed at one end while the integrated output from the other end was measured with a TRG-100 thermopile. The flashlamp was filled with air at 15 Torr. Its output reached its maximum intensity in 3 μsec and its duration at half its maximum intensity was $\sim$10 μsec.

The experiments which involved CF_3I in the presence of hexafluoroazomethane (hereafter HFAM) were conducted in a fourfold longer quartz laser tube of exactly similar design which was pumped with a flashlamp made up of four sections of the shorter one (*i.e.*, a total pumping energy of 1350 J). No mirrors were employed because of the high gain in the system. The output of the laser from one end was measured with a thermopile and from the other was fed through a light pipe to an indium antimonide detector, the signal from which was monitored by a Tektronix 555 oscilloscope.

A conventional glass vacuum system was used to mix known quantities of CF_3I and one of the added gases by several freeze–thaw cycles before introduction into the laser tube.

The extent of decomposition of CF_3I was followed by two methods. One consisted of titrating the iodine formed with N/25 sodium thiosulfate. The second consisted of measuring the volume of gases volatile at melting *n*-pentane temperature (principally C_2F_6). The two methods gave results within ±15%. Generally, the iodine titre gave a lower value for the decomposition since it was not possible to distil all of the free iodine out of the vacuum system into a sample tube. The gas measurement, although more reliable, was impractical when large amounts of other gases were added to the system.

Results

In earlier studies,[1,2] the correlation of the light output at 1.315 μ with the photochemical decomposition of CF_3I had not been attempted. Therefore, such measurements were undertaken in this work. These data are shown in

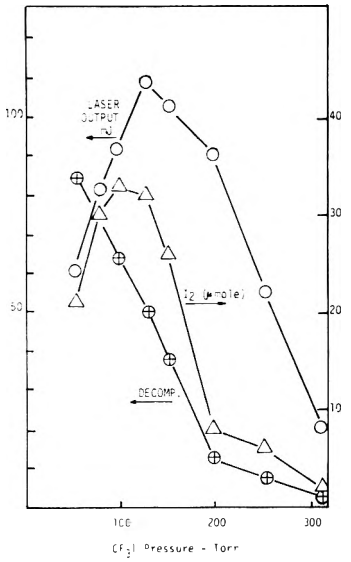

Figure 1. Flash Photolysis of CF_3I vapor.

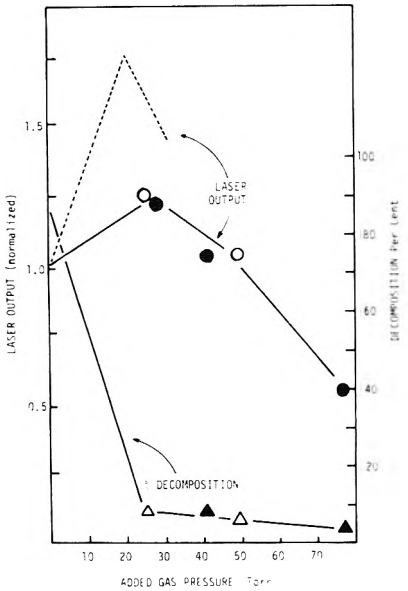

Figure 2. Effect of added gases on CF_3I Laser ($P(CF_3I)$ = 40 Torr): open circles and triangles, C_4F_6; filled circles and triangles, C_4F_8; broken line, HFAM.

Figure 1. In agreement with the observation of Kasper, Parker, and Pimentel[3] it was found that at pressures less than 200 Torr, the per cent decomposition of CF_3I was large (>10%), presumably because of the pyrolysis which accompanied the photolysis. At the pressure (~130 Torr) at which the output of the laser was a maximum, the overall decomposition was 50%.

In Figures 2 and 3, the effect of adding C_4F_6 or C_4F_8 on the performance of the laser are shown. The suppression of the production of iodine by a thermal route in the presence of a large excess of argon was first reported by Kasper, Parker, and Pimentel.[4] Addition of C_4F_8 seems much more effective in suppressing the production of iodine. The behavior of C_4F_6 is quite similar to that of C_4F_8.

The effects of the addition of HFAM at two different initial pressures of CF_3I are shown in Tables I and II. These data are normalized and entered in Figures 1 and 2 as well for purpose of comparison to the other additives. The variations in the intensity of the laser in the presence

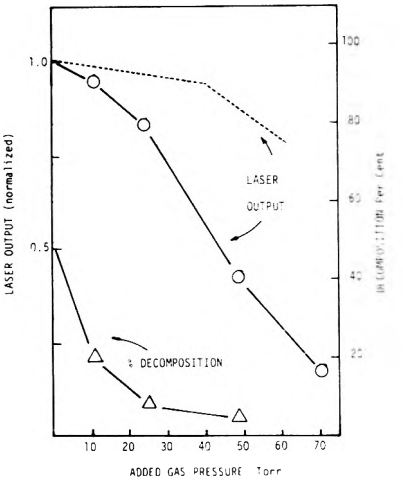

Figure 3. Effect of added gases on CF_3I laser ($P(CF_3I)$ = 130 Torr): open circle and triangles, C_4F_6; broken line, HFAM.

TABLE I: Laser Output as a Function of HFAM Pressure

CF_3I, Torr	HFAM, Torr	Output, mJ
40	0	265
40	10	360
40	20	460
40	30	385

TABLE II: Laser Output as a Function of HFAM Pressure

CF_3I, Torr	HFAM, Torr	Output, mJ
100	0	610
100	40	570
100	60	470

of HFAM as a function of time as recorded in the oscilloscope are given in Figures 4 and 5. These results could be duplicated to within ±10% when care was taken to outgas the system and mix the ingredients well.

It can be seen at $P(CF_3I)$ = 40 Torr, the addition of HFAM can increase the output of the laser by 80% while the other gases cause an increase of 10% or less. The profile of the laser output shows that the beneficial effect of HFAM persists over the entire duration of the laser emission.

Discussion

From previous studies[5] on the photochemistry of HFAM, it was expected that its effect in this system would be threefold. The first and least specific one is as an inert diluent gas in the manner of argon.[4] Both C_4F_6 and C_4F_8 molecules closely approximate HFAM in their molecular weight while C_4F_8 should offer some chemical similarity to HFAM as a quencher. It can be expected that HFAM would also have reduced the pyrolytic decomposition of CF_3I in the manner of C_4F_6 and C_4F_8 although direct analytical measurements were not performed. It is evident from the experiments with C_4F_6 and C_4F_8 that this cooling effect is in itself insufficient to account for the increased output of the laser at a pressure of CF_3I of 40 Torr when HFAM was added.

The second one is as a source of CF_3 radicals (eq 3).

$$CF_3NNCF_3 + h\nu \longrightarrow 2CF_3 + N_2 \quad (3)$$

The secondary reactions of $CF_3\cdot$ in the photolysis of CF_3I

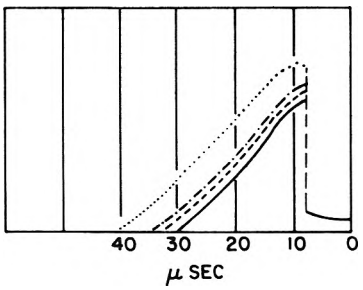

Figure 4. Oscilloscope trace of emission at 1.315 μ: $P(CF_3I)$ = 40 Torr; P(HFAM) = 0 (unbroken line); 10 (dashed line); 20 (dotted line); 30 (dash-dotted line).

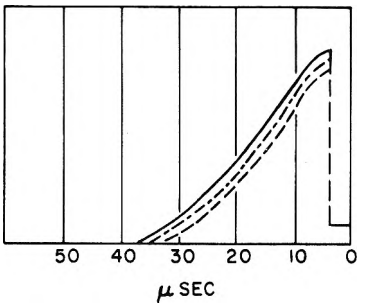

Figure 5. Oscilloscope trace of emission at 1.315 μ: $P(CF_3I)$ = 100 Torr; P(HFAM) = 0 (unbroken line); 40 (dash-dotted line); 60 (dashed line).

have been discussed.[1,6,7]

$$CF_3 + I_2 \longrightarrow CF_3I + I \quad (4)$$

$$CF_3 + I_{3/2} \longrightarrow CF_3I \quad (5)$$

$$CF_3 + I_{1/2} \longrightarrow CF_3I \quad (6)$$

$$CF_3 + CF_3I \longrightarrow C_2F_6 + I_{1/2} \quad (7)$$

Reaction 4 removes molecular iodine from the system and thus scavenges a powerful quencher of $I_{1/2}$,[4] but it also introduces one atom of $I_{3/2}$ which would affect the population inversion. The buildup of I_2 is a slow process which occurs by a three-body recombination.[1] Therefore, reaction 4 would be of importance only toward the end of the pumping flash. Reaction 5 would be a useful process since it would serve to sustain the population inversion. It may well explain the principal beneficial action of an additional source of CF_3· radicals. Reaction 6, if it leads to CF_3I in its ground electronic state (vibrationally excited), would be deleterious to the operation of the laser. But if it leads to CF_3I in its electronically excited state, the reaction may be reversible. Reaction 7 offers yet another way[1,7] in which CF_3 radicals can increase the concentration of $I_{1/2}$ and contribute to the lasing. This reaction has been invoked[7] to explain the growth in the concentration of $I_{1/2}$ atoms after the flashlamp has stopped pumping *via* photodissociation. This action could exist in concert with steps (4), (5), and (6).[8]

A third mode of action of HFAM is as a trap for CF_3 radicals derived from itself as well as from CF_3I according to (8) and (9).[5] It is known[5b] that HFAM is extremely effective in this respect. The experiments in which C_4F_6 was added to CF_3I were meant to see if this molecule would also serve as a trap for CF_3 radicals and if so, what effect it would have on the lasing. Since C_4F_6 was no different from C_4F_8 in this respect it can be concluded that either the former is an ineffective trap (which involves a further tacit assumption that CF_3 radicals somehow promote the laser output) or that trapping the CF_3 radicals does not have any effect on the laser action.

$$CF_3 + CF_3NNCF_3 \longrightarrow (CF_3)_2NNCF_3 \quad (8)$$

$$CF_3 + (CF_3)_2NNCF_3 \longrightarrow (CF_3)_2NN(CF_3)_2 \quad (9)$$

Much of the discussion so far is applicable only to the laser action at an initial pressure of CF_3I of 40 Torr. When the pressure is increased to 100 Torr, the chemistry of the CF_3I laser, even in the absence of added gases seems unclear. The increase in the output of the laser from 40 to 130 Torr (Figure 1) may be due to increased absorption of the pumping radiation. The sharp maximum at about 130 Torr is probably due to progressive increase in the output from the above reason being conpensated by a quenching process. The most likely quenching agent is CF_3I itself. The results of Donovan and Husain[9] show that as a quencher for $I_{1/2}$, CF_3I is moderately efficient. It may also be noted that Aldrige[2] has observed the fall off in the output of the iodine laser at pressure >100 Torr when CF_3I was used as the photolytic gas.

In the region above 100 Torr, none of the added gases seem capable of augmenting the output of the laser. Under these conditions, the more intense absorption of CF_3I (although its maximum does not coincide with that of HFAM)[10] may prevent the complete photolytic decomposition of HFAM. The undecomposed HFAM would then trap a part of the CF_3 radicals and cause a decrease in the output of the laser. Ultraviolet absorption spectra do show that in the first weak absorption of HFAM, there is some interference from CF_3I (P = 100 Torr) but no analytical work was undertaken to show that some HFAM survived the photolytic flash. There is need for further study of the chemistry of this laser at pressures greater than 100 Torr.

We are investigating the effect of alternative sources of CF_3 radicals on the photochemical iodine laser.

Acknowledgment. The authors wish to thank Dr. P. P. Sorokin for his advice and encouragement during the course of this work.

References and Notes

(1) A critical review has been presented by V. Yu. Zalesski, *Soviet Phys. JETP*, **34**, 474 (1972).
(2) F. T. Aldrige, *Appl. Phys. Lett.*, **22**, 180 (1973).
(3) J. V. V. Kasper, J. H. Parker, and G. C. Pimentel, *Appl. Phys. Lett.*, **5**, 231 (1964).
(4) J. V. V. Kasper, J. H. Parker, and G. C. Pimentel, *J. Chem. Phys.*, **43**, 1827 (1965).
(5) (a) J. R. Dacey and D. M. Young, *J. Chem. Phys.*, **23**, 1302 (1955); (b) G. O. Pritchard, H. I. Schiff, and A. F. Trotman-Dickenson, *Trans. Faraday Soc.*, **52**, 849 (1956); (c) J. C. Amphlett and E. Whittle, *ibid.*, **62**, 664 (1966).
(6) T. Ogawa, G. A. Carlson, and G. C. Pimentel, *J. Phys. Chem.*, **74**, 2090 (1970).
(7) K. Hohla and K. L. Kompa, *Chem. Phys. Lett.*, **14**, 445 (1972).
(8) It may appear that a test for the relative importance of the various individual steps could consist of the introduction of free radicals other than CF_3 in this system. For example, CH_3 radicals may participate in reactions analogous to (4), (5), and (6) but not in (6a). However, the use of CH_3NNCH_3 instead of HFAM quenched the output of the laser totally.
(9) R. J. Donovan and D. Husain, *Trans. Faraday Soc.*, **62**, 2023 (1966).
(10) J. C. Calvert and J. N. Pitts, Jr., "Photochemistry," Wiley, New York, N. Y., 1956, p 453, 527.

Competitive and Noncompetitive Electron Capture of Nitrous Oxide with Sulfur Hexafluoride and Electron Thermalization in the Gas-Phase Radiolysis of Xenon[1]

Yoshihiko Hatano* and Hiroshi Shimamori

Laboratory of Physical Chemistry, Tokyo Institute of Technology, Meguro-ku, Tokyo, Japan *(Received June 28, 1973; Revised Manuscriot Received February 11, 1974)*

Publication costs assisted by Tokyo Insitute of Technology

The effect of the addition of SF_6 on the nitrogen yield in the gas-phase radiolysis of Xe, which is an "electron supplier," containing 3~20 mol % of N_2O has been investigated. The decreasing nitrogen yield at higher concentrations of SF_6 (~2 mol % in Xe) is almost independent of the composition of the mixtures. The relative rate of the electron capture process of N_2O to that of SF_6 decreases apparently by a factor of 10^2 with increase in the N_2O mole per cent. The kinetic treatment shows that nitrogen formation in this system results from two different electron capture processes of N_2O, that is, the dissociative electron attachment to N_2O during the course of its thermalization and the nondissociative thermal electron attachment to N_2O by a three-body process. The rate constant for electron capture by SF_6 is estimated to be $\sim 10^{-12}$ cm^3 molecule^{-1} sec^{-1} which is much lower than that generally recognized. The yield of nitrogen nonscavengeable by SF_6 has been briefly discussed.

Introduction

Electrons ejected from a gas by irradiation have kinetic energy in excess of that of the gas molecule. This excess energy is eventually dissipated by elastic and inelastic collisions until the electrons are in thermal equilibrium with gas molecules. In polyatomic molecule gases as treated in ordinary radiation chemistry, however, it has been considered that the thermal electrons, not the epithermal, play a major role in most electron reactions because of the rapidness of their thermalization.[2]

Thus far the thermalization or the energy loss of low-energy electrons in many gases has been studied by several workers;[2-4] the results of this work suggested that the energy loss of electrons in polyatomic molecules occurs mainly by inelastic collisions, whereas in rare gases it occurs by elastic collisions alone. Therefore it may be expected that in a mixture of a rare gas and polyatomic molecules electrons become thermalized more slowly than in pure polyatomic molecule gas.

In the present study we chose the Xe-N_2O system as the mixture described above, and investigated the effect of the addition of SF_6 as an effective thermal-electron scavenger on the product yields. Nitrous oxide here is expected to behave not only as a polyatomic molecule, but also as an effective electron scavenger to form the measurable products. The competitive and noncompetitive electron capture of N_2O with SF_6 and the interaction of electrons with polyatomic molecules during the course of their thermalization have been discussed.

The combination of Xe with N_2O has the additional advantage that the possibility of charge transfer from Xe^+ to N_2O and Penning ionization of N_2O by excited Xe atoms may be excluded.

Experimental Section

Xe (stated purity 99.9%) containing nitrogen and krypton as impurities supplied by Takachiho-Shoji Co. was degassed carefully by freeze-pump-thaw cycles. Since, however, its mass spectrometric and gas chromatographic analyses showed no impurities, the purity may actually be better than 99.99%. N_2O and SF_6 also supplied by Takachiho-Shoji Co. were used after the usual degassing.

The mixtures, all at about 720 mm total pressure, were irradiated with ^{60}Co γ rays at room temperature or slightly above. The dose rate was 2.9×10^{19} eV g^{-1} hr^{-1} or $(3.7 \pm 0.2) \times 10^{13}$ eV cm^{-3} sec^{-1} in Xe, and the total dose was 1.45×10^{20} eV g^{-1}, which was determined by Fricke dosimetry making appropriate corrections for electron density.

All irradiations were carried out in 50-ml cylindrical glass vessels fitted with break-off tips which, prior to use, were baked in air at 500° and then pumped at least for 1 hr down to 10^{-5} mm. The vessels were sealed at −196° while open to the vacuum system.

After irradiations, the sample vessels were attached to a vacuum line and the seals were broken. The final products, noncondensable at −196°, nitrogen and oxygen, were collected by Toepler pump and analyzed gas chromatographically using a 5-m column of molecular sieve 5A at about 60°.

It may be considered that the products in the radiolysis of Xe-N_2O mixtures result ultimately from the decomposition of N_2O. The initial products in the radiolysis of N_2O are N_2, O_2, and NO, but NO and O_2 are known to react to form NO_2 in a cold trap.[5] The initial G values before NO and O_2 react in the cold trap are calculated from the experimentally measured quantities. Since the decomposition mode of N_2O can be written as

$$(2a + b)N_2O \longrightarrow (2a + b/2)N_2 + aO_2 + bNO$$

the initial amounts of the products expressed in G values are $G(N_2) = 2a + b/2$, $G(O_2) = a$, and $G(NO) = b$. If $g(N_2)$ and $g(O_2)$ denote the G values of N_2 and O_2 calculated from the experimentally measured amounts of those products, taking into account the presence of the reaction $O_2 + 2NO \rightarrow 2NO_2$ in the cold trap, we obtain $g(N_2) = G(N_2) = 2a + b/2$, $g(O_2) = a - b/2$. Therefore $G(N_2) = g(N_2)$, $G(O_2) = (1/3)(g(N_2) + g(O_2))$, and $G(NO) = (1/3)(2g(N_2) - 4g(O_2))$ or $2G(N_2) - 4G(O_2)$.

Results and Discussion

The yields of products were calculated as the number of molecules formed per 100-eV energy absorbed by Xe only, and were corrected for the yields of N_2 and O_2 arising from the direct radiolysis of N_2O, using $G(N_2) = 10.1$, $G(O_2) = 3.8$ for binary mixtures (no SF_6), and $G(N_2) = 8.0$, $G(O_2) = 3.2$ for ternary mixtures.[6] This is an approximate correction done simply on the basis of electron fraction and the maximum correction is about 15% of the N_2 yield for the 20% N_2O mixture.

Figure 1 shows that variations of $G(N_2)$, $G(O_2)$, and $G(NO)$ in the radiolysis of Xe–N_2O mixtures as a function of N_2O mole per cent. Each increases with the increase of N_2O mole per cent, and shows a tendency to reach a plateau value, $G(N_2) = 6.1$, $G(O_2) = 2.7$, $G(NO) = 1.4$. When SF_6 (up to 2 mol % in Xe) was added to the mixtures, each G value decreased. The larger the amount of N_2O in the mixture becomes, the more rapidly $G(N_2)$ decreases by the addition of SF_6 (Figure 2). The rapid decrease of $G(N_2)$ in Figure 2 is very analogous to that in the gas-phase radiolysis of N_2O itself[6] or of hydrocarbon containing N_2O[7] while the gradual decrease of $G(N_2)$ in Figure 2 in the case of low concentrations of N_2O is exceptional in the gas-phase radiolysis. Both $G(O_2)$ and $G(NO)$ also decreased by the addition of SF_6, especially $G(NO)$ which fell to nearly zero.

Since SF_6 has an exceedingly large cross section for thermal electron attachment, the decrease of the yields by the addition of SF_6 may be due to the following reactions

$$e_{th}^- + SF_6 \xrightarrow{k_1} SF_6^- \quad (1)$$

$$SF_6^- + Xe^+ \xrightarrow{k_2} \text{no } N_2, O_2, \text{ or NO} \quad (2)$$

Electrons freed from Xe have initially large kinetic energies. They degrade through the collisions with N_2O molecules or Xe atoms and eventually become thermal electrons. The reactions involved are

$$Xe \longrightarrow Xe^+ + e^{-*} \quad (3)$$

$$e^{-*} + Xe \xrightarrow{k_4} e_{th}^- + Xe \quad (4)$$

$$e^{-*} + N_2O \xrightarrow{k_5} e_{th}^- + N_2O \quad (5)$$

where e^{-*} is an energetic (not thermal) electron. In the course of degradation, however, there exists the possibility of dissociative attachment to N_2O of electrons having energies of 2~3 eV above thermal[8]

$$e^{-*} + N_2O \xrightarrow{k_6} N_2 + O^- \quad (6)$$

Electrons created in the ionization (3) may carry out in part reaction 6 before they are thermalized by the process 4 or 5.

Chantry[9] showed that reaction 6, below 2-eV electron energy, requires an activation energy, which is based on the fact that the cross section of O^- formation is temperature dependent below 2 eV, whereas it is independent of temperature above 2 eV. Ferguson, *et al.*,[10] using geometrical considerations of N_2O^-, have predicted that the nondissociative electron attachment to N_2O should have an activation energy required to form stable N_2O^- in the bending mode. The existence of stable N_2O^- has been reported by Paulson,[11] and Phelps and Voshall.[12] Since the N_2–O bond dissociation energy and the electron affinity of O atom are 1.67 and 1.47 eV, respectively, the energy of the electron in reaction 6 should have a threshold greater than 0.2 eV. Warman and Fessenden[13,14] have suggested that the capture of electrons below about 0.2 eV may

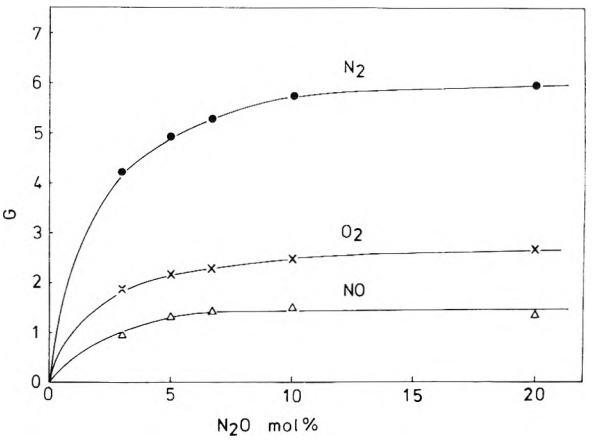

Figure 1. Yields of the products in the radiolysis of Xe–N_2O mixtures as a function of N_2O mole per cent. The values of $G(O_2)$ and $G(NO)$ are calculated using the relations $G(O_2) = (1/3)(g(N_2) + g(O_2))$ and $G(NO) = 2G(N_2) - 4G(O_2)$.

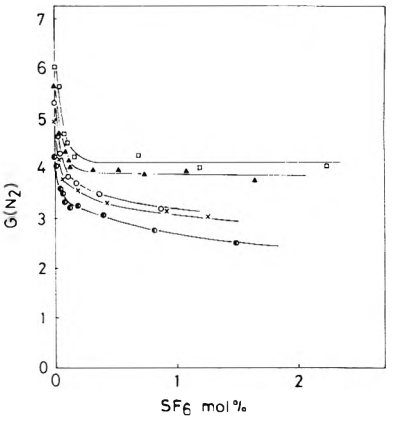

Figure 2. Effect of SF_6 on $G(N_2)$ (N_2O mole per cent): ●, 3%; ×, 5%; ○, 6.7%; ▲, 10%; □, 20%.

occur nondissociatively *via* a three-body process because of the requirement of collisional stabilization of N_2O^-. Thus, we assume here the thermal or near-thermal electron capture by N_2O to be a three-body process followed by the formation of stable N_2O^-

$$e_{th}^- + N_2O \xrightarrow[(+M)]{k_7} N_2O^- \quad (7)$$

where k_7 is the effective two-body rate constant and M is a third body. Subsequently N_2O^- reacts with Xe^+ to produce N_2

$$N_2O^- + Xe^+ \xrightarrow{k_8} N_2 + O + Xe \quad (8)$$

Since the formation of NO has been almost completely inhibited by the addition of SF_6, the thermal electron capture of N_2O may be responsible for its formation. The neutralization of N_2O^- with Xe^+ may lead partly, instead of (8), to NO

$$N_2O^- + Xe^+ \xrightarrow{k_9} NO + N + Xe \quad (9)$$

Another important process in which electrons disappear is the direct neutralization with Xe^+ [15]

$$e_{th}^- + Xe^+ \xrightarrow{k_{10}} Xe' \quad (10)$$

It is known that O^- produced by electron impact for electron energies covering the range of 0~2.5 eV has ki-

TABLE I: Values of K and A in Eq a Obtained from Figure 3

	f 4	9	14	19	32
K^a	1.9	1.9	2.0	1.8	1.8
A^b	7.0×10^{-4}	2.5×10^{-3}	6.6×10^{-3}	1.3×10^{-2}	3.0×10^{-2}

[a] Each value has an error limit of ±0.1. [b] Each significant figure in A has an error limit of ±0.2.

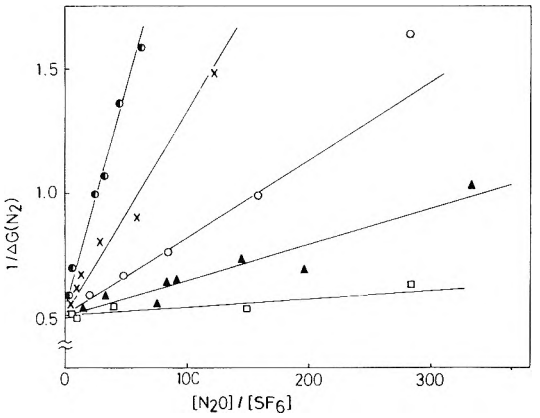

Figure 3. Plot of $1/\Delta G(N_2)$ as a function of $[N_2O]/[SF_6]$. Each line corresponds to a plot for a definite mole per cent of N_2O: ◐, 3%; ×, 5%; ○, 6.7%; ▲, 10%; □, 20%.

netic energy distributions below about 1 eV,[9] and that the cross section of the reaction $O^- + N_2O \rightarrow N_2 + O_2^-$ is near zero for O^- kinetic energies below about 2.5 eV.[11] The evidence for the reaction $O^- + N_2O \rightarrow N_2 + O_2^-$ has been reported by Burtt and Henis.[16] They have measured the pressure dependence of the intensity of O_2^- using negative ion mass spectrometer. However, Moruzzi and Dakin[17] in their study of negative ion-molecule reactions in N_2O have found that on purifying the N_2O the intensity of O_2^- reduces to a very minor peak, which indicates that the impurity is responsible for the formation of O_2^-. Also recently Marx, *et al.*,[18] have detected no O_2^- in the reaction of O^- with N_2O. Thus O^- may not be responsible for the formation of N_2 and may be consumed by the neutralization with Xe^+

$$O^- + Xe^+ \xrightarrow{k_{11}} O + Xe \qquad (11)$$

Assuming that O atoms produced in (8) and (11) are in the ground state and cannot produce N_2,[19] the decrement of the yield of N_2 by the addition of SF_6 is equivalent to the amount of thermal electrons captured by SF_6. Therefore according to the above competition for thermal electrons, there the following relation should exist between the decrement of the nitrogen yield, $\Delta G(N_2)$, and the concentrations, $[N_2O]$ and $[SF_6]$[20]

$$\frac{1}{\Delta G(N_2)} = \frac{1}{K}\left(1 + A\frac{[N_2O]}{[SF_6]}\right) \qquad (a)$$

where

$$K = \frac{k_5 + k_4 f}{k_5 + k_6 + k_4 f} G_N(e^{-*}) \qquad f = \frac{[Xe]}{[N_2O]}$$

$$A = \frac{k_7}{k_1}\left(1 + \frac{k_{10}}{k_7}\sqrt{\frac{10^{-2} G(e^{-*}) D}{k_a}}\,\frac{1}{[N_2O]}\right)$$

$$k_a = \frac{\sum_i k_i [X_i^-]}{\sum_i [X_i^-]} \qquad (i = 2, 8, 9, 10, 11)$$

and D is the dose rate in eV cm^{-3} sec^{-1}, X_i^- is the negative-ion species involved in reaction i, and k_a is the average value of all the rate constants of neutralizations involved. Since no large difference has been observed[21] between the rate of ion-ion neutralization and that of ion-electron neutralization, it seems reasonable to assume k_a nearly equals k_{10}. $G_N(e^{-*})$ is the G value of electrons contributing to nitrogen formation, and is not equal to $G(e^{-*})$, 4.6, calculated from the W value of Xe, since thermal electrons partly lead to produce NO as described before. Since $G_N(e^{-*})$ is equal to $(k_8/(k_8 + k_9))G(e^{-*})$ where the values of k_8 and k_9 are not known, we have transformed $G_N(e^{-*})$ to $G(e^{-*}) - (k_9/(k_8 + k_9))G(e^{-*})$, and estimated an approximate value of $G_N(e^{-*})$ by equating $(k_9/(k_8 + k_9))G(e^{-*})$ to the G value of electrons contributing to form NO. Assuming that O and N atoms formed by (8), (9), and (11) ultimately recombine through NO_2 to produce NO and O_2,[22] though the rate constants in ref 22 do not allow one to calculate exactly how much NO and O_2 is formed, we can say that one electron leads to the formation of two NO molecules as maximum. Since $G(NO)$ is about 1.4 in the present case, the G value of electrons which contribute to form NO is ~0.7; therefore, the value of $G_N(e^{-*})$ is ~3.9.

According to eq a for a fixed composition of Xe-N_2O mixtures plots of $1/\Delta G(N_2)$ *vs.* $[N_2O]/[SF_6]$ should be straight lines of slope A/K, which is shown in Figure 3. From the slopes and the intercepts calculated using least-squares fit of the data, K and A can be obtained for each f as listed in Table I.

It is noted that in this treatment the concentrations of SF_6 in Figure 2 employed are limited to about 10% of the N_2O concentration for all mixtures. We are concerned with the effect of a small amount of SF_6 on the yields of products, in which SF_6 exclusively plays the role of a thermal-electron scavenger and the other effect, such as the thermalization of electrons by SF_6, may be excluded. In fact the experiment on higher concentration of SF_6 (3~5% of the amount of Xe), though they are not presented in this paper, gave lower values of the yields of products than those expected from the smooth curves in Figure 2, and if one plots those lower values on Figure 3, all the points near the intercepts would begin to deviate from the straight lines. From these facts the above treatment seems to be reasonable only when the lower concentration region of SF_6 is used.

Table I shows that within experimental error K is nearly constant (~1.9) despite of the variation of f. This is fulfilled if

$$k_4 f \ll k_5 + k_6 \qquad (b)$$

and then

$$K = \frac{k_5}{k_5 + k_6} G_N(e^{-*}) \qquad (c)$$

Other possibilities such as $k_4 f >> k_5 + k_6$ or $k_6 << k_5 + k_4 f$ may be excluded, since in both cases K (= 1.9) should be equal to $G_N(e^{-*})$ estimated above to be 3.9.

Equation b shows that rare gas molecules are ineffective for the thermalization of electrons in comparison with polyatomic molecules. This is a reasonable conclusion and

is consistent with the results obtained by other methods.[2-4]

Substituting $K = 1.9$ and $G_N(e^{-*}) = 3.9$ into eq c gives $k_5/(k_5 + k_6) = 0.5$, which shows that the formation of N_2 in this Xe–N_2O system may be originated from two kinds of electrons which have different ranges of energies, about the half of which are thermal and scavengeable by SF_6.

It must be pointed out, however, that the above conclusion may be influenced to some extent by the Hornbeck–Molnar process, which for Xe can be written as follows

$$Xe^* + Xe \longrightarrow Xe_2^+ + e^- \qquad (12)$$

where Xe* must have energies above the appearance potential of Xe_2^+ (11.2 eV). It has been suggested that the electrons produced by the Hornbeck–Molnar process may contribute to the W values of rare gases.[23,24] If this process occurs completely in our case, the situation is not changed at all. If on the contrary, however, N_2O would happen to quench the Xe* atom, the Hornbeck–Molnar process might be suppressed, and then $G(e^{-*})$ might have a value lower than that expected from the W value of Xe.

Table I shows that the value of A largely depends on f. Taking N_2O as the third body in reaction 7,[25] one can express A as follows

$$\frac{A}{[N_2O]} = \frac{k^{III}}{k_1} + \frac{k_{10}}{k_1}\sqrt{\frac{10^{-2}G(e^{-*})D}{k_a}}\,\frac{1}{[N_2O]^2} \qquad (d)$$

where k^{III} is the third-body rate constant. Since, however, an attempt to show a linearity of $A/[N_2O]$ *vs.* $1/[N_2O]^2$ has failed (Figure 4a), it seems necessary to assume the following additional processes, namely, the collisional detachment of an electron from unstable SF_6^{-*} [26]

$$e_{th}^- + SF_6 \xrightarrow{k_{13}} SF_6^{-*} \qquad (13)$$

$$SF_6^{-*} + Xe \xrightarrow{k_{14}} SF_6 + Xe + e_{th}^- \qquad (14)$$

In the case of the collision of SF_6^{-*} with N_2O, SF_6^{-*} might be stabilized immediately without ejecting the electron

$$SF_6^{-*} + N_2O \xrightarrow{k_{15}} SF_6^- + N_2O \qquad (15)$$

In such cases one can rewrite eq d as

$$\frac{A}{[N_2O](1 + fk_{14}/k_{15})} = \frac{k^{III}}{k_{13}} + \frac{k_{10}}{k_{13}}\sqrt{\frac{10^{-2}G(e^{-*})D}{k_a}}\,\frac{1}{[N_2O]^2} \qquad (e)$$

Assuming that processes 14 and 15 occur on every collision, the application of the Langevin rate equation[27] to those processes gives $k_{14}/k_{15} = 0.82$. Plots of $A/[N_2O](1 + 0.82f)$ *vs.* $1/[N_2O]^2$ fit in a good straight line in Figure 4b, where its slope and intercept give $k_{13} = \sim 10^{-12}$ cm^3 molecule^{-1} sec^{-1} and $k^{III} = \sim 10^{-34}$ cm^6 molecule^{-2} sec^{-1} assuming $k_a \simeq k_{10} = 2 \times 10^{-6}$ cm^3 ion^{-1} sec^{-1}.[28] The latter can be compared with the values 6×10^{-33} cm^6 molecule^{-2} sec^{-1},[12-14] and 3.3×10^{-33} cm^6 molecule^{-2} sec^{-1}.[29] The fact that the value of k^{III} estimated here is not close to these may probably be due to the crude assumptions made. The value of k_{13} is approximately equal to that obtained by Hasted and Beg,[26] but is nearly a factor of 10^5 lower than those obtained by other workers.[30] This large discrepancy in k_{13} could not clearly be explained.[31]

Finally, the part of $G(N_2)$ nonscavengeable by SF_6 is briefly discussed. The amount of nitrogen produced by the dissociative electron attachment (6) is included in it.

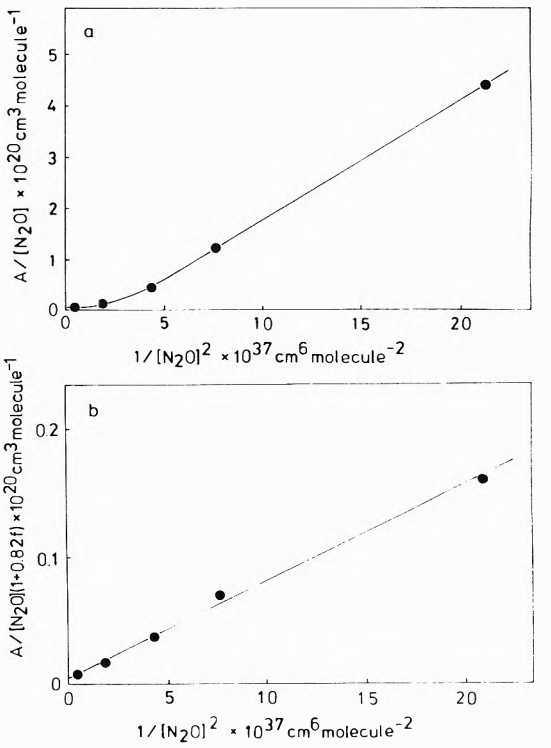

Figure 4. Dependence of A on the concentration of N_2O: (a) relation between $A/[N_2O]$ and $1/[N_2O]^2$ based on eq d; (b) relation between $A/[N_2O](1 + 0.82f)$ and $1/[N_2O]^2$ based on eq e.

Since, however, it can easily be pointed out in Figure 1 that the nitrogen yield is in excess of the total yield of electrons deduced from the W value of Xe, part of the nitrogen is formed *via* nonionic processes. The lack of dependence of K on f may also suggest that the electron–positive ion neutralization is not responsible for the gradual increase of $G(N_2)$ with the increase of N_2O mole per cent as shown in Figure 1. An important process for the nonionic formation of N_2 in Xe–N_2O mixtures might possibly be an excitation energy transfer to N_2O from metastable Xe atoms, Xe**, formed *via* direct excitation[32]

$$Xe^{**} + N_2O \longrightarrow N_2 + O + Xe \qquad (16)$$

Decomposition of N_2O during the course of electron thermalization (5)[33] might also be responsible for "nonionic" nitrogen formation

$$e^{-*} + N_2O \longrightarrow e_{th}^- + N_2 + O \qquad (17)$$

Further work is needed to resolve this question.

References and Notes

(1) This work received financial assistance from Kurata Memorial Foundation.
(2) J. M. Warman and M. C. Sauer, Jr., *J. Chem. Phys.*, **52**, 6428 (1970).
(3) V. A. J. Van Lint, *IEEE Trans. Nucl. Sci.*, **NS-11**, 266 (1964).
(4) L. G. Christophorou and J. G. Carter, *Chem. Phys. Lett.*, **2**, 607 (1968).
(5) B. P. Burtt and J. F. Kircher, *Radiat. Res.*, **9**, 1 (1958).
(6) S. Takao, S. Shida, Y. Hatano, and H. Yamazaki, *Bull. Chem. Soc. Jap.*, **41**, 2221 (1968).
(7) G. R. A. Johnson and J. M. Warman, *Trans. Faraday Soc.*, **61**, 1709 (1965).
(8) D. Rapp and D. D. Briglia, *J. Chem. Phys.*, **43**, 1480 (1965).
(9) P. J. Chantry, *J. Chem. Phys.*, **51**, 3369 (1969).
(10) E. E. Ferguson, F. C. Fehsenfeld, and A. L. Schmeltekopf, *J. Chem. Phys.*, **47**, 3085 (1967).
(11) J. F. Paulson, *J. Chem. Phys.*, **52**, 959 (1970).
(12) A. V. Phelps and R. E. Voshall, *J. Chem. Phys.*, **49**, 3246 (1968).
(13) J. M. Warman and R. W. Fessenden, *J. Chem. Phys.*, **49**, 4718 (1968).

(14) J. M. Warman, R. W. Fessenden, and G. Bakale, *J. Chem. Phys.*, **57**, 2702 (1972).
(15) The neutralization, $e^{-*} + Xe^{+} \rightarrow Xe''$, may not directly be important for product formation, since the re-ejection of electron from Xe'' may easily occur.
(16) B. P. Burtt and J. Henis, *J. Chem. Phys.*, **41**, 1510 (1964).
(17) J. L. Moruzzi and J. J. Dakin, *J. Chem. Phys.*, **49**, 5000 (1968).
(18) R. Marx, G. M. Mauclaire, F. C. Fehsenfeld, D. B. Dunkin, and E. E. Ferguson, *J. Chem. Phys.*, **58**, 3267 (1973).
(19) S. Takao, Y. Hatano, and S. Shida, *J. Phys. Chem.*, **75**, 3178 (1971).
(20) When including the negative charge transfer from N_2O^- to SF_6 in this mechanism, the kinetic treatment does not give relation a nor explain the experimental results.
(21) S. G. Lias, R. E. Rebbert, and P. Ausloos, *J. Chem. Phys.*, **57**, 2080 (1972).
(22) P. Harteck and S. Dondes, *J. Chem. Phys.*, **29**, 234 (1958).
(23) R. L. Platzmann, *Int. J. Appl. Radiat. Isotopes*, **10**, 116 (1961).
(24) L. Kevan, paper presented at the IV International Congress on Radiation Research, Evion, France, June 1970.
(25) It has been reported that Ar is much more ineffective than N_2O as the third body; R. W. Fessenden, J. M. Warman, and G. Bakale, Quarterly Report of Mellon Institute Radiation Research Laboratory, July–September 1969.
(26) J. B. Hasted and S. Beg, *Brit. J. Appl. Phys.*, **16**, 1779 (1965).
(27) F. C. Fehsenfeld, *J. Chem. Phys.*, **53**, 2000 (1970).
(28) J. M. Richardson, *Phys. Rev.*, **82**, 318 (1952).
(29) E. L. Chaney and L. G. Christophorou, *J. Chem. Phys.*, **51**, 883 (1969).
(30) Almost all the published values of k_{13} have been summarized by K. G. Monthes, E. Schultes, and R. N. Schindler, *J. Phys. Chem.*, **76**, 3758 (1972).
(31) It might be at least partly due to the fact that SF_6 can also capture the electrons not completely thermalized.
(32) D. H. Stedman and D. W. Setser, *J. Chem. Phys.*, **52**, 3957 (1970).
(33) J. T. Sears, *J. Phys. Chem.*, **73**, 1143 (1969).

Electron Spin Resonance Study of γ-Irradiated Silver Diethyl Phosphate

W. A. Bernhard* and F. S. Ezra

Department of Radiation Biology and Biophysics, School of Medicine and Dentistry, The University of Rochester, Rochester, New York 14642 *(Received November 7, 1973)*

Publication costs assisted by Department of Radiation Biology and Biophysics, Atomic Energy Project, University of Rochester

γ irradiation of silver diethyl phosphate (AgDEP) at 77 K results in the formation of the $\dot{C}H_2CH_2O\text{-}P(O_2)OC_2H_5^-$ radical. Selective line broadening of the esr spectrum is observed and attributed to a restricted motion of the $\dot{C}H_2CH_2$– moiety. Due to the electron-scavenging ability of the silver ions, other electron addition products, $CH_3\dot{C}H_2$ and $C_2H_5O\dot{P}O_2^-$, are not formed. Instead, the presence of Ag^0 is detected at 77 K. Concurrent with the decay of $\dot{C}H_2CH_2OP(O)_2OC_2H_5^-$ at 200 K is the appearance of a spectrum ascribed to $CH_3\dot{C}HOP(O)_2OC_2H_5^-$. The latter free radical decays at room temperature.

Introduction

The exposure of esters of phosphoric acid to γ irrradiation at 77 K results in the formation of three types of free radicals: (I) alkyl radicals formed by splitting a C–O bond in an electron addition reaction; (II) free radicals derived by hydrogen atom abstraction, usually from the carbon adjacent to the ester oxygen, through ionic intermediates; and (III) the alkyl phosphite radical generated by cleavage of a phosphorus–oxygen bond.[1-3] The mechanism for the formation of the last species has not been established; although, dissociative electron attachment has been proposed for phosphite radicals in γ irradiated metaphosphate glasses.[4]

We have recently characterized these three types of free radicals in γ irradiated magnesium diethyl phosphate (MgDEP) and have noted an enhanced stability due to the crystal lattice.[5-7] An effort, therefore, is being made to assess the effect of environment on free-radical production in γ irradiated dialkyl phosphates in the solid state.

Ag^+ ions are known to be efficient electron scavengers.[4,8,9] Their presence in the irradiation of phosphate esters is expected to suppress the formation of type I and III radicals. It is the aim, in this communication, to identify the free-radical intermediates in γ irradiated polycrystalline silver diethyl phosphate (AgDEP) and to determine the role of the silver ion in the radiation damage process.

Experimental Section

Methods for synthesis of AgDEP, γ irradiation of polycrystalline samples at 77 K, and recording of esr data have been reported previously.[5,6] All esr data were recorded at X band and variable temperature studies were done using the Varian variable temperature accessory. Measurements of g value were done using DPPH (g = 2.0036) as a standard.

Results and Discussion

Methyl Hydrogen Abstraction. A 77 K esr spectrum, centered at g = 2.0034 and attributed to the $\dot{C}H_2CH_2OP(O)_2OC_2H_5^-$ radical in γ irradiated AgDEP, is shown in Figure 1a. Interaction of the electron with two α and two β hydrogen nuclei can be resolved. In 90% α ^{13}C labeled AgDEP ($(CH_3{}^{13}CH_2O)_2PO_2Ag$) γ irradiated at 77 K, hyperfine coupling to the ^{13}C nucleus is also observed (Figure 2). Based solely on the magnitude of this coupling (15.0 ± 0.5 G), which is comparable to those reported for the $^{13}CH_3\dot{C}H_2$[10] and $\dot{C}H_2{}^{13}COO^-$ [11] radicals, it is concluded that the hydrogen is abstracted from ^{12}C at position 2 (Figure 3a).

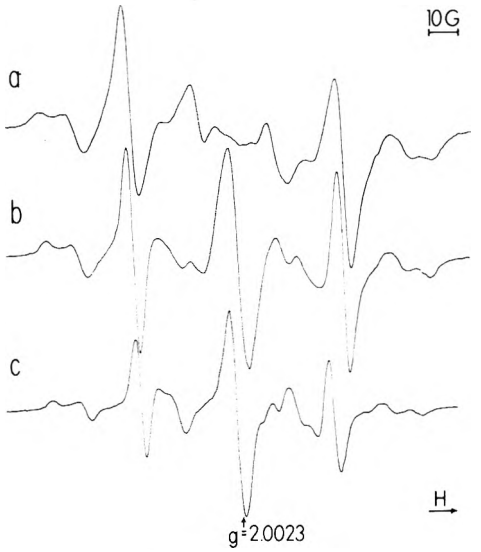

Figure 1. Esr spectra of $\dot{C}H_2CH_2OP(O)_2OC_2H_5^-$ in polycrystalline AgDEP γ irradiated at 77 K. First derivative scan recorded at X band, modulation amplitude = 2.5 G, microwave power = 0.1 mW: (a) T = 77 K, (b) T = 100 K, (c) T = 160 K.

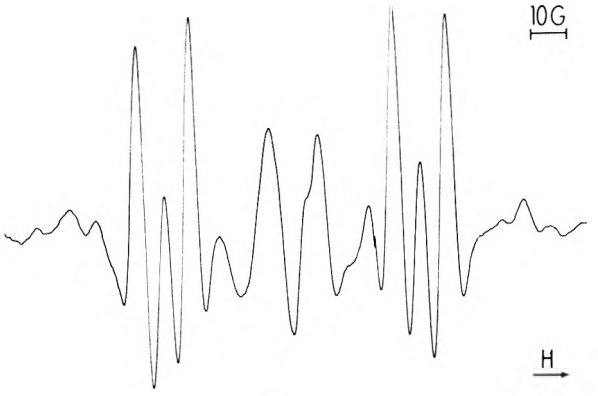

Figure 2. Esr spectrum of $\dot{C}H_2{}^{13}CH_2OP(O)_2OC_2H_5^-$ in 90% α-^{13}C polycrystalline AgDEP γ irradiated at 77 K. Second derivative scan recorded at X band, modulation amplitude = 5 G, microwave power = 5.0 mW, and T = 110 K.

Coupling to the two β protons, which are magnetically nonequivalent, is isotropic with $A_1^{H\beta}$ = 33.2 and $A_2^{H\beta}$ = 40.2 ± 0.5 G. The large magnitudes of the hyperfine coupling indicate that the $\dot{C}H_2CH_2O$- fragment attains an equilibrium conformation in which the two β protons are approximately 30° from the p orbital axis of the odd electron.[12] This conformation has been observed to be most stable for β-substituted ethyl radicals of the type $RMCH_2\dot{C}H_2$ when the atom M is from the first row of the periodic table.[13,14] In the present case, if the Heller-McConnell relationship is used

$$A^{\beta}_{Hyper} = \rho(C_0 + C\cos^2\theta)$$

where C_0 = 2 G, C = 50 G, and $\rho \sim 1$, the dihedral angles between each of the C_1-H_β bonds and the p orbital are calculated to be 29 and 38°, respectively (Figure 3b).

Nonequivalence of the β-hydrogen atoms requires that the radical fragment be either static or, assuming only rotation about the C_2-C_1 bond, undergo a rotation restricted by a twofold potential barrier. Equivalence of the α protons, observed in preliminary single-crystal data, eliminates the former possibility. Thus, the $H_2\dot{C}$- fragment is subject to a rotational motion which allows the hydrogens to remain predominantly in an equilibrium plane. This is expected to give rise to a deviation from axial symmetry in the α-proton hyperfine coupling.[5] However, such a deviation could not be resolved in AgDEP because of relatively large line widths ($\Delta H_{pp} \sim 6$ G).

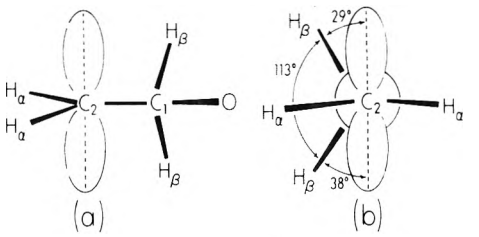

Figure 3. Two views of the $\dot{C}H_2CH_2O$- moiety in the $\dot{C}H_2CH_2OP(O)_2OC_2H_5^-$ radical: (a) perpendicular to C-C bond, (b) parallel to C-C bond.

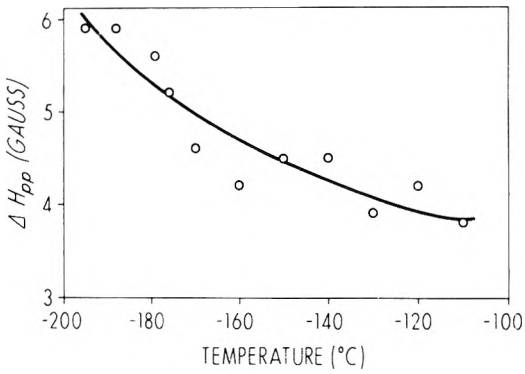

Figure 4. Plot of peak-to-peak line width measured from the $M_I^{\alpha} = 0$, $M_I^{\beta} = \pm 1$ transition in the $\dot{C}H_2CH_2OP(O)_2OC_2H_5^-$ radical as a function of temperature.

The effect of temperature on the spectrum of $\dot{C}H_2CH_2OP(O)_2OC_2H_5^-$ is shown in Figure 1b and 1c. At 77 K, the $M_I^{\beta} = 0$ components of the β proton transitions are broader than the $M_I^{\beta} = \pm 1$. As the sample is annealed, these line widths become equivalent, the magnitude of coupling to each β proton decreases and the nonequivalence in the two β protons is diminished. $A_1^{H\beta}$ decreases from 33.2 to 30.5 G and $A_2^{H\beta}$ from 40.2 to 30.5 G as the sample temperature is increased from 77 to 190 K. Selective line broadening of the spectral lines between 77 and 100 K implies that the motion of the $\dot{C}H_2CH_2OP\lessdot$ fragment is more complex than just a simple rotation about the C-C bond. This motion must generate an out of phase modulation of the β protons.[15]

All of the absorption lines in the spectrum become narrower with increasing temperature. This is due to an increasing freedom of motion of the $\dot{C}H_2$ fragment. The peak-to-peak line width as measured from the $M_I^{\alpha} = 0$, $M_I^{\beta} = \pm 1$ transition is plotted in Figure 4 as a function of temperature; however, a theoretical evaluation of the line narrowing has not been attempted. At 200 K, where transition lines are well resolved, principal values for the α proton hyperfine tensor are $A_\perp^{H\alpha}$ = 19.5 and $A^{H\alpha}$ = 30.0 ± 0.5 G. In addition to the changes in the α and β proton esr parameters, the ^{13}C coupling in $\dot{C}H_2{}^{13}CH_2OP\lessdot$ decreases within the 77-200 K temperature range from 15.0 to 14.0 ± 0.5 G. The radical eventually decays and cannot be detected above 200 K.

Reduced Silver Ion (Ag^0). Besides the $\dot{C}H_2CH_2O$-$P(O)_2OC_2H_5^-$ spectrum at 77 K, a larger magnetic field scan at high gain reveals the presence of a doublet of absorption lines with a 505 ± 10 G splitting and g = 1.990.

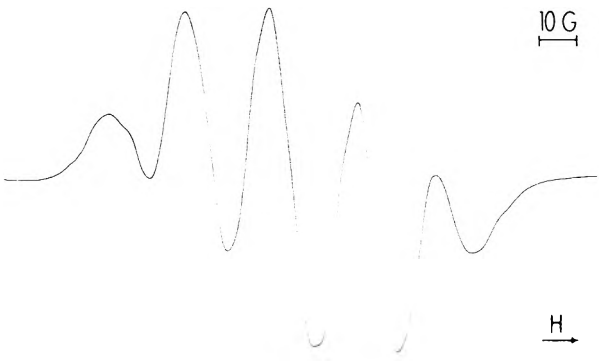

Figure 5. Esr spectrum of $CH_3\dot{C}HOP(O)_2OC_2H_5^-$ radical in polycrystalline AgDEP γ irradiated at 77 K. First derivative scan recorded at X band, modulation amplitude = 5 G, microwave power = 1.0 mW, and T = 77 K. Sample is annealed to 200 K and returned to 77 K.

The latter spectrum is attributed to Ag^0 in which the odd electron is assumed to reside in the 5s orbital. Contributions to the interaction with the silver nucleus, therefore, arise from spin density in the 5s orbital and from polarization of inner s orbitals. The 505-G coupling in AgDEP represents a 20–25% reduction in magnitude of interaction relative to that in the Ag^0 free atom.[16] Because of the large line widths, $\Delta H_{pp} \sim 50$ G, additional hyperfine structure due to the presence of the two naturally occurring isotopes, $^{109}Ag^0$ ($I = \frac{1}{2}$, natural abundance = 48.18%, $\mu_n = -0.130$) and $^{107}Ag^0$ ($I = \frac{1}{2}$, natural abundance = 51.82%, $\mu_n = -0.113$), could not be resolved.

Broadening of absorption lines and reduction in hyperfine coupling has been reported for Ag^0 trapped in different matrices and is caused by interaction of the silver 5s odd electron with the environment.[9,16,17] The broadening is a consequence of either electron exchange between reduced silver and neighboring silver ions or the presence of magnetically distinct lattice sites. In AgDEP, the silver ion is coordinated to four oxygen atoms and it has been suggested that at least one of the Ag–O bonds possesses significant covalent character.[18] Interaction of Ag^0 with the lattice results in a redistribution of the spin density from the 5s orbital onto the neighboring oxygen atoms. Moreover, the covalency in the Ag–O bonds leads to a reduction of the polarization contribution to the hyperfine coupling.

The silver atom eventually decays, probably as a result of its ability to complex with its environment. In the present case, Ag^0 is annealed out at 200 K. It is assumed that the decay does not occur through the Ag_2^+ intermediate ($Ag^0 + Ag^+ \rightarrow Ag_2^+$)[9] since no such intermediate is detected.

The white polycrystalline AgDEP turns orange upon γ irradiation at 77 K and in subsequent annealing to 200 K the orange color disappears. Since no such color changes have been observed in other γ irradiated diethylphosphate salts, except for cadmium diethyl phosphate which turns yellow, it is assumed that the orange color in AgDEP results from absorption by the trapped silver atoms.[16]

Methylene Hydrogen Abstraction. The spectrum of $\dot{C}H_2CH_2OP(O)_2OC_2H_5^-$ is gradually annealed out by increasing the temperature from 77 to 200 K and is replaced by a spectrum of comparable intensity consisting of a 23-G quintet of broad absorption lines (Figure 5). This second carbon centered radical, attributed to $CH_3CHOP(O)_2OC_2H_5^-$, might be formed in part by inter- or intramolecular conversion of $\dot{C}H_2CH_2OP(O)_2OC_2H_5^-$. But it was not possible to establish a one-to-one relationship between these two radicals because of the large degree of overlap in the two spectra.

The $CH_3\dot{C}HOP\lessgtr$ spectral lines become narrower upon raising the temperature and at 250 K, a 7.0-G coupling to the phosphorus is resolved. The radical subsequently decays by annealing the sample to room temperature. A complete determination of the ^{31}P hyperfine coupling parameters in $CH_3\dot{C}HOP\lessgtr$ was not possible because of the lack of resolution. But the parameters should be comparable to those in MgDEP.[7] The phosphorus atom in MgDEP[19] and AgDEP[18] lies close to the two C–C–O planes of the diethyl phosphate anion. The angles between the C–C–O planes and O–P bonds are 2 and 18° in AgDEP and 1 and 14° in MgDEP. Assuming that there are no large changes in conformation upon abstraction of the hydrogen, the phosphorus will remain close to the nodal plane of the unpaired electron in the $CH_3\dot{C}HOP(O)_2OC_2H_5^-$ radical. Consequently any contribution to the interaction of the electron with the ^{31}P nucleus from hyperconjugation will be minimized. Since the major contribution comes from hyperconjugation the net coupling is expected to be small.[7]

Conclusions

It is apparent, from the present work, that the environment does have an effect on the formation of free radicals in γ irradiated phosphate esters. In silver diethyl phosphate (AgDEP), the Ag^+ ion acts as an electron sink, preventing the formation of the ethyl and ethyl phosphite radicals

$$(C_2H_5O)_2PO_2^- \longrightarrow e^- + (C_2H_5O)_2P\dot{O}_2 \quad (1)$$

$$Ag^+ + e^- \longrightarrow Ag^0 \quad (2)$$

$$(C_2H_5O)_2PO_2^- + e^- \not\longrightarrow \dot{C}_2H_5 + C_2H_5OPO_3^{2-} \quad (3)$$

$$(C_2H_5O)_2PO_2^- + e^- \not\longrightarrow C_2H_5O\dot{P}O_2^- + OC_2H_5^- \quad (4)$$

On the other hand, formation of the hydrogen abstraction radicals is not suppressed by Ag^+. This implies that hydrogen is lost subsequent to an electron removal step such as that in reaction 1. Though, in this case, there is no direct evidence for the formation of $(C_2H_5O)_2P\dot{O}_2$ the following intermolecular ion–molecule reaction[3] seems probable

$$(C_2H_5O)_2P\dot{O}_2 + (C_2H_5O)_2PO_2^- \longrightarrow (C_2H_5O)_2PO(OH) + CH_3\dot{C}HOP(O)_2OC_2H_5^- \text{ (or } \dot{C}H_2CH_2OP(O)_2OC_2H_5^-) \quad (5)$$

An alternative pathway, for the production of $CH_3\dot{C}HOP\lessgtr$, is by free radical conversion

$$\dot{C}H_2CH_2OP(O)_2OC_2H_5^- \longrightarrow CH_3\dot{C}HOP(O)_2OC_2H_5^- \quad (6)$$

Both hydrogen abstraction free-radical products have been observed in esters of phosphorous or phosphoric acid allowed to react with OH radicals in aqueous systems[20] and in uv irradiated alcohols.[21] The presence of water or acid in alcohols enhances the yield of radicals resulting from hydrogen abstraction at the position 2 carbon. But it is not clear at this stage what condition in the solid state governs the position of hydrogen abstraction. The question is whether the two free-radical products are formed independently or one is a precursor to the other.

References and Notes

(1) S. Sugimoto, K. Kuwata, S. Ohnishi, and I. Nitta, *Nippon Hoshasen Kobunshi Kenkyu Kyokai Nempo*, **7**, 199 (1965–1966).

(2) C. M. L. Kerr, K. Webster, and F. Williams, *J. Phys. Chem.*, **76**, 2848 (1972).
(3) K. D. Haase, D. Schulte-Frohlinde, P. Kourim, and K. Vacek, *Int. J. Radiat. Phys. Chem.*, **5**, 351 (1973).
(4) T. Feldman and A. Tre nin, *J. Chem. Phys.*, **47**, 2754 (1967).
(5) F. S. Ezra and W. A. Bernhard, *J. Chem. Phys.*, **59**, 3543 (1973).
(6) F. S. Ezra and W. A. Bernhard, *J. Chem. Phys.*, in press.
(7) W. A. Bernhard and F. S. Ezra, *J. Chem. Phys.*, in press.
(8) D. M. Brown and F. S. Dainton, *Trans. Faraday Soc.*, **62**, 1139 (1966).
(9) L. Shields, *Trans. Faraday Soc.*, **62**, 1042 (1966).
(10) R. W. Fessenden, *J. Phys. Chem.*, **71**, 74 (1967).
(11) R. Livingston, J. K. Dohrmann, and H. Zeldes, *J. Chem. Phys.*, **53**, 2448 (1970).
(12) R. W. Fessenden, *J. Cnim. Phys.*, **61**, 1570 (1964).
(13) D. Griller and K. U. Ingold, *J. Amer. Chem. Soc.*, **95**, 6459 (1973).
(14) P. J. Krusic, P. Meakin, and J. P. Jesson, *J. Phys. Chem.*, **75**, 3438 (1971).
(15) J. E. Wertz and J. R. Bolton, "Electron Spin Resonance Elementary Theory and Practical Applications," McGraw Hill, New York, N. Y., 1972.
(16) R. S. Eachus and M. C. R. Symons, *J. Chem. Soc. A*, 1329 (1970).
(17) L. Shields, *J. Chem. Phys.*, **45**, 2332 (1966).
(18) J. Hazel and R. L. Collin, *Acta Crystallogr., Sect. B*, **28**, 2951 (1972).
(19) F. S. Ezra and R. L. Collin, *Acta. Crystallogr., Sect. B*, **29**, 1398 (1973).
(20) A. R. Metcalfe and W. A. Waters, *J. Chem. Soc. B*, 340 (1967).
(21) R. Livingston and H. Zeldes, *J. Amer. Chem. Soc.*, **88**, 4333 (1966).

Measurement by Proton Magnetic Resonance Line Shape Analysis of a Small Barrier to Internal Rotation in *N,N'*-Di-*tert*-butylthiourea

Charalyn D. Freeman and Donald L. Hooper*

Department of Chemistry, Dalhousie University, Halifax, Nova Scotia, Canada *(Received October 29, 1973)*

Publication costs assisted by Dalhousie University

Pmr line shape analysis shows that the barrier to internal rotation about the C–N bonds in *N,N'*-di-*tert*-butylthiourea is $\Delta G^* = 11.0 \pm 0.2$ kcal mol^{-1}.

The room temperature 100-MHz spectrum of *N,N'*-di-*tert*-butylthiourea has been reported[1] to show three single peaks near $\tau 9$, with the obvious interpretation that these are the *tert*-butyl signals of the cis–cis, cis–trans, and trans–trans conformations of the thiourea. Such a simultaneous observation of the signals of all three conformational isomers in a pmr spectrum at *ca.* 40° would indicate either high barriers to the interconversion of the isomers and hence to rotation about the C–N partial double bonds or an unexpectedly large chemical shift difference between the *tert*-butyl groups of the different isomers. In the pmr spectrum of *N*-methylthiourea separate signals for the methyl groups cis and trans to the thiocarbonyl are observed[2] only at temperatures below 0° and the barrier to internal rotation has been estimated as only 13.2 kcal mol^{-1}. There is insufficient data on the barriers to internal rotation in monosubstituted thioureas or thioamides to allow prediction of the effect of increasing the size of alkyl substituents, however, for a series of *N,N*-dialkyl acetamides increasing the size of the alkyl groups is reported[3] to lower the barrier. It seems then that the barrier to internal rotation in di-*tert*-butylthiourea should be comparable to that in *N*-methylthiourea unless steric interactions are enough to make the *tert*-butyl case anomalous. We have disproved the possibility of such an anomaly by recording low-temperature pmr spectra of di-*tert*-butylthiourea.

At room temperature 60- and 100-MHz spectra of di-*tert*-butylthiourea, both samples from commercial suppliers and those freshly prepared by reaction of *tert*-butylamine with *tert*-butylisothiocyanate, show only a single *tert*-butyl peak with intensity nine times that of the NH peak observed in, *e.g.*, acetone or DMSO solution. Additional high-field peaks are observed only when the sample begins to decompose after long standing in solution.

At temperatures below −55° the single *tert*-butyl peak splits into two peaks of approximately equal area, with no additional signals observed in the 60-MHz spectrum to −98°. From the coalescence temperature (218°K) and the limiting chemical shift difference (19.8 Hz at 60 MHz) a barrier $\Delta G^* = 11.0$ kcal mol^{-1} is estimated for a 5% solution of di-*tert*-butylthiourea in ⅓ toluene-d_8 and deuteriochloroform. For a 5% solution in deuteriochloroform coalescence temperature (217°K) and limiting chemical shift difference (13.0 Hz at 60 MHz) measurements give $\Delta G^* = 11.1$ kcal mol. Line shape analysis for temperatures at and below coalescence, using the iterative line shape program of Saunders,[4] refine these measurements to $\Delta G^* = 10.9 \pm 0.2$ and $\Delta G^* = 11.1 \pm 0.2$ kcal mol^{-1}, respectively.

The limiting chemical shift difference between the two *tert*-butyl signals increases by 6.8 Hz at 60 MHz on going from deuteriochloroform to ⅓ toluene-d_8 and deuteriochloroform, indicating that one of the low-temperature signals corresponds to *tert*-butyl groups cis to the thiocarbonyl and the other to groups trans to the thiocarbonyl. As the two signals are of approximately equal intensity, it appears that the time-dependent process monitored by low-temperature spectra is the interconversion of the two cis–trans conformational isomers. This is somewhat unexpected as inspection of molecular models indicates that

the cis–cis conformer should be subject to minimal steric interactions and hence be favored at low temperature. However, the infrared spectrum of this compound also shows[5] approximately equal areas for the bands assigned as the cis and trans NH stretching vibrations.

Acknowledgment. Financial assistance by the National Research Council of Canada is gratefully acknowledged.

References and Notes

(1) R. K. Gosavi, U. Agarwala, and C. N. R. Rao, *J. Amer. Chem. Soc.*, **89**, 235 (1967).
(2) A. S. Tompa, R. D. Barefoot, and E. Price, *J. Phys. Chem.*, **73**, 435 (1969)
(3) R. M. Hammaker and B. A. Gugler, *J. Mol. Spectrosc.*, **17**, 356 (1965).
(4) M. Saunders in "Magnetic Resonance in Biological Systems," A. Ehrenberg, Ed., Pergamon Press, New York, N. Y., 1967.
(5) C. N. R. Rao, K. G. Rao, A. Goel, and D. Balasubramanian, *J. Chem. Soc. A*, 3077 (1971).

Electronic Structure of Oxovanadium(IV) and Copper(II) Dicyclohexyldithiophosphinate Complexes

Henry J. Stoklosa, Gerald L. Seebach, and John R. Wasson*

Department of Chemistry, University of Kentucky, Lexington, Kentucky 40506 *(Received June 25, 1973; Revised Manuscript Received February 7, 1974)*

The unusually stable vanadyl(IV) and copper(II) dicyclohexyldithiophosphinate complexes, $VO[S_2P(C_6H_{11})_2]_2$ and $Cu[S_2P(C_6H_{11})_2]_2$, have been prepared and characterized using infrared, mass, electronic, and electron spin resonance spectroscopy. The esr spectra of the complexes exhibit considerable phosphorus superhyperfine splitting in the solid state and solution which is essentially isotropic. The electronic spectra are interpreted in terms of crystal field calculations and the properties of the complexes are discussed in terms of extended-Hückel molecular orbital calculations for the model compounds $VO(S_2PX_2)_2$ and $Cu(S_2PX_2)_2$ (X = H,F).

Introduction

Within recent years transition metal complexes with dithiophosphate (I) and dithiophosphinate (II) ligands have received considerable attention.[1] The electron spin resonance (esr) spectra of the copper(II) and oxovanadium(IV) (hereafter referred to as vanadyl) complexes of these ligands are of particular interest since they exhibit appreciable ^{31}P superhyperfine splittings attributed[2] to delocalization about the chelate ring in the copper(II) complexes and transannular interactions in the vanadyl complexes. One of the purposes of the present work was to make a more detailed inquiry into the origin of the observed ^{31}P superhyperfine splittings as well as the ^{75}As superhyperfine splitting in the esr spectra of vanadyl dithiocacodylate, $VO[S_2As(CH_3)_2]_2$, in various solvents.[3]

I II

M = metal ion
n = oxidation state of the metal
R = alkyl or aryl group

In general, copper(II) dithiophosphate and -phosphinate complexes tend to be unstable. They tend to decompose into polymeric copper(I) compounds and oxidized forms of the ligands. However, they have been trapped in the corresponding diamagnetic nickel(II) host lattices.[1,4,5] The vanadyl complexes have been studied in solution[1,2,6] and characterized in the solid state.[6] Generally, the vanadyl complexes are sensitive to air and water. We have found that stable copper(II) and vanadyl complexes result from the interaction of ammonium dicyclohexyldithiophosphinate with aqueous solutions of the appropriate metal salts. The esr and optical spectra of these complexes have been examined in the solid state, solution, and in various host lattices. Iterative extended-Hückel molecular orbital and crystal field calculations have been utilized to describe the electronic structures of these complexes.

Experimental Section

Ammonium dicyclohexyl dithiophosphinate, $NH_4S_2P(C_6H_{11})_2$, was obtained from Aldrich Chemical Co., Milwaukee, Wisc., and used without further purification. The other chemicals employed in these experiments were of reagent or spectroscopic grades. Elemental analyses were performed by Chemalytics, Inc., Tempe, Ariz.

Oxobis(dicyclohexyl dithiophosphinato)vanadium(IV), $VO[S_2P(C_6H_{11})_2]_2$, $VO(dtp)_2$. This compound was prepared by adding a methanolic solution of ammonium dicyclohexyl dithiophosphinate to a methanolic solution of hydrated vanadyl sulfate to which sufficient water had been added to dissolve the salt completely. The blue complex was isolated by filtration, washed with ether, and stored in a desiccator over anhydrous calcium chloride for 2 days.

Anal. Calcd: 48.88% C, 7.52% H, 21.45% S. Found: 48.02% C, 7.26% H, 21.1% S. Melting point (uncorrected): 218°.

Bis(dicyclohexyl dithiophosphinato)copper(II), $Cu[S_2P(C_6H_{11})_2]_2$, $Cu(dtp)_2$. This brown complex was prepared as above using a 2:1 ligand to metal ratio.

Anal. Calcd: 49.2% C, 7.6% H, 21.9% S. Found: 53% C, 9.2% H, 22% S.

Difficulties with the C and H analyses were noted. C and H analyses were consistently high while the sulfur analyses were reproducible within ±0.1%. Blue diamagnetic bis(dicylohexyl dithiophosphinato)nickel(II) and white bis(dicyclohexyl dithiophosphinato)zinc(II), to be described in detail elsewhere, were also prepared by the above procedure. The vanadyl and copper(II) doped samples of the zinc and nickel complexes were prepared using mixed solutions of the metal salts.

Infrared spectra (4000–200 cm^{-1}) were measured with a Perkin-Elmer 621 instrument using Nujol mulls on cesium iodide plates and potassium bromide pellets. Electronic absorption spectra were obtained with a Cary Model 14 recording spectrometer using matched 1.0-cm quartz cells and a mull technique described previously.[7] Mass spectra were obtained using a double-focusing Hitachi Perkin-Elmer RMU-7 spectrometer. Routine spectra were run with a resolution of about one part in 2000 with the ionization energy maintained at approximately 70 eV. Electron spin resonance spectra of finely ground compounds and solutions were obtained using the X-band instrument and techniques previously described.[8] Calculations were performed on the IBM 360-65 computer at the University of Kentucky Computer Center.

Results and Discussion

The vanadyl complex, $VO[S_2P(C_6H_{11})_2]_2$, is stable with respect to room conditions indefinitely. The compound decomposes in oxygenated noncoordinating solvents within 1 day, the solutions turning from blue to green. The compound is highly soluble in coordinating solvents but the solutions decompose within minutes. The mass spectrum of the complex exhibits a parent peak at m/e 589. This result, agreeing with the calculated molecular weight, indicates that the complex is monomeric. The ready solubility of $VO(dtp)_2$ in common solvents as well as failure to observe any esr lines attributable to dimers in solution indicate that $VO(dtp)_2$ is also monomeric in solution.

The copper(II) complex, $Cu[S_2P(C_6H_{11})_2]_2$, is slightly soluble in noncoordinating solvents without apparent decomposition. It is slightly soluble in coordinating solvents but decomposition takes place within 1 day. The mass spectrum gives a parent peak agreeing with the calculated molecular weight of the complex.

Infrared Spectra. Figure 1 gives stick diagrams of the infrared spectra of the complexes and ammonium dicyclohexyldithiophosphinate over the range in which metal–ligand vibrations can be expected to occur. Since the spectra above 900 cm^{-1} are largely due to ligand vibrational modes, they have been omitted. Metal–sulfur stretching frequencies are expected in the region 400–200 cm^{-1}. We have tentatively identified ν(V–S) at 325 cm^{-1} in accord with Cavell's work[6] and ν(Cu–S) at 293 cm^{-1}. Due to the lack of normal coordinate analyses for complexes of this type only tentative metal–sulfur stretching frequency assignments are possible. The vanadyl V=O stretching frequency occurs at 1005 cm^{-1}. This is similar to ν(V=O) found for vanadyl dithiocarbamates[9] and is consistent with the formulation of the complex as a monomeric species. Cavell, *et al.*,[6] found that $VO(S_2PF_2)_2$ and

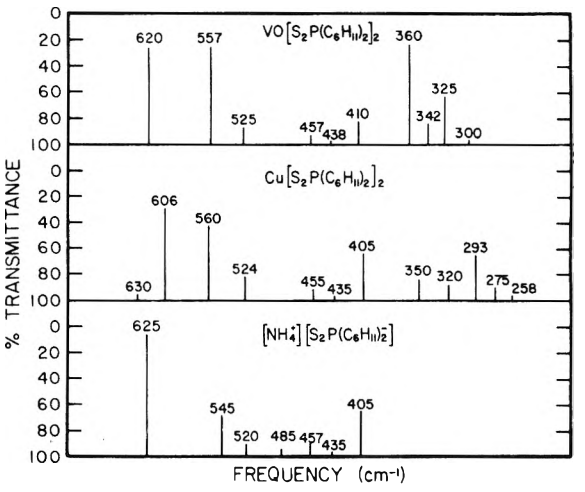

Figure 1. Infrared spectra of dicyclohexyldithiophosphinate complexes in the 650–200-cm^{-1} region.

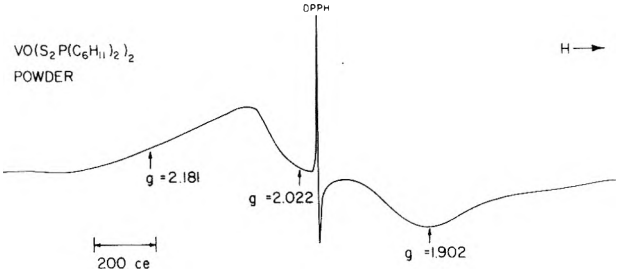

Figure 2. Electron spin resonance spectrum of powdered $VO[S_2P(C_6H_{11})_2]_2$. The g values are field markers. ν = 9.361 GHz.

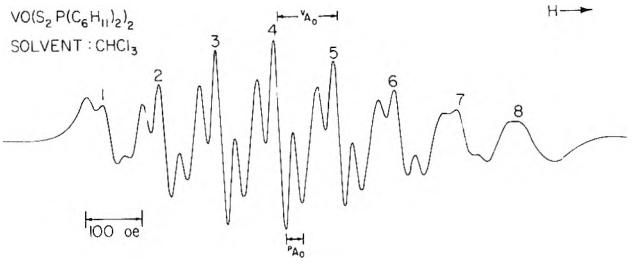

Figure 3. Esr spectrum of $VO[S_2P(C_6H_{11})_2]_2$ in chloroform. The numbered peaks indicate transitions due to the vanadium nuclear hyperfine splitting.

$VO[S_2P(CF_3)_2]_2$ exhibited ν(V=O) at 860 and 870 cm^{-1}, respectively, and postulated V=O···V=O interactions in the solid state. The monomeric nature of the dicyclohexyldithiophosphinate complexes of concern here can be safely attributed to the bulkiness of the cyclohexyl groups and this is additionally supported by inspection of Prentice-Hall framework and Benjamin-Maruzen molecular models. The tentative assignment of ν(Cu–S) is not unreasonable in view of the normal coordinate analysis of the vibrational spectra of nickel dithiocarbamate.[10]

Electron Spin Resonance Spectra. The esr spectrum of a powdered sample of $VO[S_2P(C_6H_{11})_2]_2$, $VO(dtp)_2$, shown in Figure 2 is atypical for a vanadyl complex since usually only one line is observed. The spectrum in Figure 2 undoubtedly arises from the partial resolution of the ^{51}V hyperfine splitting brought about by magnetic dilution afforded by the bulky cyclohexyl groups. The isotropic solution spectrum of $VO(dtp)_2$ in chloroform is given in Figure 3 where it can be seen that the eight ^{51}V hyperfine lines

TABLE I: Electron Spin Resonance Data

Compound	Lattice	$\langle g \rangle^a$	$g_1{}^b$	g_2	g_3	× 10^4 cm^{-1} $\langle {}^MA \rangle^c$	${}^MA_1{}^d$	${}^MA_2$	${}^MA_3$	$\langle {}^PA \rangle^e$	${}^PA_1{}^d$	${}^PA_2$	${}^PA_3$
$VO[S_2P(C_6H_{11})_2]_2$	CH_2Cl_2	1.988				100				28.2			
	Ni(II) complex	1.973	1.980	1.980	1.959	100	63	63	177	30.1	31.9	31.9	28.4
$Cu[S_2P(C_6H_{11})_2]_2$	CH_2Cl_2	2.066				80				6.2			
	Pure Powder	2.057	2.028	2.028	2.115								
	Ni(II) complex	2.047	2.006	2.011	2.124	71.4	39.3	14.1	170.7		5.4		5.8
	Zn(II) complex	2.066	2.012	2.014	2.171	74.1	54.0	35.7	140.9		5.5		5.9

[a] $\langle g \rangle$ = g isotropic or $1/3(g_1 + g_2 + g_3)$. [b] $g_1 = g_2 = g_\perp$ for axial geometry. Note that $g_\parallel < g_\perp$ for vanadyl complexes and $g_\parallel > g_\perp$ for copper complexes. The nuclear hyperfine and phosphorus superhyperfine coupling constants listed are those associated with the corresponding g values. [c] $\langle {}^MA \rangle$ = metal isotropic electron spin–nuclear spin hyperfine coupling constant or $1/3({}^MA_1 + {}^MA_2 + {}^MA_3)$. [d] $A_1 = A_2 = A_\perp$ for axial geometry. [e] $\langle {}^PA \rangle$ = phosphorus-31 superhyperfine splitting.

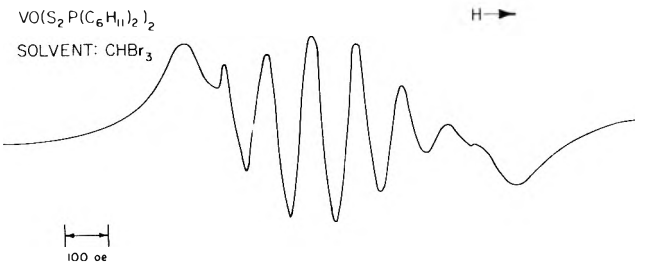

Figure 4. Esr spectrum of $VO[S_2P(C_6H_{11})_2]_2$ in bromoform.

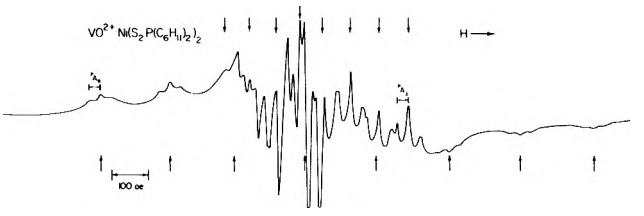

Figure 5. Esr spectrum of $VO[S_2P(C_6H_{11})_2]_2$ doped into the corresponding powdered diamagnetic nickel(II) complex. The arrows pointing upward indicate the parallel absorptions while the downward arrows indicate the perpendicular absorptions.

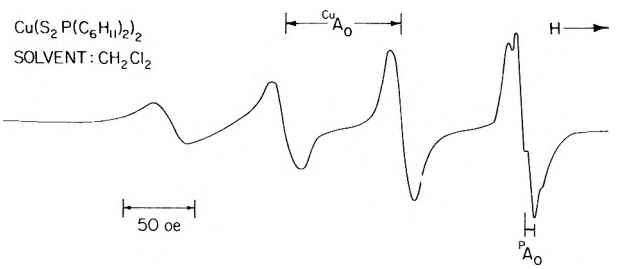

Figure 6. Esr spectrum of $Cu[S_2P(C_6H_{11})_2]_2$ in dichloromethane.

are each split into three components with intensity 1:2:1 by the presence of two equivalent phosphorus (^{31}P, $I = \frac{1}{2}$) nuclei in the molecule.[2] The solution spectrum is described by the spin Hamiltonian

$$H = g_0\beta H\hat{S}_z + {}^MA_0\hat{S}_z{}^M\hat{I}_z + {}^{31P}A_0\hat{S}_z{}^{31P}\hat{I}_z \qquad (1)$$

where g_0 is the isotropic g value, β is the Bohr magneton, H is the applied magnetic field and ${}^MA_0$ and ${}^{31P}A_0$ are the metal and phosphorus hyperfine splitting constants, respectively. $\hat{S}_z$ is the electron spin operator and ${}^M\hat{I}_z$ and ${}^{31P}\hat{I}_z$ are the nuclear spin operators. The esr parameters for $VO(dtp)_2$ are summarized in Table I. The solution parameters were checked by simulation of the spectrum using a computer program provided by Professor McClung, University of Alberta. The solution spectrum of $VO(dtp)_2$ in bromoform (Figure 4) is not a simple isotropic spectrum, the ^{31}P superhyperfine splitting is not evident and the vanadium nuclear hyperfine lines are considerably broadened. This type of spectrum arises from the failure of the molecule to tumble sufficiently rapidly in solution to produce an isotropic spectrum due to viscosity, inertia, and molecular diameter effects.[11] For complexes with large molecular diameters (~20 Å) such spectra are expected to be routinely encountered. The evaluation of accurate esr parameters from spectra of the type shown in Figure 4 is difficult. The powder esr spectrum of $VO(dtp)_2$ diluted into the related nickel(II) complex is shown in Figure 5. Magnetic dilution is achieved and vanadium hyperfine and ^{31}P superhyperfine splittings are resolved (Table I). Doping $VO(dtp)_2$ into the corresponding zinc(II) complex gave a spectrum with considerable overlapping of hyperfine lines which could not be unambiguously interpreted. This may be a result of distortion of the complex when placed in the tetrahedral zinc complex which gives rise to three g values which differ only slightly and the corresponding hyperfine and superhyperfine absorptions. Distortion of the copper(II) complex takes place, as noted below, when it is doped into the zinc compound. The spectrum of $VO(dtp)_2$ doped into the nickel(II) complex is accounted for using the axially symmetric spin Hamiltonian

$$H = g_\parallel\beta H_z\hat{S}_z + g_\perp\beta(H_x\hat{S}_x + H_y\hat{S}_y) + {}^MA^M\hat{I}_z\hat{S}_z + {}^MB({}^M\hat{I}_x\hat{S}_x + {}^M\hat{I}_y\hat{S}_y) + {}^{31P}A({}^{31P}\hat{I}_x\hat{S}_x + {}^{31P}\hat{I}_y\hat{S}_y + {}^{31P}\hat{I}_z\hat{S}_z) \quad (2)$$

where $g_\parallel$ and $g_\perp$ are the axial g values, the other quantities have their usual significance, and the last term implies that the ^{31}P superhyperfine splitting is isotropic. For practical purposes the later is true except for a slight lattice effect and experimental uncertainty due to the nature of the powder spectra. This result is in accord with similar measurements on related systems.[1,2,6] The esr parameters are listed in Table I.

The esr spectrum of a powdered sample of brown $Cu[S_2P(C_6H_{11})_2]_2$, $Cu(dtp)_2$, is indicative of a tetragonal geometry with $g_\parallel = 2.115$ and $g_\perp = 2.028$. No hyperfine splitting is resolved in the spectrum of the pure complex. However, the solution esr spectrum of the copper(II) complex in dichloromethane (Figure 6) shows not only the copper hyperfine lines but also splitting of the high-field peak into three components by two equivalent phosphorus nuclei along with an additional splitting due to superposition[2] of ^{63}Cu and ^{65}Cu isotope lines. The esr spectra of $Cu(dtp)_2$ doped into the corresponding powdered diamagnetic nickel(II) (Figure 7) and zinc(II) (Figure 8) complexes can be interpreted by standard methods using a rhombic spin-Hamiltonian operator.[12] The effective D_{2h} symmetry of the copper(II) chelate is expected to be asso-

TABLE II: Electronic Spectra

Compound	Solvent	ν_1, kK	ϵ_1[a]	$f_1 \times 10^4$[b]	ν_2, kK	ϵ_2	$f_2 \times 10^4$	ν_3, kK	ϵ_3	$f_3 \times 10^4$	ν_4, kK	ϵ_4	$f_4 \times 10^4$
$VO[S_2P(C_6H_{11})_2]_2$	Chlorobenzene	9.76	10.4	2.30	(13.7)	14.2[d]	1.31	16.8	46.4	6.85	(24.4)	32.0	6.33
	Dichloromethane	9.71	8.4	1.37	(14.2)	15.4	1.93	16.7	40.8	6.34	(24.4)	21.0	4.24
	Bromoform	9.71	25.3	2.19	(14.3)	20.3		16.4	37				
	Nujol mull[c]	9.8	[0.26]		(13.5)	[0.36]		16.5	[0.57]		(24.5)	[0.42]	
$Cu[S_2P(C_6H_{11})_2]_2$	Dichloromethane	(10.3)[d]	125		14.7	405	164						
	Dichloroethane	(10.3)	115		14.7	385	149						
	Nujol mull[c]	11.0	[0.10]		15.0	[0.50]		(18.0)	[1.00]				

[a] Molar absorptivity. [b] Oscillator strengths, f, were calculated using the expression $f = 4.60 \times 10^{-9} \epsilon_{max} \nu_{1/2}$ where ϵ_{max} is the molar absorptivity of the band maximum and $\nu_{1/2}$ is the band width at half-height expressed in wave numbers: C. J. Ballhausen, *Progr. Inorg. Chem.*, **2**, 251 (1960). [c] The ϵ values listed in brackets are absorbance values which are presented only in order to indicate relative band intensities. [d] Parentheses indicate a shoulder. [e] ν_2 and the corresponding parameters for $VO(dtp)_2$ were obtained using the program BIGAUSS (ref 14).

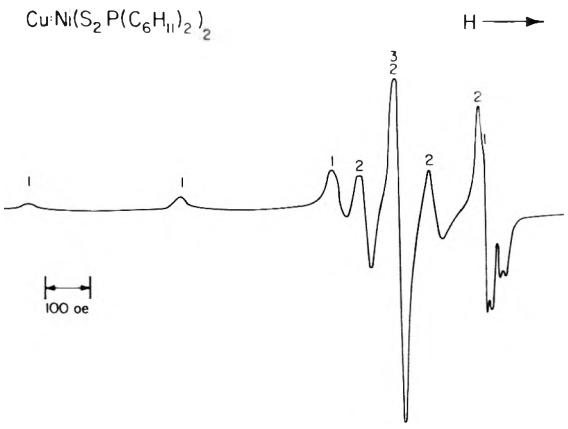

Figure 7. Esr spectrum of $Cu[S_2P(C_6H_{11})_2]_2$ doped into the nickel(II) complex, powder spectrum. The numbers indicate the hyperfine components.

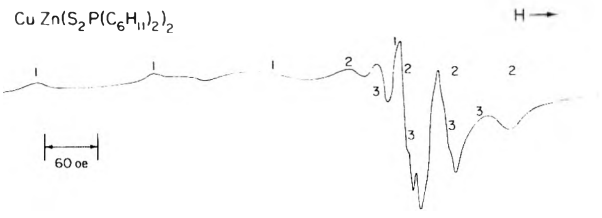

Figure 8. Esr spectrum of $Cu[S_2P(C_6H_{11})_2]_2$ doped into the zinc(II) complex, powder spectrum. The numbers indicate the hyperfine components.

ciated with three g values in accord with this result. The dramatic change in the spectrum which occurs upon doping the complex into the tetrahedral zinc chelate indicates that the copper(II) complex undergoes a marked distortion from its normal geometry. Spectra of samples at several levels of doping did not result in any improved resolution of the phosphorus superhyperfine splitting over that shown in Figures 7 and 8. The observed ^{31}P superhyperfine splitting was strongly indicative of the isotropic result obtained for the vanadyl chelate. The esr parameters for the copper chelate are summarized in Table I. The changes in the copper nuclear hyperfine coupling constants upon doping into the zinc complex is also consistent with the suggestion that the complex is forced to assume a tetrahedral type of geometry.

The isotropic ^{31}P superhyperfine splitting in complexes such as $Cu(dtp)_2$ has been attributed[2] to electron delocalization *via* sulfur to the phosphorus atoms whereas a direct $V(3d_{x^2-y^2})$-P(3s) transannular interaction can be employed to account for the isotropic ^{31}P splitting in vanadyl chelates. These mechanisms giving rise to the ligand superhyperfine splitting are taken up in more detail in a subsequent section describing the results of iterative extended-Hückel molecular orbital (EHMO) calculations for model complexes similar to $Cu(dtp)_2$ and $VO(dtp)_2$. The isotropic ^{31}P splitting is given by the familiar expression[13]

$$^{31}P A = \frac{8\pi}{3} g_e g_n \beta_e \beta_n |\psi_{3s}(0)|^2 c_s^2 \quad (3)$$

where c_s is the coefficient of the P 3s orbital in the molecular orbital containing the unpaired electron and $|\psi_{3s}(0)|^2$ is the 3s electron density at the nucleus. The experimental evaluation of c_s^2 is achieved[13] by taking the ratio of the observed ^{31}P superhyperfine splitting, A_{obsd}, to that calculated, A_{calcd}, for an unpaired electron residing in a P 3s orbital,[13] *i.e.*

$$c_s^2 = A_{obsd}/A_{calcd} = A_{obsd}/3640 \text{ G} \quad (4)$$

From the solution spectra (Table I) c_s^2 was found to be 0.0084 and 0.0018 for $VO(dtp)_2$ and $Cu(dtp)_2$, respectively. For oxovanadium(IV) and copper(II) dithiophosphate complexes c_s^2 was found[2] to be 0.0135 and 0.0026, respectively, while $c_{4s}^2 = 0.0132$ from the esr spectrum of oxobis(dimethyl dithioarsinato)vanadium(IV).[3] The result for $VO(dtp)_2$ is in good agreement with the value (0.0093) found for $VO[S_2PR_2]_2$ (where R = C_6H_5–, CH_3–, and CF_3–)[6] showing that substituent effects in the dithiophosphinates are rather minimal and that, while the steric properties of the cyclohexyl groups contribute to the stability of the dtp complexes with respect to external reactants, there is no steric effect on the electronic structure. The esr spectrum of the corresponding $Cu[S_2P(C_6H_5)_2]_2$ complex[2] yields $c_s^2 = 0.0016$ in agreement with the preceding conclusion.

Electronic Spectra. The electronic spectrum of $VO(dtp)_2$ in dichloromethane (Table II) is shown in Figure 9. The calculated spectrum shown agrees with the experimental spectrum when five Gaussian component bands are assumed. The spectrum was calculated using the program BIGAUSS.[14] The spectrum of $VO(dtp)_2$ is characteristic of vanadyl dithiophosphinate complexes[6,15] but is not typical of vanadyl compounds in general[16] since more than two or three bands are observed. The band at about 10 kK (1 KK = 1000 cm^{-1}) is of uncertain origin[6,15] and it has been suggested[6] that it is due to oxidation of vanadyl dithiophosphinates. However, we have found that exposure of solution of $VO(dtp)_2$ to air and bubbling oxygen through the solutions results in disappearance of the band at about 10 kK. Three alternate possible origins for the band at 10 kK can be proposed: (1) additional "c–d" transitions which occur due to the low symmetry (C_{2v}) assumed for $VO(dtp)_2$, (2) low-lying lig-

TABLE III: Results of Crystal Field Calculations for VO(dtp)$_2$, and Cu(dtp)$_2$, Electronic Transitions (kK)

Compound	α_2/α_4	α_4^S, kK	$yz \leftarrow x^2 - y^2$	$xz \leftarrow x^2 - y^2$	$xy \leftarrow x^2 - y^2$	$z^2 \leftarrow x^2 - y^2$
VO(dtp)$_2$[a]	0.90	11.7	13.41	13.81	16.93	71.55
			$xy \leftarrow z^2$	$xy \leftarrow x^2 - y^2$	$xy \leftarrow xz$	$xy \leftarrow yz$
Cu(dtp)$_2$[b]	0.90	−7.0	10.44	11.72	13.65	13.79
	0.90	−7.5	11.18	12.56	14.62	14.78
	0.90	−8.0	11.93	13.40	15.60	15.76

[a] $\alpha_4^{O^{2-}}$ = 94.50 kK (ref 19 and 20); S–V–S chelate angle = 88°, O–V–S angle = 105°. [b] S–Cu–S chelate angle = 88°.

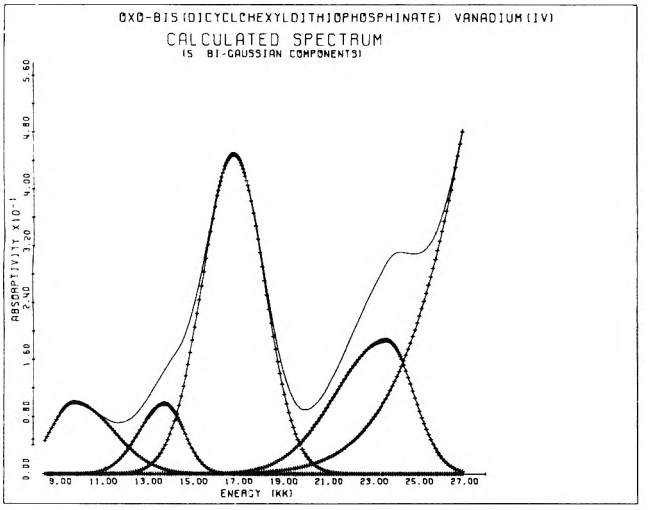

Figure 9. Electronic spectrum of VO[$S_2P(C_6H_{11})_2$]$_2$ in chloroform. The solid line is the observed spectrum which has been subjected to a Gaussian analysis using the program BIGAUSS.

and → metal charge transfer transitions due to the presence of sulfur ligands, and (3) transitions associated with the presence of an isomer with approximate trigonal bipyramidal geometry. The latter possibility is suggested by the geometry found[17] for the vanadyl chelate of 8-hydroxyquinaldine. These possibilities will be taken up in the ensuing discussion of the results of extended-Hückel molecular orbital (EHMO) calculations. The electronic spectrum of the copper(II) dicyclohexyldithiophosphinate complex (Table II) in chloroform and dichloromethane consists of a broad band with a maximum at 14.7 kK ($\epsilon_{max} \approx 400$) and a very weak shoulder at 10.3 kK ($\epsilon_{max} \approx 120$). Since these bands are of such low energy, they can be attributed to "d–d" bands with high intensity due to substantial metal–ligand covalency. The assignments of the transitions of the copper(II) compounds are considered in the following section.

Crystal Field and Molecular Orbital Calculations. In order to provide an increased understanding of the spectral and magnetic properties of VO(dtp)$_2$ and Cu(dtp)$_2$ crystal field and EHMO calculations were performed. The crystal field calculations employed the method of Companion and Komarynsky[18] and a computer program previously described.[19] Details of this explicit method[18] for d^1 and d^9 ion complexes, its simplification using elementary group theory, and evaluation of ligand crystal field parameters[19,20] are discussed elsewhere. The general coordinate system given in Figure 10 was employed in both the crystal field and MO calculations. For the copper(II) complex effective D_{2h} symmetry was assumed. The symmetry orbitals for VO(dtp)$_2$ and Cu(dtp)$_2$ were generated by standard projection operator techniques.

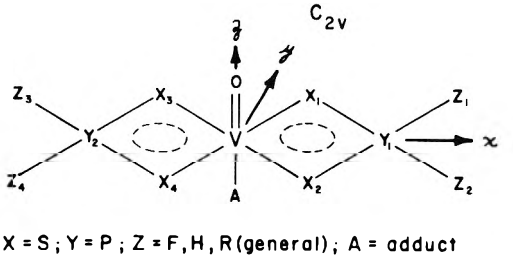

Figure 10. Coordinate system employed in crystal field and extended Hückel molecular orbital calculations. The sulfur (X) and phosphorus (Y) atoms lie in the *xy* plane. Fluorine and hydrogen atoms (see Figures 11–14) lie in the *xz* plane. For the vanadyl complex the doubly bonded oxygen atom and an trans-axial donor atom lie along the *z* axis. This coordinate system also applies to Figures 11–14.

The value of the ligand field splitting parameter, α_4 (= $6Dq$), for the dicyclohexyldithiophosphinate ion was obtained using the spectrum of the chromium(III) complex[21] and Jørgensen's expression[22]

$$10Dq \cong f(\text{ligands})\,g(\text{metal}) \times 10^3 \text{ cm}^{-1} \qquad (5)$$

A value of f(ligands) = 0.78 was thus obtained. The parameters employed in the calculations are summarized in Table III along with the calculated transition energies. Justifications of the parameters employed are discussed elsewhere.[19,20] In the absence of crystallographic data for VO(dtp)$_2$ and Cu(dtp)$_2$ a value of 88° was assumed for the S–M–S chelate angle. The calculated ground states are in agreement with more qualitative considerations as well as the results of EHMO calculations. For VO(dtp)$_2$ the calculations show that the e_π^* level in the Ballhausen–Gray C_{4v} model[16] is split only 0.4 kK upon lowering the effective symmetry to C_{2v}. Since the splitting of the e_π^* level is so small, it is unlikely that such a splitting will be observed under room temperature conditions and the C_{4v} model appears appropriate even for C_{2v} chelates. It is noted that Belford, *et al.*,[23] have reported low-temperature spectroscopic data for oxobis(2,4-pentanedionato)vanadium(IV) consistent with a ~0.4-kK splitting of the e_π^* level. The calculated transition energies ~13.8 and 16.9 kK for VO(dtp)$_2$ are in good agreement with experiment (Table II). The band appearing at about 24 kK can be assigned to a $d_{z^2} \leftarrow d_{x^2-y^2}$ promotion[16,24] which is not calculated using the crystal field model[19,20] since the metal d-orbital coefficient is small. MO calculations[16,24] show that transition $d_{z^2} \leftarrow d_{x^2-y^2}$ which best corresponds to the "d ← d" classification of crystal field theory occurs at about 70 kK, a value in accord with the $\alpha_4^{O^{2-}}$ parameter chosen in the crystal field calculations performed here. The band at about 10 kK in the spectrum of VO(dtp)$_2$, which appears as a tail in the spectra of vanadyl β-diketonates[23] and $VOCl_5^{3-}$,[25] is ruled out as a "d–d" transition by virtue of the crystal field calculations. The presence of

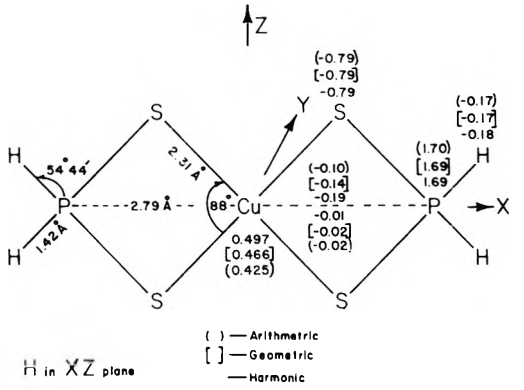

Figure 11. Geometry and EHMO results for $Cu(S_2PH_2)_2$. The left-hand side shows the assumed geometry and the right-hand side gives the results of EHMO calculations. Numbers directly above an atom indicate the net charge. Numbers between Cu and P above the line are the reduced overlap populations and those below the line refer to the product of Cu d_{xy} and P $3p_y$ orbital coefficients in the ground state. Arithmetic, geometric, and harmonic refer to the approximations employed for the off-diagonal matrix elements.

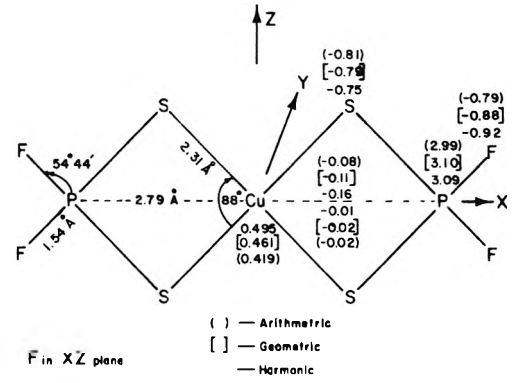

Figure 12. Geometry and EHMO results for $Cu(S_2PF_2)_2$.

a trigonal bipyramidal isomeric form of the complex is ruled out by the line widths of the solution esr spectrum and the failure to separate isomers chromatographically. It is noted that MO calculations for vanadyl complexes show a clustering of filled levels in the order of 1 eV below the ground state. We propose the assignment of the band at ~10 kK in various vanadyl complexes to arise from a filled predominantly ligand level $\rightarrow d_{x^2-y^2}$ (or d_{xy}) promotion. The comparatively weak intensity of the band at ~10 kK suggests that it is enhanced by increased metal-ligand covalency in sulfur complexes and by lower symmetries in complexes of the type[24] $VOCl_2$ (tetramethylurea)$_2$. For the tetramethylurea complex, $VOCl_2(TMU)_2$, Kuska and Yang[24] have suggested that a related transition at 9.8 kK be assigned to a $d_{xz} \leftarrow d_{xy}$ transition, however, the assignment is a bit suspect. The crystal field calculations for $Cu(dtp)_2$ (Table III) indicate the one-electron d energy level sequence $xy > z^2 > x^2 - y^2 > xz > yz$ and the calculated transitions are in fair accord with experiment. This assignment of one-electron levels is not unambiguous due to the well-known phenomenological nature of the calculations and the EHMO calculations, discussed below, are not particularly helpful.

Bond distances and angles employed in the EHMO calculations, given in Figures 11-14, were assumed on the basis of results of crystallographic studies of related complexes[1] and phosphorus compounds.[26] The EHMO calculations were performed using Hoffmann's program[27] which

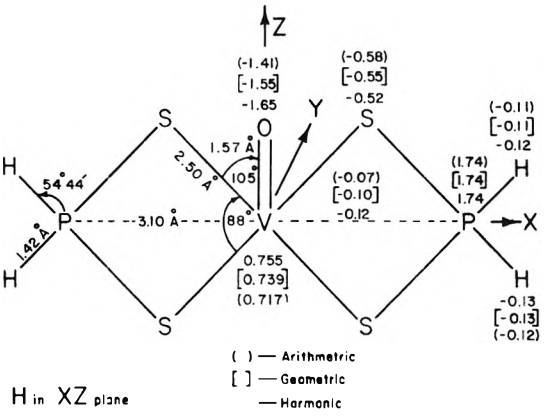

Figure 13. Geometry and EHMO results for $VO(S_2PH_2)_2$.

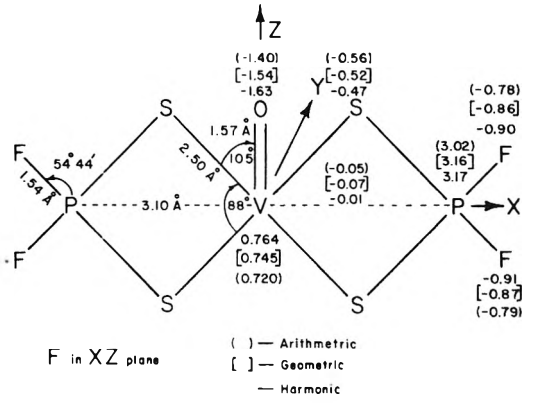

Figure 14. Geometry and EHMO results for $VO(S_2PF_2)_2$.

was obtained from Indiana University Quantum Chemistry Program Exchange and modified to permit inclusion of a central metal atom. Calculations were performed iteratively until the output charge on the metal, obtained using a Mulliken[28] population analysis, was within 0.01 of the input charge. To economize on computer time initial charges assumed were those obtained using Sanderson's electronegativity method.[29] The *model* compounds $VO(S_2PX_2)_2$ and $Cu(S_2PX_2)_2$ (X = H and F) were chosen for the calculations since they could be considered representative of both dithiophosphinate and dithiophosphate complexes, the results for the high-symmetry model compounds could be readily interpreted and calculations for the dicyclohexyl derivatives would be prohibitively expensive. Also, had the dicylohexyl groups been included the MO's of interest would probably be buried in a plethora of ligand levels. The metal valence state ionization potentials (VOIP's) were those of Basch, Viste, and Gray.[30] Using an additional approximation introduced by Schachtschneider, *et al.*,[31] in their calculations for vanadocene the metal VOIP's are given by

$$H_{ii} = -(Aq^2 + Bq + C)$$

where A, B, and C are parameters obtained from spectroscopic data on the free atom and ions and q is the net charge on the atom. Average ligand VOIP's were taken from the tabulation given by Ballhausen and Gray.[32]

The off-diagonal matrix elements of the effective Hamiltonian were estimated by the arithmetic mean or Mulliken-Wolfsberg-Helmholz[33] approximation, *i.e.*

$$H_{ij} = -0.5\, KS_{ij}(H_{ii} + H_{jj})$$

TABLE IV: Results of Extended-Hückel MO Calculations for $Cu(S_2PX_2)_2$ (X = H, F)

X = H						X = F					
Transitions, cm^{-1}	Arith[a]	Transitions, cm^{-1}	Geom[a]	Transitions, cm^{-1}	Harm[a]	Transitions, cm^{-1}	Arith	Transitions, cm^{-1}	Geom	Transitions, cm^{-1}	Harm
$A_g \leftarrow B_{1g}$	8070	$A_g \leftarrow B_{1g}$	9773	$B_{2g} \leftarrow B_{1g}$	9597	$B_{3g} \leftarrow B_{1g}$	8475	$B_{3g} \leftarrow B_{1g}$	9794	$B_{3g} \leftarrow B_{1g}$	9922
$B_{3g} \leftarrow$	8728	$B_{3g} \leftarrow$	9923	$B_{3g} \leftarrow$	9936	$B_{2g} \leftarrow$	8506	$B_{2g} \leftarrow$	10,222	$A_u \leftarrow$	10,403
$B_{2g} \leftarrow$	9178	$B_{2g} \leftarrow$	10,656	$A_g \leftarrow$	11,207	$A_g \leftarrow$	8754	$A_g \leftarrow$	10,906	$B_{2g} \leftarrow$	11,564
$A_g \leftarrow$	9317	$A_g \leftarrow$	11,499	$B_{2u} \leftarrow$	13,337	$A_g \leftarrow$	9019	$A_g \leftarrow$	11,210	$B_{2u} \leftarrow$	12,148
$B_{2g} \leftarrow$	13,579	$B_{2g} \leftarrow$	11,536	$A_u \leftarrow$	13,484	$A_u \leftarrow$	13,834	$A_u \leftarrow$	11,755	$A_g \leftarrow$	13,061
Metal configuration											
3d	9.401		9.524		9.609		9.422		9.546		9.461
4s	0.526		0.550		0.572		0.517		0.543		0.569
4p	0.643		0.460		0.315		0.640		0.446		0.294
Cu–P ROP[b]	−0.099		−0.140		−0.185		−0.079		−0.115		−0.164

[a] Arithmetic, geometric, and harmonic or reciprocal mean approximations for off-diagonal matrix elements. [b] Reduced overlap population (ref 38).

TABLE V: Results of Extended-Hückel MO Calculations for $VO(S_2PX_2)_2$ (X = H, F)

X–H, V–S = 2.40 Å						X = H, V–S = 2.50 Å					
Transitions, cm^{-1}	Arith	Transitions, cm^{-1}	Geom	Transitions, cm^{-1}	Harm	Transitions, cm^{-1}	Arith	Transitions, cm^{-1}	Geom	Transitions, cm^{-1}	Harm
$B_1 \leftarrow A_1$	6296	$B_1 \leftarrow A_1$	6316	$B_1 \leftarrow A_1$	6314	$B_1 \leftarrow A_1$	5990	$B_1 \leftarrow A_1$	5904	$B_1 \leftarrow A_1$	5826
$B_2 \leftarrow$	6434	$B_2 \leftarrow$	6431	$B_2 \leftarrow$	6406	$B_2 \leftarrow$	6110	$B_2 \leftarrow$	6006	$B_2 \leftarrow$	5907
$A_1 \leftarrow$	15,469	$A_1 \leftarrow$	15,908	$A_1 \leftarrow$	15,956	$A_2 \leftarrow$	12,840	$A_2 \leftarrow$	13,316	$A_2 \leftarrow$	13,646
$A_2 \leftarrow$	16,803	$A_2 \leftarrow$	17,404	$A_2 \leftarrow$	17,718	$A_1 \leftarrow$	14,459	$A_1 \leftarrow$	14,818	$A_1 \leftarrow$	14,927
$B_2 \leftarrow$	62,803	$B_2 \leftarrow$	63,027	$B_2 \leftarrow$	61,643	$A_1 \leftarrow$	62,628	$A_1 \leftarrow$	62,148	$A_1 \leftarrow$	60,909
Metal configuration											
3d	3.041		3.298		3.500		3.061		3.234		3.428
4s	0.450		0.422		0.400		0.467		0.440		0.421
4p	0.807		0.561		0.360		0.805		0.577		0.403
$2C_iC_jS_{ij}$[b]	1.1×10^{-4}		1.8×10^{-4}		3.0×10^{-4}		4.5×10^{-4}		3.4×10^{-4}		2.6×10^{-4}
V–P ROP	−0.083		−0.190		−0.141		−0.075		−0.099		−0.123
X = F, V–S = 2.40 Å						X = F, V–S = 2.50 Å					
$B_1 \leftarrow A_1$	7382	$B_1 \leftarrow A_1$	7553	$B_1 \leftarrow A_1$	7698	$B_1 \leftarrow A_1$	7091	$B_1 \leftarrow A_1$	7219	$B_1 \leftarrow A_1$	7298
$B_2 \leftarrow$	7416	$B_2 \leftarrow$	7629	$B_2 \leftarrow$	7870	$B_2 \leftarrow$	7138	$B_2 \leftarrow$	7292	$B_2 \leftarrow$	7434
$A_1 \leftarrow$	16,698	$A_1 \leftarrow$	17,219	$A_1 \leftarrow$	17,357	$A_2 \leftarrow$	13,958	$A_2 \leftarrow$	14,767	$A_2 \leftarrow$	15,385
$A_2 \leftarrow$	17,915	$A_2 \leftarrow$	18,735	$A_2 \leftarrow$	19,397	$A_1 \leftarrow$	15,697	$A_1 \leftarrow$	16,248	$A_1 \leftarrow$	16,469
$B_2 \leftarrow$	70,509	$B_2 \leftarrow$	70,391	$A_1 \leftarrow$	51,168	$B_2 \leftarrow$	73,592	$A_1 \leftarrow$	70,907	$A_1 \leftarrow$	51,579
Metal configuration											
3d	3.016		3.251		3.461		2.977		3.203		3.384
4s	0.452		0.426		0.408		0.468		0.445		0.429
4p	0.829		0.584		0.385		0.827		0.606		0.431
$2C_iC_jS_{ij}$	-3.1×10^{-3}		-3.4×10^{-3}		-3.9×10^{-3}		-2.6×10^{-3}		-3.0×10^{-3}		-3.4×10^{-3}
V–P ROP	−0.059		−0.078		−0.109		−0.190		−0.054		−0.099

[a] Arithmetic, geometric, and harmonic or reciprocal mean approximations for off-diagonal matrix elements. [b] $2C_iC_jS_{ij}$ = twice the product of V $3d_{x^2-y^2}$ and P 3s orbital orbital coefficients and overlap integral for the A_1 ground state. [c] Reduced overlap population (ref 38).

with K set[27] equal to 1.75. Off-diagonal matrix elements were also evaluated by the geometric[16] and harmonic or reciprocal[34] mean approximations, *i.e.*

$$H_{ij} = -KS_{ij}(H_{ii}H_{jj})^{1/2}$$

and

$$H_{ij} = -KS_{ij}[2(H_{ii}H_{jj})/(H_{ii} + H_{jj})]$$

respectively.

Slater orbital exponents for the metal ions were those employed by Zerner and Gouterman in their calculations for porphyrin complexes.[35] Ligand atom Slater orbital exponents were simple averages of the energy optimized valence shell orbital exponents listed by Clementi and Raimondi.[36]

The results of the EHMO calculations for the model compounds $Cu(S_2PX_2)_2$ (X = H,F) are summarized in Figures 11 and 12 and Table IV. The (H)F-P-F(H) angle was assumed tetrahedral in all of the calculations. It is noted that $Cu(S_2PF_2)_2$ does not exist, the acid HS_2PF_2 forms[37] only the Cu(I) complex upon reaction with copper(II) chloride. This is reflected in the low charges on the copper atoms and the large negative charges calculated for the sulfur atoms. The large positive changes calculated for the phosphorus atoms bound to fluorine are in accord with electronegativity considerations. Of particular interest are the reduced overlap populations[38] between the copper and phosphorus atoms. The reduced overlap populations show that there is an antibonding interaction across the chelate ring. The product of the metal d_{xy} and phosphorus $3p_y$ coefficients in the ground state is also negative indicating the d_π-p_π interaction is also antibonding. The negative reduced overlap populations are also consistent with the expected repulsion between the copper and phosphorus positively charged centers. The data in Table IV show that the calculated energies of the first five electronic transitions, using the "hole" formalism, vary considerably with the substituent on the phosphorus atom and the mean approximation employed for the off-diagonal matrix elements and do not agree with those found using phenomenological crystal field theory (Table III) except with respect to the symmetry of the ground state. Ligand levels are mixed in among the "d" levels and the calculated "d ← d" transitions would be expected to be obscured by ligand → metal charge-transfer transitions. The failure of the EHMO calculations to provide semiquantitative electronic transition energies can be linked to the assumptions employed concerning the bond distances and angles in the complexes as discussed below. It is noted, however, that neither the copper nor the phosphorus s orbitals appear in the ground state of the $Cu(S_2PX_2)_2$ complexes. This shows that the EHMO model cannot be employed to account for nuclear and superhyperfine interactions without the introduction of other considerations. van der Avoird, *et al.*,[39] employed the distorted actual geometry of bis(dithiocarbamato)copper(II) rather than D_{2h} (slightly idealized) symmetry in order to introduce metal s orbitals into the ground state. Lowering the symmetry of the $Cu(S_2PX_2)_2$ complexes would enable a crude evaluation of the hyperfine and superhyperfine interactions but it is unlikely that the electronic transition energies would improve.

Due to the lack of structural data for VOS_4 complexes two V-S bond distances were assumed in the EHMO calculations, the results of which are summarized in Figures 13 and 14 and Table V. The charge distributions and reduced overlap populations are reasonable in terms of the type of complexes of concern. The calculated charges on the ligands seem a little high compared to other vanadyl compounds[24] but it is noted that the dithiophosphates can reduce vanadyl to vanadium(III).[40]

The symmetry combinations of basis functions show that the A_1 ground states of vanadyl chelates involve considerable mixing of metal d, s, and p orbitals. Since phosphorus s orbitals are included in the ground state, appreciable phosphorus superhyperfine splitting in the esr spectra of the complexes can be expected and is observed for vanadyl dithiophosphate[1,2] and dithiophosphinate[1,2,6] chelates as well as related dithioarsinate[3] compounds.

The crystal field calculations gave the energy level scheme: $a_1(d_{x^2-y^2}) < b_2(d_{yz}) < b_1(d_{xz}) < a_2(d_{xy}) < a_1(d_{z^2})$. The EHMO calculations for all of the complexes agree with the crystal field ground state. Although the xz and yz levels are close together, the EHMO calculations uniformly indicate the levels are interchanged compared to the crystal field model. For a V-S distance of 2.40 Å the "d" energy level sequence $a_1 < b_1 < b_2 < a_2 < b_2$ holds generally for the $VO(S_2PX_2)_2$ complexes but this is considered unrealistic since qualitative and semiquantitative arguments show that the d_{z^2} antibonding level must lie highest. For a V-S distance of 2.50 Å and "d" energy level sequence $a_1 < b_1 < b_2 < a_2 < a_1 < a_1$ holds generally in accord with expectations. The transition energies in Table V are not in good agreement with those found (Table II) for $VO(dtp)_2$ but it must be kept in mind that the EHMO calculations are for *model* compounds. Elucidation of the energy levels of VOS_4 complexes awaits crystallographic studies and subsequent single-crystal electronic spectral investigations. The present work indicates that the Ballhausen-Gray[16] type model is also satisfactory for low-symmetry vanadyl complexes.

The V-P reduced overlap populations in the $VO(S_2PX_2)_2$ complexes show that the V-P interactions are antibonding. However, the quantity $2c_ic_jS_{ij}$ (where i = V $3d_{x^2-y^2}$ and j = P 3s and S_{ij} is the corresponding overlap integral) for the A_1 ground states shows that there is a transannular V-P bonding interaction in the $VO(S_2PH_2)_2$ complex whereas the interaction is of an antibonding type in $VO(S_2PF_2)_2$ as in the $Cu(S_2PX_2)_2$ complexes. $\langle {}^PA \rangle$ for $VO(S_2PF_2)_2$ is 59.6 g,[6] larger than any values reported[1,2,6] for any other vanadyl dithiophosphate or dithiophosphinate complexes. Apparently, the type of interaction across the chelate ring is not as important as the magnitude of the phosphorus 3s coefficient in the ground state.

In summary, the unusually stable complexes $VO(dtp)_2$ and $Cu(dtp)_2$ have been prepared and characterized by a variety of techniques. Crystal field and EHMO calculations agree on the symmetry of the ground states but not particularly well with regard to calculated transition energies and one-electron "d" levels. The assumed geometries employed in the EHMO calculations are consistent with available structural data but, apparently, are not completely appropriate for the problem to which they were addressed.

Acknowledgment. The authors are grateful to Professor R. E. D. McClung, University of Alberta, and Professor N. D. Chasteen, University of New Hampshire, for esr spectra simulation programs, Professor R. G. Cavell, University of Alberta for the program BIGAUSS and Dr. H. E. Montgomery, U. S. Naval Nuclear power School for the extended-Hückel MO program. The esr spectrometer em-

ployed in this work was purchased with the aid of National Science Foundation Grant No. GP-18397.

References and Notes

(1) J. R. Wasson, G. M. Woltermann, and H. J. Stoklosa, *Top. Current Chem.*, **35**, 65 (1973).
(2) J. R. Wasson, *Inorg. Chem.*, **10**, 1531 (1971).
(3) B. J. McCormick, J. L. Featherstone, H. J. Stoklosa and J. R. Wasson, *Inorg. Chem.*, **12**, 692 (1973).
(4) N. D. Yordanov and D. Shopov, *Chem. Phys. Lett.*, **16**, 60 (1972).
(5) R. K. Cowsik and R. Srinivasan, *Chem. Phys. Lett.*, **16**, 183 (1972).
(6) R. G. Cavell, E. D. Day, W. Byers, and P. M. Watkins, *Inorg. Chem.*, **11**, 1591 (1972).
(7) J. R. Wasson, *Chem.-Anal.*, **56**, 36 (1967).
(8) G. M. Woltermann and J. R. Wasson, *J. Phys. Chem.*, **77**, 945 (1973).
(9) B. J. McCormick, *Can. J. Chem.*, **47**, 4283 (1969).
(10) G. Durgaprasad, D. N. Sathyanarayana, and C. C. Patel, *Can. J. Chem.*, **47**, 631 (1969); K. A. Jensen, B. M. Dahl, P. H. Nielsen, and G. Borch, *Acta Chem. Scand.*, **25**, 2029 (1971); **26**, 2241 (1972).
(11) H. J. Stoklosa, H. L. Huffman, and J. R. Wasson, *J. Inorg. Nucl. Chem.*, **35**, 2584 (1973).
(12) A. D. Toy, S. H. H. Chaston, J. R. Pilbrow, and T. D. Smith, *Inorg. Chem.*, **10**, 2219 (1971).
(13) P. W. Atkins and M. C. R. Symons, "The Structure of Inorganic Radicals," American Elsevier, New York, N. Y., 1967, pp 20–22.
(14) P. E. Rakita, S. J. Kopperl, and J. P. Fackler, Jr., *J. Inorg. Nucl. Chem.*, **30**, 2139 (1968).
(15) A. Muller, V. V. K. Rao, and E. Diemann, *Chem. Ber.*, **104**, 461 (1971).
(16) C. J. Ballhausen and H. B. Gray, *Inorg. Chem.*, **1**, 111 (1962); J. Selbin, *Chem. Rev.*, **65**, 153 (1965); *Coord. Chem. Rev.*, **1**, 293 (1966).
(17) M. Shiro and Q. Fernando, *Chem. Commun.*, 63 (1971).
(18) A. L. Companion and M. A. Komarynsky, *J. Chem. Educ.*, **41**, 257 (1964).
(19) J. R. Wasson and H. J. Stoklosa, *J. Chem. Educ.*, **50**, 185 (1973).
(20) H. J. Stoklosa and J. R. Wasson, *J. Inorg. Nucl. Chem.*, **36**, 227 (1974); D. K. Johnson, H. J. Stoklosa, J. R. Wasson, and H. E. Montgomery, *ibid.*, in press.
(21) E. R. Price and J. R. Wasson, unpublished results.
(22) C. K. Jørgensen, *Struct. Bonding (Berlin)*, **1**, 3 (1966); B. N. Figgis, "Introduction to Ligand Fields," Interscience, New York, N. Y., 1966, pp 242–245.
(23) M. V. Valek, W. A. Yeranos, G. Basu, P. K. Hon, and R. L. Belford, *J. Mol. Spectrosc.*, **37**, 228 (1971).
(24) H. A. Kuska and P.-H. Yang, "Bonding Studies of Bis(tetramethylurea)dichlorooxovanadium(IV)," submitted for publication; Abstracts of the 5th Central Regional Meeting of the American Chemical Society, Cleveland, Ohio, May 13–15, 1973.
(25) R. A. D. Wentworth and T. S. Piper, *J. Chem. Phys.*, **41**, 3884 (1964).
(26) D. E. C. Corbridge, *Top. Phosphorus Chem.*, **3**, 57 (1966).
(27) R. Hoffmann, *J. Chem. Phys.*, **39**, 1397 (1963).
(28) R. S. Mulliken, *J. Chem. Phys.*, **23**, 1833, 1841 (1955).
(29) R. T. Sanderson, "Inorganic Chemistry," Reinhold, New York, N. Y., 1967; H. J. Stoklosa, *J. Chem. Educ.*, **50**, 290 (1973).
(30) H. Basch, A. Viste, and H. B. Gray, *J. Chem. Phys.*, **44**, 10 (1966).
(31) J. H. Schachtschneider, R. Prins, and P. Ros, *Inorg. Chim. Acta*, **1**, 462 (1967).
(32) C. J. Ballhausen and H. B. Gray, "Molecular Orbital Theory," W. A. Benjamin, New York, N. Y., 1964, p 122.
(33) M. Wolfsberg and L. Hemlholz, *J. Chem. Phys.*, **20**, 837 (1952).
(34) W. A. Yeranos, *J. Chem. Phys.*, **44**, 2207 (1966).
(35) M. Zerner and M. Gouterman, *Inorg. Chem.*, **5**, 1699 (1966); *Theor. Chim. Acta*, **4**, 44 (1966).
(36) E. Clementi and D. L. Raimondi, *J. Chem. Phys.*, **38**, 2686 (1963).
(37) F. N. Tebbe and E. L. Muetterties, *Inorg. Chem.*, **9**, 629 (1970).
(38) J. J. Kaufman, *Int. J. Quantum Chem.*, **15**, 495 (1967).
(39) C. P. Keijzers, H. J. M. de Vries, and A. van der Avoid, *Inorg. Chem.*, **11**, 1338 (1972).
(40) C. Furlani, P. Porta, A. Sgamellotti, and A. A. G. Tomlinson, *Chem. Commun.*, 1046 (1969).

CNDO/2 Study of NH···O Hydrogen Bonds in Ions, Zwitterions, and Neutral Molecules

R. D. Singh and D. R. Ferro*

Istituto di Chimica delle Macromolecole del CNR, 20133 Milano, Italy *(Received November 30, 1973)*

Publication costs assisted by the Istituto di Chimica delle Macromolecole

CNDO/2 calculations have been carried out on a number of hydrogen bonded systems, including ammonia, ammonium, imidazole, and glycine as proton donors and formic acid, formate ion, and glycine as acceptors. The interaction energy at intermolecular separations larger than the equilibrium distance has been interpreted as the sum of the electrostatic energy and an attractive potential U_{HB} for each H bond. A moderate dependence of U_{HB} on the nonlinearity of the H bond is observed, while in the case of two H bonds or of a bifurcated H bond, the additivity of U_{HB} is found to hold with good approximation. The magnitude of U_{HB} greatly increases when varying the donor and/or the acceptor from neutral molecule to zwitterion and to ion.

Introduction

Considerable attention has been given to the study of hydrogen bonds of N-H···O type, which play an important role in stabilizing the secondary and tertiary structures of polypeptides. In a recent paper McGuire, *et al.*,[1] have pointed out the importance of a suitable empirical hydrogen bond potential function for the study of the conformations of macromolecules. They have derived hydrogen bond potentials in a variety of relevant systems by calculating the interaction energy between simple molecules using CNDO/2 and empirical methods. Such functions may be useful in the empirical expression of the conformational energy of a macromolecule. Thus one can write total conformational energy[2] as

$$E_{conf} = \Sigma U_{tors} + \Sigma U_{nb} + \Sigma U_{HB} + E_{el} \qquad (1)$$

where the four components on the right-hand side represent the torsional, nonbonded, hydrogen bond and the electrostatic energies, respectively.[3]

However, the energetics of the hydrogen bonds formed between a proton donor and a proton acceptor, of which either or both bear an electric charge, is little known and only few theoretical papers have dealt with it.[4] The main reason for this lack of interest is that the ionic groups of molecules of biological significance in water are normally solvated and their interaction is therefore screened by the solvent. On the other hand, the protein structures determined by the X-ray diffraction show examples of ionic bonds, while at times H bonds and electrostatic interactions appear to stabilize the substrate-enzyme or hapten-antibody complexes.[5-7] Amino acids and oligopeptides are found as ions and zwitterions in the solid state and as such are linked by strong hydrogen bonds; similar H bonds may, therefore, be formed also between the ionizable groups of macromolecules when favorable conditions are met.

From their nmr and esr studies of angiotensin II, Weinkam and Jorgensen[8] have concluded that in this octapeptide and its several analogs the C terminus tripeptide his-pro-phe, exists in a cyclic structure stabilized by an ion-dipole interaction between the COO^- group and the histidine ring. In an attempt to study the conformation of angiotensin II and to confirm the findings of these authors by conformational energy calculations, we were faced with the problem of using an appropriate empirical hydrogen-bond potential function for the $COO^-\cdots H\text{-}N$ type of interaction. Due to the lack of the experimental information on such interactions, we had to resort to independent quantum mechanical calculations in order to gain insight about the hydrogen bond potential function to be used in our empirical expression of the conformational energy.

We have, therefore, undertaken a systematic study of hydrogen bonds of the type N-H···O in small systems consisting of ions, zwitterions, and neutral molecules, using Pople and Segal's[9] CNDO/2 method. In all these systems, ammonia, ammonium, imidazole, and both the canonical and the zwitterion forms of glycine have been taken as proton donors; formic acid, formate ion, and both the forms of glycine as acceptors.

The present study is, therefore, aimed at seeing whether in the conformational calculations on systems in which charged groups form H bonds (a) one can apply the computational scheme of eq 1, *i.e.*, describe the hydrogen bonding, also in such cases, by a simple function to be added to the electrostatic and nonbonded energies; and if so, (b) the functions U_{HB} are the same as for a normal hydrogen bond.

Method

Since the most important quantities responsible for the intermolecular interaction are the charge distribution and thus the electrostatic energy, we have used the complete neglect of differential overlap (CNDO/2) method which yields a reasonable charge distribution. This method has already been applied to such calculations[1] and its details can be referred to elsewhere.[9] In the study of intermolecular hydrogen bonds, it is generally observed that upon the optimization with respect to internal coordinates CNDO/2 predicts too short O···H distances and overestimates the dimerization energies. However, when the two monomers are held rigid and calculations are done at experimental hydrogen bond length, a fairly reasonable value is obtained for the energy of formation of hydrogen bond. Since CNDO/2 underestimates the repulsive interactions, it follows that this method can provide satisfactory information only in the attraction region of the potential energy, and some other method is required to determine the depth of the minimum and the shape of the potential in the repulsion region. The information obtained by these two methods, in the two regions, when compounded together with proper weight to reproduce some experimental quantities, could lead to the complete hydrogen bond potential. Due to the lack of experimental knowledge of hydrogen bonds in our systems, we, at present, have restricted our studies in the attraction region; even in this region, however, it remains to be seen if the quantitative validity of the derived potential is based on experimental facts.

We have used the CNDO/2 method to calculate the intermolecular interaction in several systems forming one or more hydrogen bonds of the N-H···O type, as a function of O···H distance (R_{OH}), limiting the analysis of our results to the range of R_{OH} above its approximate equilibrium value of 1.75 Å. The interaction energy $E(R_{OH})$ between the two molecules, defined as the difference between the energy of the dimer and the sum of the energies of the two isolated components, has been calculated by holding rigid the two molecules and translating one of them along a straight line (shown by the arrow in the figures). A modification was made to Segal's original program[10] which enabled us to use the final molecular orbitals of one calculation as the initial guess for the following one; this led to a significant reduction of the computer time required for calculating the curves $E(R_{OH})$.

The interaction energy calculated using *ab initio* MO methods in hydrogen bonded systems when split into electrostatic, exchange, charge transfer, polarization, and dispersion interaction components appears to provide a physically meaningful interpretation.[11] A similar but more simplistic decomposition of the total interaction energy is implied in the empirical calculations. Thus in the case of two interacting rigid molecules eq 1 becomes

$$E_{inter} = \Sigma U_{nb} + \Sigma U_{HB} + E_{el} \qquad (2)$$

and we analyze the CNDO/2 results to see whether the behavior of E supports such an empirical expression of the interaction energy. The first term of E_{inter} is the pairwise sum of the nonbonded interactions (extended over all the atom pairs except the O···H ones involved in hydrogen bonding), each represented by a repulsive part and the attractive dispersion energy. At the intermolecular distances we are dealing with, the repulsive contribution to the nonbonded term is negligible; whereas CNDO/2, which is an approximate SCF method, neglects the dispersion energy. We may, therefore, conclude that ΣU_{nb} is not included in E. The second term ΣU_{HB} arises from each intermolecular hydrogen bond, and each U_{HB} is a function of only the distances between the atoms directly involved in the hydrogen bonding (H, O, and perhaps C and N as well). Thus in order for eq 2 to be of general application it must be possible to express the difference between the total interaction and the electrostatic energy by a simple sum of terms

$$E - E_{el} = \Sigma U_{HB} \qquad (3)$$

independently of (a) the relative orientation of the molecules, (b) the number of hydrogen bonds formed, and (c)

TABLE I:[a] Internal Coordinates of the Isolated Monomers

	Glycine[b]		Imidazole[c]			Formic acid	
	Zwitterion	Canonical form				Neutral	Ion
C^{α}–C′	1.46	1.46	C_1–C_2	1.36	C–N	1.08	1.09
C^{α}–N	1.45	1.47	C_2–N_3	1.36	C=O	1.24	1.25
C′=O	1.30	1.27	N_3–C_4	1.31			
			C_4–N_5	1.32	C–O	1.31	
C′–O	1.30	1.36	N_5–C_1	1.39	O–H	1.00	
C^{α}–H	1.09	1.09					
N–H	1.00	1.00					
O–H		1.00					
			C_1–C_2–N_3	107.0	O–C=O	124.3	124.0
C^{α}–C′=O	119.5	123.0	C_2–N_3–C_4	110.0	H–C=O	117.85	118.0
C^{α}–C′–O	119.5	116.0	N_3–C_4–N_5	109.0	H–C–O	117.85	118.0
N–C^{α}–C′	109.5	109.5	C_4–N_5–C_1	108.0			
C′–O–H	109.5	109.5	N_5–C_1–C_2	106.0	C–O–H	107.8	

[a] All the bond lengths are in Ångstrom units and angles in degrees. [b] All H atoms are tetrahedrally attached to C^{α} and N, with one NH bond lying in the $NC^{\alpha}C'O$ plane. [c] Each hydrogen is placed in the ring plane at 1.00 Å on the bisector of the corresponding ring angle.

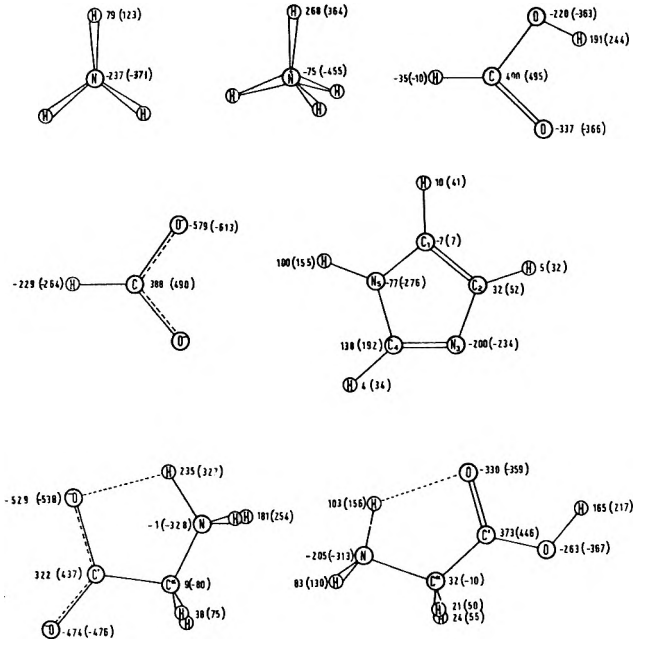

Figure 1. CNDO/2 and CNDO/2 (ON) (in parentheses) net charges on the atoms for the above conformations of the molecules participating in the intermolecular interaction. The values given should be divided by 1000 to obtain electronic charge units.

the substituents attached to the atoms forming the hydrogen bond. Therefore $E - E_{el}$ was plotted as a function of R_{OH} for different configurations of the dimers, and eq 3 was fitted by the least-squares method. First U_{HB} was expressed as a function of R_{OH} only, *i.e.*, the effect of nonlinearity of the hydrogen bond was neglected. However, it was found that the fitting is significantly improved by introducing a direction-dependent term to account for the nonlinearity of N–H···O bond. The final form for U_{HB} selected for the attraction range of the R_{OH} distance is

$$U_{HB} = -AR_{OH}^{-n}[1 - \alpha \sin^2 (\widehat{NH\cdots O})] \qquad (4)$$

Our approach to the study of the nature of the hydrogen bond is very similar to that of McGuire, *et al.*,[1] but we deviate from them in the following three points.

(a) As discussed above, to derive the hydrogen bond potential we do not substract the nonbonded term from the total interaction energy. The error due to this term, not accounted for by CNDO/2, is of the order of 0.5 kcal/mol in small systems, but it would have been a few times bigger in the case of larger systems as glycine-glycine (see Results and Figure 8).

(b) We calculate the electrostatic energy in the usual monopole approximation

$$E_{el} = \Sigma_i \Sigma_j \frac{q_i q_j}{r_{ij}} \qquad (5)$$

q_i and q_j being the fractional charges on the atoms i and j, respectively, calculated by CNDO/2 population analysis, and r_{ij} being their separation. On the contrary, McGuire, *et al.*, calculate the charge distribution by means of a population analysis based on overlap normalization.[12] Although the overlap normalized (ON) charges may represent a better approximation to the true electron distribution, they are not consistent with the CNDO scheme, and a fictitious dielectric constant equal to 2 had to be added to obtain the convergence of E_{el} to E at large distances. The dipole moment calculated by CNDO/2 is in agreement with the experimental value when the atomic dipoles, arising mainly from the lone pairs, are added to the dipole calculated from the net charges. We agree then that these charges must be altered to reproduce the total dipole moment by means of a point charge distribution only; but they are consistent with the CNDO energy and must be used as such to interpret E in terms of E_{el} and other contributions.

(c) Finally, unlike McGuire, *et al.*, we have not tried to determine the repulsive part of U_{HB}. For each curve also the nonbonded interactions were calculated and only the points corresponding to negative values of ΣU_{nb} were included in the fitting of $E - E_{el}$. This procedure avoided errors due to omission of the repulsive interactions, but in the case of distorted hydrogen bonds it restricted the range of fitting above R_{OH} = 2 Å. In most cases, however, it is found that inclusion of points corresponding to even smaller value of R_{OH}, and thus, to a (small) positive value of ΣU_{nb}, does not significantly affect the fitting.

Definition of the Dimers. The monomers of the hydrogen bonded dimers treated in the present paper are illustrated in Figure 1, where the fractional CNDO/2 and ON charges (in parentheses) are given for each atom. The molecular internal coordinates used in our calculations are reported in Table I. The values for the two forms of glycine are those reported by Oegerle and Sabin,[13] except for the CCO angle of the carboxylate group, which here corre-

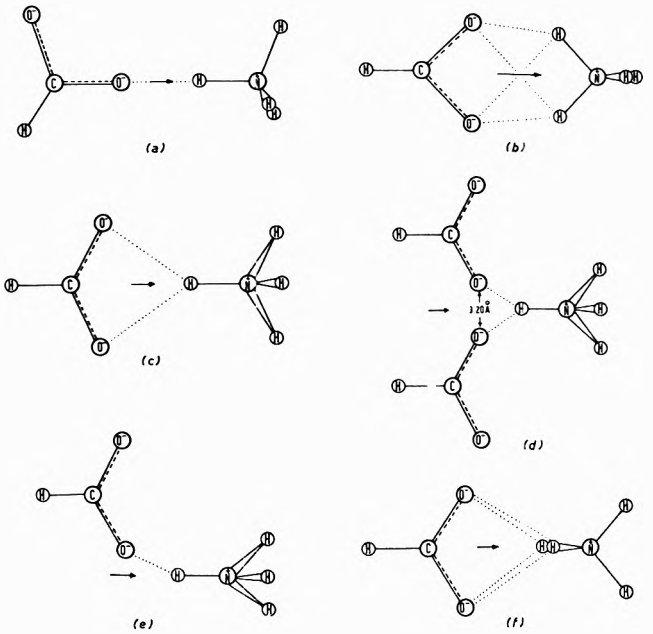

Figure 2. Conformations of linear, distorted, bifurcated, mono-, and multihydrogen bonded dimers of ammonia and formate ions. The arrows indicate the directions of translation of one molecule with respect to the other and the dotted lines are used to represent hydrogen bonds.

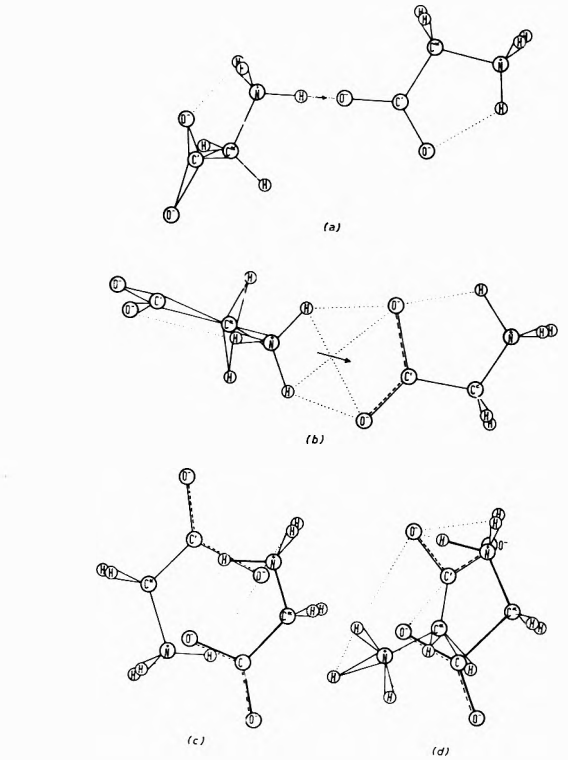

Figure 3. Zwitterionic dimers of glycine. The inter- and intramolecular hydrogen bonds are shown by dotted lines. The directions of translation in cases a and b are indicated by the arrows.

sponds to a lower value of the CNDO/2 energy of the isolated molecule.

In a first set of calculations ammonium and ammonia as proton donors were allowed to form the hydrogen bonds with formate ion and formic acid in all the four possible combinations taking two at a time: A (ammonium···formate), B (ammonium···formic acid), C (ammonia···formate), and D (ammonia···formic acid). Figure

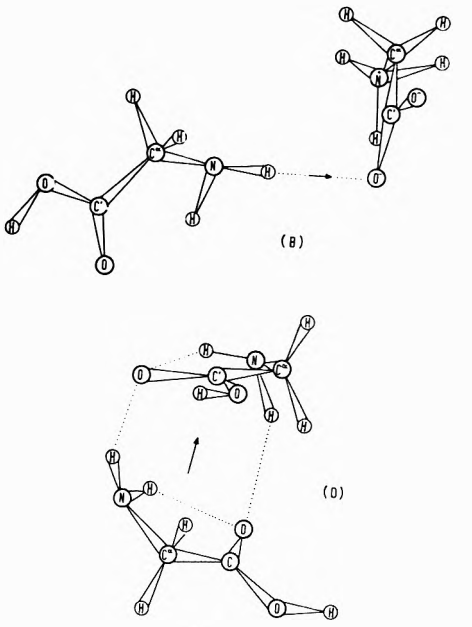

Figure 4. Dimers of glycine. The upper part shows the dimer zwitterionic glycine···glycine (B), and the lower part glycine ···glycine (D). The dotted lines represent the hydrogen bonds and the arrows indicate the directions of translation of one molecule with respect to the other

2, which is restricted to the system A, *i.e.*, ammonium···formate, shows all the relative orientations of the interacting molecules. The corresponding arrangements for systems B, C, and D can be obtained from Figure 2 by removing one of the free protons (the one lying above the plane of the figure in the cases a through e) from ammonium and/or by adding one proton to the free oxygen. Only the dimers a, d, and e have been considered for the combinations C and D. In all the cases the heavy atoms are coplanar; the configuration of case d is similar to the bifurcated H bond formed in the crystal of α-glycine by the COO^- groups of two parallel molecules; e is derived from d by removing one acceptor molecule.

Dimers of glycine were then studied, as this is the simplest example of a zwitterion. The structures considered are shown in Figures 3 and 4. Except in case a of Figure 3, where the two molecules were set on the same plane to form a linear H bond, a preliminary scan was performed to find favorable orientations of the dimers by empirical energy calculation. In the case of two zwitterions three energy minima were found: the two most stable, c and d, showing a center and an axis of symmetry, respectively, are compact structures in which van der Waals contacts are important and they gave rise to practical difficulties in translating the molecules; therefore the curve $E - E_{el}$ was not calculated for them. The constraint of exact linearity was applied to obtain the dimer of case B, and two almost linear and equivalent hydrogen bonds were obtained in case D.

We examined the linear hydrogen bonds formed by imidazole with the formate ion and the glycine zwitterion. The first system is shown in Figure 5a; in the latter case the formate ion is replaced by the glycine molecule oriented as the mirror image of the donor of Figure 3a.

Finally, for a comparison with the hydrogen-bonded dimers also a few pairs of molecules not linked by H bonds were studied; those discussed in the next section are presented in Figure 5*b*, 5*g*, and 5*h*.

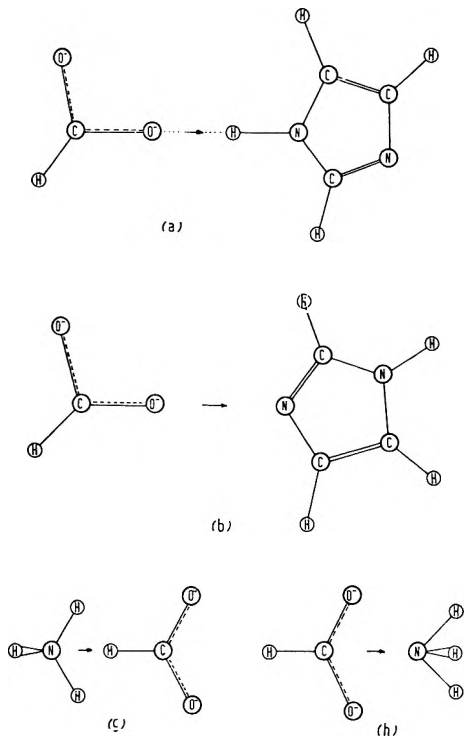

Figure 5. Hydrogen bonded (a) and nonhydrogen bonded (b) dimers of imidazole and formate ion. g and h represent two differently oriented nonhydrogen bonded dimers of ammonia and formate ion. Arrows indicate the directions of translation of one molecule with respect to the other.

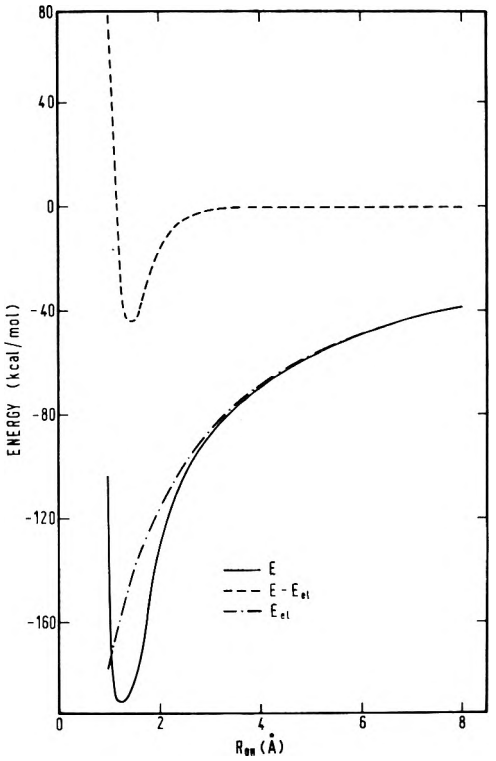

Figure 6. R_{OH} dependence of the CNDO/2 interaction energy E, the intermolecular electrostatic energy E_{el}, and their difference $E - E_{el}$ in case b of the ammonium···formate dimer.

Results and Discussion

Illustrative examples of the interaction energy E, calculated by using the CNDO/2 method, the electrostatic energy calculated from the CNDO/2 charges, and the difference $E - E_{el}$ are shown in Figures 6-8. The order of magnitude of E differs considerably in the three systems. In each case, for values of R_{OH} greater than 6 Å, E_{el} converges to E within an uncertainty of the order of the computational errors (0.05 kcal/mol). In the case of the glycine dimer shown in Figure 8, subtraction of the nonbonded energy contribution from $E - E_{el}$ leads to a physically inconsistent result, since a positive value of the order of 2 kcal/mol is predicted for the hydrogen bond potential at the O···H distance of *ca.* 2.5 Å. These facts quantitatively support our interpretation of the CNDO/2 interaction energy in terms of the electrostatic and the hydrogen bond components only.

The values of E and $E - E_{el}$ calculated at some R_{OH} distances, together with the corresponding fitted values ΣU_{HB}, are listed in Tables II-IV. The coefficients A and α were determined by the least-squares fitting for several integral values of n in the expression (5) of U_{HB}; all the structures of Tables II-IV, except the dimers c and d of the glycine zwitterion, were included. In all the cases the best fit corresponded either to $n = 5$ or 6, except for imidazole···formate where it was 4; therefore the A's and the α's for the values 5 and 6 of n are reported in Table V, where we give also the root-mean-square deviation corresponding to the best potential $U_{HB} = -AR_{OH}^{-n}$. In the following paragraphs we will examine the difference $E - E_{el}$ as a function of R_{OH} separately for the types of systems described in the previous section.

Ammonium (or Ammonia)···Formate (or Formic Acid). The collection of dimers shown in Figure 2 constitutes a variety of situations sufficient to investigate the R_{OH} dependence of $E - E_{el}$ and its additivity in multihydrogen bonded systems. A cumulative inspection of Fig-

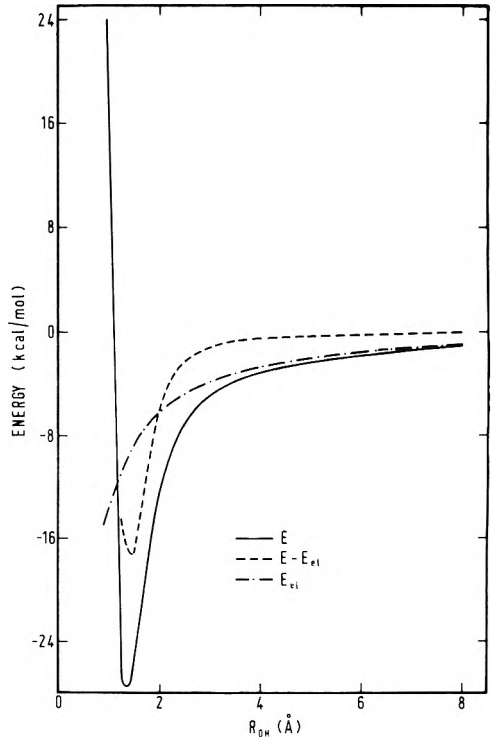

Figure 7. R_{OH} dependence of CNDO/2 interaction energy E, intermolecular electrostatic energy E_{el}, and their difference $E - E_{el}$ in the case of imidazole···formate dimer.

TABLE II: Interaction Energies for Hydrogen Bonded Dimers at Various R_{OH} Distances

Configuration	R_{OH}, Å	E, kcal/mol	$E - E_{el}$, kcal/mol	ΣU_{HB}	E, kcal/mol	$E - E_{el}$, kcal/mol	ΣU_{HB}
		$NH_4^+ \cdots HCOO^-$			$NH_3 \cdots HCOO^-$		
a	1.75	−119.38	−22.99	−25.17	−9.55	−7.75	−8.36
	1.85	−111.20	−17.95	−18.04	−7.88	−6.25	−6.33
	2.00	−101.10	−12.12	−11.30	−5.80	−4.33	−4.29
	2.15	−93.25	−8.11	−7.32	−4.25	−3.00	−3.00
	2.50	−80.80	−3.32	−2.96	−2.34	−1.37	−1.40
	4.00	−57.00	−0.48	−0.17	−0.62	−0.19	−0.13
b	2.02	−132.60	−16.76	−19.99	−7.49	−5.23	−6.38
	2.17	−121.70	−11.81	−11.96	−5.82	−3.81	−4.43
	2.51	−103.58	−4.78	−5.22	−3.29	−1.71	−2.18
	4.01	−69.35	−0.47	−0.38	−0.98	−0.23	−0.23
c	2.15	−119.36	−12.97	−13.23	−6.90	−5.33	−5.00
	2.30	−110.01	−8.91	−8.93	−5.25	−3.84	−3.65
	2.50	−100.20	−5.32	−5.53	−3.67	−2.44	−2.49
	4.00	−65.98	−0.44	−0.34	−0.83	−0.29	−0.25
d	2.00	−209.28	−18.58	−17.40	−8.41	−6.60	−5.24
	2.15	−194.91	−13.79	−11.68	−6.94	−5.23	−3.93
	2.30	−183.06	−9.96	−8.08	−5.58	−3.98	−3.30
	3.00	−147.88	−2.75	−1.73	−2.47	−1.31	−0.88
e	2.00	−107.09	−9.85	−8.70	−4.00	−3.05	−2.62
	2.15	−99.32	−7.05	−5.84	−3.24	−2.35	−1.97
	2.30	−92.97	−4.94	−4.04	−2.56	−1.72	−1.51
	3.00	−74.63	−1.17	−0.86	−1.07	−0.47	−0.44
f	2.55	−112.70	−4.92	−6.81	−2.97	−1.60	−2.16
	2.85	−100.33	−2.66	−3.51	−2.23	−1.00	−1.28
	3.30	−69.19	−1.19	−1.48	−0.92	−0.49	−0.64

TABLE III: Interaction Energies for Hydrogen Bonded Dimers at Various R_{OH} Distances

Configuration	R_{OH}, Å	E, kcal/mol	$E - E_{el}$, kcal/mol	ΣU_{HB}	E, kcal/mol	$E - E_{el}$, kcal/mol	ΣU_{HB}
		$NH_4^+ \cdots HCOOH$			$NH_3 \cdots HCOOH$		
a	1.75	−23.73	−11.82	−12.01	−3.65	−3.09	−3.29
	1.85	−20.38	−9.35	−9.09	−3.14	−2.65	−2.49
	2.00	−16.36	−6.43	−6.16	−2.32	−1.91	−1.68
	2.15	−13.39	−4.40	−4.30	−1.61	−1.27	−1.17
	2.50	−9.20	−1.94	−2.01	−0.65	−0.43	−0.55
	4.00	−3.95	−0.39	−0.19	−0.09	−0.03	−0.05
d	2.00	−32.80	−10.44	−10.22	−2.86	−2.36	−2.38
	2.15	−27.63	−7.59	−7.30	−2.35	−1.89	−1.74
	2.30	−23.49	−5.36	−5.34	−1.73	−1.31	−1.31
	3.00	−13.59	−0.81	−1.49	−0.44	−0.19	−0.38
e	2.00	−16.85	−4.94	−5.11	−1.41	−1.14	−1.19
	2.15	−14.21	−3.54	−3.65	−1.17	−0.92	−0.87
	2.30	−12.11	−2.46	−2.67	−0.87	−0.65	−0.65
	3.00	−7.01	−0.51	−0.75	−0.22	−0.09	−0.10
		Imidazole···Formate			Imidazole···$^+$Gly$^-$		
a	1.75	−18.57	−11.23	−11.07	−4.07	−6.25	−6.44
	1.85	−15.94	−9.07	−8.87	−3.74	−5.06	−4.88
	2.00	−12.72	−6.47	−6.49	−3.31	−3.49	−3.30
	2.10	−11.05	−5.15	−5.34	−2.96	−2.38	−2.30
	2.50	−7.03	−2.27	−2.65	−2.32	−0.93	−1.08
	4.00	−3.15	−0.24	−0.08	−1.03	−0.11	−0.10

ures 9–12 gives an idea of the relative strengths of various types of hydrogen bonds.

First of all one observes that the lowest curve in all the figures always corresponds to the linear hydrogen bond (a), while the curves of cases b through e, all representing variously distorted H bonds, lie close to it. This fact suggests that, besides being a function of R_{OH}, U_{HB} must possess a moderate dependence on the nonlinearity of atoms N, H, and O.

Secondly the three $E - E_{el}$ curves of cases e (one H bond), b (two equivalent H bonds), and c (two H bonds having the donated proton in common) fall fairly close to each other when normalized to one hydrogen bond. An even stronger indication of the additivity of $E - E_{el}$ stems from the comparison of curves d and e (Figures 11–13); the interaction of the proton with two acceptor molecules (bifurcated H bond) yields a value of $E - E_{el}$ per H bond almost equal to that with one acceptor in the same condition. A note of caution should however be added while making a quantitative comparison of the interaction energies; since we are studying the effect of hydrogen bonding when acceptor and donor approach each other, the isolated acceptor in case d is defined as the complex of the two formate (or formic acid) molecules at the O-O separation of 3.2 Å, and E_{el} is therefore computed using the charge distribution of this complex. In systems A and B, because

TABLE IV: Interaction Energies for Hydrogen Bonded Dimers at Various R_{OH} Distances

Configuration	R_{OH}, Å	E, kcal/mol	$E - E_{el}$, kcal/mol	ΣU_{HB}	R_{OH}, Å	E, kcal/mol	$E - E_{el}$, kcal/mol	ΣU_{HB}
			$^-Gly^+\cdots{}^-Gly^+$				$^-Gly^+\cdots Gly$	
a	1.75	−23.97	−9.88	−10.44	1.85	−7.37	−5.03	−5.11
	1.85	−20.81	−7.74	−7.48	1.96	−6.00	−3.97	−3.82
	2.00	−16.91	−5.17	−4.68	2.10	−4.42	−2.74	−2.71
	2.15	−14.01	−3.40	−3.04	2.50	−1.97	−0.98	−1.13
	2.50	−9.78	−1.29	−1.23	4.00	−0.19	−0.11	−0.11
	4.00	−4.01	−0.13	−0.07			Gly···Gly	
b	2.00	−29.64	−7.77	−7.75	1.87	−6.97	−5.49	−5.73
	2.49	−18.44	−2.15	−2.16	2.02	−5.04	−3.80	−3.61
	2.99	−13.18	−0.65	−0.76	2.17	−3.74	−2.70	−2.35
	3.98	−8.09	−0.16	−0.15	2.63	−1.24	−0.60	−0.74
c		−42.75	−10.38	−6.59	4.10	−0.17	+0.01	−0.05
d		−43.54	−9.47	−7.16				

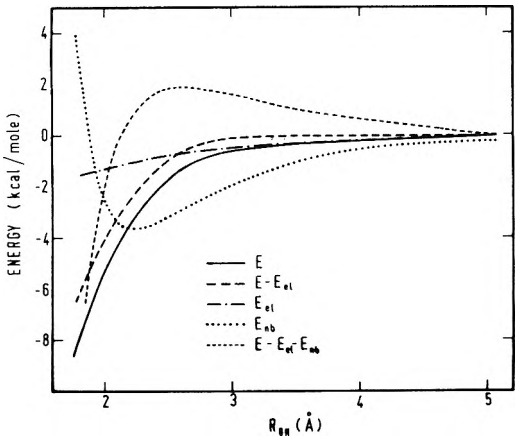

Figure 8. Variation of different types of intermolecular energies with R_{OH} in the case of the glycine···glycine dimer. E_{nb} is the empirical nonbonded interaction term; of particular interest is the fact that $E - E_{el} - E_{nb}$ is largely positive at $R_{OH} \simeq 2.50$ Å.

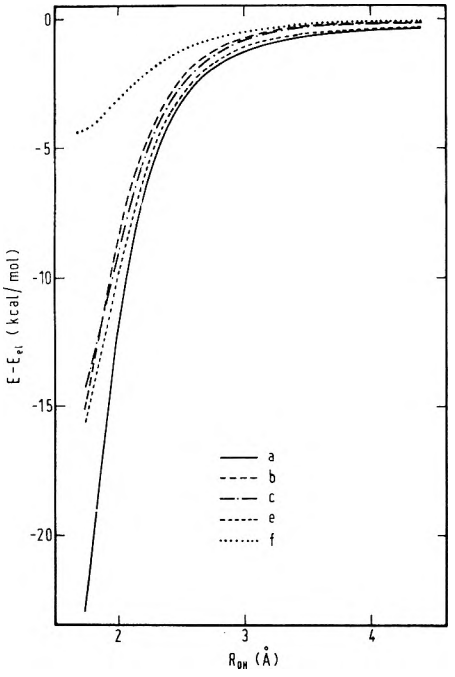

Figure 9. A plot of $E - E_{el}$ *vs.* R_{OH} for various conformations of the ammonium···formate dimer. Curves a, b, c, e, and f refer to the corresponding situations of Figure 2. For comparison the curves b and c have been normalized the one H bond by dividing $E - E_{el}$ by 2.

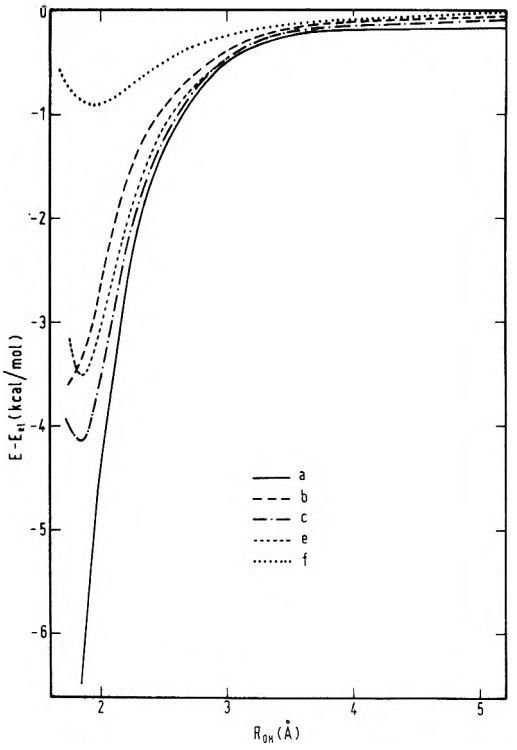

Figure 10. A plot of $E - E_{el}$ *vs.* R_{OH} for various conformations of the ammonia···formate dimer. Curves b and c are normalized to one H bond.

of the mutual polarization of the two anions, E_{el} so computed differs significantly (almost by 4 kcal/mol at R_{OH} = 2 Å in A) from the value relative to the charge distribution of the isolated formate ion. There is then a lack of additivity of the total interaction energy arising from E_{el} rather than from U_{HB}; in fact it does not occur with systems C and D where the acceptor is a neutral molecule.

The configuration of dimer f is obtained from b by rotating the donor by 90° about the C–N axis, so that for any given C–N separation the distances R_{OH} only differ in the two structures. Upon rotation it is observed that E increases much more than E_{el}; the result is a large positive change of $E - E_{el}$ (*e.g.*, 11 and 3.5 kcal/mol, respectively, in A and B for R_{OH} in b equal to 2 Å), which then is due only to the breaking of two hydrogen bonds partially balanced by the formation of four long and more distorted ones. This result shows that with good approximation, also in the case of charged molecules, $E - E_{el}$ does not

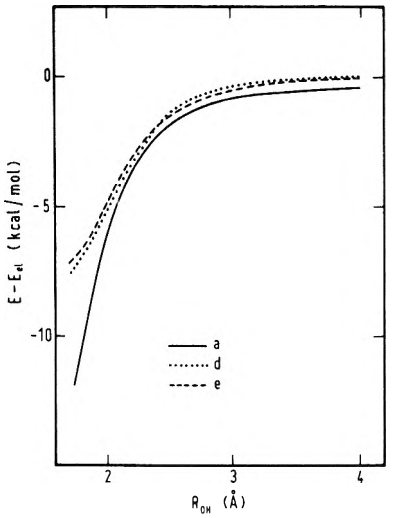

Figure 11. A plot of normalized $E - E_{el}$ *vs.* R_{OH} for the various conformations of ammonium···formic acid dimer. Curves a, d, and e refer to the corresponding dimer conformations.

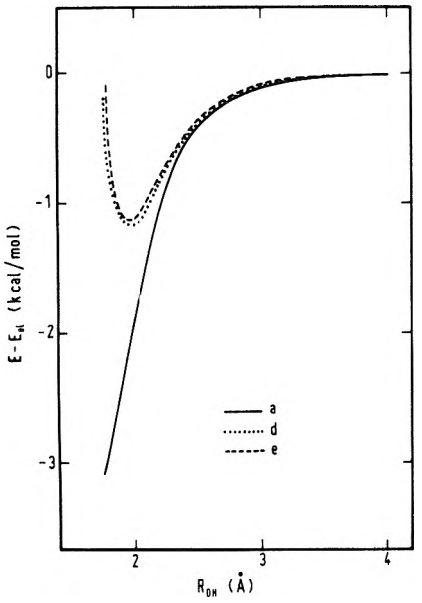

Figure 12. A plot of normalized $E - E_{el}$ *vs.* R_{OH} for the various conformations of the ammonia···formic acid dimer. Curves a, d, and e refer to the corresponding dimer conformations.

arise from the polarization induced by ions or dipoles *independently* of the positions of the hydrogens, but it is essentially a function of the coordinates of the atoms forming the H bonds. If this statement were exact then E_{el} should equal E when two polar molecules interact without hydrogen bonding, whereas a certain polarization effect is to be expected. An estimate of the amount of $E - E_{el}$ not arising from hydrogen bonding can then be obtained by comparing the curves relative to configurations g and h (Figure 5) of $HCO_2^-\cdots NH_3$ with those of the hydrogen bonded dimers; in particular, cases b, c, and h differ from each other only by a rotation through N. The comparison (Figure 14) is very rough, since $E - E_{el}$ is plotted as a function of the distance R_{CN}, taken rather arbitrarily as a measure of the intermolecular separation. It shows any way that in nonbonded systems, at intermolecular distances corresponding to normal hydrogen bonds, the correction to E_{el} due to the charge redistribution is only a

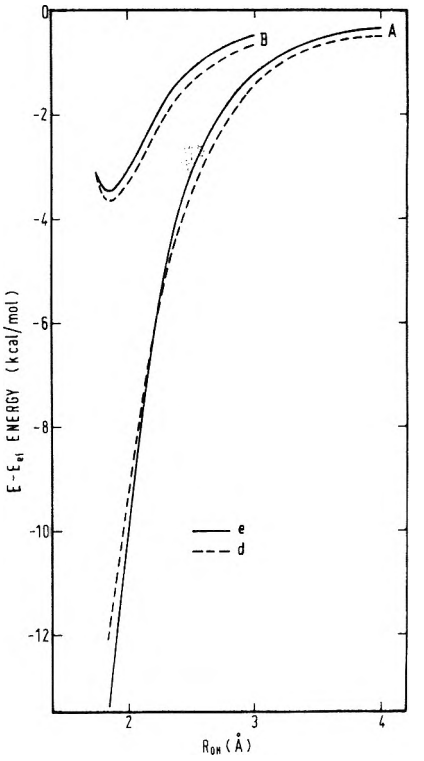

Figure 13. Comparison between the normalized $E - E_{el}$ curves of cases d and e for the systems ammonium···formate (A) and ammonia···formate (B).

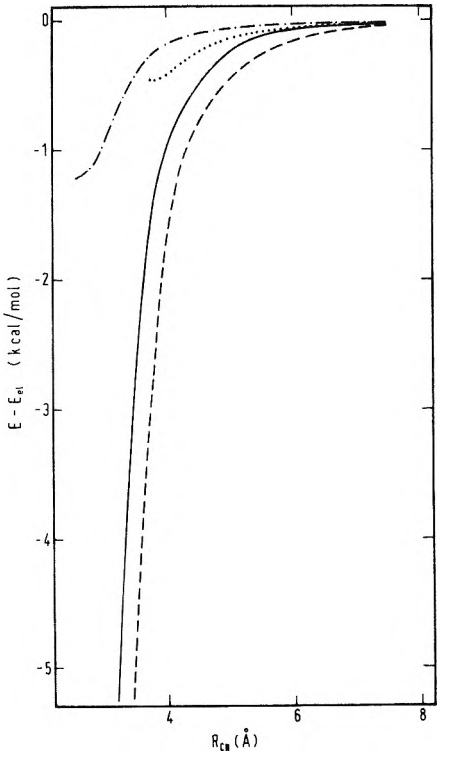

Figure 14. A plot of $E - E_{el}$ *vs.* R_{CN} for the nonhydrogen bonded dimers g (– · –) and h (· · · ·) of ammonia···formate, compared with the curves of the hydrogen bonded cases b (——) and c (- - -).

small fraction of the hydrogen bond energy. The calculation also offers an estimate of a typical error committed in the empirical calculations of the conformational energy

TABLE V: Best Fit Coefficients A, α, and n of the Potential Function U_{HB}

		$n = 5$			$n = 6$			
Donor	Acceptor	A, kcal mol Å^5	α	σ	A, kcal mol Å^6	α	σ	σ_0[a]
NH_4^+	$HCOO^-$	383	0.53	1.01	723	0.36	0.92	1.36
NH_3	$HCOO^-$	137	0.61	0.48	256	0.41	0.55	0.71
NH_4^+	HCOOH	197	0.27	0.30	366	0.10	0.44	0.47
NH_2	HCOOH	54	0.46	0.11	100	0.31	0.16	0.22
$^-Gly^{+}$[b]	$^-Gly^+$	163	0.65	0.24	300	0.48	0.23	0.57
Gly	$^-Gly^+$	111		0.10	213		0.16	
Gly	Gly	63		0.21	122		0.20	
Imidazole	$HCOO^-$	194		0.36	356		0.78	
Imidazole	$^-Gly^+$	106		0.14	195		0.29	

[a] Root-mean-square deviation for $\alpha = 0$. The values reported correspond to the best n, which varies from 5 to 7. [b] Represents $^-OOC-CH_2-NH_3^+$.

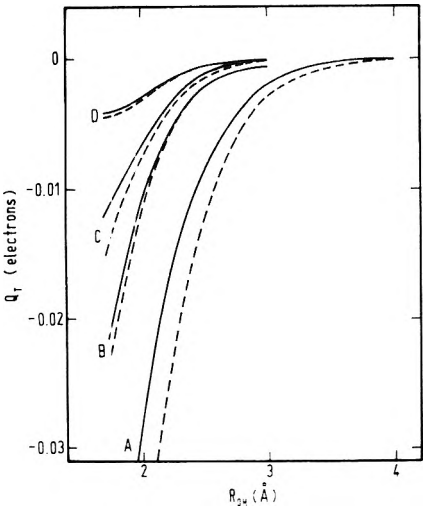

Figure 15. A plot of the charge Q_T transferred (per H bond) from donor to acceptor for cases d (——) and e (- - -) of the four combinations ammonium···formate (A), ammonia···formate (B), ammonium···formic acid, (C) and ammonia···formic acid (D).

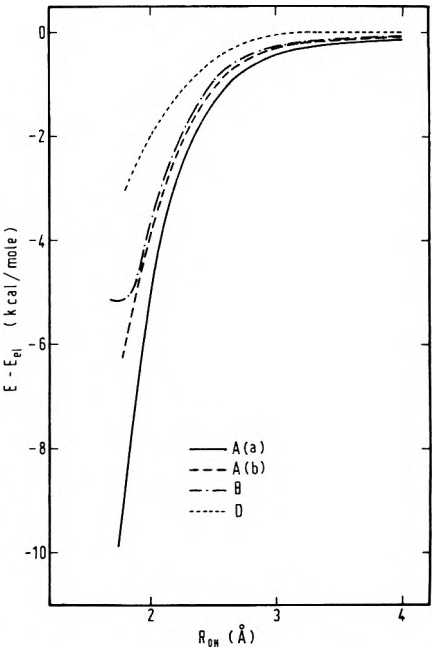

Figure 16. A plot of normalized $E - E_{el}$ vs. R_{OH} for the glycine dimers. Curves A(a), A(b), C, and D refer to the corresponding situations in Figures 3 and 4.

where the charge distribution is kept constant while varying the molecular conformation.

The features of the results discussed above are common to the four systems considered. However, the magnitude of $E - E_{el}$ at a given R_{OH} greatly increases in going from the dipole···dipole to the ion···dipole and to the ion ···ion type of interaction. This fact is quantitatively expressed by the best fit coefficients A of U_{HB}, reported in Table V. The improvement of the two-parameter fitting (*i.e.*, accounting for the angular dependence) over the one, can be immediately visualized by comparing the root-mean-square deviations σ_0 in the last column of this table, with the lowest value of σ. In general, the error is almost halved when the nonlinearity of the hydrogen bond is accounted for in the present way. The residual error may be partially due to the analytical form selected for U_{HB}, but is mainly contributed by the different situations which we try to fit with the same potential. Although the discrepancies do not show a regular trend, cases b seem the most deviating ones.

While we do not attempt to interpret the potential U_{HB} quantitatively in terms of the charge transfer and the polarization components, the results indicate that both must be important. For example, one observes rather a good correlation between the magnitude of the coefficients A of the four types of hydrogen bonds and the total charge Q_T transferred from the proton acceptor to the donor. Figure 15 shows also that the transferred charge in the bifurcated case approaches the corresponding value in the equally distorted single hydrogen bonds but the differences are larger than those between their energies. We finally observed a moderate dependence of Q_T on the distortion of the H bonds. On the other hand, the charge transfer and the hydrogen bond energy are greatly enhanced when the donor and/or the acceptor is an ion. A comparison of cases B and C shows that this effect grows with the polarizability of the molecule interacting with the ion.

Glycine Dimers. The three combinations A, B, and D of the two forms of glycine (Figures 3 and 4) differ from the ones described previously for the replacement of the ion with the zwitterion. The effect is that the differences between the strengths of the hydrogen bonds in the three cases are reduced, probably because the polarization caused by the binding ion is partially balanced by the opposite ion on the other side of the molecules. The $E - E_{el}$ curves for these systems are reported is Figure 16. The two forms a and b of the zwitterion dimer show again that there is a significant effect of distortion on the hydrogen bond energy and on the total charge transferred. The latter can be seen in the upper part of Figure 17, whereas the

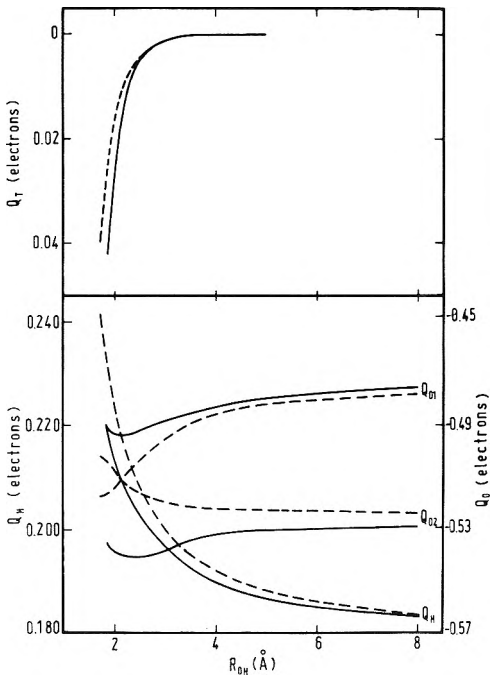

Figure 17. Charge redistribution due to hydrogen bonding in the dimers of zwitterionic glycine. Dashed lines refer to one linear H bond (case a), while solid lines refer to two distorted H bonds (b). Upper half shows the variation of Q_T *vs.* R_{OH}. Lower half shows the behavior of the fractional CNDO/2 charges on hydrogen bonded hydrogens and oxygens. In the case of two hydrogen bonds the variation of the charges on the two bonded hydrogens is exactly the same, whereas on the two oxygens is different because one of them (O_2) is intramolecularly bonded. Worth noting is the susceptibility of these charges even at large intermolecular distances, in contrast to Q_T and $E - E_{el}$ which approach zero at $R_{OH} \simeq 3$ Å.

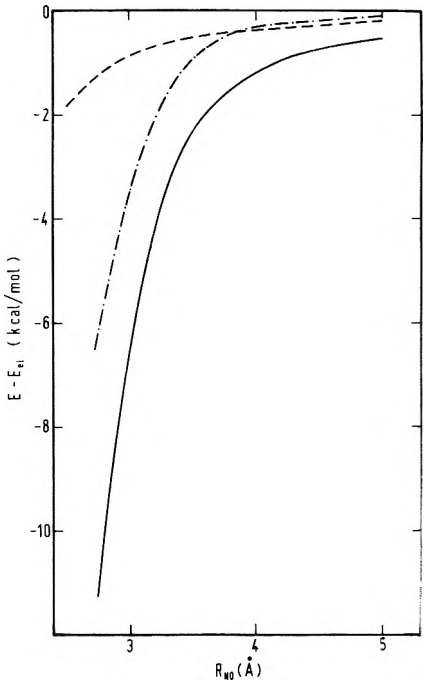

Figure 18. A plot of $E - E_{el}$ *vs.* R_{NO} for the hydrogen bonded dimers imidazole···formate (——) and imidazole···zwitterionic glycine (-·-·-·), and for the nonhydrogen bonded imidazole···formate dimer.

lower part of this figure shows the behavior of the net charges on the atoms directly involved in the hydrogen bonding. An important feature of these curves that deserves a special mention is the nature of Q_T and the net charges at large distances. It can be noticed that while Q_T drops to zero at $R_{OH} \simeq 3.5$ Å, the net charges remain experiencing the influence of the interacting molecule up to much larger distances. The charge redistribution due to the H-bond formation qualitatively agrees with the one normally found by other MO calculations,[11] namely, an increase of the electron density on the electronegative atom carrying the proton and also on the electronegative atom forming the bond, and a decrease on the hydrogen and on the atom (C here) bonded to the electronegative atom. However, the variation of the individual charges does not appear to be correlated with the H-bond potential. A redistribution of the charges in the dimer upon the formation of the hydrogen bond and a good correlation of the variation of Q_T with that of hydrogen bond energy supports the fact that the hydrogen bonding is a collective interaction.

The three $E - E_{el}$ curves A, B, and D referring to the linear H bonds are much closer to each other than those in ion···ion and related systems. Thus, while the coefficient A is not very different in gly···gly and ammonia···formic acid as one should expect, in the case of the zwitterionic dimer it is less than a half the value of $HCOO^- \cdots NH_4^+$. Yet the differences in the hydrogen bond strengths are large enough (A:B:D $\sim$ 3:2:1) to convince one not to use the same H-bond potential function for neutral and charged groups. Concerning the large disagreement between $E - E_{el}$ and ΣU_{HB} for the two cases c and d of the zwitterionic dimer, we notice that both structures present several very distorted H bonds; the error may arise from having overestimated the distortion parameter α.

Imidazole as a Proton Donor. Since the aromatic ring of imidazole is more polarizable than ammonia one could expect stronger hydrogen bonds when the former acts as the proton donor. Such appears to be the case when imidazole forms a linear hydrogen bond with the formate ion (Figure 5a); the coefficient A is 40% larger than that in ammonia···formate and a similar behavior is offered by Q_T. When the imidazole molecule is rotated until the nonprotonated N is colinear with the C=O bond (Figure 5b), $E - E_{el}$ becomes small compared with its value in the hydrogen bonded configuration at the same R_{ON} distance. Again the polarization effect is small unless the O and H atoms come close, and so the increase of A when imidazole replaces ammonia is mainly due to the strengthening of the H bond. Contrary to this, such an increase is not observed when imidazole replaces a glycine molecule bonded to the zwitterion of glycine. Table V shows that the coefficient A of imidazole···$^+$gly$^-$ is even slightly smaller than that of gly···$^+$gly$^-$. Calculations on some more systems are, therefore, needed to analyze the importance of the substituents.

Conclusions

The results of the present CNDO/2 calculations support the empirical representation of the interaction energy between the hydrogen bonded molecules as the sum of the intermolecular electrostatic energy and one potential U_{HB} (function of R_{OH} and N···O) for each hydrogen bond being formed; to these terms the dispersion energy, not accounted for by CNDO, should be added. Of particular interest is the result that the additivity of U_{HB} holds also in the case of bifurcated hydrogen bonds.

The attractive coefficients A determined by us show that the parameters of the hydrogen bond potential functions to be used in the empirical energy calculations vary greatly according to whether neutral molecules, zwitterions, or ions participate in the hydrogen-bonding. Further work is needed to test the applicability of U_{HB} and to extend it to shorter distances; for this purpose lattice energy calculations of crystals of the above molecules may be useful.

Acknowledgment. One of us (R. D. S.) wishes to express his thanks to the National Research Council of Italy for having assisted him financially throughout the course of this investigation.

References and Notes

(1) R. F. McGuire, F. A. Momany, and H. A. Scheraga, *J. Phys. Chem.*, **76**, 375 (1972).
(2) H. A. Scheraga, *Advan. Phys. Org. Chem.*, **6**, 103 (1968).
(3) In this work we are not concerned with the torsional energies. It suffices to say that usually they are represented by a cosine function of the dihedral angle, such that when added to nonbonded and electrostatic contributions reproduce the experimental barriers to rotation in small model systems.
(4) (a) P. A. Kollman and L. C. Allen, *J. Amer. Chem. Soc.*, **92**, 6101 (1970); (b) P. J. Hay, W. J. Hunt, and W. J. Goddard, *ibid.*, **94**, 8301 (1972).
(5) R. E. Dickerson and I. Geis, "The Structure and Action of Proteins," Harper and Row, New York, N. Y., 1969, pp 73, 83, and 93.
(6) M. Yudkin and R. Offord, "A Guidebook to Biochemistry," University Press, Cambridge, 1971, pp 24 and 46–49.
(7) A. S. V. Burgen, O. Jardetzsky, J. C. Metcalfe, and N. W. Wade-Jardetzsky, *Proc. Nat. Acad. Sci. U. S.*, **58**, 447 (1967).
(8) R. J. Weinkam and E. C. Jorgensen, *J. Amer. Chem. Soc.*, **93**, 7033 (1971); *ibid.*, **93**, 7038 (1971).
(9) J. A. Pople and G. A. Segal, *J. Chem. Phys.*, **44**, 3289 (1966).
(10) G. A. Segal, Quantum Chemical Exchange Program, No. 91, QCPE, Indiana University.
(11) P. A. Kollman and L. C. Allen, *Chem. Rev.*, **72**, 283 (1972).
(12) J. F. Yan, F. A. Momany, R. Hoffmann, and H. A. Scheraga, *J. Phys. Chem.*, **74**, 420 (1970).
(13) W. R. Oegerle and J. R. Sabin, *J. Mol. Struct.*, **15**, 131 (1973).

Charge-Transfer Complexes in Organic Chemistry. XI.[1] Effect of Acceptors on the Properties of Charge-Transfer Complexes Formed by Cyclic Anhydrides

J. B. Nagy,[2] O. B. Nagy,* and A. Bruylants

Laboratoire de Chimie Générale et Organique, Université Catholique de Louvain, Institut Lavoisier, Place L. Pasteur, B-1348 Louvain-la-Neuve, Belgium *(Received July 27, 1973; Revised Manuscript Received January 14, 1974)*

π–π and n–π type charge-transfer complexes with fixed donor moiety and variable acceptor moiety were examined. The thermodynamic and spectroscopic properties of these complexes were analyzed as a function of the properties of the acceptors. Several new electron affinity values for the acceptors were determined and their magnitude was interpreted in the light of the molecular electronic structure.

In a previous paper[3] we examined the variation of the properties of charge-transfer complexes (CT complexes) formed by tetrachlorophthalic anhydride (TCPA) with aromatic π donors when the latter were changed. In the present paper we wish to report a similar study on the n–π and π–π type CT complexes of several cyclic anhydrides (Table I).

The main purpose is to examine the behavior of various CT complexes when their acceptor moiety is varied.

Although the different presently known acceptors were already compared and their acceptor strength carefully analyzed,[4] only a few studies were devoted to closely related acceptors. The homologous series of polynitrobenzenes[4-6,8] and of substituted *p*-benzoquinones[4,7-9] were studied in detail.

The importance of this type of study should be emphasized since it permits one to establish how the properties of the acceptor molecule may influence those of the whole CT complex.

According to the theory of weak complexes a direct relationship exists between the CT band position $\bar{\nu}_{max}$ and the electron affinity of the acceptor, E_A[4]

$$h\nu_{CT} = -E_A + C_1 + \frac{C_2}{C_1 - E_A} \quad (1)$$

C_1 and C_2 are constants characteristic mainly of the donor moiety. Since the last term on the right-hand side of eq 1 turns out to be negligible, one should obtain a straight line with unit slope when plotting $h\nu_{CT}$ against E_A both expressed in eV units. This prediction has already been verified experimentally by Briegleb[10] and by Foster[8] who used either the actual electron affinity values or the half-wave reduction potentials, $E_{1/2}$, which are closely related to them[10]

$$E_A = -E_{1/2} + 1.41 \quad (2)$$

The intercept of eq 1 is given approximately by

$$C_1 = I_D + E_C - W_0 \quad (3)$$

where I_D is the ionization energy of the donor; E_C represents the Coulomb interaction energy of the two oppositely charged ions resulting from the complete transfer of one electron from the donor to the acceptor; W_0 represents the interaction energy between the donor and the acceptor due to other factors than charge-transfer.

Since in practice $|I_D + E_C| \gg |W_0|$, eq 3 reduces to

$$C_1 \simeq I_D + E_C \quad (4)$$

It is noteworthy that only very few E_A values are known at present and their reliability is often questionable.[10]

TABLE I: Cyclic Anhydrides Used in the Present Study

Name	Symbol
Tetrachlorophthalic anhydride	TCPA
Tetrabromophthalic anhydride	TBPA
3,6-Dichlorophthalic anhydride	DCPA
4-Nitrophthalic anhydride	4NPA
3,5-Dinitrophthalic anhydride	3,5NPA
Homophthalic anhydride	HPA
Phthalic anhydride	PA
1,8-Naphthalenedicarboxylic anhydride	NA
2,3-Pyridinedicarboxylic anhydride	PCA
Maleic anhydride	MA

The study of CT complexes presents an extremely useful approach to overcome the difficulties. If a series of CT complexes with fixed donor and variable acceptor moieties is examined, new electronaffinity values can be extracted from the plot $h\nu_{CT}$ *vs.* E_A.

Results and Discussion

All the CT complexes studied in 1,2-dichloroethane (DCE) presented a new electronic absorption band either well separated from the components' absorption or showing up as a shoulder (Figure 1).

Table II gives the results obtained by using the Scatchard equation for the π–π type CT complexes of acenaphthene (ACE) with the various anhydrides. The 1:1 stoichiometric composition of such complexes was previously established.[1,3] The concentration of the anhydrides varied between 3×10^{-3} and 2×10^{-2} *M*. The range of concentration of the donor is 0.1–1.1 *M*. The saturation factors are 0.2–0.7, except for DCPA (0.15) and this value must be regarded with caution. The extinction coefficient of the complexes does not vary with temperature showing that contact interactions are unimportant.[1,3,11]

The thermodynamic and spectroscopic data are also collected in Table II. The enthalpies of complex formation do not show any change with temperature. This precludes the presence of isomeric CT complexes of different $\Delta H°$.[1,3,12] The low values for $\Delta H°$ indicate that ACE forms only relatively weak complexes with the anhydrides under study. This is corroborated by the low ionic character (i%) of the CT bond.

The entropy values, ranging from −2 to −12 eu, are negative in all cases. It seems that the increase in entropy due to partial desolvation of the donor and acceptor molecules cannot counter balance the considerable entropy loss accompanying the complex formation. The desolvation effect is the greatest for MA and the smallest for TCPA, TBPA, and 3,5NPA. This is in accord with the different solvation of the acceptors due to their different size. More important, however, is the solvation of the CT complex which is governed mainly by its polarity due to the charge-transfer; that is the more polar the complex the better it is solvated. This effect works in an opposite manner to the effect of the partial desolvation resulting in the observed entropy sequence. Good correlation exists between $\Delta H°$ and $T\Delta S°$ (Figure 2). The slope is close to unity (1.20 ± 0.08) showing that the entropy varies almost as much as the enthalpy. Therefore it cannot be supposed that the entropy factor remains constant when a series of CT complexes with variable acceptor moiety is considered. Nevertheless, the observed $\Delta H°/T\Delta S°$ relationship is rather surprising as no such relationship could be obtained for complexes of variable donor moiety.[3]

The molar extinction coefficient ϵ does not vary regularly with $\bar{\nu}_{max}$ while the oscillator strength f gives an excellent correlation (Figure 3) ($f = -0.105\ (\pm 0.013)\bar{\nu}_{max} + 6.12\ (\pm 0.31)$). Thus f represents much better than ϵ the charge-transfer transition intensity.[1] Since the correlation obtained satisfies the general theory,[4] *i.e.*, f decreases with increasing $\bar{\nu}_{max}$, no correction was carried out for solvent complexation effects.[1] This latter is supposed to vary only slightly from acceptor to acceptor.

The transition moment μ_T of the charge-transfer band is about 2 D[15] for all complexes studied.

The complexes of 1,4-diazabicyclo[2.2.2]octane (DBO) with the anhydrides are of the n–π type. They are stronger than the corresponding π–π type complexes of ACE as indicated by the lower $\bar{\nu}_{max}$ values. The thermodynamic data show clearly that this is indeed the case: K for the complex DBO–PA[16] is equal to 0.9 M^{-1} at 40°, $\Delta H°$ = −4.2 kcal mol^{-1}, $T\Delta S°$ = −4.4 kcal mol^{-1} on the other hand for the complex ACE–PA we have $K = 0.0_9\ M^{-1}$ at 44°, $\Delta H°$ = −1.3 kcal mol^{-1}, and $T\Delta S°$ = −2.8 kcal mol^{-1}.

TCPA also forms stronger complexes with n donors: the value K_{kin} = 5.6 M^{-1} at 20° for the complex DBO–TCPA[17] is to be compared with K_{uv} = 2 M^{-1} at 20° for the complex ACE–TCPA.[18]

The half-band width for the complexes of ACE increases slightly with $\bar{\nu}_{max}$. The relationship is far from

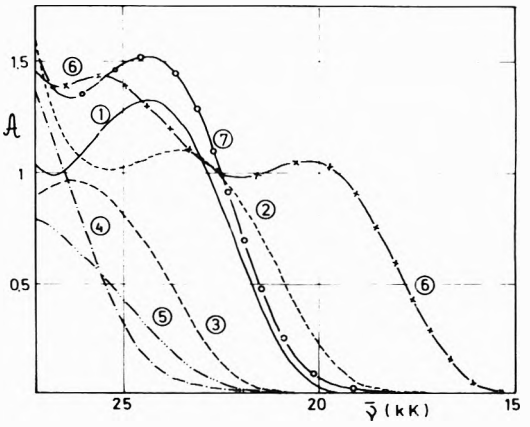

Figure 1. Electronic spectra of the CT complexes of cyclic anhydrides with ACE in 1,2-dichloroethane at T = 20° (concentrations in parentheses in *M*): 1, TCPA (3×10^{-3}) + ACE (0.436); 2, 4NPA (6.0×10^{-3}) + ACE (0.416); 3, DCPA (1.2×10^{-2}) + ACE (0.140); 4, PA (2.4×10^{-2}) + ACE (0.555); 5, MA (2×10^{-2}) + ACE (0.313); 6, 3,5NPA (1.666×10^{-3}) + ACE (0.555); 7, TBPA (3×10^{-3}) + ACE (0.60).

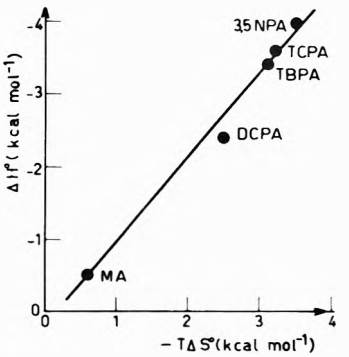

Figure 2. Relationship between $\Delta H°$ and $T\Delta S°$ for the complexes of ACE with various cyclic anhydrides in DCE.

TABLE II: Variation of Thermodynamic and Spectroscopic Data with Acceptor Properties for the Complexes ACE–Anhydrides at 20° in DCE[g]

Anhydride	E_A, eV	K, M^{-1}	$\Delta G°$, kcal mol^{-1}	$\Delta H°$, kcal mol^{-1}	$-T\Delta S°$, kcal mol^{-1}	$\bar{\nu}_{max}$, kK	$\bar{\nu}_{max} - \bar{\nu}_{1/2}$, cm^{-1}	ϵ_{max}, M^{-1} cm^{-1}	$f \times 10^2$	μ_T, D	i%[h]
TCPA	0.58[c]	2.1 ± 0.1	−0.43 ± 0.03	−3.6 ± 0.5	3.2 ± 0.5	24.3	2300	940	3.5	1.8	5
TBPA[a]	0.7[e]	1.8 ± 0.05	−0.33 ± 0.03	−3.4 ± 0.4	3.1 ± 0.4	24.25	2300	960	3.6	1.8	5
DCPA	0.5[e]	0.8 ± 0.04	+0.13 ± 0.05	−2.4 ± 0.4	2.5 ± 0.4	26.15	2600	800	3.4	1.7	3
3,5NPA[b]	1.1[d]	2.5 ± 0.1	−0.53 ± 0.04	−4.0 ± 0.4	3.5 ± 0.4	20.3	2400	1030	4.0	2.0	6
4NPA	0.5[a]	~0.6				23.75	2700				
MA	0.57[c]	0.7 ± 0.03	+0.1 ± 0.03	−0.5 ± 0.1	0.6 ± 0.1			220			
PA	0.15[c]	~0.1		−1.0[f]							

[a] Reference 13. [b] Reference 14. [c] Reference 10. [d] Calculated from the relationship $\bar{\nu}_{max}/E_A$ of the complexes formed with pyrene.[11,14] [e] Calculated from eq 6 and verified by eq 7. [f] Calculated from $A = \epsilon K C_A^0 C_D^0$, where C_A^0 and C_D^0 are the initial concentrations for the acceptor and donor molecules, respectively; A is the absorbancy. [g] The errors are given as standard errors; the propagation of errors was also taken into account. [h] Per cent ionic character of the CT band following Briegleb:[1] $i(\%) = |\Delta H°|/(|\Delta H°| + h\nu_{CT})$, 10[2].

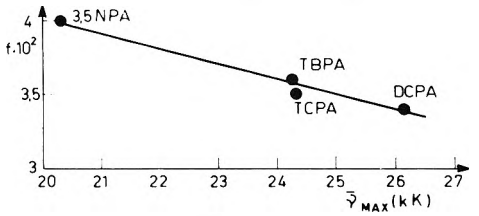

Figure 3. Variation of f with $\bar{\nu}_{max}$ for the complexes of ACE with various cyclic anhydrides in DCE at $T = 20°$.

being perfect but it can be seen that when the stability decreases the complexes become looser. For the complexes of DBO, the half-width $\bar{\nu}_{max} - \bar{\nu}_{1/2}$ seems to be independent of $\bar{\nu}_{max}$.

The complexes of *N*-dimethylaniline (DMA) are of borderline type between n–π and π–π. Indeed DMA is an n donor due to its free electron pair on the nitrogen but it is also a π donor due to its benzene ring. This is shown by the behavior of $\bar{\nu}_{max}$ values; the CT absorptions are either hypsochromic or bathochromic with respect to the corresponding values for DBO (Table III). The mixed character of DMA can also be inferred from the solvent effect studies on charge-transfer maxima when similar substituted benzene molecules are used as solvent[19] or from the properties of complexes formed by aniline.[20-22] A further support comes from the fact that the slope of the straight line obtained by plotting $\bar{\nu}_{max}$ of the complexes of DBO against $\bar{\nu}_{max}$ of the complexes of DMA is not unity. Since the same is true in the case when the complexes of ACE (π–π) are correlated with those of DBO (n–π), one can say that DBO and DMA are donors of different type. However this latter explanation should be handled with caution, since no satisfactory explanation exists at present for the deviation of the slopes from unity.[23]

As starting point of determining new electronaffinity values we used the E_A values for TCPA, MA, and PA as given by Briegleb[10] (Table III).

The E_A of 3,5NPA was obtained by interpolation from the empirical relationship $h\nu_{CT} = -E_A + 3.42$ established for the CT complexes of pyrene.[10,14] When ACE is the donor, the points of the plot $h\nu_{CT}/E_A$ follow closely the theoretical straight line of unit slope.

The equation obtained with the theoretical slope

$$h\nu_{CT} = -E_A + 3.73 \qquad (5)$$

was used to calculate the E_A values of TBPA and DCPA. A similar procedure (Table III) for the complexes when DBO or DMA were taken as donors in benzene (B) solution, yielded the equation

TABLE III: Spectroscopic Data of the Complexes of Anhydrides Formed with DBO and DMA in Benzene at 20°

	DBO		DMA		
Anhydride	$\bar{\nu}_{max}$, kK	$\bar{\nu}_{max} - \bar{\nu}_{1/2}$, cm^{-1}	$\bar{\nu}_{max}$, kK	$\bar{\nu}_{max} - \bar{\nu}_{1/2}$, cm^{-1}	E_A, eV
TCPA	22.6	2950	21.85	2900	0.58[a]
DCPA	24.25	2850	23.45	3050	0.5[a]
PA	26.5	3050	~27		0.15[a]
MA	25.45	3150	24.65		0.57[a]
4NPA	22.75	2950			0.5[a]
NA	25.15	2900	27.0		0.35[b]
PCA	25.8				0.32[b]
HPA	25.3	2350			0.33[c]

[a] For the values see Table II. [b] Calculated from eq 6 and verified by eq 7. [c] Calculated from eq 6.

$$h\nu_{CT} = -E_A + 3.48 \qquad (6)$$

From this equation the E_A values for NA, PCA, and HPA could be calculated (Table III).

In order to check the validity of the new E_A values, they have been compared to the corresponding half-wave reduction potential ($E_{1/2}$) of the acceptors.[13,24] The empirical relationship obtained

$$E_A = -0.99\,(\pm 0.04)E_{1/2} + 1.42\,(\pm 0.04) \qquad (7)$$

shows that despite the different estimating procedures the proposed E_A values are essentially correct.[25] This expression differs only slightly from eq 2.[26] It should be noted that the different E_A values satisfy simultaneously eq 5 and 6 (the 4NPA is an exception) valid for π–π and n–π CT complexes, respectively; this represents a further support of the reliability of the new E_A values.

According to eq 4, the two quantities I_D or E_C can be determined if one of them is known. Using I_D = 7.7 eV for ACE,[3] I_D = 7.2 eV for DBO,[27] and I_D = 7.3 eV for DMA[28] the following Coulomb energies could be calculated: E_C = −3.97 eV for the complexes of ACE, E_C = −3.72 eV for the complexes of DBO, and E_C = −3.82 eV for the complexes of DMA. These values are in good agreement with E_C = −3.3 ± 0.5 eV as suggested by Mulliken and Person.[23]

Considering the ±(0.1–0.2) eV uncertainties attached to the I_D values one can say that the Coulomb energies remain constant when passing from π donors to n donors for the same π acceptor.

Similar constancy of E_C is observed for complexes of π donors when π acceptors and σ acceptors are compared as

shown by theoretical and experimental considerations.[29] These findings are in disagreement with earlier suggestions that different E_C values must be used for π-π and π-σ complexes.[10]

The apparent insensitivity of E_C toward the nature of the complexing partners is somewhat surprising. Even if we suppose, as an extreme situation, that the intermolecular distance remains constant, the charge transfer and the charge distribution for π-π and n-π complexes are certainly different enough to cause a variation in E_C. Our results suggest that beside these factors the intermolecular distance does also change resulting in a constant E_C term. The charge transfer in n-π complexes is greater than in π-π complexes. Therefore the Coulomb interaction should be stronger in the former. It follows from the constancy of E_C that the intermolecular distance should be smaller for π-π than for n-π complexes. Unfortunately, this is not borne out in practice.

We wish to note that we use Briegleb's E_A values[10] to establish our equation on account of the greater number of data available. It should be kept in mind that these values were calculated using chloranil as reference. They are by about 1 eV lower than those given by Batley and Lyons.[30] These authors established an absolute electron affinity scale using the iodine atom as a standard.[31] The new E_A values may be interpreted in terms of the electronic structure of the acceptors.

The presence of the benzene ring in PA reduces considerably the electron affinity compared to MA. The introduction of two chlorine atoms in the 2,6 positions as in DCPA seems to correct for this and raises the electron affinity almost up to that of MA. Further substitution by chlorine as in TCPA has almost no effect.[32]

It appears that one nitro group in the 4 position is as efficient as two chlorine atoms in raising the electron affinity. An additional nitro group as in 3,5NPA doubles approximately the E_A value. Therefore 3,5NPA belongs to the class of relatively strong acceptors such as 2,4,7-trinitro-9-fluorenone (E_A = 1.1 eV), dibromopyromellitic dianhydride (E_A = 1.1_6 eV), or dichloro-*p*-benzoquinones[10] (E_A = 1.1_5 eV).

The higher E_A value for TBPA (0.7 eV) than for TCPA (0.5_8)[33] follows well the trend observed for the corresponding substituted *p*-benzoquinones: E_A (*p*-bromanil) > E_A (*p*-chloranil).[10,30]

The pyridine ring in PCA is more of an electrocaptor than the benzene ring in PA as could be expected. It is interesting to note that PCA has about the same electron affinity as NA.

Experimental Section

The preparations of TCPA, DCPA, PA, 4NPA, NA, and 3,5NPA have already been described.[16] ATBP, PCA, HPA (Aldrich products), and MA (UCB product for analysis) were used without further purification. The purification of DCE and of B was previously described.[16]

Apparatus. All spectra were taken on an Unicam SP 800 spectrophotometer, calibrated by the holmium spectrum. Their accuracy is ±100-150 cm^{-1}. The solutions studied were thermostated within ±0.1°.

Acknowledgments. We thank Mrs. A. Zador-Tits and F. Billastre for technical assistance.

References and Notes

(1) Part IX. L. Hevesi, E. Wolfson-Davidson, J. B. Nagy, O. B. Nagy, and A. Bruylants, *J. Amer. Chem. Soc.*, **94**, 4715 (1972). Part X. *Bull. Soc. Chim. Belg.*, in press.
(2) Taken in part from the Ph.D. Thesis of J. B. Nagy, Louvain, 1970.
(3) Part VIII. J. B. Nagy, O. B. Nagy, and A. Bruylants, *Bull. Soc. Chim. Belg.*, **82**, 337 (1973).
(4) G. Briegleb, "Elektronen-Donator-Acceptor-Komplexe," Springer Verlag, Berlin, 1961.
(5) B. Dale, R. Foster, and D. Ll. Hammick, *J. Chem. Soc.*, 3986 (1954).
(6) S. D. Ross, M. Bassin, and J. Kuntz, *J. Amer. Chem. Soc.*, **76**, 4176 (1954).
(7) R. Foster, D. Ll. Hammick, and P. J. Placito, *J. Chem. Soc.*, 3881 (1956).
(8) R. Foster, "Organic Charge-Transfer Complexes," Academic Press, London, 1968.
(9) R. Foster and C. A. Fyfe, *Trans. Faraday Soc.*, **62**, 1400 (1966).
(10) G. Briegleb, *Angew. Chem., Int. Edit. Engl.*, **3**, 617 (1964).
(11) L. E. Orgel and R. S. Mulliken, *J. Amer. Chem. Soc.*, **79**, 4839 (1957).
(12) C. D. Johnson and R. E. Bowen, *J. Amer. Chem. Soc.*, **87**, 1655 (1965).
(13) H. Lion, Mémoire de fin d'études, Institut Techniques Supérieur d'Assistants de Laboratoire et de Diététiciens, Louvain, 1971.
(14) S. Dupire, Thèse de Licence, U.C.L. Louvain, 1971.
(15) For the method used to calculate *f* and μ_T see ref 1.
(16) Part XIV. D. Mukana, J. B. Nagy, O. B. Nagy, and A. Bruylants, manuscript in preparation.
(17) Part V. J. B. Nagy, O. B. Nagy, and A. Bruylants, *Bull. Soc. Chim. Belg.*, **82**, 539 (1973).
(18) The comparison of *K* values determined by kinetics (K_{kin}) and by spectrophotometry (K_{uv}) is legitimated by the fact that the agreement between the measurements by these different techniques is satisfactory as can be judged from the following data: complex triethylamine-TCPA in *n*-chlorohexane K_{kin} = 10, K_{uv} = 8; in 1,2-dichloroethane K_{kin} = 13, K_{uv} = 10.5; in benzene K_{kin} = 5.2, K_{uv} = 5.2; in mesitylene K_{kin} = 1.3, K_{uv} = 1.3; complex triethylamine-DCPA in 1,2-dichloroethane K_{kin} = 10, K_{uv} = 13; complex pyridine-TCPA in benzene K_{kin} = 0.6, K_{uv} = 0.6. All the constants in M^{-1} units were measured at 20°. The good agreement between K_{kin} and K_{uv} is insensitive to the change of solvent (the highest discrepancy is about 30%). The K_{kin} values are taken from ref 17.
(19) Part VI. O. B. Nagy, J. B. Nagy, and A. Bruylants, *J. Chem. Soc., Perkin Trans. 2*, 968 (1972).
(20) D. C. Mukherjee and A. K. Chandra, *J. Phys. Chem.*, **68**, 477 (1964).
(21) B. B. Wayland and R. S. Drago, *J. Amer. Chem. Soc.*, **86**, 5240 (1964).
(22) W. R. Carper, R. M. Hedges, and H. N. Simpson, *J. Phys. Chem.*, **69**, 1707 (1965).
(23) R. S. Mulliken and W. B. Person, "Molecular Complexes, A Lecture and Reprint Volume," Wiley, New York, N. Y., 1969.
(24) J. B. Nagy, O. B. Nagy, and H. Lion, results to be published.
(25) The E_A value of HPA does not follow eq 7. For explanation see ref 24.
(26) For other acceptors Briegleb obtained[10] $E_A = -1.04E_{1/2} + 1.39$.
(27) A. M. Halpern, J. L. Roebber, and K. Weiss, *J. Chem. Phys.*, **49**, 1348 (1968).
(28) G. Briegleb and J. Czekalla, *Z. Elektrochem.*, **63**, 6 (1959).
(29) J. L. Lippert, M. W. Hanna, and P. J. Trotter, *J. Amer. Chem. Soc.*, **91**, 4035 (1969).
(30) M. Batley and L. E. Lyons, *Nature (London)*, **196**, 573 (1962).
(31) When the absolute scale E_A values are used, the same procedure yields $E_C \approx -2.8$ eV for the complexes under study. It should be noted that this value corresponds to the lower limit proposed by Mulliken and Person.[23]
(32) Similar trend is observed for the reactivity of these anhydrides with triethylamine in benzene.[16]
(33) This is in agreement with the higher Hammett σ value for bromine than for chlorine.

Uncoupled Representations in Hydrogen Isotope Exchange Reactions

J. L. Garnett* and J. C. West

Department of Physical Chemistry, The University of New South Wales, Kensington, New South Wales 2033, Australia
(Received October 29, 1973)

A mathematical analysis of the rate equations for both stepwise and multiple exchange of hydrogen isotopes in molecules containing N kinetically equivalent exchangeable hydrogen atoms is presented. The solutions are obtained in terms of a transform function $E_m(t)$ which can be used to transform experimental data to an uncoupled representation. This uncoupled representation provides N independent tests for correspondence between experimental data and the kinetic assumptions. The application of the uncoupled representation to the analysis of experimental data is illustrated for (i) stepwise exchange using literature data for the deuteration of ammonia and neopentane on *heterogeneous* platinum and nickel and (ii) multiple exchange using the deuteration of benzene with a *homogeneous* $PtCl_4^{2-}$ catalyst. Very frequently undeuterated substrate is exchanged with a fully enriched deuterium source and therefore an Appendix of the constants necessary for transformation of experimental data under these conditions is provided.

1. Introduction

The catalyzed exchange of protium and deuterium atoms in hydrocarbon molecules has been observed in both *heterogeneous* and *homogeneous* systems. Two classes of reaction are common: (a) between chemically different species and (b) between chemically identical positions in identical species. Reactions in class a are *exchange* reactions whereas those in class b are *redistribution* reactions. Mass spectrometric analysis is widely used to determine the distribution of deuterium isotope over the various isotopic species. This technique yields the fraction of molecules containing $0,1,\ldots,i,\ldots,N$ deuterium atoms (denoted by $d_0,d_1,\ldots,d_i,\ldots,d_N$), the molecules themselves being denoted by D_i. In principle, these data contain detailed information on the reaction mechanism, but their correct interpretation in some instances involves mathematical complications. The development of uncoupled representations for kinetic systems has considerably facilitated evaluation of experimental data.[1] In particular, the uncoupled representation for stepwise redistribution reactions permits simple graphical evaluation of the experimental data.[2]

Many exchange reactions occur in a stepwise manner without an appreciable isotope effect. Recently an elegant method for integration of the rate equations in stepwise redistribution reactions with arbitrary initial conditions was derived.[2] The solutions were obtained in terms of a system of orthogonal polynomials, the properties of which can be used to transform experimental data to an uncoupled representation.

Bolder and coworkers[3] have presented the general solution for stepwise exchange with arbitrary conditions of s, where s represents the fraction of hydrogen atoms in the deuterating agent that is deuterium. In the absence of an isotope effect, the reaction sequence for stepwise exchange in a molecule containing N chemically equivalent exchangeable hydrogen atoms may be schematically written

$$D_i + D_s \underset{(i+1)s}{\overset{(N-i)s}{\rightleftharpoons}} D_{i+1} + H_s \quad (i = 0,1,\ldots,N-1) \qquad \text{(I)}$$

where D_s and H_s refer to the deuterated and protonated species in the deuterating agent. A solution was also derived for the special, and frequently used initial condition, $s = 1$. In this case the $d_i(t)$ were given by the binomial expression

$$d_i(t) = \binom{N}{i} p^i q^{N-i} \qquad (1.1)$$

where p and q are defined by

$$Np = \sum_{i=0}^{N} i d_i(t) \qquad (1.2)$$

$$Nq = \sum_{i=0}^{N} (N-i) d_i(t) \qquad (1.3)$$

$$p + q = 1 \qquad (1.4)$$

However, there are numerous cases where multiple exchange occurs. Bolder and coworkers[3] found that if a steady-state approximation is introduced the rate equations can be solved, but the expressions for the $d_i(t)$ are obtained in a surveyable form only when the deuterium content of the deuterating agent remains constant. Physically this implies an infinite pool of deuterating reagent, but in many systems is a reasonable approximation, and is especially true during the initial stages of the reaction. There have been many kinetic treatments of both stepwise and multiple systems, but the two referred to are the most important and contain references to earlier literature.

In this paper the concept of uncoupled representations will be extended to include multiple exchange in molecules containing N chemically equivalent exchangeable hydrogen atoms, provided s remains constant. For completeness the analysis will also be presented for stepwise exchange (*i.e.*, class a reactions) under the same conditions. As an illustration, the methodology will be applied to exchange in ammonia, neopentane, and benzene. A reference Appendix of constants is provided to facilitate transformation of experimental data to the uncoupled representation in cases where the initial condition $s = 1$ is valid.

2. Experimental Section

The procedure adopted for the *homogeneous* exchange of benzene with deuterioacetic acid was a modification of that described previously.[4] Na_2PtCl_4 (Matthey Garrett) was used without further purification. All reactions were carried out in sealed ampoules under air. Aliquots (2 ml) of the stock platinum(II) catalyst solution containing Na_2PtCl_4 (16 mg) in 50 mol % deuterium oxide-deuterioacetic acid mixture that was 0.02 *M* in DCl and benzene (0.25 ml) were sealed off and allowed to react at 100° in an oil bath. After cooling, the ampoules were opened, water was added, and the benzene removed with a Pasteur pipet. The benzene was analyzed for deuterium content by low voltage mass spectrometry (Hitachi-Perkin-Elmer RMS4).

3. Method for Stepwise Exchange Systems

(*a*) *Solution of Rate Equations.* Stepwise exchange is represented by the system in eq I and the corresponding rate expressions are

$$k^{-1}(\mathrm{d}/\mathrm{d}t)d_i(t) = r(i+1)d_{i+1}(t) - [(r-s)i + Ns]d_i(t) + s(N-i+1)d_{i-1}(t) \quad (3.1)$$

with s, and therefore $r = 1 - s$, constant this system of equations can be solved by the method of Corio.[2] Alternatively, the $d_i(t)$ can be transformed according to (3.2) and the time dependence of the transformed function $E_m(t)$ can be determined. This method is presented because it can be readily extended to include multple exchange (section 4). $E_m(t)$ is defined as

$$E_m(t) = \sum_{i=0}^{N} K_m(i)d_i(t) \quad (3.2)$$

where $K_m(i)$ is the Krawtchouk polynomial of degree m in the discrete variable i. These polynomials satisfy the difference equation

$$s(N-i)K_m(i+1) - [(r-s)i + sN - m]K_m(i) + irK_m(i-1) = 0 \quad (3.3)$$

The Krawtchouk polynomials are generated by the function

$$(1-sx)^{N-i}(1+rx)^i = \sum_m K_m(i)x^m \quad (3.4)$$

and are given explicitly by the formula

$$K_m(i) = \sum_{j=0}^{m}(-1)^{m-j}\binom{i}{j}\binom{N-i}{m-j}s^{m-j}r^j \quad (3.5)$$

The mathematical theory of Krawtchouk polynomials has been presented earlier.[5,6] Substitution of (3.2) into (3.1) yields

$$k^{-1}(\mathrm{d}/\mathrm{d}t)E_m(t) = k^{-1}\sum_{i=0}^{N} K_m(i)[r(i+1)d_{i+1}(t) - \{(r-s)i + Ns\}d_i(t) + s(N-i+1)d_{i-1}(t)] \quad (3.6)$$

It can be shown that (3.6) simplifies on rearrangement to

$$k^{-1}(\mathrm{d}/\mathrm{d}t)E_m(t) = \sum_{i=0}^{N} riK_m(i-1) - \{(r-s)i + Ns\}K_m(i) + s(N-i)K_m(i+1)]d_i(t) \quad (3.7)$$

By comparing (3.3) and (3.7) it follows that

$$k^{-1}(\mathrm{d}/\mathrm{d}t)E_m(t) = -\sum_{i=0}^{N} mK_m(i)d_i(t) = -mE_m(t) \quad (3.8)$$

Therefore, the $E_m(t)$ are the uncoupled solutions for (I) and can be found by integrating (3.8).

$$E_m(t) = E_m(0)\exp(-mkt) \quad (3.9)$$

Graphs of $\ln E_m(t)$ against t will be straight lines with slope $-mk$. The system of equations in (3.9) gives N independent estimates of k and provides an exhaustive test for the kinetic assumptions.

If required, the $d_i(t)$ can be obtained from the $E_m(t)$ by using the orthogonality relationship

$$\sum_{i=0}^{N}\omega(i)K_n(i)K_m(i) = (sr)^n\binom{N}{n}\delta_{nm} \quad (3.10)$$

where $\delta_{nm} = 0$, for $n \neq m$; and $\delta_{nm} = 1$, for $n = m$. $\omega(i)$ is defined by

$$\omega(i) = \binom{n}{i}s^i r^{N-i} \quad (3.11)$$

Therefore

$$d_i(t) = \sum_{m=0}^{N}\left[(sr)^m\binom{N}{m}\right]^{-1}\omega(i)K_m(i)E_m(t) \quad (3.12)$$

Alternatively

$$d_i(t) = \sum_{m=0}^{N} a_m\omega(i)K_m(i)_x \exp(-mkt) \quad (3.13)$$

where

$$a_m = \left[(sr)^m\binom{N}{m}\right]^{-1}\sum_{i=0}^{N}K_m(i)d_i(0) \quad (3.14)$$

(*b*) *Solutions for Special Initial Conditions.* If undeuterated compound is used initially then $d_0(0) = 1$. From (3.14)

$$a_m = \left[(sr)^m\binom{N}{m}\right]^{-1}K_m(0) = (-1)^m r^{-m} \quad (3.15)$$

where from (3.4) and (3.13) it can be shown that

$$d_i(t) = \binom{N}{i}[r + s\exp(-kt)]^{N-i}[1-\exp(-kt)]^i s^i \quad (3.16)$$

The substitutions (3.17) and (3.18) are made

$$p = s[1 - \exp(-kt)] \quad (3.17)$$

$$q = r + s\exp(-kt) \quad (3.18)$$

and $p + q = 1$ since $s + r = 1$. With these substitutions (3.16) becomes

$$d_i(t) = \binom{N}{i}p^i q^{N-i} \quad (3.19)$$

This is precisely the relationship in (1.1) provided (1.2) and (1.3) are satisfied. The result can be obtained by performing the summation indicated in (1.2) with the $d_i(t)$ in (3.19).

Very often undeuterated organic is used as substrate and the deuterating agent is fully deuterated (*i.e.*, $s = 1$, $r = 0$). For this particular system the $K_m(i)$ are greatly simplified; $K_m(i)$ becomes

$$K_m(i) = (-1)^m\binom{N-i}{m} \quad (3.20)$$

Since these initial conditions are frequently used it is convenient to refer to tabulated values of $K_m(i)$. In Appendix I values for $K_m(i)$, with these initial conditions, have been

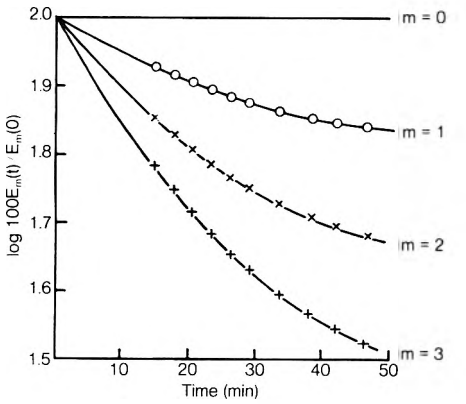

Figure 1. Plot of log $[100E_m(t)/E_m(0)]$ *vs.* time for exchange in ammonia. Data taken from Kemball.[7]

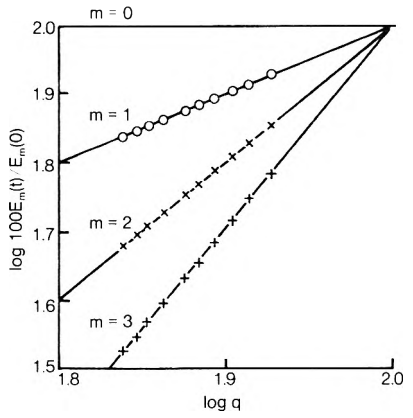

Figure 2. Plot of log $[100E_m(t)/E_m(0)]$ *vs.* log q for exchange in ammonia. Data taken from Kemball.[7]

tabulated for $N = 1,2,\ldots,10$. The initial condition also yields

$$E_m(0) = (-1)^m\binom{N}{m} \tag{3.21}$$

If, however, s does not remain constant during the reaction the $E_m(t)$ transformation is still useful for these initial conditions (*i.e.*, initially $s = 1$). For stepwise exchange and variable s, Bolder and coworkers[3] have shown that

$$d_i(t) = \binom{N}{i}p^i q^{N-i} \tag{3.22}$$

Therefore

$$E_m(t) = \sum_{i=0}^{N}(-1)^m\binom{N-m}{m}\binom{N}{i}p^i q^{N-i} \tag{3.23}$$

This expression can be simplified to yield

$$E_m(t) = (-1)^m q^m\binom{N}{m} \tag{3.24}$$

Alternatively

$$E_m(t)/E_m(0) = q^m \tag{3.25}$$

Equations 3.24 and 3.25 suggest a simple test for a stepwise reaction. A plot of log $[(-1)^m E_m(t)]$ or log $[E_m(t)/E_m(0)]$ *vs.* log q for the data should yield a straight line with slope m. There will be N independent tests for consistency, but the rate constant k must be obtained from the time progress of either p or q.

$$p(\infty) - p(t) = p(\infty)\exp[-kt/p(\infty)] = q(t) - q(\infty) \tag{3.26}$$

(*c*) *Application of Method to Ammonia Exchange.* Kemball[7] has shown that exchange between deuterium and ammonia over a variety of metal films, including nickel and platinum, proceeds *via* a stepwise process (eq II). He numerically integrated the rate equations and

$$NH_3 + D_2 \overset{\text{metal}}{\rightleftharpoons} NH_2D + HD \tag{II}$$

compared the solutions with the data. Mikovsky and Wei[8] have calculated the $d_i(t)$ for this system from the binomial expression and have shown that the results are consistent with the data. Both these methods involve complicated curve fitting and a more attractive function for demonstrating this consistency is the transform $E_m(t)$. In Figure 1, log $[100E_m(t)/E_m(0)]$ for Kemball's data is plotted against time. Because s varied considerably during this reaction (actually some 50%), the curves are not linear. The nonlinearity is particularly obvious for the smaller values of m because these $E_m(t)$ are more heavily weighted with the higher deuterated species. However, plots of log $[100E_m(t)/E_m(0)]$ against log q are linear and clearly demonstrate that the reaction conforms to the stepwise exchange mechanism over the range studied (Figure 2).

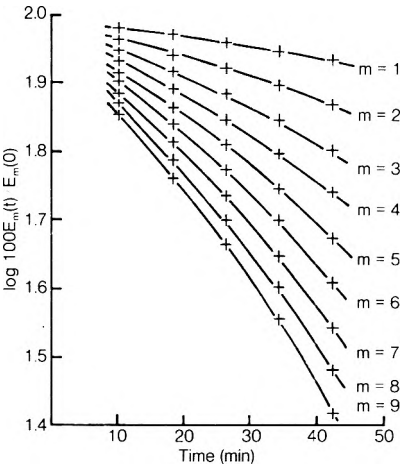

Figure 3. Plot of log $[100E_m(t)/E_m(0)]$ *vs.* time. Results taken from ref 9.

(*d*) *Application of Method to Neopentane Exchange.* A second example is taken from the data of Kemball[9] on the deuteration of neopentane on metal films.

$$\begin{array}{c}CH_3\\|\\CH_3{-}C{-}CH_3\\|\\CH_3\end{array} + D_2 \rightleftharpoons \begin{array}{c}CH_3\\|\\CH_3{-}C{-}CH_2D\\|\\CH_3\end{array} + HD \tag{III}$$

The *tert*-butyl ion was used as a measure of the reaction progress. In Figure 3, log $[100E_m(t)/E_m(0)]$ is plotted against time and in Figure 4, log $[100E_m(t)/E_m(0)]$ is plotted versus log q. The results in Figure 4 clearly show stepwise character and the curves in Figure 3 reflect the variation in s.

4. Method for Multiple Exchange Systems

(*a*) *Solutions for Molecules with N Equivalent Hydrogen Atoms in the Reactive State.* Multiple exchange is possible if a small fraction of all the molecules in the system are converted to a particular state from which they are capable of undergoing exchange. A multiple exchange

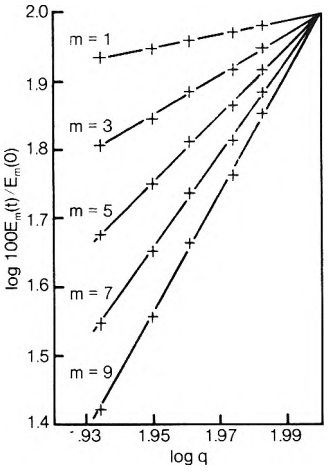

Figure 4. Plot of log $[100E_m(t)/E_m(0)]$ *vs.* log q. Results taken from ref 9.

reaction is defined as a process in which a molecule after passing through the transition state for the exchange of one hydrogen atom does not necessarily return to the normal state, but to a relatively stable and, with respect to exchange, reactive state (designated *). In the system chosen at the end of this section to illustrate the principle of the proposed method, the exchange of benzene is used in the presence of homogeneous $PtCl_4^{2-}$ catalyst.[4,10] The proposed mechanism[4] for this deuteration is shown in eq IV where A denotes the reactive state (*).

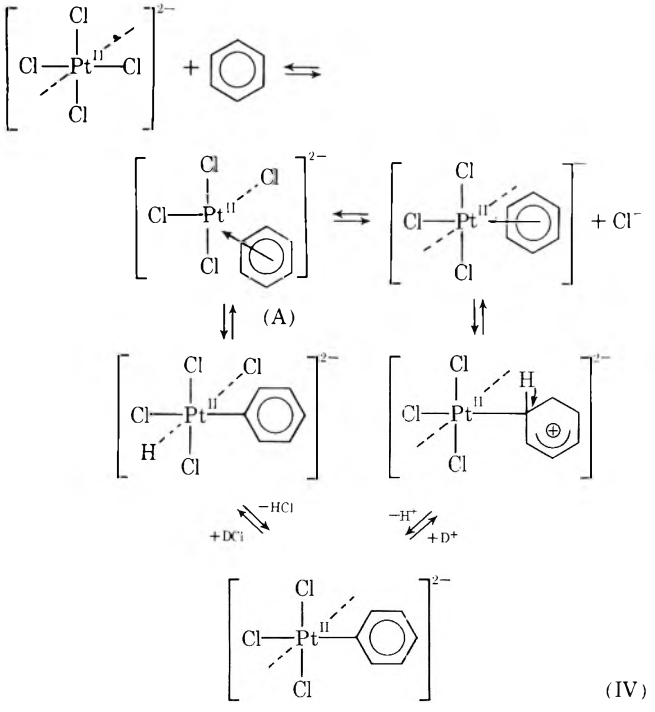

(IV)

In general, the mechanism for multiple exchange in molecules with symmetrical activation can be schematically written

$$D_i + C \underset{k_{-1}}{\overset{k_1}{\rightleftharpoons}} D_i^*$$

$$(N-i)k_2 \Big\downarrow \Big\uparrow (i+1)k_{-2} \qquad (i = 0, 1, \ldots, N-1) \qquad \text{(V)}$$

$$D_{i+1} - C \underset{k_{-1}}{\overset{k_1}{\rightleftharpoons}} D_{i+1}^*$$

TABLE I: Time Progress for Deuterium Incorporation into Benzene from D_2O in Acetic Acid in the Presence of Na_2PtCl_4[a]

Time, hr	Deuterium distribution[b]						
	D_0	D_1	D_2	D_3	D_4	D_5	D_6
1	67.6	5.9	5.9	5.8	5.7	5.3	3.8
2.1	45.9	8.2	8.8	9.4	10.0	10.1	7.6
3	33.5	8.7	9.8	11.0	12.8	13.8	10.4
4	23.8	8.4	10.0	12.1	15.1	17.4	13.2
5.1	15.9	7.8	9.8	12.8	17.2	20.8	15.7
6	12.1	6.9	9.3	13.0	18.5	23.0	17.2

[a] Reaction conditions as in Experimental Section. [b] By low voltage mass spectrometry.

where s is assumed to remain constant. If this is not so, then the substitutions $k_2's = k_2$ and $k_{-2}'r = k_{-2}$ are made. C refers to the catalyst in homogeneous systems or to the active sites in heterogeneous catalysis. $C(t)$ is then the concentration of catalyst in the former system and the number of active sites in the latter system at time t.

The rate equations for the system are

$$(\mathrm{d}/\mathrm{d}t)C(t) = -k_1 \sum_{j=0}^{N} d_j(t) + k_{-1} \sum_{j=0}^{N} d_j^*(t) \qquad (4.1)$$

$$(\mathrm{d}/\mathrm{d}t)d_i^*(t) = k_1 C(t) d_i(t) - k_{-1} d_i^*(t) + (N-i+1)k_2 d_{i-1}^*(t) - [ik_{-2} + (N-i)k_2] d_i^*(t) + (i+1)k_{-2} d_{i+1}^*(t) \qquad (4.2)$$

$$(\mathrm{d}/\mathrm{d}t)d_i(t) = -k_1 C(t) d_i(t) + k_{-1} d_i^*(t) \qquad (4.3)$$

This system of equations can be solved if the reasonable approximation that $C(t)$ remains constant is made, but the analysis is mathematically intricate and can be greatly simplified by assuming that in addition to $C(t)$ remaining constant, a steady-state exists in the $d_i^*(t)$ for most of the reaction.[3] If there is no isotope effect then

$$k_{-2} = \frac{r}{s} k_2 \qquad (4.4)$$

It can be shown that the stationary value of $C(t)$ is the equilibrium concentration. Therefore we let

$$C(t) = C_e \qquad (4.5)$$

where C_e is constant.

The $(\mathrm{d}/\mathrm{d}t)d_i^*(t)$ in (4.2) are set to zero and with (4.4) gives

$$k_1 C_e d_i(t) - k_{-1} d_i^*(t) + \frac{k_2}{s}\{(N-i+1)s d_{i-1}^*(t) - [(r-s)i + sN] d_i^*(t) + (i+1)r d_{i+1}^*(t)\} = 0 \qquad (4.6)$$

Equations 4.3 and 4.5 can be solved by the method of Bolder and coworkers[3] but a more elegant approach is to use the Krawtchouk polynomials to obtain the solutions in terms of the uncoupled representations. The $d_i(t)$ and $d_i^*(t)$ are transformed by the relationships

$$E_m(t) = \sum_{i=0}^{N} K_m(i) d_i(t) \qquad (4.7)$$

$$E_m^*(t) = \sum_{i=0}^{N} K_m(i) d_i^*(t) \qquad (4.8)$$

These transforms are applied to (4.3) to give

$$(\mathrm{d}/\mathrm{d}t)E_m(t) = -k_1 C_e E_m(t) + k_{-1} E_m^*(t) \qquad (4.9)$$

By transforming (4.6) it can be shown (as in section 3)

TABLE II: Tabulation of $K_m(i)$ for $N = 10$, $s = 1$

m \ i	0	1	2	3	4	5	6	7	8	9	10
0	1	1	1	1	1	1	1	1	1	1	1
1	−10	−9	−8	−7	−6	−5	−4	−3	−2	−1	0
2	45	36	28	21	15	10	6	3	1	0	0
3	−120	−84	−56	−35	−20	−10	−4	−1	0	0	0
4	210	126	70	35	15	5	1	0	0	0	0
5	−252	−126	−56	−21	−6	−1	0	0	0	0	0
6	210	84	28	7	1	0	0	0	0	0	0
7	−120	−36	−8	−1	0	0	0	0	0	0	0
8	45	9	1	0	0	0	0	0	0	0	0
9	−10	−1	0	0	0	0	0	0	0	0	0
10	1	0	0	0	0	0	0	0	0	0	0

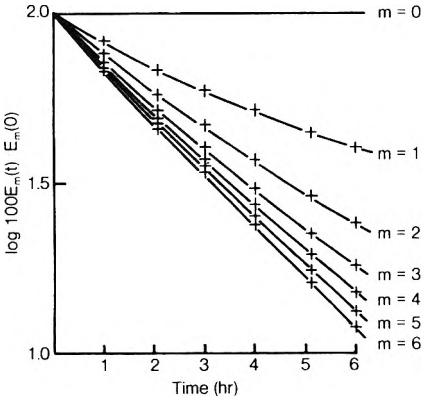

Figure 5. Plot of log $[100E_m(t)/E_m(0)]$ *vs.* time for exchange in benzene. Data taken from Table I.

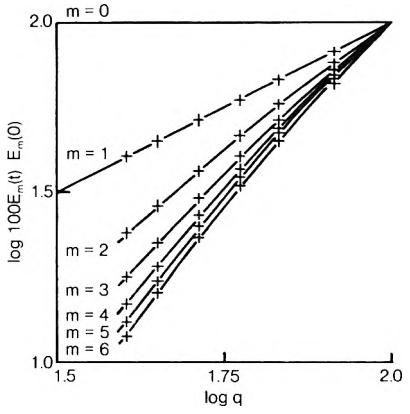

Figure 6. Plot of log $[100E_m(t)/E_m(0)]$ *vs.* log q for exchange in benzene. Data taken from Table I.

that

$$k_1C_eE_m(t) - k_{-1}E_m^*(t) - \frac{k_2}{s}mE_m^*(t) = 0 \qquad (4.10)$$

It follows that

$$E_m^*(t) = \frac{k_1sC_e}{k_{-1}s + k_2m}E_m(t) \qquad (4.11)$$

Substituting (4.11) into (4.9) yields

$$(d/dt)E_m(t) = \frac{-k_1k_2mC_e}{k_{-1}s + k_2m}E_m(t) \qquad (4.12)$$

It follows that

$$E_m(t) = E_m(0)\exp(-\lambda_m t) \qquad (4.13)$$

where

$$\lambda_m = \frac{k_1k_2C_em}{k_{-1}s + k_2m} \qquad (4.14)$$

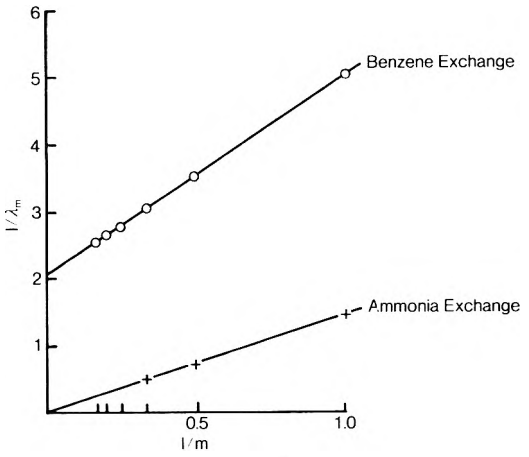

Figure 7. Plot of $1/\lambda_m$ *vs.* $1/m$ for exchange in benzene and ammonia. λ_m is defined in eq 4.14: (+) plot for exchange in ammonia, data as in Figures 1 and 2; (O) plot for exchange in benzene, data as in Figures 5 and 6.

Plots of ln $E_m(t)$ against time for multiple exchange, with constant s, and a steady state in the $d_i^*(t)$ should be linear with slope $= -\lambda_m$. Unlike stepwise exchange, the λ_m are not linear functions of m but are given by (4.14). Agreement between the experimentally determined λ_m and (4.14) provides a convenient test for the kinetic assumptions in the model. However, (4.14) is easier to handle if rearranged to

$$1/\lambda_m = \frac{s}{k_1C_eK_R}\frac{1}{m} + \frac{1}{k_1C_e} \qquad (4.15)$$

where

$$K_R = k_2/k_{-1} \qquad (4.16)$$

Plots of $1/\lambda_m$ against $1/m$ should be linear and K_R can be used as a measure of the multiplicity.

$$K_R = s(\text{intercept/slope}) \qquad (4.17)$$

The solutions for stepwise and multiple exchange are formally similar (compare (3.9) and (4.13)). If (4.12) is used to represent both stepwise and multiple systems, then a straight line through the origin (in eq 4.15) indicates a stepwise process.

(*b*) *Application of Method to Benzene Exchange.* The homogeneous $PtCl_4^{2-}$ catalyzed exchange between benzene and deuterated aqueous acetic acid follows multiple kinetics[10] (eq IV, Table I) and therefore it is particularly interesting to compare the results for this reaction with those for stepwise reactions. In Figures 5 and 6, log [100 $E_m(t)/E_m(0)$] is plotted against time and log q, respec-

tively. Two features are apparent. First, neither plot produces a linear function (because s is not constant) and secondly, the initial slopes in Figure 5 do not increase proportionally with m.

In Figure 7, $1/\lambda_m$ is plotted against $1/m$ for exchange reactions with benzene (multiple) and ammonia (stepwise). Both sets of results give linear plots and show the validity of eq 4.15 for the stepwise and multiple exchange systems.

The present procedure thus demonstrates that for an isotope exchange process possessing either stepwise or symmetrical multiple character, the transform $E_m(t)$, which is defined in eq 3.2, greatly simplifies the treatment of the mass spectral kinetic data.

Acknowledgments. The authors thank the Australian Research Grants Committee and the Australian Institute of Nuclear Science and Engineering for the support of this research.

Appendix I

A tabulation of $K_m(i)$ is provided for the special initial conditions: undeuterated organic substrate and a fully deuterated source of deuterium (*i.e.*, $s = 1$, $r = 0$). The table is for $N = 10$. Tables for $N = 1$ to 9 are readily obtained as subtables of this Table II.

In general for $N = y$; $y = 1$ to 9, subtract $(10 - y)$ from all values of i at the top of Table II and disregard all columns for which i becomes negative. Then use only the first y rows of Table II to complete the tabulation for $N = y$. For example, if $N = 6$, subtract 4 from the values of i and disregard the first four columns. Use only the first six rows to complete the table.

References and Notes

(1) J. Wei and C. D. Prater, *Advan. Catal.*, **13**, 203 (1962).
(2) P. L. Corio, *J. Phys. Chem.*, **74**, 3853 (1970), and references therein.
(3) H. Bolder, G. Dallinga, and H. Kloosterziel, *J. Catal.*, **3**, 312 (1964), and references therein.
(4) R. J. Hodges and J. L. Garnett, *J. Phys. Chem.*, **72**, 1673 (1968).
(5) G. Szego, "Orthogonal Polynomials," American Mathematical Society, New York, N. Y., 1959, pp 35–37.
(6) P. L. Corio, *Int. J. Quantum Chem.*, **6**, 289 (1972).
(7) C. Kemball, *Proc. Roy. Soc., Ser. A*, **214**, 413 (1952).
(8) R. J. Mikovsky and J. Wei, *Chem. Eng. Sci.*, **18**, 253 (1963).
(9) C. Kemball, *Trans. Faraday Soc.*, **50**, 1344 (1954).
(10) J. L. Garnett and J. C. West, unpublished data.

Virial Theorem Decomposition of Molecular Force Fields

Gary Simons* and Jay L. Novick

Department of Chemistry, Wichita State University, Wichita, Kansas 67208 *(Received December 17, 1973)*

A procedure for decomposing a molecular force field into its (1) electronic kinetic and (2) electronic and nuclear potential components is developed. By applying this procedure to the triatomic species N_2O, HCN, CS_2, CO_2, SO_2, O_3, SeO_2, ClO_2, BO_2^-, H_2S, H_2O, H_2Se, ClCN, OCS, GeF_2, NCO^-, OF_2, and NO_2, a set of structural rules regarding the signs of various T and V components of the Born–Oppenheimer potential is obtained. The signs of the equilibrium values of $\partial T/\partial\theta$, $\partial^2 V/\partial\theta^2$, $\partial^2 V/\partial R\partial\theta$, $\partial^2 V/\partial R_1\partial R_2$, $\partial^3 V/\partial R^2\partial\theta$, $\partial^3 T/\partial R\partial\theta^2$, $\partial^3 V/\partial R_1\partial R_2\partial\theta$, $\partial T/\partial R$, $\partial^2 V/\partial R^2$, and $\partial^3 T/\partial R^3$ are shown to be generally negative, while the signs of the respective derivatives of the other components are positive. A discussion of the physical significance of the rules is given, and the decomposition procedure is used to assess the virtues and defects of three recently proposed model functions.

I. Introduction

As witnessed by the number of recent review articles which deal with the subject,[1-4] the determination of molecular force fields including cubic and often quartic force constants has become an area of considerable research activity. There are now in the literature cubic or quartic force fields of varying degrees of accuracy for nearly 20 triatomic species,[5-23] and several more ambitious studies have been reported.[24-26] Given the difficulty and expense of determining accurate potential surfaces from *ab-initio* computations,[27] these "experimental" force fields remain a primary source of information concerning the interactions between atoms in molecules. The determination and interpretation of these fields is a formidable task, however, which has led several investigators to propose simple model potential functions.[28-36] These models provide additional physical content for the empirically determined force constants, and may eventually lead to the construction of model potentials for molecules about which there is little or no experimental data.

In section II of this paper we demonstrate that by employing the polyatomic quantum-mechanical virial theorem in the form derived by Nelander,[37] one may rigorously decompose a molecular force field into its kinetic and potential components (the components due (1) to the electronic kinetic energy and (2) the electron–nuclear, electron–electron, and nuclear–nuclear electrostatic interactions, respectively). Since no physical model, empirical rule, or approximate wave function is employed, the resulting kinetic (T) and potential (V) constants may be regarded as "experimental," subject only to the errors involved in the determination of the force constants.

By inspecting the T and V fields of a number of triatomic molecules, we have discovered several relationships of apparently general validity, which describe the way T and V contribute to certain force constants; these are given in section III. These rules may prove useful in assessing the reliability of experimental force fields or of computed potential surfaces, but more importantly, they allow for an increased understanding of the "whys" of bonding and structure: for example, we show that in essentially all cases the kinetic energy tends to open the bond angles of bent triatomics, while the potential tends to close the angles.

Further, the experimental T and V fields may be employed to analyze physical models of force fields. In section IV we use this approach to assess the virtues and defects of three recently proposed model functions.

II. Decomposition of Force Fields

The Born-Oppenheimer potential or force field of a polyatomic molecule may be expressed as a sum of kinetic and potential components

$$W(\{R_j\},\{\theta_k\}) = V(\{R_j\},\{\theta_k\}) + T(\{R_j\},\{\theta_k\}) \quad (1)$$

where $\{R_j\}$ are a set of internuclear distances and $\{\theta_k\}$ a set of angles which together are *sufficient* to determine the molecular structure. Nelander[37] has shown that these quantities are related by the polyatomic virial theorem

$$V = 2W + \Sigma_i R_i(\partial W/\partial R_i) \quad (2)$$

where i runs over the set j, with all members of $\{R_j\}$ except R_i held constant during each differentiation. For a triatomic molecule, eq 2 may be written

$$V(R_1, R_2, \theta) = 2W(R_1, R_2, \theta) + R_1\partial W/\partial R_1 + R_2\partial W/\partial R_2 \quad (3a)$$

or

$$T(R_1, R_2, \theta) = -W(R_1, R_2, \theta) - R_1\partial W/\partial R_1 - R_2\partial W/\partial R_2 \quad (3b)$$

where R_1, R_2, and θ are the two bond lengths and the bond angle. By successively differentiating eq 3, one straightforwardly obtains a series of expressions relating various derivatives of T and V to derivatives of W.[36] If the derivatives are then evaluated at the equilibrium geometry, the T and V fields may be expressed in terms of the molecular force field. Thus if the force field W is written as

$$W = \sum_{\substack{i+j+k\le N \\ i,j,k\ge 0}} (\partial^{(i+j+k)}W/\partial q_1^{\,i}\partial q_2^{\,j}\partial q_3^{\,k}|_e q_1^{\,i} q_2^{\,j} q_3^{\,k}/i!\,j!\,k! \quad (4)$$

where the q's are the displacement coordinates $R_1 - R_{1e}$, $R_2 - R_{2e}$, and $\theta - \theta_e$, and $|_e$ indicates the derivatives are evaluated at the equilibrium geometry, then eq 3 and its derivatives allow one to determine the kinetic field

$$T = \sum_{\substack{i+j+k\le N-1 \\ i,j,k\ge 0}} (\partial^{(i+j+k)}T/\partial q_1^{\,i}\partial q_2^{\,j}\partial q_3^{\,k}|_e q_1^{\,i} q_2^{\,j} q_3^{\,k}/i!\,j!\,k! \quad (5)$$

and the analogous potential field. Note that an Nth order force field determines $N-1$th order T and V fields.

We have determined the T and V constants for a number of triatomic molecules. Unfortunately, the derivatives of W are not normally known to high accuracy, and errors in the force constant values are magnified in the determination of the T and V constants. Although experimental uncertainties are not necessarily closely related to statistical dispersions, we have treated the dispersions (when available) as errors, and carried them through the calculations. The final "uncertainties" are not quantitatively correct, but they do suggest which derivative values are meaningful and which are not. Some results are presented in Tables I–VII.

TABLE I: Linear Angle Derivatives for Bent Triatomics[a,b]

Molecule	$\partial T/\partial\theta$	$\partial V/\partial\theta$	% error	Ref
SO_2	−1.51	1.51	27	10
O_3	−1.38	1.38	28	12
SeO_2	−0.05	0.05	67	13
ClO_2	−0.49	0.49		14
H_2S	−0.36	0.36		16
H_2O	−0.86	0.86	24	17
H_2Se	−0.23	0.23		16
GeF_2	0.06	−0.06		21
OF_2	−0.59	0.59		1
NO_2	−1.55	1.55	3	23

[a] In this and following tables, T and V are in milliergs, R_1 and R_2 are in angstroms, and θ is in radians. [b] In this and following tables, % error is per cent uncertainty in T component derivative determined from statistical dispersions; see text.

TABLE II: Quadratic Angle Derivatives for Linear Triatomics

Molecule	$\partial^2T/\partial\theta^2$	$\partial^2V/\partial\theta^2$	% error	Ref
N_2O	3.10	−2.43	11	5
HCN	0.61	−0.35	18	6
CS_2	1.71	−1.14	2	8
CO_2	2.04	−1.26	1	9
BO_2^{-a}	−2.42	3.09	8	15
BO_2^{-b}	1.10	−0.43	10	15
ClCN	−0.42	0.77	20	18
OCS	1.46	−0.81	39	19
NCO^{-a}	−1.33	2.07	10	22
NCO^{-b}	2.23	−1.50	5	22
NCO^{-c}	2.30	−1.57	7	22

[a] In KCl matrix. [b] In KBr matrix. [c] In KI matrix.

TABLE III: Quadratic Bond-Angle Derivatives for Bent Triatomics

Molecule	$\partial^2T/\partial R\partial\theta$	$\partial^2V/\partial R\partial\theta$	% error	Ref
SO_2	4.76	−4.24	11	10
O_3	5.32	−4.78	88	12
SeO_2	−0.40	0.42	210	13
ClO_2	−15.19	15.35		14
H_2S	1.00	−0.86		16
H_2O	0.68	−0.23	152	17
H_2Se	0.11	−0.03	158	16
GeF_2	0.78	−0.80		21
OF_2	2.04	−1.83		1
NO_2	0.80	−0.14		23

III. Structural Rules

An inspection of Tables I–VII reveals a number of rules regarding the signs and magnitudes of various T and V derivatives.

1. In bent triatomics the kinetic component of the Born-Oppenheimer energy favors larger angles while the potential component favors smaller angles ($\partial T/\partial\theta < 0$, $\partial V/\partial\theta > 0$). This rule is rather surprising, as it attributes the same type of energetics to diverse molecules such as SO_2 and H_2O; nevertheless, it is well supported by the data. Nine of the ten molecules listed in Table I obey the rule, and the uncertainties in the force constants of the

TABLE IV: Quadratic Bond–Bond Derivatives

Molecule	$\partial^2 T/\partial R_1 \partial R_2$	$\partial^2 V/\partial R_1 \partial R_2$	% error	Ref
N_2O	−0.26	1.29	318	5
N_2O[a]	3.68	−2.65		20
HCN	1.58	−1.80	48	6
CS_2	3.02	−2.38	9	8
CO_2	5.28	−4.02	9	9
SO_2	3.44	−3.32	10	10
O_3	2.78	−1.05	171	12
SeO_2	1.01	−0.98	188	13
ClO_2	16.72	−16.63		14
BO_2^-[b]	4.82	−3.72		15
BO_2^-[c]	4.71	−3.63		15
H_2S	−0.08	0.07	714	16
H_2O	1.42	−1.54	74	17
H_2Se	0.41	−0.43	208	16
ClCN	3.49	−3.10	5	18
OCS	−6.08	7.12	238	19
GeF_2	0.12	0.14		21
NCO^-[b]	8.77	−7.52		22
NCO^-[c]	8.17	−6.96		22
NCO^-[d]	7.07	−5.94		22
OF_2	2.11	−1.28		1
NO_2	1.27	0.87	140	23

[a] In N_2 matrix. [b] In KCl matrix. [c] In KBr matrix. [d] In KI matrix.

TABLE V: Cubic Bond[2] Angle Derivatives for Bent Triatomics

Molecule	$\partial^3 T/\partial R^2 \partial\theta$	$\partial^3 V/\partial R^2 \partial\theta$	% error	Ref
SO_2	9.54	−12.72		10
O_3	17.06	−20.60	74	12
ClO_2	170.9	−161.7		14
H_2S	2.4	−3.2		16
H_2O	51.69	−52.67	63	17
NO_2	0.10	−0.68		23

exception, GeF_2, may be quite large. Hence we conclude that conventional arguments which attribute the large bond angle in H_2O to proton-proton repulsions[38] are not totally correct; the unshielded protons may indeed cause the large bond angle, but only indirectly, by shaping the electron distribution which determines $\partial T/\partial\theta$.

2. In linear triatomics V favors bending while T opposes bending ($\partial^2 T/\partial\theta^2 > 0$, $\partial^2 V/\partial\theta^2 < 0$, $|\partial^2 T/\partial\theta^2| > |\partial^2 V/\partial\theta^2|$). This rule is also well supported by the data, as shown in Table II. Five molecules obey the rule, in two cases (BO_2^- and NCO^-) KBr and KI matrix results agree with the rule, and in one case the rule is disobeyed. When taken together, rules 1 and 2 support an interpretation of T as the kinetic energy of a "particle-in-a-sector"[28-31] (any motion which increases the sector size decreases T). Moreover, rules 1 and 2 suggest that a model in which increased bending leads to increased attractive electrostatic interactions might be appropriate for V. A purely point-charge model would predict $\partial^2 V/\partial\theta^2$ to be positive, however, so higher terms are necessary.

3. In bent symmetric triatomics the kinetic bond-angle interaction is positive ($\partial^2 T/\partial R\partial\theta > 0$) *while the respective potential interaction is negative.* As shown in Table III, eight molecules obey this rule, while ClO_2 and SeO_2 do not. The uncertainty in the SeO_2 derivative is so great (210%), however, that this value is meaningless. The ClO_2 data are for an excited state, which may be atypical; no statistical dispersions were given for this molecule. This rule is also in accord with the "particle-in-a-sector" idea.

4. T makes a positive contribution to the bond-bond interaction force constant; V makes a negative contribution ($\partial^2 T/\partial R_1\partial R_2 > 0$, $\partial^2 V/\partial R_1\partial R_2 < 0$). Seventeen of the data sets in Table IV obey this rule. All of the data sets which disobey the rule, two partially and three completely, possess large or unknown dispersions. Hence this observation appears to be of quite general validity, applying to molecules with both positive and negative force constants. This result provides a new basis for the rule of Linnett and Hoare,[32,39] which states that molecules with localized bonding electrons have negative force constants and molecules with nonlocalized bonding electrons have positive force constants. The positive kinetic derivative should have a larger magnitude when there are nonlocalized bonding electrons.

TABLE VI: Cubic Bond-Angle[2] Derivatives

Molecule	Bond	$\partial^3 T/\partial R\partial\theta^2$	$\partial^3 V/\partial R\partial\theta^2$	% error	Ref
N_2O	N–N	−5.96	4.28	42	5
HCN	C–H	2.37	−0.48	152	6
HCN	C–N	1.06	−1.72	63	6
CS_2	C–S	−4.72	3.99	12	8
CO_2	C–O	−4.24	3.02	14	9
SO_2	S–O	−10.16	7.86	18	10
O_3	O–O	−9.40	5.34	317	12
ClO_2	Cl–O	35.48	−37.68		14
BO_2^-[a]	B–O	−4.14	4.84		15
BO_2^-[b]	B–O	−1.37	0.08		15
H_2S	H–S	4.76	−4.86	99	16
H_2O	H–O	6.46	−7.27	110	17
ClCN	C–N	−4.67	3.90	15	18
ClCN	C–Cl	−5.84	6.43	6	18
OCS	C–S	−3.61	2.39	236	19
OCS	C–O	−9.71	9.52	152	19
N_2O	N–O	−6.28	4.71	31	5
NO_2	N–O	−4.19	3.12		23
NCO^-[a]	C–O	−11.24	12.70		22
NCO^-[b]	C–O	−5.43	3.88		22
NCO^-[c]	C–O	−5.56	4.13		22
NCO^-[a]	C–N	−4.54	3.53		22
NCO^-[b]	C–N	−4.14	3.25		22
NCO^-[c]	C–N	−4.87	3.81		22

[a] In KCl matrix. [b] In KBr matrix. [c] In KI matrix.

TABLE VII: Cubic Bond–Bond Angle Derivatives for Bent Triatomics

Molecule	$\partial^3 T/\partial R_1\partial R_2\partial\theta$	$\partial^3 V/\partial R_1\partial R_2\partial\theta$	% error	Ref
SO_2	2.67	−3.56	9	10
O_3	−11.59	10.10	98	12
ClO_2	−15.19	15.35		14
H_2S	1.00	−0.86		16
H_2O	0.68	−0.23	152	17
NO_2	1.02	−2.19		23

5. For bent triatomics, $\partial^3 T/\partial R_1^2\partial\theta > 0$ *and* $\partial^3 V/\partial R_1^2\partial\theta < 0$. All six molecules in Table V support this rule. Note that for most molecules, $\partial^2 T/\partial R_1\partial\theta$ and $\partial^3 T/\partial R_1^2\partial\theta$ have the same sign; ordinarily a differentiation leads to a sign reversal.

6. For both linear and nonlinear triatomics, $\partial^3 T/\partial R\partial\theta^2 < 0$ *and* $\partial^3 V/\partial R\partial\theta^2 > 0$. Fourteen of the nineteen interactions displayed in Table VI obey this rule. The hydride molecules HCN, H_2O, and H_2S seems to be exceptions, but the estimated errors are quite large in these cases. As in rule 3, ClO_2 is an exception. There generally is a sign reversal between $\partial^2 T/\partial R\partial\theta$ and $\partial^3 T/\partial R\partial\theta^2$.

7. For nonlinear triatomics, $\partial^3 T/\partial R_1\partial R_2\partial\theta > 0$ *and* $\partial^3 V/\partial R_1\partial R_2\partial\theta < 0$. Four of the six cases listed in Table VII satisfy this relation. O_3 and ClO_2 do not, but both values are presumed to have large uncertainties.

8. Individual bond stretches follow the same pattern as in diatomics: $\partial T/\partial R_1 < 0$, $\partial V/\partial R_1 > 0$; $\partial^2 T/\partial R_1^2 > 0$, $\partial^2 V/\partial R_1^2 < 0$; $\partial^3 T/\partial R_1^3 < 0$, $\partial^3 V/\partial R_1^3 > 0$; $|\partial^n T/\partial R_1^n| \geq |\partial^n V/\partial R_1^n|$. This rule is, of course, not surprising. It is in accord with earlier observations[16] and values for particular derivatives are available from the authors.

Attempts to obtain a structural rule for $\partial^3/\partial R_1^2 \partial R_2$ derivatives failed, as the data are scattered and expected uncertainties are quite large.

The structural rules proposed here should not, of course, be accepted as "final." It is quite possible that new and improved data could modify some of the conclusions, and that molecules with unusual bonding patterns may be exceptions. Nevertheless, we believe that the proposed rules are basically correct, and that they will apply to the great majority of triatomic molecules.

IV. Model Force Fields

An exact model force field will automatically predict proper values for derivatives of T and V. If, however, a model is employed which does not predict all force constants precisely, then one may decompose the model force field into its kinetic and potential components to determine which terms are being treated accurately and which are not. In the following we report the results of such analyses of three model functions.

A. The Parr-Brown Model. Parr and Brown[28,29] have proposed that a Born–Oppenheimer potential function of the form

$$W = W_1/R_1 + W_2/R_2 + W_{11}/R_1^2 + W_{22}/R_2^2 + W_{12}/R_1R_2 + W_{112}/R_1^2R_2 + W_{122}/R_1R_2^2 + W_G \csc(\theta/2)/R_1R_2 \quad (6)$$

be employed to describe linear triatomics. They determined the W coefficients by a least-squares fit to the force constants for CO_2, OCS, HCN, and N_2O.[29] The W_1, W_2, W_{11}, and W_{22} coefficients were interpreted using a point-charge and particle-in-a-box model earlier found useful for diatomics;[40,41] the W_G term was justified by a particle-in-a-sector argument.

Smith and Overend have suggested[30,31] that eq 6 be modified to

$$W = W_1/R_1 + W_2/R_2 + W_{11}/R_1^2 + W_{22}/R_2^2 + W_1^6/R_1^6 + W_2^6/R_2^6 + W_{12}/R_1R_2 + W_\theta \tan^2[1/2(\pi - \theta)]/R_1^2R_2^2 \quad (7)$$

They used this function to study CO_2, CS_2, OCS, HCN, ClCN, and N_2O. Both the original and modified functions yielded force constants in reasonable agreement with experimental values.

By inspecting the T and V derivatives obtained from the original Parr–Brown potential function for CO_2, OCS, HCN, and N_2O, we have found that out of 84 distinct T and V derivatives, nine disagree in sign with the experimental values (three for CO_2, two for OCS, one for HCN, and three for N_2O). Some of the discrepancy is due to derivatives of the type $\partial^3 T/\partial R_1^2 \partial R_2$ and $\partial^3 V/\partial R_1^2 \partial R_2$; we regard the experimental values for these quantities as unreliable. In other cases, calculated derivatives which disagree with experiment but are in accord with the rules outlined in section III may, in fact, be more reliable than the experimental ones. Thus we distinguish between the 11 "unconfirmed" discrepancies for these molecules, and the four "confirmed" discrepancies, cases in which calculated values disagree both with experiment *and* with the rules of section III. For the potential function of eq 6, confirmed sign discrepancies occur for $\partial^2 V/\partial\theta^2$ of OCS, $\partial^2 V/\partial\theta^2$ of CO_2, $\partial^3 V/\partial R_{N\text{-}O}\partial\theta^2$ of N_2O, and for $\partial^3 V/\partial R_{N\text{-}N}\partial\theta^2$ of N_2O. There are no confirmed discrepancies for any kinetic derivatives or for any non-angle-dependent potential derivatives.

In the Smith and Overend studies of these same molecules, there are 18 unconfirmed discrepancies, but only one confirmed discrepancy ($\partial^2 V/\partial R_1 \partial R_2$ for HCN). The high number of unconfirmed discrepancies is due either to questionable terms involving $\partial^3/\partial R_1^2 \partial R_2$ or to cases in HCN and OCS where the predicted derivatives agree with the structural rules but the experimental values do not. Thus the modified potential function eq 7 is somewhat more accurate than eq 6, and supports the structural rules of section III. This function is also successful in treating CS_2 and ClCN, where there are six unconfirmed but only one confirmed discrepancy.

B. The Anderson Potential Function. Anderson has recently proposed[33,34] a potential function of the form

$$W(R_1, R_2, \theta) = W_D(R_1) + W_D(R_2) + A/R_3^N - B/(R_1 + \eta R_2)^n \quad (8)$$

where the W_D are functions obtained from the respective diatomic molecules *via* a Poisson's equation approach,[42] η is a scale parameter, and N is taken to be either 2 or 4. He evaluated his potential function for CO_2, CS_2, OCS, HCN, H_2O, SO_2, and O_3. For the two linear symmetric species, CO_2 and CS_2, a virial theorem analysis of his results shows that there are no confirmed or unconfirmed discrepancies; eq 8 seems to describe quite accurately this kind of molecule. These results are superior to those reported by Parr and Brown[29] and Smith and Overend.[31]

For the two nonsymmetric molecules, OCS and HCN, there are 17 unconfirmed and 4 confirmed discrepancies; these results are inferior to those reported in section IVA. Three of the four confirmed discrepancies involve derivatives of V.

The three nonlinear molecules, H_2O, SO_2, and O_3, are more difficult to model successfully. Anderson's results contain 20 unconfirmed and 10 confirmed discrepancies. All of the confirmed discrepancies involve angle-dependent derivatives, five of T and five of V. Thus the virial theorem analysis suggests that Anderson's function is quite accurate for symmetric linear species, somewhat less accurate for nonsymmetric linear molecules, and significantly less accurate for nonlinear triatomics.

C. Point-Charge Point-Dipole Model. One of us has recently proposed a point-charge point-dipole model for V which contains two parameters: q, a bond charge, and μ, a point dipole on the central atom.[36] The suggested form of V was

$$V(R_1, R_2, \theta) = -20(q^2e^2/9R_1) - 20(q^2e^2/9R_2) - 10[q\mu e \cos(\theta/2)/3R_1^2] - 10[q\mu e \cos(\theta/2)/3R_2^2] + [22q^2e^2/9(R_1^2 + R_2^2 - 2R_1R_2\cos\theta)^{1/2}] - [2q^2e^2/3(R_1^2 + 1/4R_2^2 - R_1R_2\cos\theta)^{1/2}] - [2q^2e^2/3(1/4R_1^2 + R_2^2 - R_1R_2\cos\theta)^{1/2}] \quad (9)$$

The parameters were evaluated using approximate relations obtained from the virial theorem and their values were shown to be in accord with chemical intuition. Approximate values for $\partial^3 W/\partial R_1^3$ and $\partial^2 W/\partial\theta^2$ were predicted.[36] Now that experimental values for $\partial V/\partial R_1$ and $\partial V/\partial\theta$ are available, we have determined q and μ parameters for

CO_2, CS_2, SO_2, O_3, SeO_2, ClO_2, BO_2^-, H_2S, H_2O, H_2Se, and OF_2. The new q values are generally larger than those obtained previously ($q_{old}(H_2O) = 1.16$, $q_{new}(H_2O) = 1.60$; $q_{old}(CO_2) = 2.30$, $q_{new}(CO_2) = 3.62$), so the connection between q values and bond orders is now less satisfactory.

Values for derivatives of V were calculated, and their signs were compared to those predicted by the structural rules. We found that the signs of $\partial^2V/\partial R_1^2$, $\partial^2V/\partial R_1\partial\theta$, $\partial^3V/\partial R_1^3$, and $\partial^3V/\partial R_1\partial R_2\partial R_3$ are predicted correctly, the signs of $\partial^2V/\partial R_1\partial R_2$, $\partial^2V/\partial\theta^2$, and $\partial^3V/\partial R_1^2\partial\theta$ are incorrect, and results for $\partial^3V/\partial R_1\partial\theta^2$ are ambiguous. Thus, our conclusions are in agreement with those obtained by Ray and Parr.[43] The initial formulation of the model appears to be chemically useful at the simple quadratic valence force field level, but an improved expression for V, capable of correctly predicting more derivatives, will require the inclusion of other electrostatic interactions, such as point charge point quadropole or point dipole point dipole terms.

V. Conclusion

The virial theorem decomposition technique is a useful procedure for extracting physical information from empirically determined force fields. By decomposing the force fields of a number of triatomic molecules, we have developed a set of rules regarding the contributions of T and V to molecular structure. The rules have been shown to be of interpretive value, and can be further employed to study the strengths and weakness of model force fields.

Acknowledgment. The generous support provided by the Wichita State University Research Committee is gratefully acknowledged.

References and Notes

(1) Y. Morino, *Pure Appl. Chem.*, **18**, 323 (1969).
(2) J. Overend, *Ann. Rev. Phys. Chem.*, **21**, 265 (1970).
(3) T. Shimanouchi in "Physical Chemistry: An Advanced Treatise," Vol. 4, H. Eyring, D. Henderson, and W. Jost, Ed., Academic Press, New York, N. Y., 1970, Chapter 6.
(4) T. Shimanouchi and I. Nakagawa, *Ann. Rev. Phys. Chem.*, **23**, 217 (1972).
(5) I. Suzuki, *J. Mol. Spectrosc.* **32**, 54 (1969).
(6) T. Nakagawa and Y. Morino, *Bull. Chem. Soc. Jap.*, **42**, 2212 (1969).
(7) D. F. Smith and J. Overend, *J. Chem. Phys.*, **54**, 3632 (1971).
(8) J. Giguere, V. K. Wang, and J. Overend, *Spectrochim. Acta, Sect. A*, **29**, 1197 (1973).
(9) I. Suzuki, *J. Mol. Spectrosc.* **25**, 479 (1968).
(10) A. Barbe, L. Secroun, and P. Pourre, *J. Phys.*, **33**, 209 (1972).
(11) T. Tanaka and Y. Morino, *J. Mol. Spectrosc.*, **33**, 538 (1970).
(12) D. F. Smith, *Spectrochim. Acta, Sect. A*, **29**, 1517 (1973).
(13) H. Takeo, E. Hirota, and Y. Morino, *J. Mol. Spectrosc.*, **34**, 370 (1970).
(14) J. C. D. Brand, R. W. Redding, and A. W. Richardson, *J. Mol. Spectrosc.*, **34**, 399 (1970).
(15) D. F. Smith, *J. Chem. Phys.*, **58**, 4776 (1973).
(16) K. Kuchitsu and Y. Morino, *Bull. Chem. Soc. Jap.*, **38**, 814 (1965).
(17) D. F. Smith and J. Overend, *Spectrochim. Acta, Sect. A*, **28**, 477 (1972).
(18) C. Murchison and J. Overend, *Spectrochim. Acta., Sect. A*, **27**, 1801 (1971).
(19) Y. Morino and T. Nakagawa, *J. Mol. Spectrosc.*, **26**, 496 (1968).
(20) D. F. Smith, J. Overend, R. Spiker, and L. Andrews, *Spectrochim. Acta, Sect. A*, **28**, 87 (1972).
(21) H. Takeo, F. Curl, and D. W. Wilson, *J. Mol. Spectrosc.*, **38**, 464 (1971).
(22) D. F. Smith and J. Overend, *J. Chem. Phys.*, **58**, 1636 (1973).
(23) D. F. Smith and J. Overend, *Spectrochim. Acta, Sect. A*, **28**, 2387 (1972).
(24) Z. Cihla and A. Chedin, *J. Mol. Spectrosc.*, **40**, 337 (1971).
(25) Y. Morino, K. Kuchitsu, and S. Yamamoto, *Spectrochim. Acta, Sect. A*, **24**, 335 (1968).
(26) J. M. Riveros, *J. Chem. Phys.*, **51**, 1269 (1969).
(27) M. Krauss, *Ann. Rev. Phys. Chem.*, **20**, 39 (1970).
(28) R. G. Parr and J. E. Brown, *J. Chem. Phys.*, **49**, 4849 (1968).
(29) J. E. Brown and R. G. Parr, *J. Chem. Phys.*, **54**, 3429 (1971).
(30) D. F. Smith, Jr., and J. Overend, *J. Chem. Phys.*, **53**, 2411 (1970).
(31) D. F. Smith, Jr., and J. Overend, *J. Chem. Phys.*, **57**, 523 (1972).
(32) K. Machida and J. Overend, *J. Chem. Phys.*, **50**, 4429 (1969).
(33) A. B. Anderson, *J. Chem. Phys.*, **56**, 4228 (1972).
(34) A. B. Anderson, *J. Chem. Phys.*, **57**, 4143 (1972).
(35) V. K. Wang and J. Overend, *Spectrochim. Acta, Sect. A*, **29**, 1623 (1973).
(36) G. Simons, *J. Chem. Phys.*, **56**, 4310 (1972).
(37) B. Nelander, *J. Chem. Phys.*, **51**, 469 (1969).
(38) C. A. Coulson, "Valence," 2nd ed, Oxford University Press, London, 1961.
(39) J. W. Linnett and M. F. Hoare, *Trans. Faraday Soc.*, **45**, 844 (1949).
(40) R. G. Parr and R. F. Borkman, *J. Chem. Phys.*, **49**, 1055 (1968).
(41) R. F. Borkman, G. Simons, and R. G. Parr, *J. Chem. Phys.*, **50**, 58 (1969).
(42) A. B. Anderson and R. G. Parr, *J. Chem. Phys.*, **55**, 5490 (1971).
(43) N. K. Ray and R. G. Parr, *J. Chem. Phys.*, **59**, 3934 (1973).

Aromatic Radical Cation Formation on the Intracrystal Surfaces of Transition Metal Layer Lattice Silicates

T. J. Pinnavaia,* Peter L. Hall, Sharmaine S. Cady, and M. M. Mortland

The Department of Chemistry and the Departments of Crop and Soil Science and Geology, Michigan State University, East Lansing, Michigan 48824 *(Received October 29, 1973)*

Publication costs assisted by Michigan State University

The adsorption of selected aromatic molecules on the intracrystal surfaces of Fe(III) and VO^{2+} exchange forms of a layer lattice silicate (hectorite) has been studied by ir, uv-visible, and esr spectroscopy. In addition to aromatic radical cation formation, type II species, which exhibit an intense charge-transfer band in the ir region and vibrational frequencies that are substantially shifted relative to the parent molecule, are formed with benzene on the Fe(III) exchange form and with anisole and thiophene on both Fe(III) and VO^{2+} exchange forms. The complexes are identical with those previously observed on Cu(II) layer lattice silicates. It is suggested that the type II species are *associated* radical cations formed by electron transfer from the parent molecule to the metal ion. Toluene radical cation formation is accompanied by polymerization, and the polymer apparently inhibits radical cation association.

Introduction

In an earlier report[1] from these laboratories it was shown that the chemisorption of benzene on the interlamellar surfaces of copper(II) montmorillonite under dehydrating conditions results in the formation of two distinct species distinguishable by infrared spectroscopy: a green-yellow type I complex containing a planar C_6H_6 ring, and an intensely red type II species in which the ring no longer appears to be planar and aromaticity is apparently lost or greatly perturbed. The type I benzene is observed under conditions where the degree of hydration of the mineral is greater than that necessary for formation of type II benzene, and the two forms can be reversibly interconverted by adding or removing controlled amounts of water. Phenol and alkyl-substituted benzenes have been found to form only type I complexes,[2,3] but both type I and type II species have also been observed with anisole and related aromatic ethers,[4] biphenyl, naphthalene, and anthracene,[5] and thiophene.[6]

The vibrational spectra of the type I complexes are consistent with the aromatic ring being edge-bonded to copper(II) in a manner analogous to that found in $Ag(C_6H_6)ClO_4$[7] and $Cu(C_6H_6)AlCl_4$.[8] This mode of bonding is further supported by spectral similarities between aromatics chemisorbed on the Ag(I) exchange form of montmorillonite and the corresponding type I Cu(II) complexes.[9]

The nature of the type II species, however, is considerably less certain. The principal spectral feature of all type II aromatics is the presence of a very low energy electronic transition in the ir region which extends from *ca.* 1600 cm^{-1} to beyond 4000 cm^{-1}. They also exhibit C–C stretching and C–H deformation bands which are strongly shifted relative to those characteristic of the parent aromatic molecule. Type II benzene, for example, shows two intense C–C stretching bands at 1540 and 1480 cm^{-1} and a broad C–H deformation near 790 cm^{-1}. In comparison, the corresponding vibrations in liquid benzene are found near 1478 and 675 cm^{-1}, respectively.

In a recent esr study, Rupert[5] has found that upon formation of type II species the $g_\parallel$ and $g_\perp$ resonance components of Cu(II) are lost and a new band is obtained which exhibits a width of 3 G between points of extreme slope and a g value (2.0024) near that expected for a free spinning electron. The ratios of integrated signal intensities revealed that only a small fraction of the Cu(II) spins lost are recovered as free electron spins. He suggested that the type II species involved the formation of radical cations or divalent cations as a result of electron transfer from the arene to copper(II). The lack of proton hyperfine splitting was interpreted in terms of rapid electron exchange between the radical cation and neutral molecule or the dication. The loss of spin density was attributed to the initial formation of a dication or electron transfer between radical cations to give a dication and the neutral molecule. An alternative suggestion was that a paramagnetic complex is formed which has an unfavorable relaxation time to be detected by esr.

Rupert's suggestion of radical cation or divalent cation formation is in accord with our observation that type II anisole is oxidized to type II 4,4′-dimethoxybiphenyl[4] and with Matsunaga's discovery[10] that the uv-visible spectra of adsorbed phenolthiazine and tetrathiotetracene on Cu(II) montmorillonite are consistent with the presence of only the radical cation and divalent cation, respectively. Although Matsunaga also found that adsorbed perylene exhibits electronic bands characteristic of the radical cation, the band near 4000 cm^{-1} could not be assigned to a transition of the radical cation, the dication, or the dimeric perylene cation. It was suggested that the new perylene species is formed by interaction of radical cations and the neutral molecules.

In view of Rupert's and Matsunaga's findings it becomes of interest to determine whether type II aromatics are truly complexes formed between aromatic cations and other organic species present on the surface or if the copper ion plays an intimate role in their formation. If Cu(II) functions merely as an oxidizing agent to generate the aromatic cations needed to form an organic complex, then it should be possible to form these complexes with metal ions which are stronger oxidizing agents than Cu(II). Therefore, the present study of the chemisorption of ben-

zene and other aromatic molecules on VO^{2+} and Fe^{3+} exchange forms of a layer lattice silicate was undertaken.

Experimental Section

Preparation of Homoionic Hectorites. Hectorite was obtained from the Baroid Division of the National Lead Co. The approximate unit cell formula is $Na_{0.66}(Mg_{5.34}Li_{0.66})(Si_8)O_{20}(OH,F)_4$. This mineral is structurally similar to montmorillonite except that the negative charge on the silicate layers arises from substitution of Li(I) for Mg(II) in the octahedral layer. The vanadyl exchange form of the mineral was prepared by stirring the fraction of the clay below 2 μ esd with an 0.25 *M* aqueous vanadyl sulfate solution. The procedure was carried out three times to maximize the exchange. Excess salt was removed by repeated washing with distilled water until the washings were sulfate free. Analysis for total vanadium (Galbraith Laboratories, Knoxville, Tenn.) showed the mineral to contain 63 mequiv of VO^{2+}/100 g, in comparison to the total exchange capacity of approximately 90 mequiv/100 g. Samples of Fe(III) and Cu(II) hectorite were prepared in an entirely analogous manner using aqueous chloride solution. A sample of the vanadyl hectorite was slurried three times with a 0.5 *M* $CaCl_2$ solution to determine whether the VO^{2+} ions were exchangeable. Chemical analysis indicated that at least 80% of the VO^{2+} could be exchanged in this manner.

Cu(II)-doped Zn(II) hectorite was prepared by three successive 1-hr treatments of 10 g of the mineral in 500 ml of methanol containing 1 mequiv of $CuCl_2 \cdot 2H_2O$ and 9 mequiv of $ZnCl_2 \cdot 2H_2O$. The mineral was washed free of Cl^- with methanol. The powder was air dried, suspended in 300 ml of water for several hours to displace adsorbed methanol, and then freeze dried.

Thin, self-supporting film samples for use in the ir and uv-visible studies were formed by depositing a few milliliters of an aqueous suspension of the mineral onto a Teflon sheet, and allowing air evaporation to take place. Considerable particle orientation is obtained in this way, the basal planes of the silicate layers being aligned predominantly in the plane of the film.

Formation of Arene Complexes. Air-dried film or powder samples of VO^{2+} and Fe^{3+} hectorite were placed in a P_2O_5 desiccator containing a small beaker of the hydrocarbon. Color changes were observed as the aromatic molecules were adsorbed onto the mineral surfaces. Benzene was also adsorbed on VO^{2+} hectorite using Rupert's method of suspending the mineral in boiling benzene and removing adsorbed water by azeotropic distillation. Perylene was adsorbed on Cu(II) and Cu(II)-doped Zn(II) hectorite by suspending the mineral for 4 hr in a saturated solution of perylene in acetone at room temperature, filtering the suspension, and drying the mineral in a stream of dry nitrogen for several hours. As acetone is lost in the drying procedure, the Cu(II) saturated minerals turns from brown to purple and the Cu(II)-doped Zn(II) form changes from yellow to lavender.

Subsequent to complex formation, all samples were handled in a dry nitrogen atmosphere to avoid decomplexation of the aromatic species by moisture.

Spectroscopic Measurements. X-Band electron spin resonance spectra were recorded using a Varian E4 spectrometer operating in the range 9.48–9.52 GHz. Measurement of *g* values was made relative to a standard pitch sample. Spectra at 77°K were obtained by immersing the sample tube in a Dewar filled with liquid nitrogen. The spectrometer gain was varied depending on sample size, but care was taken to ensure that the modulation amplitude did not exceed half the line width. Infrared spectra in the range 4000–600 cm^{-1} were recorded on a Beckman IR-7 spectrophotometer. Samples were mounted in a brass cell fitted with NaCl windows. Uv-visible absorption spectra in the range 200–800 mμ were recorded on a Cary 15 spectrophotometer. A thin film of Na^+ hectorite was used as a reference sample. The sample and reference were coated with Nujol oil and sandwiched between quartz disks to reduce scattering and to protect the complexes from atmospheric moisture.

Results

Benzene. The exposure of a freshly prepared sample of Fe(III) hectorite to benzene vapor in the presence of P_2O_5 causes the mineral to turn from the yellow characteristic of hydrated Fe(III) to a deep red color. A similar color transformation occurs when the mineral is slurried in boiling benzene and the water removed by azeotropic distillation. The infrared spectrum of the chemisorbed benzene is shown in Figure 1 along with the spectra of the parent mineral and of type II benzene on Cu(II) hectorite. As can be seen from the figure, the bands at 1540, 1480, 1195, and 790 cm^{-1} are identical with those present for the type II species on the Cu(II) exchange form.[1] Also, the characteristic electronic absorption which extends from 1600 to beyond 4000 cm^{-1} is present. Matsunaga[10] has found this latter band to be centered at 4400 cm^{-1} for type II benzene on Cu(II) montmorillonite.

As shown in Figure 2a, type II benzene on Fe(III) hectorite exhibits at least two overlapping, broad absorptions in the uv-visible spectrum in the range 300–600 nm. Two well-resolved bands near 430 and 500 nm and a weak band near 560 nm are found in the spectrum of type II benzene on Cu(II) hectorite and montmorillonite.[2,10] Figure 3a and 3b illustrate that upon formation of the type II species, the broad esr resonance characteristic of Fe(III) is replaced by a new sharp band of reduced intensity and with $g = 2.0028$ and width 3.5 ± 0.3 G. A totally analogous loss of the metal ion signal and appearance of a free radical signal occurs upon type II benzene formation on Cu(II) montmorillonite[5] and hectorite. We find, in agreement with Rupert's results, that only *ca.* 1% of the Cu(II) spins lost upon type II benzene formation are recovered as free radical spins.

The observation of type II benzene on Fe(III) hectorite is in contrast to an earlier report[11] that Fe(III) layer lattice silicates absorb benzene by physical means only. The sample of Fe(III) hectorite used in the present study was freshly prepared. When the experiments were repeated using Fe(III) hectorite or montmorillonite that had been allowed to age for 3 weeks to several months or more under ambient conditions, only physically absorbed benzene was observed. It is possible that aging renders the Fe(III) exchange form inert due to formation of polymeric iron oxides or hydroxides[12] which reduce the oxidation potential of the metal ion or hinder the access of the benzene molecules to the metal ion positions on the exchange sites.

While still moist, freshly prepared vanadyl hectorite exhibits a light blue color characteristic of the aqueous vanadyl ion $VO(H_2O)_5^{2+}$. The light blue color is lost and a tan color develops when the sample is air dried or freeze dried. Subsequent exposure of the tan-colored mineral to water vapor results in fairly rapid conversion to a bright

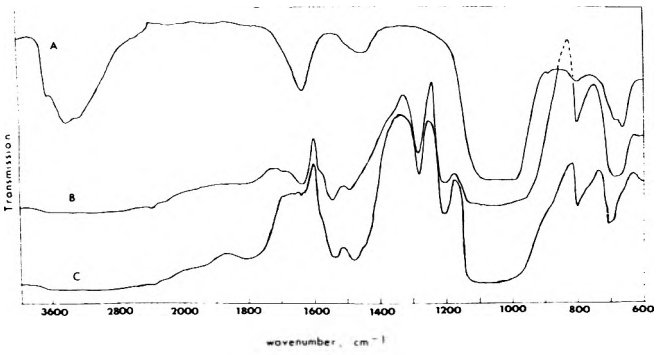

Figure 1. Infrared spectra of (a) Fe(III) hectorite, (b) type II benzene on Fe(III) hectorite, and (c) type II benzene on Cu(II) hectorite.

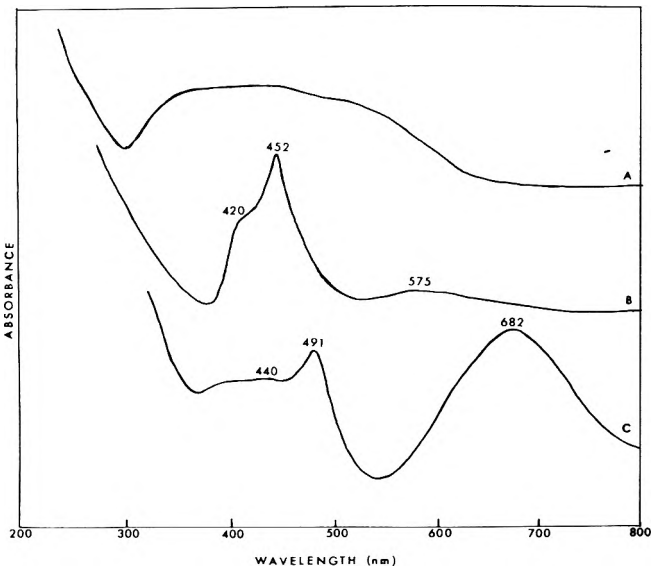

Figure 2. Uv-visible spectra of Fe(III) hectorite with (a) type II benzene, (b) chemisorbed toluene, and (c) type II anisole present on the intracrystal surfaces.

yellow color. This change is also induced, though more slowly, by atmospheric moisture. The change could not be reversed either by vacuum drying over P_2O_5 or by heating for 24 hr at 110°. X-Ray diffraction studies of the tan and yellow forms of vanadyl hectorite indicate in each case a broad (001) reflection. The average d_{001} value corresponds to about 13.0 Å for the tan form and 14.3 Å for the yellow form, compared with about 9.6 Å for the completely dehydrated mineral. One may conclude that both forms consist of randomly interstratified mono- and dimolecular layers of water between the silicate sheets, the yellow form having a greater proportion of dimolecular layers.

The infrared spectra of the tan and yellow forms in the range 4000–600 cm^{-1} exhibit bands attributable to the silicate lattice or to adsorbed water. Since the V=O stretching mode lies in the range 985 ± 50 cm^{-1} [13] the band is probably obscured by the silicate absorption centered at ~1000 cm^{-1}. The esr spectrum of the light-blue vanadyl hectorite (Figure 4a) exhibits an isotropic, eight-line spectrum characteristic of rapidly tumbling aqueous vanadyl ions. From the spectrum one obtains g = 1.971 ± 0.002 and hyperfine splitting parameter A = 110 ± 1.0 G. In contrast, the tan form exhibits an anisotropic spectrum having the appearance of an axially symmetric system (Figure 4b) which is characteristic of VO^{2+} ions in an en-

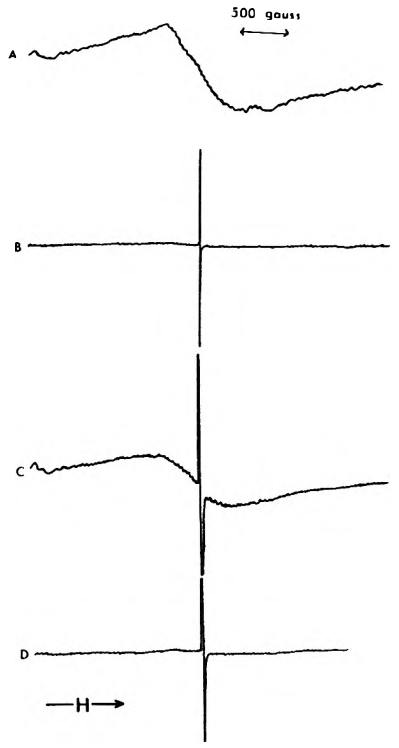

Figure 3. Esr spectra for (a) Fe(III) hectorite and Fe(III) hectorite in presence of adsorbed (b) benzene (type II), (c) toluene, and (d) thiophene (type II).

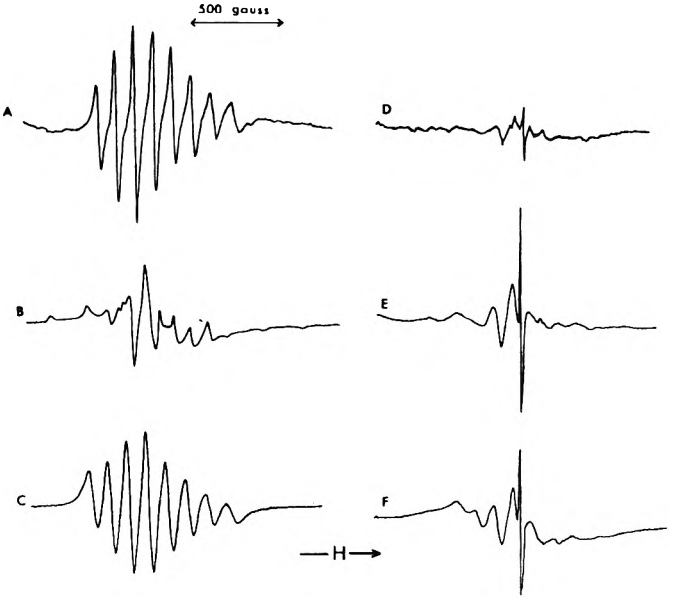

Figure 4. Esr spectra of the (a) blue, (b) tan, and (c) yellow forms of VO^{2+} hectorite and of VO^{2+} hectorite containing adsorbed (d) benzene, (e) toluene, and (f) anisole (type II).

vironment in which molecular rotation is restricted. The spectrum may be fitted approximately to the usual spin Hamiltonian.

$$\mathcal{H} = g_{\parallel}\beta H_z S_z + g_{\perp}\beta(H_x S_y + H_y S_y) + A_{\parallel} I_z S_z + A_{\perp}(I_x S_x + I_y S_y)$$

with g = 1.931 ± 0.003, A = 198.5 ± 1.0 G, and $g_{\perp}$ = 1.987 ± 0.003, $A_{\perp}$ = 79.0 ± 1.0 G. The yellow form of vanadyl hectorite, like the blue form, exhibits an isotropic

spectrum (Figure 4c) having $g = 1.974 \pm 0.002$ and $A = 110 \pm 1.0$ G. The isotropic nature of the spectrum suggests that rapid molecular rotation or Jahn-Teller rearrangement is taking place.

Irrespective of which color form of VO^{2+} hectorite is exposed to benzene vapor in presence of P_2O_5, the mineral adopts a green color. Infrared spectral bands at 1478 (C–C stretching) and 688 cm^{-1} (C–H deformation) indicate the presence of physically bound benzene.[1] However, the esr spectrum (Figure 4d) shows a weak free radical signal in addition to the VO^{2+} signal, indicating that some electron transfer does take place. Also, a band is present at 385 nm in the electron spectrum (Figure 5a) which cannot be assigned to physically adsorbed benzene. After aging several days, the green mineral turns brown and all infrared bands attributable to benzene are absent. Weak absorptions occur at 1598, 1510, 1491, and 1450 cm^{-1} which may reflect the existence of a polymeric product.

Toluene. The adsorption of toluene on Fe(III) hectorite under dehydrating conditions causes the mineral to turn dark green. The infrared spectrum exhibits C–C stretching and C–H out-of-plane deformation bands at 1495 and 738 cm^{-1}, respectively, which are indicative of physically adsorbed toluene.[2] In addition, new bands appear at 1435, 1365, 1300, and 1944 cm^{-1} which are attributable to the presence of a polymer. Extraction of the mineral with methanol or acetone yields, in addition to free toluene, a brown, waxy substance which exhibits vibration bands near those found for the adsorbed polymer. The infrared spectrum of toluene on VO^{2+} hectorite is identical with that described for the Fe(III) exchange form, and the same polymeric material can be desorbed with methanol. A polymer free of Cu(II) can also be desorbed from toluene on Cu(II) hectorite and montmorillonite under conditions where the type I complex is present, but this polymer is a red solid which exhibits strong to medium bands at 1600, 1505, 1490, 1450, 1305, 1170, 1140, 1075, 1020, 810, 55, 726, and 705 cm^{-1}. In contrast, the desorption of type II benzene from Cu(II) hectorite affords mainly free benzene. For example, the extraction of 50 g of Cu(II) hectorite containing *ca.* 4.0 g of type II benzene affords less than 5 mg of polymeric solid when extracted with methanol.

As illustrated in Figure 2b and 5b, chemisorbed toluene on Fe(III) and VO^{2+} hectorite exhibits two strong bands near 410 and 455 nm and weak bands in the region 550–650 nm. The 410- and 450-nm bands are present for toluene adsorbed on Cu(II) hectorite and montmorillonite, and two weak bands are resolved at 555 and 610 nm. The desorbed polymer exhibits bands at 402 and 430 nm.

Although there is no indication of the low-energy electronic absorption characteristic of a type II species, the esr spectra of the Fe(III), VO^{2+}, and Cu^{2+} exchange forms of hectorite containing chemisorbed toluene all show a sharp free-radical signal near $g = 2.00$, the intensity of the transition metal ion signal being significantly reduced. Figures 3c and 4e illustrate the esr spectra for toluene on the Fe(III) and VO^{2+} forms, respectively.

Anisole. The adsorption of anisole on VO^{2+} hectorite is remarkably analogous to its adsorption on the Cu(II) exchange form of the mineral. In both cases the mineral develops an intense blue color which can be rapidly transformed to a brilliant green upon exposure to atmospheric moisture. It has been previously shown in the case of Cu(II) that the blue species is a type II anisole complex, whereas the green species is a type II complex of 4,4′-dimethoxybiphenyl. Both exhibit the characteristic electronic band which extends well into the infrared. The vibration spectra of both species have been described in detail in a previous report.[4]

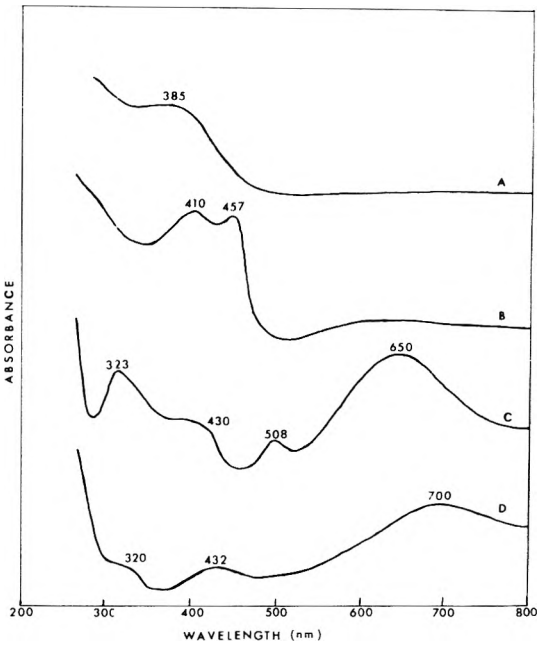

Figure 5. Uv-visible spectra of VO_2^+ hectorite with adsorbed (a) benzene, (b) toluene, (c) anisole (type II), and (d) 4,4′-dimethoxybiphenyl (type II) present on the interlamellar surfaces.

The adsorption of anisole on Fe(III) hectorite also leads to the formation of blue type II anisole. Its exposure to water vapor provides a brown product which can be desorbed with acetone. The infrared spectrum of the desorbed solid contains predominantly bands which may be attributed to 4,4′-dimethoxybiphenyl, but additional bands are present which suggest the presence of higher polymerization products. Thus type II anisole on Fe(III) hectorite is oxidized in part to 4,4′-dimethoxybiphenyl, but further oxidation probably also occurs to give higher oligomers.

Figure 2c shows the absorption bands in the uv-visible spectrum of type II anisole on Fe(III) hectorite. At least three bands are present at 440, 491, and 682 nm. On VO^{2+} hectorite these three bands are slightly shifted in energy, and a fourth band is resolved at 323 nm (*cf.* Figure 5c). Type II anisole on Cu(II) hectorite exhibits bands in the same regions.

The esr spectra of Fe(III), VO^{2+}, and Cu(II) hectorites containing type II anisole all exhibit a narrow line at $g = 2.0029$ and a weak transition metal ion signal which is significantly reduced in intensity in comparison to the original mineral. The spectrum in the case of the VO^{2+} exchange form is shown in Figure 4f. Type II 4,4′-dimethoxybiphenyl formation on VO^{2+} and Cu(II) hectorite is also accompanied by the appearance of a sharp free-radical signal at $g = 2.0029$. The brown product which forms upon exposure of type II anisole on Fe(III) hectorite to water vapor does not give rise to a free-radical signal; only the signal characteristic of Fe(III) is present under these conditions.

Thiophene. Both VO^{2+} and Fe(III) hectorite adopt a green color on exposure to thiophene and exhibit infrared spectra closely similar to the blue, type II thiophene complex recently found by Cloos and coworkers[6] on Cu(II)

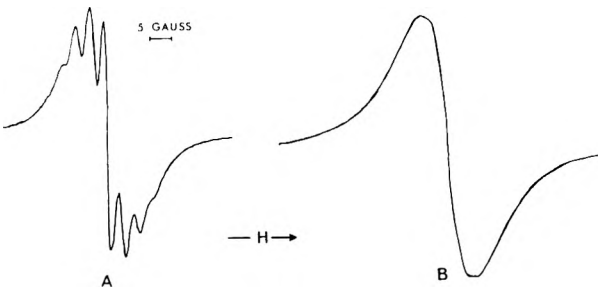

Figure 6. Esr spectra of (a) Cu(II)-doped Zn(II) hectorite and (b) Cu(II) hectorite in presence of adsorbed perylene.

montmorillonite. All three exchange forms with thiophene exhibit the characteristic infrared absorption above 1600 cm^{-1} and sharp free-radical in their esr spectra. In each case the resonance signal characteristic of the metal ion is almost entirely absent. The spectrum obtained with type II thiophene on Fe(III) hectorite is illustrated in Figure 3d.

Esr Hyperfine Splitting. Several attempts were made to observe proton hyperfine splitting of the free-radical signal associated with the chemisorption of the aromatic molecules described above. None could be observed even at 77°K for any of the systems studied. A sample of type II benzene on Cu(II) montmorillonite gave a single, sharp resonance even at 8°K. The g values and line widths observed at ambient temperature are summarized in Table I.

It was found, however, that the absorption of perylene from acetone solution onto Cu(II)-doped Zn(II) hectorite gives rise to an esr signal with $g = 2.0021 \pm 0.0003$ and nine hyperfine components separated by 3.25 G. Perylene on Zn(II) hectorite itself does not give an esr signal. The former spectrum, illustrated in Figure 6a, is essentially the spectrum previously observed for the perylene radical cation on silica–alumina catalysts.[14-17] It is to be noted that the resolved hyperfine structure is much less than can be observed for the ion solution.[18] Brouwer[15] has attributed the lower resolution of hyperfine splitting to some contribution of the anisotropic part of the paramagnetic absorption of the adsorbed ions which are neither completely free to tumble nor too rigidly fixed. Integration of the Cu(II) and perylene$^+$ signals indicates that about 3% of the Cu(II) spins lost are recovered as perylene radical cation spins.

The presence of the perylene radical cation is further verified by the presence in the uv-visible spectrum of a band at 545 nm. This band has been well established for the radical ion in solution.[19] Additional bands appear at 388, 412, 433, and 438 nm which are indicative of the presence of neutral perylene.[19] Also, a weak band at 645 nm is present which has been previously assigned to the protonated perylene ion on silica surfaces.[15] The vibrational spectrum of the adsorbed perylene is obscured by the presence of coadsorbed acetone, but the strong infrared absorption from 1600 to beyond 4000 cm^{-1} characteristic of a type II species is clearly evident.

The esr spectrum of perylene on Cu(II)-saturated hectorite gives only a single line (*cf.* Figure 6b). Apparently, increasing the surface density of radical ions results in the loss of proton hyperfine structure. This result is in accord with Rupert's suggestion that rapid electron exchange is responsible for the absence of hyperfine structure for the radical cation of benzene and substituted benzenes. Unfortunately, no hyperfine structure could be observed for the radical signal associate with type II benzene on Cu(II)-doped Zn(II) hectorite.

TABLE I: g Values and Line Widths of Esr Free-Radical Signals Associated with the Chemisorption of Aromatic Molecules on VO^{2+} and Fe(III) Hectorite[a]

Cation	Molecule	g (± 0.0001)	ΔH, G
VO^{2+}	Anisole	2.0029	0.9 ± 0.1
VO^{2+}	4,4′-Dimethoxybiphenyl	2.0029	0.7 ± 0.1
VO^{2+}	Toluene	2.0029	6.0 ± 0.5
VO^{2+}	Benzene	2.0028	8.0 ± 0.5
VO^{2+}	Thiophene	2.0037	4.0 ± 0.5
Fe^{3+}	Anisole	2.0028	3.5 ± 0.3
Fe^{3+}	Toluene	2.0029	6.5 ± 0.5
Fe^{3+}	Benzene	2.0028	3.5 ± 0.3
Fe^{3+}	Thiophene	2.0036	5.0 ± 0.5

[a] All data were obtained at ambient temperature.

Discussion

The formation of type II benzene on both Cu(II) and Fe(III) hectorite and of type II anisole, 4,4′-dimethoxybiphenyl, and thiophene on Cu(II), Fe(III), and VO^{2+} exchange forms of the mineral indicates that the role of the metal ion is simply to serve as an oxidizing agent to form organic radicals which may subsequently interact among themselves or with other organic species present on the interlamellar surfaces. The previously reported[5,11] absence of type II complex formation in the adsorption of nitrobenzene or chlorobenzene on Cu(II) layer lattice silicates or with benzene adsorption on a variety of other metal ion exchange forms of these minerals (*e.g.*, Co(II), Mn(II), Ni(II), or Cr(III)) is now readily explained in terms of unfavorable redox couples for these systems.

The oxidizing role of Cu(II), Fe(III), and VO^{2+} is further demonstrated by the conversion of type II anisole to type II 4,4′-dimethoxybiphenyl and by the oxidation of toluene to polymers or oligomers. The polymerization of benzene and related coupling reactions of other aromatic nuclei by Cu(II) and Fe(III) in homogeneous solution has been well documented by the work of Kovacic.[20,21] Thus it is not surprising that these metal ions and VO^{2+} should also oxidize aromatic molecules when present on the intracrystalline surfaces of a layer lattice silicate. Whether the structures of the toluene polymers formed on the silicate surface are analogous to those formed in solution remains to be investigated.

The exchange-narrowed free-radical esr signal associated with the formation of each of the type II species is undoubtedly due to the organic radical cation $[Ar\cdot]^+$ formed by one electron transfer from the parent molecule to the transition metal ion

$$Ar + M^{n+} \longrightarrow [Ar\cdot]^+ + M^{(n-1)+}$$

In the case of 4,4′-dimethoxybiphenyl formed from anisole, the radical cation may result from coupling of the anisole radical cation and a neutral anisole molecule.[4] No esr signal is observed at room temperature for the reduced form of the metal ion as it is either diamagnetic (Cu(I)) or a non-Kramer paramagnetic ion (Fe(II), V(III)). The presence of the radical cation of perylene in the type II perylene–Cu(II)-doped Zn(II) hectorite system is unequivocally established by the uv-visible and esr results. Moreover, the presence of $C_6H_6^+$ in the type II benzene systems is indicated by a weak band at 560 nm as $C_6H_6^+$ in organic

glasses at 77°K[22,23] and on silica gel[24] exhibits a band in this region. The band near 430 cm^{-1} may be due to the carbonium ion $C_6H_7^+$ since a band at 400 nm has been attributed to this species in liquid HF.[25] The presence of the protonated perylene ion in the type II perylene system on Cu(II)-doped Zn(II) hectorite is indicated by the band at 645 nm.

Despite the evidence for the presence of radical cations and carbonium ions in the type II systems, it is impossible to assign the infrared absorption and the vibrational spectra characteristic of the type II complexes to either of these species. Protonated benzene and perylene ions, for example, do not give rise to an electronic absorption in the infrared region.[26] If the type II species was a simple radical cation, the infrared absorption would have to be assigned to a $\sigma \rightarrow \pi$ transition. Previous attempts to observe this transition in substituted benzene radical cations have been unsuccessful.[23] The most cogent evidence disfavoring the assignment of type II species to the parent radical cation is provided by the adsorption of toluene on Cu(II), Fe(III), and VO^{2+} hectorite. Each of these systems gives rise to a sharp esr signal and a weak absorption near 555 nm which is indicative of $[C_6H_5CH_3^-]^+$;[22,23] yet, the intense ir absorption typical of a type II species is absent.

It is unlikely that the type II species are dimer radical cations of the type $(Ar)_2^+$ with eximer-like sandwich structures.[23] If this were the case, the unpaired spin on the perylene dimer cation should be equally distributed over both halves of the ion as in $(napthalene)_2^+$.[27,28] However, the coupling observed for the perylene radical on Cu(II)-doped 2n(II) hectorite is consistent with the unpaired spin being localized on a single perylene entity.

Since only a small fraction (<5%) of the Cu(II) spins lost upon type II benzene and perylene formation are recovered as radical cation spins, we suggest that the type II species are formed by coupling of the radical cations themselves. Coupling of perylene radical cations has been observed previously.[29,30] In solvents of low polarity the associated ions exhibit an intense charge transfer band in the region 6500–8300 cm^{-1}. For type II perylene on Cu(II) montmorillonite, the infrared band is centered near 4500 cm^{-1}.[10] Unfortunately, no vibrational data have yet been reported for associated aromatic radical cations.

The failure of toluene and other readily oxidized alkyl-substituted benzenes to form type II species may be explained by their polymerization or oligomerization on the interlamellar surfaces of the mineral. In the presence of a polymer, the association of the trapped radical cations may not be possible, yet rapid electron exchange between the cations and polymer could occur, accounting for the absence of proton hyperfine splitting in their esr spectra.

Acknowledgment. We thank Dr. J. Paul Rupert for helpful discussions and for providing us with a copy of ref 5 prior to its publication. The support of this research by the National Science Foundation through Grant No. GP-33878 is gratefully acknowledged.

References and Notes

(1) M. M. Mortland and T. J. Pinnavaia, *Nature (London), Phys. Sci.*, **229**, 75 (1971).
(2) T. J. Pinnavaia and M. M. Mortland, *J. Phys. Chem.*, **75**, 3957 (1971).
(3) D. B. Fenn and M. M. Mortland, Proceedings of the International Clay Conference, Madrid, Spain, 1972, p 591.
(4) B. Fenn, M. M. Mortland, and T. J. Pinnavaia, *Clays Clay Min.*, **21**, 315 (1973).
(5) J. P. Rupert, *J. Phys. Chem.*, **77**, 784 (1973).
(6) P. Cloos, D. Vande Poel, and J. P. Camerlynck, *Nature (London), Phys. Sci.*, **243**, 54 (1973).
(7) H. G. Smith and R. E. Rundle, *J. Amer. Chem. Soc.*, **80**, 5075 (1958).
(8) R. W. Turner and E. L. Amma, *J. Amer. Chem. Soc.*, **88**, 1877 (1966).
(9) D. M. Clementz and M. M. Mortland, *Clays Clay Min.*, **20**, 181 (1972).
(10) Y. Matsunaga, *Bull. Chem. Soc. Jap.*, **45**, 770 (1972).
(11) H. E. Doner and M. M. Mortland, *Science*, **166**, 1406 (1969).
(12) R. E. Grim, "Clay Mineralogy," 2nd ed, McGraw-Hill, New York, N. Y., 1968.
(13) J. Selbin, *Chem. Rev.*, **65**, 153 (1965).
(14) J. J. Rooney and R. C. Pink, *Trans. Faraday Soc.*, **58**, 1632 (1962).
(15) D. M. Brouwer, *J. Catal.*, **1**, 372 (1962).
(16) W. K. Hall, *J. Catal.*, **1**, 53 (1962).
(17) A. Terenin, V. Barachevsky, E. Kotov, and V. Kolmogorov, *Spectrochim. Acta*, **19**, 1797 (1963).
(18) A. Carrington, F. Dravnieks, and M. C. R. Symons, *J. Chem. Soc.*, 947 (1959).
(19) W. Y. Aalbersberg, G. J. Hoijtink, E. L. Mackor, and W. P. Weijland, *J. Chem. Soc.*, 3049 (1959); 3055 (1959).
(20) P. Kovacic and J. S. Ramsey, *J. Polym. Sci., Part A-1*, **7**, 111 (1969), and references therein.
(21) P. Kovacic, C. Wi, and R. W. Stewart, *J. Amer. Chem. Soc.*, **82**, 1917 (1960).
(22) W. H. Hamill in "Radical Ions," E. T. Kaiser and L. Kevan, Ed., Interscience, New York, N. Y., 1968, p 321.
(23) B. Badger and B. Brocklehurst, *Trans. Faraday Soc.*, **65**, 2582 (1969).
(24) V. A. Baracnevskii and A. N. Terenin, *Opt. Spectrosc.*, **17**, 161 (1964).
(25) G. Dallinga, E. L. Mackor, and A. A. Verrijn Stuart, *Mol. Phys.*, **1**, 123 (1958).
(26) H. H. Perkampus and E. Baumgarten, *Angew. Chem., Int. Edit. Engl.*, **3**, 776 (1964).
(27) I. C. Lewis and L. S. Singer, *J. Chem. Phys.*, **43**, 2712 (1965).
(28) O. W. Howarth and G. K. Fraenkel, *J. Amer. Chem. Soc.*, **88**, 4514 (1966).
(29) H. Kuroda, T. Sakurai, and H. Akamatu, *Bull. Chem. Soc. Jap.*, **39**, 1893 (1966).
(30) Y. Sato, M. Kinoshita, M. Sano, and H. Akamatu, *Bull. Chem. Soc. Jap.*, **42**, 3051 (1969).

On the Estimation of Ionic Entropies in Various Solvents

Cecil M. Criss

Department of Chemistry, University of Miami, Coral Gables, Florida 33124 *(Received October 29, 1973)*

Publication costs assisted by The National Science Foundation

The correspondence principle has been employed to divide recently published partial molal entropies for electrolytes in acetone and acetonitrile into their ionic components. The data are expressed in terms of the equation $\bar{S}_2°(X) = a + bS_2°(H_2O)$ where a and b are constants characteristic of the solvent and $\bar{S}°(X)$ and $S_2°(H_2O)$ are the entropies of the corresponding ions in the nonaqueous solution and water, respectively. Coefficients in the above equation for these solvents are compared with the coefficients for eight other nonaqueous solvents, deuterium oxide, and water in relation to the structural characteristics and basicities of the solvents. It is shown that solvent structure, rather than basicity, plays the predominant role in determining the value of ionic entropies. A general equation is presented which enables one to estimate ionic entropies in nonaqueous solutions for which there are no data.

A reliable means of estimating thermodynamic properties of electrolytes in nonaqueous solutions would be of considerable value to chemists and engineers. Some degree of success has been realized in the estimation of standard partial molal ionic entropies, $\bar{S}_2°$. Through the use of correspondence plots, several investigators[1-4] have divided the entropies of electrolytes in nonaqueous solutions into their ionic components and have shown that these entropies are related to the entropies of ions in water by

$$\bar{S}_2°(X) = a + b\bar{S}_2°(H_2O) \qquad (1)$$

where a and b are constants characteristic of the solvent.

Criss, Held and Luksha,[3] and Criss and Salomon[4] have employed the correspondence plot method and the "absolute" entropies of ions in water[5] in an effort to evaluate "absolute" entropies of ions in eight nonaqueous solvents and D_2O. Within the limits of experimental error, the entropies of both cations and anions (and hence any pair of ions) in the various solvents are observed to increase in the order NH_3 < DMF ≈ EtOH < MeOH < PC ≈ DMSO < NMF < F < H_2O < D_2O. This order was rationalized in terms of the inherent structure within the solvent resulting from hydrogen bonding or strong dipole–dipole interactions. The highly ordered solvents at the right end of the series presumably cause the entropies of the ions to be relatively positive because of the large entropy increase from solvent disruption, while low entropy values are exhibited by ions in solvents at the left end of the series since very little solvent disruption occurs. It was suggested[3] that entropies in various solvents could be represented by the equation

$$\bar{S}_2° = S° + \Delta S_F° + \Delta S_O° + \Delta S_D° \qquad (2)$$

where $S°$ is the inherent entropy of the ion or pair of ions,[6] $\Delta S_F°$ is the entropy change because of loss of degrees of translational freedom of the gaseous ion, $\Delta S_O°$ is the entropy of orientation of solvent in the electric field around an ion (always <0), and $\Delta S_D°$ is the entropy of disruption of the original solvent (always ≥0). For any given ion or pair of ions the first two terms are positive and independent of the solvent.[7] Criss and coworkers[3,4] further assumed that $\Delta S_O°$ for a given ionic solute would be constant in all solvents, since one can look at this term as a function of how strongly molecules are restricted and how many are restricted. Justification for this assumption was made on the basis that the interactions are electrostatic in nature and that solvent molecules of large dipoles will be strongly oriented near the ion but loosely oriented away from the ion because of the rapid decrease in field strength. On the other hand, for solvent molecules of low dipole moment, the nearest molecules are less severely restricted in their motion, but more molecules are affected since the field surrounding the ion does not diminish as rapidly. Consequently, the first three terms in eq 2 may be replaced by a constant, and since the entropy of disruption of the solvent, $\Delta S_D°$, should be directly proportional to the degree of structure in the solvent, it was proposed[3] that eq 2 be replaced by

$$\bar{S}_2° = kS_{str} + C \qquad (3)$$

where S_{str} is the "structural" entropy of the pure solvent and k and C are constants characteristic of each ion. It was further proposed that S_{str} was proportional to the difference in the actual boiling point of the solvent and the boiling point that the solvent would have if there were no strong interactions present, and eq 3 was modified to

$$\bar{S}_2° = k'\Delta T_{bp} + C \qquad (4)$$

While this equation is only approximately valid, it can be employed for estimating entropies of ions in solvents for which no data exist, if solvent structure is the major factor affecting the entropy and if one can estimate a reliable value for ΔT_{bp} for a solvent.

In contrast to the above argument, one can make a case for correlating the ionic entropies with the base strengths of the solvents. Within any solvent type (alcohols, amides, etc.), ionic entropies become more negative with the generally accepted solvent basicities. Support for this view comes from studies of enthalpies of solution or of transfer between solvents. In nearly all of the solvents that have been investigated enthalpies of solution or transfer between water and the nonaqueous solvent are in the same order as the ionic entropies. It is tempting, therefore, to conclude that the processes causing the enthalpies of solution to vary are the same that cause the variation in entropies. Since the variation in heats of solution in different solvents and the sign of the enthalpy of transfer between any two solvents has frequently been rationalized in

terms of solvent basicity,[8-13] or the coordinating ability of the solvent molecules, one might expect the entropies also to depend mainly upon the coordinating ability of the solvent. If this were the case, $\Delta S_O°$ in eq 2 would not be constant, but would become increasingly negative for those solvents that coordinate well with the ions.

At the time the proposal was put forth relating $\bar{S}_2°$ with the structural entropy of the solvents,[3] insufficient $\bar{S}_2°$ data existed to choose with certainty between the above alternative correlations. A test to differentiate between these two explanations would exist if $\bar{S}_2°$ data were available for a series of ions in a structureless solvent of low basicity and solvating power. According to the first view, ionic entropies in a structureless solvent would be very negative in spite of the fact that the solvent is an extremely weak base. On the other hand, if $\bar{S}_2°$ were dependent primarily on base strength, ionic entropies would be relatively positive in a solvent of low basicity.

Two notably poor solvating solvents that are generally considered very weak bases, and yet are relatively structureless, are acetonitrile and acetone. Recently, Abraham[14] reported entropies of transfer of electrolytes from water to several solvents, including acetonitrile and acetone. From these, and the application of the correspondence principle, absolute entropies of the ions in acetonitrile and acetone have been evaluated on a mole fraction standard state and compared with ionic entropies in other solvents. The coefficients in eq 1 for these solvents have also been evaluated and are listed in Table I, along with coefficients for other solvents. The overall trend of the ionic entropies, as indicated by the intercept, a, shows that the entropies of ions in acetone and acetonitrile are much more negative than one would expect on the basis of base strengths. The deviations from the ideal boiling points, ΔT_{bp}, for the various solvents are also listed in Table I. These were obtained by taking the difference between the actual boiling point of the solvent and the estimated ideal boiling point; that is, the boiling point the solvent would exhibit if hydrogen bonding or dipole–dipole interactions were absent. In practice the ideal boiling points are determined by way of model compounds or series of compounds of nearly identical molecular weights and shapes, but with very low dipole moments and little or no opportunity for hydrogen bonding. Considering the crude manner in which ΔT_{bp} must be estimated, the correlation between the constant a and ΔT_{bp} is remarkable. The above observations lead one to conclude that the structural characteristics of the solvents play the predominant role in determining ionic entropies and that solvent basicities or solvating power play a minor role.

Table I shows that the slope of eq 1 is constant to about 25% for all solvents, and has an average value of 0.85 ± 0.2. Consequently, for entropies of ions in water that are not too different from zero, the error introduced by assuming $b = 0.85$ for all solvents would not be large. For the alkali metal and halide ions the largest absolute aqueous ionic entropy is for I^-, which is 23.1 eu (mole fraction standard state), which would lead to a maximum error or about 4.6 eu in other solvents. Errors due to this term for other ions and for most of the solvents would be considerably less.

The data in Table I may be employed to estimate the intercept in eq 1 for other solvents. For the hypothetical ion in water having an entropy of zero, eq 1 reduces to

$$\bar{S}_2° = a$$

TABLE I: Constants for Eq 1 and the Deviation in Ideal Boiling Points for Various Solvents[a]

Solvent	a	b	Δ[c]	ΔT_{bp}[d]
D_2O	0.8	1.04	0.4	173
H_2O	0.0	1.00	0.0	174
F	− 1.5	0.63	1.5	162
NMF	− 4.8	0.66	0.4	128
PC	− 9.3	0.75	1.8	151
DMSO	− 9.9	0.92	1.9	135
MeOH	−10.8	0.82	0.7	117
EtOH	−15.8	0.76	0.6	97
DMF	−15.9[b]	0.79[b]	1.8[b]	98
AN	−18.3	0.92	0.8	105
NH_3	−22.4	0.82	2.0	57
AC	−27.6	1.11	0.7	62

[a] Constants are evaluated by a least-squares treatment of the data for the mole fraction standard state, and with the exception of acetonitrile and acetone have been determined on entropy values listed in ref 4. The data for acetonitrile and acetone are from ref 14. Slight variation in some of the constants listed here and those reported in ref 3 are due to revised data; see ref 4. [b] The constants and standard deviation for DMF do not include the entropy data for Li^+ since apparently its value is in serious error or it does not adhere to the correspondence method of treatment. [c] Δ is the standard deviation between the calculated and the experimental values. [d] Details for the evaluation of ΔT_{bp} are given in ref 3 and 4, except for the solvents, acetone and acetonitrile. For these solvents, the model compounds used in estimating ΔT_{bp} are $(CH_3)_2C{=}CH_2$ (bp −6°) and $CH_3C{\equiv}CH$ (bp −23°), respectively.

which upon substitution into eq 4 becomes

$$a = k'\Delta T_{bp} + C \qquad (5)$$

Evaluation of the constants in eq 5 gives $k' = 0.21$ and $C = -37.3$. Substituting eq 5 into eq 1, with $b = 0.85$ gives

$$\bar{S}_2°(X) = 0.21\Delta T_{bp} + 0.85\bar{S}_2°(H_2O) - 37.3 \text{ eu} \qquad (6)$$

This equation will be useful for calculating the entropy of any simple singly charged ion (on a mole fraction standard state) in any solvent for which one can estimate an accurate value of ΔT_{bp}. An error of about 1 eu is introduced for every 5° error in the estimation of ΔT_{bp}. Equation 6 reproduces 83% of the experimentally known ionic entropies[3,4] for the solvents listed in Table I within 4 eu of the experimental values. When no experimental sources of information are available it appears that eq 6 can be applied with a fair degree of reliability to estimate ionic entropies in nonaqueous solutions. For solvents for which the a and b constants have been evaluated, eq 1 can be used with an even higher degree of reliability. The constants listed in Table I reproduce 66% of the experimentally known ionic entropies to 1 eu and 97% of the experimental entropies to within 3 eu. The mole fraction ionic entropies calculated by eq 1 and 6 can be converted to the more common hypothetical 1 m standard state entropies by the equation

$$\bar{S}_{2\,m}° = \bar{S}_{2\,X}° + R \ln \frac{1000}{M}$$

where M is the molecular weight of the solvent.

Acknowledgment. The author is indebted to the National Science Foundation for their financial support of this research through Grant No. GP-39248X.

References and Notes

(1) W. M. Latimer and W. L. Jolly, *J. Amer. Chem. Soc.*, **75**, 4147 (1953).
(2) B. Jakuszewski and Taniewska-Osinska, *Lodz. Tow. Nauk. Pr. Wydz. 3.* **7**, 32 (1961); **8**, 11 (1962).

(3) C. M. Criss, R. P. Held, and E. Luksha, *J. Phys. Chem.*, **72**, 2970 (1968).
(4) C. M. Criss and M. Salomon in "Physical Chemistry of Organic Solvent Systems," A. K. Covington and T. Dickinson, Ed., Plenum Press, New York, N. Y., 1973, Part 4 of Chapter 2.
(5) There is no accepted thermodynamic method to divide entropies of electrolytes into their ionic components. However, several different nonthermodynamic arguments indicate that the absolute entropy of H^+ in water is approximately −5 eu (hypothetical 1 *m* standard state). For the discussions here and in the author's previous papers the division has been made on the above assignment. A brief review of the various entropy values reported for H^+ is given in ref 4.
(6) To avoid the problems associated with assignment of absolute entropies, one may wish to compare pairs of ions.
(7) The second term is strictly constant for only the "correct" choice of standard state. Strong arguments can be put forth in defense of either the mole fraction or the molar concentration standard state. In any event the ordering of the solvents is independent of the choice and the maximum variation in the second term because of the choice would be about 3 eu for the above series of solvents. Following previous work the mole fraction standard state is employed for the present discussion.
(8) C. V. Krishnan and H. L. Friedman, *J. Phys. Chem.*, **73**, 3934 (1969).
(9) H. L. Friedman, *J. Phys. Chem.*, **71**, 1723 (1967).
(10) G. Choux and R. L. Benoit, *J. Amer. Chem. Soc.*, **91**, 6221 (1969).
(11) E. M. Arnett and D. R. McKelvey, *J. Amer. Chem. Soc.*, **88**, 2598 (1966).
(12) R. Fuchs, J. L. Bear, and R. F. Rodewald, *J. Amer. Chem. Soc.*, **91**, 5797 (1969).
(13) J. R. Ferraro, L. I. Katzin, and G. Gibson, *J. Inorg. Nucl. Chem.*, **2**, 118 (1956).
(14) M. H. Abraham, *J. Chem. Soc., Faraday Trans. 1*, **69**, 1375 (1973).

Hydrophobic Hydration and Quadrupolar Magnetic Relaxation of Ionic Nuclei

H. G. Hertz* and M. Holz

Institut für Physikalische Chemie und Elektrochemie der Universität Karlsruhe, 75 Karlsruhe, West Germany
(Received October 1, 1973)

Experimental results regarding the nuclear magnetic relaxation rate of ^{81}Br in aqueous bromide solutions containing tetraethylammonium bromide are presented together with data for admixtures of neutral organic solutes to aqueous bromide solutions. For comparison, the ^{87}Rb magnetic relaxation in the corresponding solutions has as well been studied. The very strong relaxation effect caused on the ^{81}Br relaxation may be interpreted in terms of an entirely electrostatic theory. In the encounter configuration between bromide and the organic solute a coherency of water molecules is postulated whose electric dipoles cause the strong electric field gradient. The occurence of this structural effect is considered to be connected with the hydrophobic hydration of nonpolar groups.

1. Introduction

The present paper is a contribution to our understanding of the magnetic relaxation of halide ion nuclei such as ^{35}Cl, ^{37}Cl, ^{79}Br, ^{81}Br, and ^{127}I in aqueous solution. Knowledge of this relaxation mechanism then in turn can be helpful (to a greater or lesser degree depending on the circumstances) to obtain information concerning the structure of aqueous solutions. For all the halide ionic nuclei mentioned above the nuclear magnetic relaxation mechanism is the interaction of the nuclear quadrupole moment with the electric field gradient at the nuclear site.

In aqueous alkali halide solutions the relaxation can be understood satisfactorily in terms of field gradients produced by the electric monopoles and multipoles representing the ions and water molecules in the solution.[1-4] If we claim that the relaxation can be explained in terms of an electrostatic mechanism we are aware of the fact that this does not mean that the relaxation mechanism is really exclusively electrostatic. Distortions of the charge distributions of the ion beyond the one to be expected within the framework of the electrostatic theory (for details see ref 1) may indeed be present. But such contributions, if at all effective, are small when compared to the electrostatic effects or at best of the same order of magnitude.

In the early days of the investigation of halide nuclear magnetic relaxation it was observed by one of the present authors[5] that their relaxation rate is very large if the cations present in the solution are tetraalkylammonium ions. Later on, this effect has been studied in a more systematic way by a group of Swedish workers.[6-8] These authors tried to give an explanation of the very strong relaxation effect in terms of the peculiar hydration behavior of the (inert) alkyl groups, a hydration which has been denoted in the literature as the iceberg effect,[9,10] hydration of the second kind,[11,12] or hydrophobic hydration.[13,14] According to their treatment a certain fraction of halide ions resides in clathrate sites close to the tetraalkylammonium ions. The observed linear concentration dependence leads to the requirement that only a small fraction of anions is bound in the clathrate positions and from this it would follow that the quadrupole interaction in these positions must be very high, that is almost of the order of magnitude as it is known in a state of covalent binding. Considering this finding (and some other difficulties) we feel that their explanation cannot be considered to be fully satisfactory.

The investigation of this effect is of particular interest because relaxation studies of the halide nuclei have frequently been and will in the future be applied in order to obtain information regarding macromolecules with biolog-

ical significance.[15] In this conjunction it is of basic importance to have knowledge of all possible relaxation mechanisms which can influence the measured relaxation rates. Here the substituted ammonium ions may act as suitable model substances.

It is the purpose of the present paper to show that the anomalous relaxation effect caused by the tetraalkylammonium salts can as well be explained on an entirely electrostatic basis.

The Swedish workers[6-8] had already extended their study to a number of other cations such as mono-, di- and trialkylammonium ions, alkyl-substituted sulfonium and phosphonium ions, and to the uncharged Et_3N in order to see how specific the relaxation effect in question is. Summarizing, their finding was that the inert alkyl group has a dominant influence and that the presence of polar groups such as NH or OH causes no anomalous relaxation effect or at least reduces the effect one would obtain if the H or the total polar group is replaced by C_nH_{2n+1}, $n = 1$, 2.

We shall proceed in a similar manner, that is, we shall present experimental results regarding the relaxation effect caused by a rather wide variety of other solutes aside from the R_4N^+. By doing so we consider the tetraalkylammonium ion to be one link in a gradual transition from a purely aqueous environment of the relaxing ion to an entirely organic environment. Moreover, in order to make our approach more general we shall also present some experimental results regarding the influence of organic solutes on the magnetic relaxation of ionic nuclei which as well relax by quadrupole interaction, but which are cations or anions other than halide ions.

2. Experimental Section

Nmr line width measurements performed by the wide-line technique are easily influenced by experimental conditions. Our experience shows that especially line widths up to *ca.* 3000 Hz are often artificially broadened resulting in too high relaxation rates. In contrast to this pulsed nmr spin lattice relaxation time measurements are less affected by experimental parameters and yield more accurate results if one is able to overcome the signal-to-noise problems. Therefore, as far as possible in this work we used the pulse technique. The spectrometer was a Bruker B-KR 304 S pulse spectrometer. The resonance frequency was 12 MHz for ^{81}Br, ^{35}Cl, ^{23}Na, and ^{133}Cs and 18 MHz for ^{87}Rb and ^{1}H. To be able to measure the extremely short T_1 values of ^{81}Br, special care was taken to have maximum transmitter power (highest H_1 field) and minimum receiver dead times of the spectrometer. For measuring short T_1 values ($\leq$3 msec) we used the 180°–90° sequence whereas for longer values the 90°–90° sequence was applied. The signal-to-noise ratio was improved by using a relatively large sample volume of about 5 cm^3, a modified probe circuit, and by applying electronic signal accumulation (Ridl 400 channel analyzer). Due to the short relaxation times in the case of ^{81}Br and ^{87}Rb, about 2000 accumulations per measuring point were possible, resulting in signal-to-noise ratios greater than 50:1. The data given on the following pages are mean values of at least five measurements. Thus the experimental error is estimated to be less than ±5% in most cases.

Our result for the ^{81}Br relaxation rate, extrapolated to $c_{Br^-} \rightarrow 0$, is ($T = 25°$) $1/T_1 = 1050\ sec^{-1}$.

By direct analysis of the free induction decay (^{81}Br) and by using a Gill-Meiboom modified Carr-Purcell sequence (^{87}Rb) in some cases we determined T_2, the transverse relaxation time. T_1 and T_2 were found to be equal, thus the situation of extreme narrowing is established. For some samples the relaxation rate ratio for the isotopes ^{79}Br and ^{81}Br was measured. The results agreed within 5% with the theoretical value which one obtains from the squared ratio of the quadrupole moments of the two isotopes. To obtain the ^{14}N data we used a Varian DP 60 wide-line spectrometer with the variable frequency unit V-4210 A. The line widths measurements were performed at 4.33 MHz in side band technique. The sample temperature was held constant within ±0.5°. Unless otherwise indicated all experimental results reported were obtained at 25°. The solutions were prepared from substances of the highest purity commercially available and used without further purification. Some substances, prepared in our laboratory, were recrystallized several times before use. For the admixture experiments with alkali halide solutions stock solutions of the organic compounds were prepared to which the alkali halides were added. Solutions in which the proton relaxation times were determined were freed from oxygen by the usual pump and freeze technique.

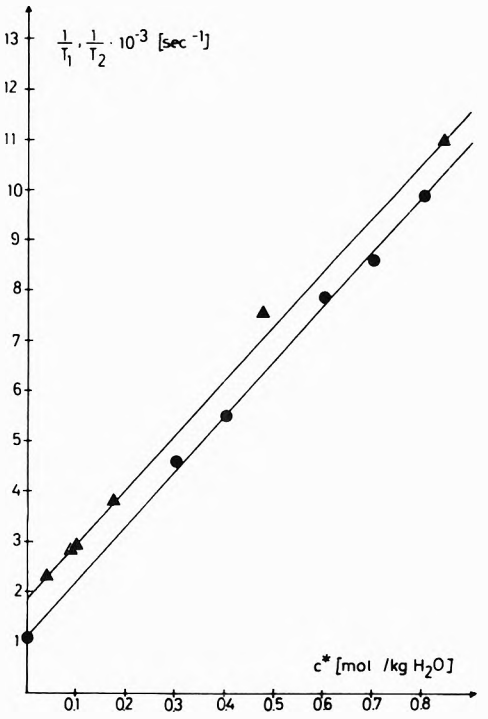

Figure 1. ^{81}Br relaxation rates in aqueous solution of Et_4NBr as a function of the concentration (25°): ●, this work; ▲, data reported by Lindman, *et al.*[6]

3. Experimental Results

3.1 ^{81}Br Relaxation in Aqueous $(C_2H_5)_4NBr$ Solutions. For our investigations we used only the tetraethylammonium ion (Et_4N^+) as a typical representative for the symmetrical tetraalkylammonium ions. It is known from the work of Lindman, *et al.*,[6] and from previous unpublished work at this laboratory that the relaxation effect on ^{81}Br increases with increasing length of the alkyl groups. Figure 1 shows the concentration dependence of the ^{81}Br relaxation rate in aqueous Et_4NBr solution. With the pulse technique higher concentration than 1 *m* could not be measured. For comparison, some results reported by Lindman, *et al.*,[6] are also given in Figure 1. These data are

converted from ^{79}Br line width measurements. As mentioned in the Experimental Section, the differential scanning wide line methods is liable to systematic line broadening. Thus, Lindman's relaxation rates are slightly larger than our's but the general pattern is the same. One important feature of Figure 1 is the linear concentration dependence. An approximately linear increase of the relaxation rate is quite generally found within a moderate range of the organic solute, *i.e.*, $c^* \leq 1$ *m*. Thus, one finds a linear increase of the relaxation rate with the Et_4NBr concentration when this salt is added to a YX solution of any concentration where Y is an alkali metal ion, and X is one of the halide ions of interest here (all except F). Likewise, the concentration dependence is substantially linear when Y is the relaxing nucleus or if the added solute is any other organic molecule. Therefore, for the following it is convenient to define a relative molal increase of the relaxation rate of the relaxing nucleus with respect to an organic solute

$$\Delta R_m = \frac{(1/T_1)_{c^*} - (1/T_1)_0}{(1/T_1)_0\, c^*}$$

where $1/T_1$ = relaxation rate of the ion nucleus, $(1/T_1)_{c^*}$ = relaxation rate at organic admixture concentration c^* (molality scale), and $(1/T_1)_0$ = relaxation rate without an organic admixture. With this definition our result for a "pure" Et_4NBr solution according to Figure 1 is ΔR_m = 10.54 m^{-1}. On the other hand, if one studies the deuteron magnetic relaxation rate in a solution of $(C_2H_5)_4NBr$ in D_2O, one finds $\Delta R_m{}^D$ = 0.29 $\bar{m}^{-1}$ ($\bar{m}$ = aquamolality, moles of salt/55.5 mole of water) for the solvent water. Since the variation of the deuteron relaxation rate measures the change in the rotational correlation time of the water molecule[12,16-19] and thereby at the same time the change of the correlation time for the quadrupolar relaxation mechanism,[1-4] it may be seen that in the presence of Et_4NBr the ^{81}Br relaxation varies much more than the correlation time, which has been emphasized previously by Lindman, *et al.*[6] In fact, this is the anomalous relaxation effect which is the subject of this paper.

3.2 Shape of the Cation. We asked the question: is the shape of the cation of substantial importance for the relaxation strength? We compared the effect of nonsymmetrical $(CH_3)_2(C_3H_7)_2NBr$ with symmetrical Et_4NBr, both cations having the same molecular formula. The result given in Table I shows that the shape of the cation is not a decisive factor for the anomalous relaxation.

3.3 Other Anions. Wennerström, *et al.*,[8] did not find competition effects among I^-, Br^-, and Cl^-. Consequently, the relaxation rate depends only on the cation present. Furthermore, the relative increase of the relaxation rate found by these authors was in the order Cl < Br < I. We confirmed these findings with some measurements as given in Table II. Another anion nucleus which relaxes by quadrupole interaction is ^{14}N. Measurements of the ^{14}N relaxation as line width measurements were feasible for CN^- and SCN^-. It may be seen from Table II that the ^{14}N relaxations in CN^- and in SCN^- in fact show an anomalous relaxation increase as Et_4N^+ is added, because the molal relative increase in the correlation time is only about 30%.

Our conclusion is that anomalous relaxation increase due to the presence of Et_4N^+ has been found for CN^- and SCN^-, thus it is not unique for halide ions.

3.4 Relaxation of Alkali Metal Cations. The alkali metal ions ^{23}Na, (^{39}K), ^{87}Rb, and ^{133}Cs all relax by quadrupole interaction and formally the theory given previously[1,2] is exactly the same for anions and cations with noble gas structure. Consequently, the question arises: do the cation nuclei also suffer an anomalous enhancement of magnetic relaxation when tetraalkylammonium ions are present? The entries of Table II show that this is not the case. The relative increase of the cation relaxation rate is roughly given by the relative increase of the correlation time, only the ^{133}Cs relaxation shows a slightly larger effect. In Figure 2 we have depicted the dependence of the ^{87}Rb relaxation on the added amount of Et_4NBr. The dashed (the theoretical) curve gives the behavior to be expected if the change of the ^{78}Rb relaxation rate is only due to the increase of the rotational correlation time of the solvent water. The relative variation of the rotational correlation time has been derived from deuteron relaxation time measurements in the usual manner.[12] One sees from Figure 2 that any anomalous or excess relaxation contribution is absent when the ^{87}Rb cation relaxation is studied.

3.5 Influence of Organic Anions on the ^{81}Br and ^{87}Rb Relaxation Rate. Next we studied a solution which is the analog to the system described in paragraph 3.4: 2 *m* RbBr + 0.5 *m* $CH_3C(CH_3)_2COONa$ in H_2O. The anion was of the most symmetric form available. The results for the ^{81}Br and ^{87}Rb relaxation in the same solution are shown in Table II. It may be seen that here as well the halide relaxation is more liable to an excess relaxation enhancement than that of the cation, inspite of the fact that the perturbing solute particle carries a negative charge. The finding that the cation nuclear quadrupole relaxation

TABLE I

Solution	$(1/T_1)^{81}_{Br}$, sec^{-1}	ΔR_m
0.8 *m* Me_2Pr_2NBr	9090	9.57
0.8 *m* Et_4NBr	9900	10.54
2 *m* KBr + 0.1 *m* Me_2Pr_2NBr	1758	5.67
2 *m* KBr + 0.1 *m* Et_4NBr	1953	7.40

TABLE II

Nucleus	Solution	$1/T_1$, $1/T_2$, sec^{-1}	ΔR_m
^{81}Br	2 *m* KBr + 2 *m* KI + 0.07 *m* Et_4NBr	1670	
	4 *m* KBr + 0.07 *m* Et_4NBr	1700	
^{81}Br	4 *m* NaBr	1470	
	4 *m* NaBr + 0.3 *m* Et_4NBr	3960	5.67
^{81}Br	2 *m* RbBr	1220	
	2 *m* RbBr + 0.5 *m* $(CH_3)_3CCOONa$	1870	1.06
^{35}Cl	4 *m* NaCl	48.1	
	4 *m* NaCl + 0.3 *m* Et_4NCl	121	5.04
^{14}N	2 *m* KCN	141.5	
	2 *m* KCN + 0.25 *m* Et_4NBr	188.5	
	2 *m* KCN + 0.5 *m* Et_4NBr	295	
	2 *m* KCN + 1 *m* Et_4NBr	496	2.5
	2 *m* KSCN	220	
	2 *m* KSCN + 0.5 *m* Et_4NBr	305	0.9
	2 *m* KSCN + 1.0 *m* Et_4NBr	398	
	2 *m* KSCN + 2.0 *m* Et_4NBr	675	
^{23}Na	3 *m* NaBr	21.1	
	3 *m* NaBr + 0.3 *m* Et_4NBr	22.5	0.22
^{87}Rb	2 *m* RbBr	391	
	2 *m* RbBr + 0.3 *m* Et_4NBr	425	0.29
	2 *m* RbBr + 0.5 *m* $(CH_3)_3CCOONa$	500	0.56
^{133}Cs	4 *m* CsBr	0.072	
	4 *m* CsBr + 0.5 *m* Et_4NBr	0.087	0.43

TABLE III

Nucleus	Solution: 2 *m* RbBr in mol % H_2O + mol % organic solute		$1/T_1$, sec^{-1}	$\Delta R_m'$	$\Delta R_m'^D$
^{87}Rb	100	0	391		
^{81}Br	100	0	1220		
^{87}Rb	80	20 MeOH	637	0.032	0.052
^{81}Br	80	20 MeOH	6666	0.223	
^{87}Rb	90	10 EtOH	730	0.087	0.115
^{81}Br	90	10 EtOH	4926	0.304	
^{87}Rb	95	5 *t*-BuOH	641	0.128	0.153
^{81}Br	95	5 *t*-BuOH	5405	0.686	
^{87}Rb	97.8	2.2 glycerol	476	0.108	
^{81}Br	97.8	2.2 glycerol	1940	0.270	
^{87}Rb	95.3	4.7 glycol	487	0.052	
^{81}Br	95.3	4.7 glycol	2410	0.208	
^{87}Rb	98.2	1.8 formamide	426	0.050	
^{81}Br	98.2	1.8 formamide	1486	0.120	
^{87}Rb	98.2	1.8 urea	439	0.068	
^{81}Br	98.2	1.8 urea	1387	0.076	
	2 *m* KBr in				
^{81}Br	99.46	0.54 Et_4NBr	3500	3.93	

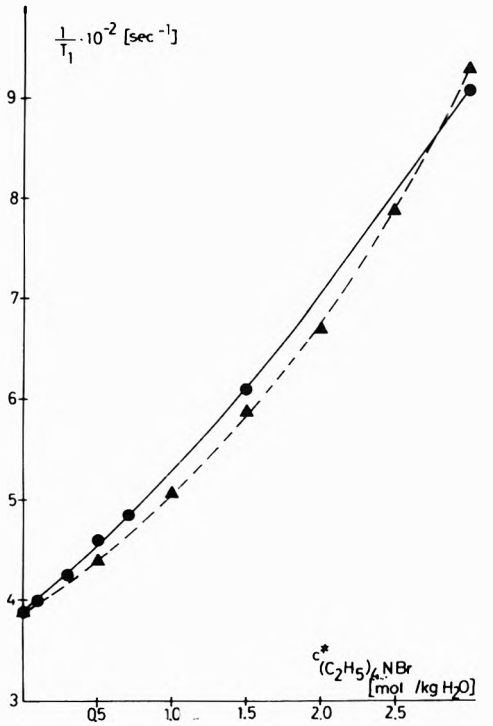

Figure 2. ^{87}Rb relaxation rate in 2 *m* RbBr to which *c** mol/kg of H_2O Et_4NBr has been added. The dashed curve represents the theoretical relaxation rate according to eq 1 (25°).

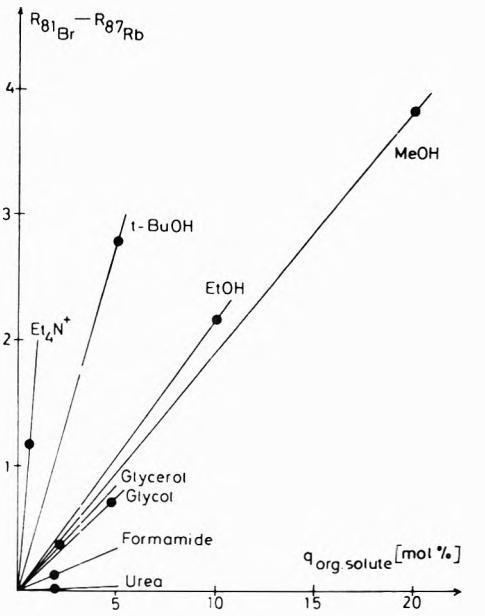

Figure 3. Difference between relative ^{81}Br and ^{87}Rb relaxation rate in 2 *m* RbBr solutions to which various organic solutes have been added (25°).

is only slightly altered by the presence of an organic ion is in accordance with measurements mentioned in ref 8.

3.6 ^{81}Br and ^{87}Rb Relaxation in the Presence of Uncharged Organic Solutes. For these solutions it is more convenient to redefine the quantity ΔR_m slightly. We write

$$\Delta R_m' = \frac{(1/T_1)_q - (1/T_1)_0}{(1/T_1)_0 q}$$

where q is the mole per cent of added organic solute and $(1/T_1)_q$ is the relaxation rate at composition q. Thus we have $\Delta R_m' \approx \frac{1}{2}\Delta R_m$. $\Delta R_m'^D$ represents the relative increase per mole per cent of the deuteron relaxation rate, *i.e.*, of the correlation time. Our results for a number of solutions are presented in Table III. The difference between the relative relaxation rates for ^{81}Br and ^{87}Rb in the same solution is shown in Figure 3. Two facts may be extracted from these data. (i) Similar to the behavior of charged organic particles,[7] for neutral organic solutes as well the relaxation effect becomes greater when more methyl or methylene groups are present and it becomes smaller when more nonpolar groups are replaced by polar groups, the size of the molecule being kept approximately unchanged. (ii) The relaxation enhancement due to the alkyl groups is observed only for the anion, as the alkyl groups are replaced by polar groups the relaxation effect of the cation and anion gradually become the same. Lastly, it may be mentioned that we observed the greatest relative increase of the ^{81}Br relaxation rate in the presence of the macroheterobicyclic compound "cryptate" as described by Lehn and coworkers.[20] The ^{81}Br relaxation in a 2 *m* KBr solution to which 0.05 *m* of the cryptate was added increased by 84%; this corresponds to $\Delta R_m \approx 17$.

3.7 Variation of Relaxation Effect with Alkali Bromide Concentration. In the next type of experiment we kept the

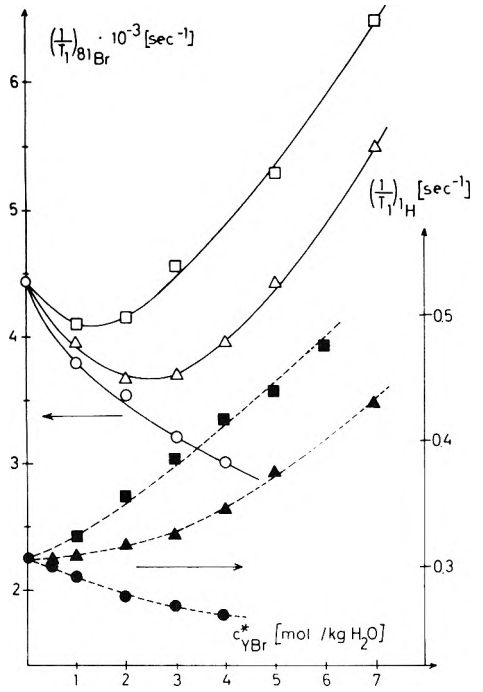

Figure 4. ^{81}Br relaxation rate (open symbols) and solvent proton relaxation rates (filled symbols) of a 0.3 *m* Et_4NBr solution to which *c** mol/kg of H_2O YBr has been added (Y = Li, Na, K): □, Li; △, Na; ○, K. Left-hand and right-hand ordinate regard the ^{81}Br and proton relaxation rate, respectively (25°).

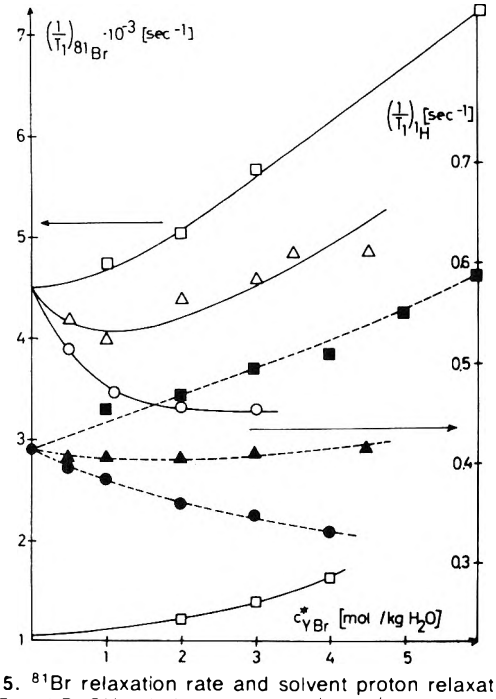

Figure 5. ^{81}Br relaxation rate and solvent proton relaxation rate of a 1.5 *m* *t*-BuOH solution to which c* mol/kg of H_2O YBr has been added (Y = Li, Na, K). For comparison the ^{81}Br relaxation rate in "pure" LiBr solution is included as the lowest curve. Other details are the same as in Figure 4.

Et_4NBr concentration constant at 0.3 *m* and varied the salt concentration YBr, where Y = Li, Na, or K. The purpose of these measurements was to see how sensitive the anomalous relaxation effect of ^{81}Br was with regard to varying amounts of alkali bromide present in the solution. The results are shown in Figure 4. The dashed curves represent the proton relaxation rate of the solvent water in the corresponding solution (the contribution of the alkyl protons to the total proton signal may be neglected). The proton as well as the deuteron relaxation rate gives an approximate representation of the concentration dependence of the correlation time entering in the quadrupole relaxation mechanism.[3] It may be seen from Figure 4 that the excess relaxation effect decreases a little when the alkali bromide concentration increases. A more quantitative evaluation of these results will be given below. Figure 5 shows the corresponding plot for the system 1.5 *m* *t*-BuOH + YBr.

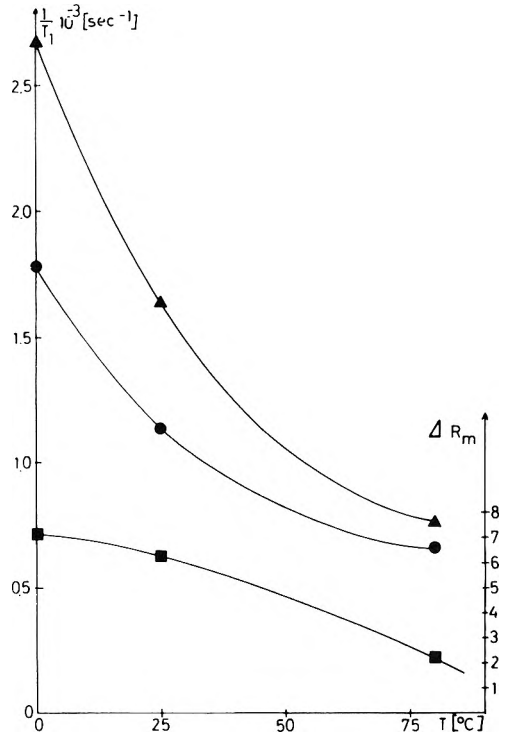

Figure 6. Temperature dependence of ^{81}Br relaxation rate in 2 *m* KBr solution (●) and in the solution 2 *m* KBr + 0.07 *m* Et_4NBr (▲). The temperature dependence of ΔR_m for Et_4NBr + 2 *m* KBr is also given (■).

TABLE IV

Solution	E_a, kcal/mol[a]	E_a, kcal/mol
2 *m* KBr	2.2 ± 0.2	2.1 ± 0.4[b]
2 *m* KBr + 0.07 *m* Et_4NBr	3.0 ± 0.2	
4 *m* KBr + 0.5 *m* Et_4NBr	4.2 ± 0.2	4.4 ± 0.2[c]

[a] This work. [b] Reference 21. [c] From ref 7 for a pure 0.5 *m* Et_4NBr solution.

3.8 Temperature Dependence. We measured the temperature dependence of the ^{81}Br relaxation rate for the two solutions: (i) 2 *m* KBr, (ii) 2 *m* KBr + 0.07 *m* Et_4NBr. It may be seen from Figure 6 that the magnitude of the anomalous relaxation effect decreases with increasing temperature. The activation energies were found as given in Table IV.

4. Evaluation of Experimental Results

4.1 General. It is our task to give an interpretation of the experimental results reported in section 3 in terms of an electrostatic model. The detailed theory on which the following treatment is based has been given elsewhere.[1,2] To begin with, we consider the isolated ion (*i.e.*, in the limit of infinite dilution). Let the ion be Br^- or Rb^+. As

has been shown previously,[1,22] the relaxation rate is given by the equation

$$\frac{1}{T_1^0} = k' \frac{m^2 c_{H_2O}' P^2 \tau_{H_2O}}{r_0^5} \quad (1)$$

$$k' = \frac{6\pi}{5} \frac{2I+3}{I^2(2I-1)} \left(\frac{eQ(1+\gamma_\infty)}{\hbar} \right)^2$$

where I is spin of relaxing nucleus, e the charge of the proton, Q the nuclear quadrupole moment, γ_∞ the Sternheimer or antishielding factor, m, the electric dipole moment of the water molecule, c_{H_2O}' concentration of water molecules (particles per cm^3), τ_{H_2O} the correlation time due to reorientational motion of water molecules, P the polarization factor (see below), and r_0 = closest distance of approach of water dipole to the center of the ion.

For the following it is important to have a clear picture of the model on which eq 1 is based. The model assumes *uniform distribution* of the centers of mass and *random dipole orientation* of the H_2O molecules over the entire space up to the surface of the ion. Thus, a hydration sphere in the usual sense is absent in this model. For the present section P is the most important quantity in eq 1 and needs further explanation. The mechanism of relaxation is based on the fluctuating electric field gradient produced by all the water molecules (*i.e.*, by point dipoles) present in the system. If all these water dipoles were entirely independent, then we would have $P = 1$. But actually they are not independent. For, if one H_2O molecule is a nearest neighbor of the ion, a second nearest neighbor cannot be anywhere, *e.g.*, it cannot have the same position as the first one. furthermore, the orientations of these two nearest neighbors are determined (at least partly) by the fact that there is a "central" ion whose hydration waters they are. Likewise, if a given water molecule is far apart from the ion, it is well known that its (water) neighbors do not have random orientation relative to this particular H_2O. Let V^w be the field gradient produced at the center of the relaxing ion by the (selected) single water molecule and let $N_w \tilde{V}^{ww}$ be the field gradient produced by the total surroundings of this water molecule. N_w = total number of water molecules in the sample. Now we express $N_w \tilde{V}^{ww}$ in terms of V^w

$$N_w \tilde{V}^{ww} = K V^w \quad (2a)$$

with K constant, $1 \geq K \geq -1$. This approximation neglects the fact that actually K depends on the separation between the ion and the "selected" water molecule.[1] It is convenient to replace the constant K by

$$K \equiv P^2 - 1$$

because the sum of the mean squared field gradient of the single water molecule, $\overline{(V^w)^2}$, and the cross-correlation contribution between this water molecule and its surroundings, $\overline{V^w N_w \tilde{V}^{ww}}$, yields $\overline{P^2 (V^w)^2}$. Then $\overline{P^2 (V^w)^2} \tau_{H_2O}$ is essentially the expression shown by eq 1.

We see that if the surroundings of the selected single H_2O does not produce any field gradient, we have $P = 1$, if the surroundings compensates the field gradient of the selected water molecule exactly, then $P = 0$, if the field gradient of the surroundings reinforces that of the single selected water molecule, then $1 < P \leq 2^{1/2}$. The restriction $K \leq 1$ is due to our approximation which takes account of only two water cross correlations. We have characterized $N_w \tilde{V}^{ww}$ as the field gradient of the "total" surroundings of the single H_2O. This means that this quantity implies an integral over the entire space. (For more quantitative details see eq 27 and 28 of ref 1 or eq 37a and 38 of ref 2.) Therefore we may call the polarization factor P as delocalized cross correlation correction.

Usually in our work we have chosen $P = \frac{1}{2}$,[1,22] *i.e.*, $(P^2 - 1) = -\frac{3}{4}$. This is close to the value

$$P = (2\epsilon + 3)/5\epsilon$$

(ϵ = dielectric constant) derived by Cohen and Reif on the basis of a continuum theory.[23]

We now return to the description of the hydration model in conjunction with eq 1 where we had said that the model does not involve any distinct hydration sphere. However, eq 1 contains the correction factor $P^2 = \frac{1}{4}$ and we may interpret this factor as a symmetry effect in the first hydration sphere, but we may as well interpret it as a general polarization effect spread over the whole solution. The (delocalized) treatment does not make any statement in this regard.

So far we were concerned with the limit of infinite dilution. Next we turn to finite concentrations of any other solute, *i.e.*, ions or uncharged particles. Consider an instantaneous configuration in which the selected single water molecule is in contact with both the relaxing ion and another solute particle. Now, in general, the quantity $N_w \tilde{V}^{ww}$ will have changed. Especially we would expect this to be so when the solute particle contains inert alkyl groups which represent a "dielectric hole" in the solution. As mentioned above, $N_w \tilde{V}^{ww}$ involves an integral over the space around the single water molecule, and if this surroundings is substantially a dielectric hole, it is well possible that $N_w \tilde{V}^{ww}$ will deviate from the former value KV^w (see eq 2a) which corresponds to a filled, polarizable hole. Therefore, if the contact situation just described occurs we write

$$N_w \tilde{V}^{ww} = N_w k_0^{ww} V_w \quad (2b)$$

with $N_w k_0^{ww} \neq K$ in general (for the mathematical definition of k_0^{ww} see eq 40 of ref 2).

The probability that the selected single water molecule is a member of the hydration sphere of the solute particle is given by

$$p_h = n_{hc} c^* / 55.5 \quad (3)$$

if we have random distribution of the solute particles relative to the relaxing ion. n_{hc} = hydration number of the solute particle and c^* = molality of solute particle. Thus, we may understand $N_w k_0^{ww} - (P^2 - 1)$ as a perturbation of the polarization $P^2 - 1$ due to the close approach of the solute molecule. Now the nuclear magnetic relaxation in the present system is due to a fluctuating electric field gradient. In fact, as the solute particle moves toward and away from the relaxing ion, the field gradient contribution $N_w \tilde{V}^{ww}$ fluctuates between the perturbed value $N_w \tilde{V}^{ww} = N_w k_0^{ww} V^w$ and the unperturbed value $(\bar{P}^2 - 1) V^w$. P may depend weakly on the composition of the solution, therefore now we have written $\bar{P}$, *i.e.*, mean value of P. As has been shown elsewhere[2] the contribution to the relaxation rate corresponding to this process is

$$\frac{1}{T_1^{ww}} = k' m^2 c_{H_2O}' \frac{75 c^* n_{hc}}{8\pi 55.5} (N_w k_0^{ww} - (\bar{P}^2 - 1)) F_{4,4}(r_0, \alpha') \tau_{H_2O}'$$

$$0 < c^* \leq 55.5/n_{hc} \quad (4)$$

where n_{hc} = hydration number of organic solute, c^* = con-

centration of organic solute (molality scale)

$$F_{n,n}(r_0,\alpha') = \frac{8\pi}{15\nu!}\left\{\sum_{k=1}^{\nu}(k-1)!\left(-\frac{1}{\alpha'}\right)^{\nu-k} r_0^{-k} + \left(-\frac{1}{\alpha'}\right)^{\nu} e^{r_0/\alpha'} E_1\left(\frac{r_0}{\alpha'}\right)\right\}$$

$\nu = 2n - 3$; $E_1(r_0/\alpha') = \int_{r_0/\alpha'}^{\infty}(e^{-y}/y)\,dy$, $\tau_{H_2O}' = \tau_{H_2O}^{hc}\tau_{pol}/(\tau_{H_2O}^{hc} + \tau_{pol})$, τ_{pol} = mean time a water molecule resides in a position close to the relaxing ion *and* the organic solute, $\tau_{H_2O}^{hc}$ = rotational correlation time of a water molecule in the hydration sphere of organic solute, and α' = ion-solute separation beyond which the effect of special structures on the ion nuclear relaxation vanishes.

It may be useful to summarize once again the qualitative meaning of eq 4: $(N_w k_0^{ww} - (\bar{P}^2 - 1))$ characterizes the amplitude of the perturbation of the field gradient caused by the surroundings of a selected water molecule, the perturbation being due to the neighborhood of the solute molecule. $F_{4,4}(\tau_0, \alpha')$ takes account of the range α' over which such a perturbation is effective. τ_{H_2O}' is the correlation time after which an instantaneous field gradient perturbation of the type considered has decayed.

We must give a brief comment how to proceed for concentrations $c^* > 55.5/n_{hc}$. If expression 4 becomes appreciable as $c^* \to 55.5/n_{hc}$, then the correction of eq 1 is large, in other words, the model implied in eq 1 no longer holds at $c^* = 55.5/n_{hc}$. In this event we have to apply another model for $c^* > 55.5/n_{hc}$ which is more suitable. The corresponding formula for the relaxation rate then must contain a parameter which takes account of the further increase of $1/T_1$ as c^*, the concentration of the organic solute, increases.

In ionic solutions of finite concentration the ions represent point charges which undergo translational thermal motion. This diffusive motion produces additional fluctuating field gradients. The corresponding contribution to the relaxation rate is given by the expression

$$\frac{1}{T_1^{ion}} = 2k'c'e^2\bar{P}^2\frac{15}{8\pi}F_{3,3}(a_c,\alpha)\tau_c' \qquad (5)$$

where c' is the ion concentration (particles/cm^3), a_c the closest distance of approach between the ions, α the thickness of ionic charge cloud

$$\tau_c' = \frac{\tau_c^*\tau_{ion}}{\tau_c^* + \tau_{ion}}$$

τ_c^* is the rotational correlation time for ion-ion vector, see ref 2, and τ_{ion} is the time after which ion has diffused a length $\approx \alpha$. The derivation of eq 5 has been given elsewhere.[2] This equation is based on the assumption that the field gradient of the point charge is coupled with a field gradient produced by the surroundings of this point charge as given by eq 2a

$$N_w\tilde{V}^{\mu w} = (\bar{P}^2 - 1)V^{\mu} \qquad \mu = c,a \qquad (6)$$

where c, a represent the cation or anion, respectively. V^{μ} is the field gradient due to a single point charge *in vacuo*, $N_w\tilde{V}^{\mu w}$ is the field gradient caused by the total surroundings of the point charge. But again, if the relaxing ion and the diffusing ion are close to one another, there may be a perturbation of the polarization state of the mutual surroundings as compared with a situation where the diffusing ion is far apart. For instance, the cation may represent a dielectric hole (tetraalkylammonium ion!). Then we have

$$N_w\tilde{V}^{cw} = N_w k_0^{cw} V^c$$

with $N_w k_0^{cw} \neq (\bar{P}^2 - 1)$. Diffusion of the ion then produces an additional fluctuation of the field gradient between the perturbed and unperturbed state. The corresponding contribution to the relaxation rate is[2]

$$\frac{1}{T_1^{cw}} = k'c'e^2(N_w k_0^{cw} - (\bar{P}^2 - 1))\frac{15}{8\pi}F_{3,3}(a_c,\alpha')\tau_c'' \qquad (8)$$

$$\tau_c'' = \frac{\tau_{pol}\tau_c^*}{\tau_{pol} + \tau_c^*}$$

where we have assumed that such an relaxation effect comes from the cation alone. For a better understanding we state the difference and analogy, respectively, between eq 8 and 4. In eq 8 $(N_w k_0^{cw} - (\bar{P}^2 - 1))$ corresponds to the amplitude of the perturbation of the field gradient caused by the surroundings of the *cation* (not of the water molecule). The perturbation is due to the close proximity of the cation and the relaxing anion. Again $F_{3,3}(a_c,\alpha')$ takes account of the range over which the perturbation is effective, τ_c'' is the correlation time after which the perturbing field gradient has vanished. Since our theory takes account only of two particle cross correlations, the contributions eq 4 and 8 appear as independent ones in eq 9 below, really they are coupled.

4.2 ^{81}Br Relaxation in Aqueous Et_4NBr Solutions. Here the total (experimental) relaxation rate $1/T_1$ is given by the sum of all the contributions eq 1, 4, 5, and 8

$$\frac{1}{T_1} = \frac{1}{T_1^0} + \frac{1}{T_1^{ww}} + \frac{1}{T_1^{ion}} + \frac{1}{T_1^{cw}} \qquad (9)$$

We have to assign the observed anomalous relaxation effect to one or more of these terms. The "normal" halide nuclear relaxation behavior in alkali halide solutions can be understood in terms of eq 9 if we put α, the ion cloud thickness parameter which appears in $1/T_1^{ion}$, about equal to the diameter of the alkali metal cation.[3] It may be shown that it is possible to explain the halide nuclear relaxation in the presence of the tetraalkylammonium ions if in $1/T_1^{ion}$ one sets $\alpha \to \infty$. But this is clearly not a satisfactory approach. Thus the effect in question must be contained in the terms $1/T_1^{ww}$ and $1/T_1^{cw}$. This means that we have to determine the quantities $N_w k_0^{ww}$ and $N_w k_0^{cw}$ from our observed data (see eq 4 and 8). If these quantities turn out to be of the order of magnitude of unity, then, according to the arguments given above (*e.g.*, one dipole parallel to the selected one) we may say that we have an electrostatic explanation of the anomalous relaxation rate. If, however, $N_w k_0^{ww}$ and $N_w k_0^{cw}$ should come out very much larger than ≈ 1, then the effect can only be due to specific "electronic" alterations of the electric field gradient at the halide nucleus.

For the numerical evaluation of eq 9 we used the quantities which are listed in Table V. These quantities, if not available from direct physical sources, were partly obtained by simple geometrical estimates, and partly their approximate correctness has been shown by previous studies of alkali halide solutions.[3,4] For further details of the evaluation see ref 26.

We are unable to give any reliable assessment regarding the ratio k_0^{ww}/k_0^{cw}. According to the general reasoning of the theory it seems to be most appropriate to set $k_0^{ww} = k_0^{cw}$. The error involved in such an assignment cannot be very large because, due to the rather large value of a_c, eq 8 represents only a small correction of the leading term $1/T_1^{ww}$.

TABLE V[a,b]

System	m	10^{-18}, esu	P	$c_{H_2O}{}^{0\prime}$	τ_{H_2O}	n_{hc}	τ_{pol}	$\tau_{H_2O}{}^{hc}$, sec	α', Å	a_c, Å	τ_{ion}	$\tau_c{}^*$	r_0, Å	$N_w k_0{}^{ww}$
Et_4NBr + H_2O	1.84	1/2	$c_{H_2O}{}^{0\prime}$	$\tau_{H_2O}{}^0 R_D$	32	$R_D\alpha'^2/12\bar{D}_0$	5×10^{-12}	2.8	6	$R_D\alpha_c^2/12\bar{D}_0$	$R_D a_c^2/3\bar{D}_0$	3.36	See Figure 7
2 *m* RbBr + H_2O +:						17								
1 *m* MeOH						20								−0.32 (+0.1)
1 *m* EtOH	1.84	1/2	$c_{H_2O}{}^{0\prime}$	$\tau_{H_2O}{}^0 R_{87Rb}$		$\alpha'^2/1.06 \times 12\bar{D}_0$	4.4×10^{-12}	2.8				3.36		−0.36 (+0.03)
1 *m* *t*-BuOH						25								−0.03 (+0.8)
0.3 *m* Et_4NBr + YBr + H_2O	1.84	1/2	$c_{H_2O}{}^{0\prime}$	$\tau_{H_2O}{}^0 R_H$	32	$R_H\alpha'^2/12\bar{D}_0$	$(R_H/1.09)5 \times 10^{-12}$	2.8	6	$R_H\alpha_c^2/12\bar{D}_0$	$R_H a_c^2/3\bar{D}_0$	3.36	See Figure 7	
1.5 *m* *t*-BuOH + YBr + H_2O	1.84	1/2	$c_{H_2O}{}^{0\prime}$	$\tau_{H_2O}{}^0 R_H$	25	$R_H\alpha'^2/12\bar{D}_0$	$(R_H/1.49)5 \times 10^{-12}$	2.8				3.36	See Figure 7	

[a] For further details see ref 26. [b] $R_D = (1/T_1)_c/(1/T_1)_0$ for deuteron relaxation.[12,15,19] $R_H = (1/T_1)_c/(1/T_1)_0$ for proton relaxation.[25] $R_{87Rb} = (1/T_1)_c/(1/T_1)_0$ for ^{87}Rb relaxation. $\bar{D}_0$ = mean self-diffusion coefficient for Br^- and organic solute (for infinite dilution).[24] $\tau_{H_2O}{}^0 = 2.5 \times 10^{-12}$ sec. $c_{H_2O}{}^{0\prime}$ = water concentration in pure water (particles/cm^3). $F_{1,4}(3.36,2.8) = 6.10 \times 10^{36}$ cm^{-3}; $F_{1,4}(6,4) = 1.59 \times 10^{21}$ cm^{-3}; $F_{1,4}(6,2.8) = 1.42 \times 10^{21}$ cm^{-3}.

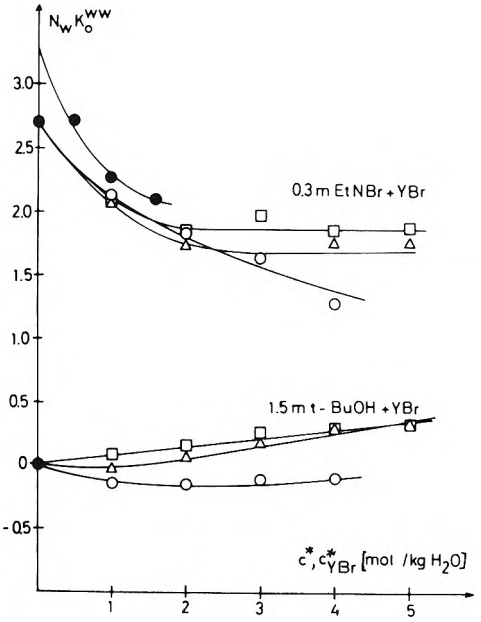

Figure 7. Structure parameter $N_w k_0{}^{ww}$ for "pure" Et_4NBr solution as a function of the concentration c* (●). $N_w k_0{}^{ww}$ for 0.3 *m* Et_4NBr + YBr solutions and 1.5 *m* *t*-BuOH + YBr solutions as a function of YBr concentration $c_{YBr}{}^*$: Y = Li (□); Y = Na (△); Y = K (○).

The results of our evaluation are given in Figure 7. It will be seen that the resulting $N_w k_0{}^{ww}$ lies between 2 and 3 which is indeed of the order of magnitude which can be accounted for on grounds of a purely electrostatic model. According to Figure 7 $N_w k_0{}^{ww}$ decreases somewhat as the concentration of Et_4NBr increases. This observation has little physical meaning because our evaluation implies the validity of eq 3. But if the tetraalkylammonium ions gain direct contact as the cation concentration increases, n_{hc}, *i.e.*, the number of surrounding water molecules *per* cation decreases, then p_h becomes smaller which in turn would yield a greater $N_w k_0{}^{ww}$ (of course N_w decreases slightly as the ion concentration increases).

4.3 Cation Nuclear Relaxation Rate in the Presence of Et_4NBr (and Related Experiments). We have to discuss the behavior described in section 3.4 and depicted in Figure 2. Now $1/T_1$ is almost exclusively given by eq 1, all other terms of eq 9 being small. The most evident reason for the vanishing of $1/T_1{}^{ww}$ will be that now $p_h \approx 0$, where p_h is the probability that a water molecule in the first hydration sphere of the relaxing ion is at the same time a member of the first hydration sphere of the organic cation (overlap of hydration spheres), *i.e.*, eq 3 is not valid. The alkali metal cation does not approach sufficiently close toward the organic cation (see also the study on selective solvation).[27] On the other hand, the results given in section 3.5 show that $p_h \neq 0$, if the relaxing nucleus is Br^- and if anions such as $(CH_3)_3CCOO^-$ are present. In fact, now the term $1/T_1{}^{ww}$ becomes effective for the anion relaxation. For Rb^+ p_h may or may not be zero, but in any case Rb^+ will approach the polar end of the anion, here the solute appears as a polarizable dipole, not as a dielectric hole.

4.4 Relaxation in the Presence of Uncharged Organic Solutes. In these solutions (see section 3.6) the relaxation rate of ^{81}Br is

$$\frac{1}{T_1} = \frac{1}{T_1{}^0} + \frac{1}{T_1{}^{ion}}(2m) + \frac{1}{T_1{}^{ww}} \qquad (10)$$

while that of ^{87}Rb is

$$\frac{1}{T_1} = \frac{1}{T_1^0} + \frac{1}{T_1^{ion}} \quad (2m) \qquad (11)$$

We have determined $N_w k_0^{ww}$ from the experimental results by aid of eq 10 and 4 for solutions with MeOH, EtOH, and *t*-BuOH. The parameters needed are listed in Table V together with the $N_w k_0^{ww}$ results derived. It may be seen that these $N_w k_0^{ww}$ are markedly smaller than those found with Et_4N^+. Three reasons for this finding may be quoted. (i) The alcohol molecules have a polar group. The n_{hc} values (listed in Table V) entering eq 3 and thus in eq 4 regard the entire solute molecule. Thus actually the hydration number of the nonpolar part is smaller. Use of n_{hc} values which are ½ of those given in Table V leads to the $N_w k_0^{ww}$ results shown in parentheses in that table. (ii) p_h according to eq 3 is the approximation of uniform distribution. Stronger anion-organic cation attraction or weaker anion neutral solute attractions than implied in eq 3 would lead to smaller and larger $N_w k_0^{ww}$ values, respectively. (iii) The presence of the electric field of the organic cation itself may cause a dipole-dipole alignment which produced an enhancement of the field gradient.

For the other uncharged organic solutes listed in Table III $N_w k_0^{ww}$ gradually approaches $\bar{P}^2 - 1 = -0.75$ as the ratio of the number of inert groups/number of polar groups decreases. For the ^{87}Rb relaxation we always have $N_w k_0^{ww} \approx P^2 - 1 = -0.75$.

4.5 Et_4NBr and t-BuOH in Alkali Bromide Solutions. This paragraph regards the experimental results presented in Figures 4 and 5. Equation 9 has to be applied, $1/T_1^{cw}$ is absent when *t*-BuOH is the organic admixture. Now the term $1/T_1^{ion}$ takes account of the increasing amount of alkali bromide present in the solution. This ionic contribution to the relaxation rate of ^{81}Br is known from previous work with "pure" alkali halide solutions.[3] The corresponding quantities (after a suitable correction due to the slight change of the correlation time) have been subtracted from the experimental data presented in Figures 4 and 5. The other parameters used are listed in Table V and the results of this evaluation, $N_w k_0^{ww}$ as a function of the YBr concentration, are shown in Figure 7. We obtain the statement from Figure 7 that the parameter $N_w k_0^{ww}$, which describes the particular water arrangement in the encounter configuration alkyl group of solute-Br^- is not sensitive with respect to high electrolyte concentrations. Since N_w decreases with increasing salt concentration (the volume of the sample is constant) a slight decrease of $N_w k_0^{ww}$ is to be expected, but even such a decrease is not evident for the solution of noncharged solutes.

As a summary we show Figure 8 which represents the anomalous relaxation effect of ^{81}Br

$$\delta = 1/T_1 - 1050 R_D \quad \text{sec}^{-1}$$
$$\approx 1/T_1^{ww} + 1/T_1^{cw}$$

$R_D = (1/T_1)_c/(1/T_1)_0$ for deuteron relaxation, for the solutions 0.5 *m* Me_4NBr, 0.5 *m* Et_4NBr, and 0.5 *m* Pr_4NBr, and 1 *m* MeOH, 1 *m* EtOH, and 1 *m* *t*-BuOH as a function of the hydration number n_{hc} ($1/T_1 = 1050$ sec^{-1} for ^{81}Br in the limit of infinite dilution). For the alcohols $1/T_1$ is extrapolated to $c_{Br^-} \to 0$. The hydration numbers n_{hc} are obtained from a simple geometrical estimate; the concentration of the alcohols is twice that of the ammonium ions because only half of the hydration sphere regards the inert part of the molecule. It is clearly demonstrated by this picture that the same physical effect is concerned with the solution of tetraalkylammonium ions and aliphatic alcohols.

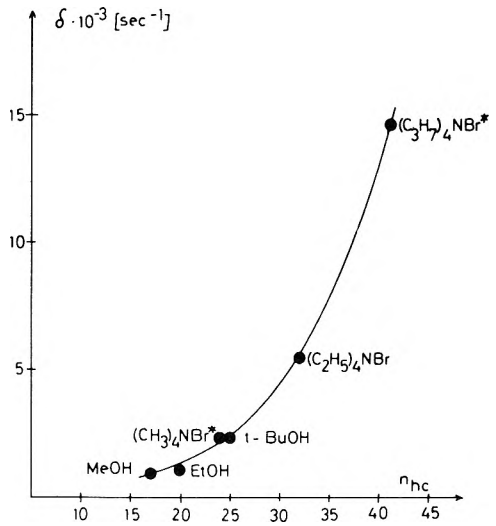

Figure 8. Excess relaxation effect of organic solutes in aqueous solution on the ^{81}Br relaxation rate in dependence of estimated hydration number n_{hc}. For details see text. The asterisk shows corrected values from Lindman, *et al.*[7]

5. Interpretation of the Anomalous Relaxation Effect in Terms of a "Localized" Model

So far our interpretation of the anomalous relaxation effect was based on the statement that in the encounter configuration inert solute-Br^- ion there is some parallel dipole polarization relative to a selected water molecule or at least less quenching of the mean gradient produced by the water dipole. We denoted this approach as a delocalized one because no geometrical details are involved, *i.e.*, nothing is said where, relative to the approaching particles, structural peculiarities occur and of what nature they are. Now Figure 9 leads us to the localized model. At the hydrophobic interface we see a number of water molecules which show substantially parallel dipole orientation. The positive and negative ends of the water molecules point toward the bulk water and the dielectric hole, respectively.[28,29] Recently it has been shown experimentally that the water protons surrounding CH_3 groups predominantly point toward the bulk water.[30,31] In pure H_2O the water molecules form tetrahedral H bonds but here the orientating torque on the H_2O probably comes about as a combined effect of the dielectric hole acting on the dipole and quadrupole moment of the molecule. This is the hydrophobic hydration. If a dipole resides in the hole, then the electric field at the hydrating H_2O is quite different and the particular torque producing the hydrophobic hydration is absent.

In Figure 9 the coordination number of Br^- is assumed to be 6. Three of these water molecules are members of the hydrophobic hydration sphere as well. Now let us consider for a moment an isolated hydrated Br^- ion with coordination (= hydration) number $n_h = 6$. Then, corresponding to this hydration model $1/T_1^0$ may be written[1]

$$\frac{1}{T_1^0} = \frac{9}{4\pi} k' \frac{m^2}{r_0^8} n_h \tau_c (1 - e^{-6\lambda}) \qquad (12)$$

This formula implies a well-defined hydration number (here $n_h = 6$) and *radial orientation* of the water dipoles.

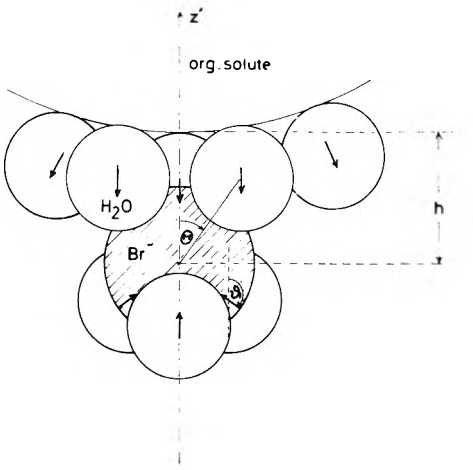

Figure 9. Br^- ion in contact with hydrophobic hydration sphere of large organic solute particle. The circular arrows indicating angles are not in the paper plane.

λ is a parameter which describes the width of the lateral angular distribution of the hydration water. $\lambda \to \infty$ means isotropic lateral distribution, $\lambda \to 0$ corresponds to exact positions of the water molecules on octahedron sites. τ_c is the correlation time for the vectors connecting the ion center with the point dipoles, here $\tau_c \approx 2.5 \times 10^{-12}$ sec. We may determine λ from the experimental ^{81}Br relaxation rate. One finds $\lambda = 0.01$ which corresponds to a high degree of order. In fact, actually the order in the hydration sphere of Br^- is less than this, the small relaxation rate is due to random dipole orientation and loose packing, as described in connection with eq 1, but for our present treatment we substitute for the real hydration sphere of Br^- an effective one which is ordered. This procedure is convenient as will be shown shortly, it does not restrict the generality of our arguments.

Let us return to the situation depicted in Figure 9. We see that now three of the previously radially oriented water molecules are replaced by water molecules belonging to the hydrophobic hydration sphere. Their orientation is parallel to the z' axis which in turn is perpendicular to the hydrophobic surface. These three water's have axial symmetry with respect to z'. The angular position and orientation of a water molecule is given by the angles θ and ϑ, respectively, as indicated in Figure 9. The electric field gradient $V_{z'z'}$ at the Br^- nucleus caused by one water molecule may be shown to be[22]

$$V_{zz} = \frac{3m}{r_0^4}\{[\sin\vartheta\sin\theta + \cos\vartheta\cos\theta](5\cos^2\theta - 1) - 2\cos\vartheta\cos\theta\} \quad (13)$$

and with radial orientation of the water dipoles, $\vartheta = \theta$

$$V_{z'z'} = \frac{3m}{r_0^4}(3\cos^2\theta - 1) \quad (14)$$

The angle θ for the octahedrally located water molecule is $\theta = 54° 44'$. This is the "magic" angle for which $\cos^2\theta = \frac{1}{3}$, thus, according to eq 14, for radial dipole orientation we have $V_{z'z'} = 0$. Consequently the contribution of the three waters on octahedral positions may be neglected, this is also essentially valid when these three waters do not have strict radial orientation and are more widely distributed over space corresponding to the situation around Br^-. Thus we are left with the field gradient generated by the three water molecules sitting on the hydrophobic surface. For one dipole parallel to the axis z', *i.e.*, $\vartheta = 0$, we have

$$V_{z'z'} = \frac{3m}{r_0^4}(5\cos^3\theta - 3\cos\theta) \equiv \frac{3m}{r_0^4}F(\theta) \quad (15)$$

If the Br^- just comes in contact with the close packed water of the hydrophobic hydration sphere one finds $\theta = 28° 50'$ ($h = 4.33$ Å), if Br^- approaches further toward the hydrophobic surface, the waters are pushed aside, θ increases (h decreases), finally, Br^- is in contact with the hydrophobic surface, now one finds $\theta_{max} = 80° 90'$ ($h_{min} = 1.96$ Å). The field gradient may be calculated for any θ according to eq 15. At $\theta = 39° 10'$ $V_{z'z'}$ vanishes, and at $\theta = 63° 36'$ $V_{z'z'}$ attains its maximum absolute value. Let us consider the effect of a neutral hydrophobic particle first, then, according to the general theory of quadrupolar relaxation[32] we have the relaxation rate in the configuration shown in Figure 9

$$\left(\frac{1}{T_1}\right)^{hydr} = \frac{3}{40}\frac{2I+3}{I^2(2I-1)}\left(\frac{eQ(1+\gamma_\infty)}{\hbar}\right)^2\left(3\frac{3m}{r_0^4}F(\theta)\right)^2\tau_c \quad (16)$$

The correlation time τ_c is the lifetime of the configuration given in Figure 9; we set $\tau_c \approx 5 \times 10^{-12}$ sec, this is the rotational correlation time of a water molecule in the hydrophobic hydration sphere.[12] Table VI gives some results as calculated with eq 16.

TABLE VI

θ	$F(\theta)$	h, Å	$(1/T_1)^{^{81}Br^{hydr}}$ (calcd), sec^{-1} [a]
28° 50′	+0.74	4.33	7,520
54° 44′	−0.77	3.34	6,964
63° 30′	−0.9	2.89	11,126
80° 90′	−0.49	1.96	3,300

[a] We have set $r_0 = 3.36$ Å; $\vartheta = 0$.

We compare these data with experimental results. We assume $n_{hc} = 25$ for t-BuOH, then, since $55.5/n_h = 2.2$ at 1.1 m one-half of all water molecules are in the hydration sphere of t-BuOH. But at this concentration the probability that a given Br^- is in a configuration as given in Figure 9 is $\approx$ one-half because the three water's which are members of the alcohol's hydration sphere may as well be located at the polar part of t-BuOH. For such Br^- the relaxation rate is $(1/T_1)^{free} = 1290$ sec^{-1} where only the change of the correlation time has been taken into account. The observed relaxation rate at 1.1 m is $(1/T_1)^{obsd} = 3560$ sec^{-1}, and from

$$\left(\frac{1}{T_1}\right)^{obsd} = \left(\frac{1}{T_1}\right)^{free} + \frac{1}{2}\left(\left(\frac{1}{T_1}\right)^{hydr} - \left(\frac{1}{T_1}\right)^{free}\right) \quad (17)$$

we find $(1/T_1)^{hydr} = 5830$ sec^{-1} which is in good agreement with the entries of Table VI.

The entries in Table VI have been calculated with $r_0 = 3.36$ Å. Clearly we have no precise knowledge of r_0, but we are only interested in an order of magnitude comparison. Thus, even if r_0 should be larger by 10%, $(1/T_1)^{hydr}$ in Table VI would still be of the order of 10^3 sec^{-1}, that is, we have demonstrated that our model with a "localized" electrostatic field gradient can account for the observed quadrupolar relaxation effect.

The condition $\vartheta = 0$ was introduced in conjunction with our model of the hydrophobic hydration. We have to examine whether our results remain valid when the three

water dipoles, *e.g.*, point toward the center of a smaller hydrophobic solute particle. We give two numerical examples. One calculates from a corresponding formula similar to eq 16: $(1/T_1)^{hydr} = 10{,}000\ sec^{-1}$ with $\vartheta = 60°$, $\theta = 28°$; $(1/T_1)^{hydr} = 12{,}000\ sec^{-1}$ with $\vartheta = 30°$, $\theta = 54° 44'$.

Moreover, it may be shown (see below) that even for $\vartheta = \theta$, *i.e.*, radial orientation of the water dipoles with respect to the relaxing nucleus, $(1/T_1)^{hydr}$ is of the order $10^4\ sec^{-1}$ provided ϑ is sufficiently different from the magic angle. Thus we arrive at the much more general result that for the explanation of the anomalous relaxation effect, it is sufficient to postulate in the encounter configuration the existence of a triplet of water molecules with more or less coherent dipole orientation which is closely packed to the halide anion.

For Rb^+ the "crown" of three waters closely attached to the ion is not formed; therefore, the relaxation behavior is normal. Likewise, in the neighborhood of a polar solute, obviously the water molecules are not closely packed to the halide ion. It is tempting to consider the dipole orientation in the hydrophobic hydration layer as described above as being the cause for the attraction or "adsorption" of the anions, a tendency which is not effective for the alkali metal cation.

Next we turn to the tetraalkylammonium ion. Now the field gradient due to the cation charge is superimposed on that of three waters, consequently (for $\vartheta = 0$)

$$\left(\frac{1}{T_1}\right)^{hydr} = \frac{3}{40}\,\frac{2I+3}{I^2(2I-1)}\left(\frac{eQ(1+\gamma_\infty)}{\hbar}\right)^2\left\{\frac{9m}{r_0^4}F(\theta)+\frac{2e}{a_c^3}\right\}^2\tau_c \tag{18}$$

where a_c is the separation between the two ions. We notice that now the sign of $F(\theta)$ becomes important, for small separations the field gradient of the point charge reduces that of the three dipoles. We give three numerical examples for Et_4N^+ which are calculated from eq 18: $(1/T_1)^{hydr} = 11{,}000\ sec^{-1}$ with $\vartheta = 0$, $\theta = 28° 50'$, $a_c = 7.8$ Å, $(1/T_1)^{hydr} = 30{,}000\ sec^{-1}$ with $\vartheta = 28.50,'$ $\theta = 28° 50'$, $a_c = 7.8$ Å, $(1/T_1)^{hydr} = 6400\ sec^{-1}$ with $\vartheta = 0$, $\theta = 63° 30'$, $a_c = 6.9$ Å. In a theoretical treatment by Friedman and coworkers[33] the separation $a_c \approx 7.5$ Å was found to correspond to the maximum of the anion–cation pair distribution function. The second numerical example given above represents radial orientation of water molecules with regard to the bromide nucleus. The above figures have to be compared with the experimental results: for Et_4N^+ $n_{hc} \approx 30$, from this it follows that at 0.9 *m* all Br^- anions are in a configuration as shown in Figure 9, because 55.5/30 = 1.8. The experimental relaxation rate at this concentration is $(1/T_1)^{obsd} = 11{,}000\ sec^{-1}$. Thus $(1/T_1)^{obsd} \approx (1/T_1)^{hydr}$.

As a result of this section we obtain the statement that the localized model approach yields a full confirmation of the delocalized approach presented in the previous section. Molecular arrangements may indeed be constructed which, on an entirely electrostatic basis, produce strong additional relaxation effects, that is, there is a justification to account for the large $N_w k_0^{ww}$ values found in section 4 in terms of an electrostatic mechanism.

Lastly we examine whether the greatest ^{81}Br relaxation rates observed in very concentrated Et_4NBr solutions, $c^* \approx 7$ *m*, can be understood in terms of the electrostatic theory. Now essentially all water molecules should be attached closely to the anion, but an ordering which produces cubic symmetry at the Br^- nucleus is not expected. For this situation we may apply eq 12 with $\lambda \to \infty$, *i.e.*, for random lateral positions of the H_2O's

$$\frac{1}{T_1} = \frac{9}{4\pi}\,k'\,\frac{m^2}{r_0^8}\,n_h\tau_c \tag{16a}$$

At $c^* = 1.8$ *m* we had $\tau_c \approx 5 \times 10^{-12}$ sec, then from the fact that at 6.8 *m* EtNBr the deuteron relaxation rate of the solvent water yields a value 4.3 times larger than that at 1.8 *m*,[12] we obtain $\tau_c \approx 2.2 \times 10^{-11}$ sec at $c^* = 6.8$ *m*. This gives with eq 16a $(1/T_1)^{calcd} = 150{,}000\ sec^{-1}$. On the other hand, if we drop the condition of radial orientation of the dipoles and apply the model of closest packed ($n_h = 6$) randomly orientated hydration dipoles (see eq 57 of ref 1) then

$$\frac{1}{T_1} = \frac{5}{4\pi}\,k'\,\frac{m^2}{r_0^8}\,n_h\tau_{H_2O}$$

Now with $\tau_{H_2O} = \tau_c$ we find $(1/T_1)^{calcd} = 88{,}000\ sec^{-1}$. The experimental result of Lindman, *et al.*,[6] is $(1/T_1)^{obsd} = 89{,}000\ sec^{-1}$. It is clear that here and above any precise numerical agreement is fortuitous, but the agreement of the order of magnitude is convincing. If close packing around the cation Rb^+ is absent up to the highest concentration we would expect that eq 1 holds over the entire range.

Acknowledgment. Financial support of the Fonds der Chemischen Industrie is gratefully acknowledged.

References and Notes

(1) H. G. Hertz, *Ber. Bunsenges. Phys. Chem.*, **77**, 531 (1973).
(2) H. G. Hertz, *Ber. Bunsenges. Phys. Chem.*, **77**, 688 (1973).
(3) H. G. Hertz, M. Holz, R. Klute, G. Stalidis, and H. Versmold, *Ber. Bunsenges. Phys. Chem.*, **78**, 24 (1974).
(4) H. G. Hertz, M. Holz, G. Keller, H. Versmold, and C. J. Yoon, *Ber. Bunsenges. Phys. Chem.*, **78**, 24 (1974).
(5) H. G. Hertz, *Ber. Bunsenges. Phys. Chem.*, **67**, 311 (1963).
(6) B. Lindman, S. Forsen, and E. Forslind, *J. Phys. Chem.*, **72**, 2805 (1968).
(7) B. Lindman, H. Wennerstrom, and S. Forsen, *J. Phys. Chem.*, **74**, 754 (1970).
(8) H. Wennerstrom, B. Lindman, and S. Forsen, *J. Phys. Chem.*, **75**, 2936 (1971).
(9) H. S. Frank and M. W. Evans, *J. Chem. Phys.*, **15**, 507 (1945).
(10) H. S. Frank and W. Y. Wen, *Discuss. Faraday Soc.*, **24**, 133 (1957).
(11) H. G. Hertz, *Ber. Bunsenges. Phys. Chem.*, **68**, 907 (1964).
(12) H. G. Hertz and M. D. Zeidler, *Ber. Bunsenges. Phys. Chem.*, **68**, 821 (1964).
(13) F. Franks in "Hydrogen-Bonded Solvent Systems," A. K. Covington and P. Jones, Ed., Taylor and Francis, London, 1968, p 31.
(14) F. Franks in "Water, a Comprehensive Treatment," Vol. 2, F. Franks, Ed., Plenum Press, London, 1973, p 1.
(15) T. R. Stengle and J. D. Baldeschwieler, *Proc. Nat. Acad. Sci. U. S.*, **55**, 1020 (1966).
(16) See, *e.g.*, H. G. Hertz, *Progr. Nucl. Magn. Resonance (NMR) Spectrosc.*, 3, 159 (1967).
(17) M. D. Zeidler in ref 14, p 509.
(18) E. v. Goldammer and M. D. Zeidler, *Ber. Bunsenges. Phys. Chem.*, **73**, 4 (1969).
(19) E. v. Goldammer and H. G. Hertz, *J. Phys. Chem.*, **74**, 3734 (1970).
(20) (a) B. Dietrich, J. M. Lehn, and J. P. Sauvage, *Tetrahedron Lett.*, **34**, 2889 (1969). (b) We wish to thank Professors Lehn, Strasbourgh, for supplying us with this material.
(21) D. E. O'Reilly, G. E. Schacher, and K. Schug, *J. Chem. Phys.*, **39**, 1756 (1963).
(22) H. G. Hertz, *Z. Elektrochem., Ber. Bunsenges. Phys. Chem.*, **65**, 20 (1961).
(23) M. H. Cohen and F. Reif, "Solid States Physics," Vol. 5, F. Seitz and D. Turnbull, Ed., Academic Press, New York, N. Y., 1957, p 321.
(24) H. G. Hertz, B. Lindman, and V. Siepe, *Ber. Bunsenges. Phys. Chem.*, **73**, 542 (1969).
(25) L. Endom, H. G. Hertz, B. Thul, and M. D. Zeidler, *Ber. Bunsenges. Phys. Chem.*, **71**, 1008 (1967).
(26) M. Holz, Thesis, Karlsruhe, 1973.
(27) P. Neggia, M. Holz, and H. G. Hertz, *J. Chim. Phys.*, **71**, 56 (1974).

(28) F. H. Stillinger and A. Ben-Naim, *J. Chem. Phys.*, **47**, 4431 (1967).
(29) J. E. B. Randles, "Water and Hetero Interfaces—Liquid/Colloid Particles," XVème Conseil International de Chimie, Bruxelles, 1972.
(30) H. G. Hertz and C. Rädle, *Ber. Bunsenges. Phys. Chem.*, **77**, 531 (1973).
(31) H. G. Hertz and W. Y. Wen, to be submitted for publication.
(32) See, *e.g.*, A. Abragam, "The Principles of Nuclear Magnetism," Oxford University Press, London, 1961.
(33) P. S. Ramathan, C. V. Krishnan, and H. L. Friedman, *J. Solution Chem.*, **11**, 237 (1972).

Studies of Counterion Binding by Poly(vinylsulfonate)[1]

John Hen and Ulrich P. Strauss*

School of Chemistry, Rutgers University, the State University of New Jersey, New Brunswick, New Jersey 08903

(Received November 19, 1973)

Publication costs assisted by the National Institutes of Health

The interactions of poly(vinylsulfonate) with hydrogen, silver, and selected alkali and alkaline earth metal ions have been studied by dilatometry, dialysis equilibrium, and viscosity methods, employing tetramethylammonium ion as a competing cation. A desolvation parameter, θ_v, defined as the ratio of the observed volume change to that estimated for complete desolvation of the site-bound species and hence considered a measure of the tightness of binding, correlates well with the degree of binding as determined from dialysis equilibrium. The preference of the poly(vinylsulfonate) follows the order $Ag^+ > K^+ > Na^+ > H^+ \approx Li^+ > TMA^+$, for the univalent cations, and $Ba^{2+} > Mg^{2+}$ for the divalent cations. The viscosity results show that, in general, the contractive effect by the cations on the molecular dimensions parallels the degree and tightness of binding. However the effect of hydrogen ion appears to be exceptionally weak. This result is taken to indicate that the small hydrogen ion, in contrast to the metal ions, does not cross link the polyion through simultaneous site binding to two sulfonate groups widely separated along the polymer contour. The results obtained here with poly(vinylsulfonate) are interpreted in the light of comparable findings with other polyelectrolytes.

Introduction

It has been shown that the interactions between polyions and counterions frequently exhibit pronounced specificities which may be attributed to solvation effects.[2] Among methods which have been found useful in demonstrating such specificities are the determination of polyion selectivities for competing counterions by dialysis equilibrium,[3] the comparison of the effect of different counterions on the polyion molecular dimensions by viscosity,[4-6] and the measurement of volume changes accompanying ion exchange processes by dilatometry.[7] In this paper we are presenting the results obtained by applying these methods to the interactions of poly(vinylsulfonate) (PVS) with selected pairs of the cations H^+, Li^+, Na^+, K^+, Ag^+, Mg^{2+}, Ba^{2+}, and tetramethylammonium ion (TMA^+). In most instances the TMA^+ which interacts very weakly with the polyion has been taken as one of the competing ions and may be considered a reference against which the other cations are measured. It is hoped that the correlation of the results obtained from the different experimental methods will lead to a better understanding of the mechanism of the "site binding" of counterions by poly(vinylsulfonate) in particular and also by polyelectrolytes in general.

Experimental Section

Materials. Poly(vinylsulfonic acid) (HPVS) was prepared by the polymerization of vinylsulfonic acid following the procedure of Eisenberg and Mohan.[5] The vinylsulfonic acid monomer was generated from its sodium salt, obtained from American Hoechst Corp., by the method of Breslow and Hulse.[8] The polyacid was neutralized with sodium hydroxide and the resulting poly(sodium vinylsulfonate) (NaPVS) was purified by repeated precipitations of its aqueous solutions into methanol. The granular white solid was dried *in vacuo* at 60°. Low molecular weight impurities were removed by exhaustive dialysis against conductivity water. The average molecular weight of the NaPVS was estimated to be 1.0×10^5 from viscosity measurements in 1.00 *M* NaCl at 32.4°.[9] The NaPVS was stored at 4° in the form of a 0.75 *N* stock solution from which all solutions used in this work were derived by appropriate dilution and dialysis.

All inorganic chemicals were obtained commercially in Reagent Grade form.

Dialysis Equilibrium. Solutions of PVS which had previously been brought to the desired cation form by exhaustive dialysis against the desired electrolyte and tested, where necessary, for the complete elimination of sodium ion by atomic absorption were placed into Visking cellulose casing bags, each provided with a glass bead. The bags were tumbled in the desired "outside" solution which was changed at least three times. Final equilibration was attained by tumbling for 48 hr at 30.0 ± 0.1°. The outside solution was prepared to contain two cations at a total normality close to 0.2. In those experiments involving silver the anion was nitrate; in all others it was chloride.

The concentrations of alkali and alkaline earth metal ions in the final inside and outside solutions were deter-

mined with a Techtron Model AA-4 atomic absorption spectrophotometer. Potassium, sodium, and lithium were measured with solutions diluted to 10^{-4} to 10^{-3} *M*. The presence of PVS, TMA^+, H^+, or Ag^+ did not affect the accuracy of the results. The analysis for Ba^{2+} which was carried out in the concentration range from 10^{-3} to 10^{-2} equiv/l. was sensitive to the concentration of Cl^-. Therefore the calibration curve was constructed at 0.2 *M* chloride ion. Magnesium was determined from 10^{-5} to 10^{-4} *N*. The calibration procedure was adjusted for the observed effect of PVS on the Mg^{2+} analysis.

Silver and chloride ions were determined potentiometrically in aqueous 60% acetic acid. The analysis for nitrate ion was carried out by the Devarda method.[10] Hydrogen ion was determined by potentiometric titration.

The PVS normality was measured by replacing all cations with hydrogen ion in a Dowex-50X8 ion-exchange column and analyzing the effluent for hydrogen ion concentration. From this value the total concentration of cations in the original inside solution was calculated, and the PVS normality was deduced from the electroneutrality condition. Knowledge of the total cation concentration also allowed the calculation of the TMA^+ molarity.

Dilatometry. Volume changes were measured at 30° as described previously in Linderstrom-Lang dilatometers immersed in a thermostated bath controlled within 0.001°.[7,11]

Viscosity. Viscosimetric measurements were carried out at 30° in a Cannon-Ubbelohde four-bulb dilution viscometer. Viscosities were extrapolated to zero shear rate. No shear dependence was observed.

The procedure in obtaining the appropriate solutions was as follows. An inside solution of known PVS concentration was transferred from the dialysis bag of one of the dialysis equilibrium runs into the viscometer. After its viscosity was obtained, dilutions were made with the outside solution of the same dialysis equilibrium experiment in order to keep the chemical potentials of the simple electrolyte components constant. The solvent viscosity used for the calculation of the specific viscosity was that of the outside solution.

Results and Discussion

Dialysis Equilibrium. A general treatment for obtaining a relation between binding parameters from dialysis equilibrium data involving two univalent counterions has been given previously.[3] The results of the treatment can be expressed in the form

$$\frac{\beta_1}{(C_1^+)_0} - \frac{\beta_2}{(C_2^+)_0} = \frac{\beta_1'}{(C_1^+)_0} - \frac{\beta_2'}{(C_2^+)_0} \equiv \delta_{12} \qquad (1)$$

where the desired quantities β_1 and β_2 are the fractions of sulfonate groups neutralized by bound cations C_1^+ and C_2^+, while the experimentally determined parameters β_1' and β_2' are defined by the relation

$$\beta_k' = \frac{(C_k^+)_i - (C_k^+)_o}{(PVS)} \qquad k = 1, 2 \qquad (2)$$

Parentheses indicate normalities, and the subscripts o and i refer to the outside and inside solutions, respectively. Equation 1 does not uniquely define the binding parameters β_1 and β_2, but the parameter δ_{12}, unambiguously defined by eq 1 in terms of the experimental quantities β_k' and $(C_k^+)_0$, is a useful measure of the preference of the polyelectrolyte for counterion 1 over counterion 2. An additional criterion is needed to obtain individual values for β_1 and β_2. The only requirement for the validity of eq 1 is that there are no *specific* interactions between the polyion and the *free* counterions; *i.e.*, any specific interactions must occur with the *bound* counterions. A criterion which is likely to satisfy this requirement is the identification of the bound ions with those predicted to be "condensed" by the theory of Manning.[12] For our experimental condition this criterion becomes

$$\beta_1 + \beta_2 = 0.64 \qquad (3)$$

Results from competitive dialysis equilibrium experiments involving two univalent cations are given in Tables I and II. Because of their application to the dilatometry and viscosity results to be given below, the data involving tetramethylammonium ion as one of the cations are given in detail in Table I. It should be noted that in the case of the silver ion result, the lowest value of β_1 compatible with eq 1 (corresponding to $\beta_2 = 0$) is 0.68, *i.e.*, greater than 0.64, perhaps indicating some covalent contribution to the binding. Since under these circumstances no condensation of TMA^+ would be expected, the value of 0.68 is assumed to be the correct one. The quantity δ_{12} which indicates the preference of the polyion for C_1^+ over C_2^+ appears to show some tendency to decrease with increasing ratio $(C_1^+)_0/(C_2^+)_0$ for a given cation pair, similar to observations made with ion exchange resins.[13] However, the effect is not clear cut, and further substantiation is needed. The variations in δ_{12} from one cation pair to another are quite definite and indicate the affinity order $Ag^+ > K^+ > Na^+ > H^+ > Li^+ > TMA^+$.

Direct competitive dialysis equilibrium studies of pairs of these cations at approximately equal normalities of 0.1 each in the outside solution led to values of δ_{12} which are presented in Table II, where cation 1 is indicated along the top and cation 2 along the left-hand side. As can be seen, exact additivity, *i.e.*, $\delta_{kl} + \delta_{lm} = \delta_{km}$, is not generally obtained, and perhaps should not be expected since the polyelectrolyte is in different states in 1-1 mixtures of C_k^+ and C_l^+, C_l^+ and C_m^+, and C_k^+ and C_m^+. However, in many instances deviations from additivity are small, and with the exception of the Li^+-H^+ pair, the affinity order observed in the cation-TMA^+ systems is maintained. In the case of the Li^+-H^+ pair, Li^+ seems to be preferred over H^+ in direct competition, in contrast to the indirect comparison relative to TMA^+ where H^+ was preferred over Li^+. The comparisons relative to K^+ and Ag^+ seem to indicate a very slight preference of PVS^- for Li^+ over H^+, while no preference is found relative to Na^+. Apparently the intrinsic affinities of PVS^- for Li^+ and H^+ are approximately equal, so that small changes in state of the PVS^- can affect the observed order.

Dialysis equilibrium results with Mg^{2+} and Ba^{2+} in competition with TMA^+ are given in Table III. The whole of the excess of the divalent ion in the inside solution was assumed to be due to binding, and therefore β_k was taken as equal to β_k', defined in terms of normalities as in eq 2. Barium ion appears to be bound considerably more strongly than magnesium ion, as is seen from a comparison of the values of $\beta_k/(C_k^{2+})_0$ in the last column of Table III.

Dilatometry. Table IV gives the volume changes resulting from the following type of experiment: 2 ml of initial solution I containing PVS in the TMA^+ form and TMACl were mixed with 2 ml of initial solution II containing the indicated cation C_1^{n+}, with the total chloride normality brought to 0.2 with TMACl.[14] The concentration of

TABLE I: Competitive Dialysis Equilibria of Univalent Cations and Tetramethylammonium Ion

C_1^+	$(C_1^+)_0$	$(C_2^+)_0 = (TMA^+)_0$	(PVS^-)	β_1'	β_2'	δ_{12}	β_1	β_2
Li^+	0.0488	0.1495	0.0638	0.266	0.591	1.5	0.213	0.427
	0.0740	0.1239	0.0647	0.383	0.490	1.2	0.296	0.344
	0.1005	0.0993	0.0658	0.486	0.374	1.1	0.375	0.265
Na^+	0.0480	0.1495	0.0629	0.339	0.513	3.6	0.288	0.352
	0.0693	0.1281	0.0628	0.481	0.401	3.8	0.396	0.244
	0.0940	0.1124	0.0696	0.560	0.294	3.3	0.463	0.177
K^+	0.0509	0.1115	0.0631	0.471	0.440	5.3	0.392	0.248
	0.0756	0.1290	0.0611	0.597	0.288	5.7	0.506	0.134
	0.1018	0.1138	0.0644	0.658	0.205	4.7	0.553	0.087
	0.1512	0.0496	0.0620	0.813	0.087	3.6	0.617	0.023
H^+	0.0962	0.1110	0.0741	0.485	0.338	2.0	0.395	0.245
Ag^+	0.1062	0.0822	0.0791	0.807	0.102	6.4	0.68	0

TABLE II: Values of δ_{12} from Competitive Dialysis Equilibria of Univalent Cations in Poly(vinylsulfonate) Solutions

C_2^+	C_1^+ Ag^+	K^+	Na^+	Li^+	H^+
TMA^+	6.4	4.7	3.3	1.1	2.0
H^+	5.1	3.2	2.1	1.4	
Li^+	4.9	3.0	2.1		
Na^+		1.5			
K^+	2.4				

TMACl in solution I was adjusted so that the final solution, resulting from mixing solutions I and II, would closely imitate the composition of one of the inside solutions of the dialysis equilibrium experiments described in Tables I and III. Preliminary experiments agreed with earlier findings that a number of secondary effects, including those arising from the dilution of the solutes on mixing and from any possible interaction of TMA^+ with the polyion, are negligible.[7] The composition of the final solutions is described in columns 1-4 of Table IV. Column 5 contains ΔV_P, the measured volume change expressed for convenience in units of milliliters per equivalent of PVS^-.

We would like to determine the volume change, Δv, for the reaction (per equivalent of C^{n+} and PVS^-)

$$\frac{1}{n}C^{n+} + PVS^- = C_{1/n}PVS \tag{4}$$

If we identify β_1 with the fraction of sulfonate groups which has undergone reaction 4 then we have

$$\Delta v = \Delta V_P/\beta_1 \tag{5}$$

Equation 5 must be interpreted with some caution. Reaction 4 may occur in several stages involving different extents of solvation change and hence also varying volume change.[15-17] All these stages are likely to exist simultaneously in a polyelectrolyte solution, so that, more exactly, we should have

$$\Delta V_p = \sum_j \beta_{1j}\Delta v_j \tag{6}$$

were Δv_j and β_{1j} correspond to stage j of reaction 4. The parameters β_1 and Δv in eq 5 thus represent two interdependent average quantities the estimate of one of which determines the value for the other.

The values of Δv obtained by eq 5 using the values of β_1 estimated from the dialysis equilibrium data are given in column 7 of Table IV. Several features of these results appear noteworthy. First, the magnitude of the Δv values is substantial and comparable to magnitudes obtained in simple acid-base reactions.[11] Second, for a given C_1-PVS system, Δv appears to be roughly constant, in some cases with a slight tendency to decrease with increasing β_1. Such a tendency has also been observed with polyphosphates[7] and polycarboxylates.[17] Third, on comparing the values of Δv for the various C_1-PVS systems we note significant differences which should be an indication of the extent to which bound water is released from the interacting ionic species and thereby also of the strength of the interaction. However, the various cations are hydrated to different extents in their free state, and to obtain a meaningful comparison the values of Δv should be examined relative to the hypothetical volume change, Δv_{max}, which would result from reaction 4 if the product was completely desolvated. We therefore define a desolvation parameter, θ_v, by the expression

$$\theta_v = \Delta v/\Delta v_{max} \tag{7}$$

The estimation of Δv_{max} is carried out *via* the relation

$$\Delta v_{max} = \Delta V_P^e + \Delta V_C^e \tag{8}$$

where ΔV_P^e and ΔV_C^e represent the contributions per equivalent of polyion and cation, respectively. The quantity ΔV_P^e may be obtained from the equation

$$\Delta V_P^e = V_P^i - \bar{V}_P \tag{9}$$

The partial monomolal volume of the polyanion, $\bar{V}_P$, has been reported to be 48.1 ml/equiv.[16] The intrinsic monomolal volume, V_P^i, is difficult to determine experimentally for strong polyacids. We have estimated this quantity be a displacement method using molecular models. Molecular models of PVS of different chain lengths were constructed from Courtauld atomic models. The average monomolecular volume displaced by immersing these models into a container filled with styrofoam balls was taken to represent V_P^i. The size of the styrofoam spheres was chosen so as to represent water molecules on the scale of the Courtauld models. In this way V_P^i for PVS^- was determined to be 59.0 ml/equiv, resulting in ΔV_P^e = 10.9 ml/equiv.

The molecular model method was tested with polyacrylate ion for which V_P^i can be assumed to be equal to the experimentally determined partial monomolal volume of undissociated poly(acrylic acid). A recently reported value of the latter is 46.7 ml/equiv.[16] Our molecular model method gave 48.2 ml/equiv.

The quantity ΔV_C^e may be estimated from the relation

$$\Delta V_C^e = V_C^i - \bar{V}_C \tag{10}$$

where V_C^i is the intrinsic volume per equivalent of bound desolvated cation and $\bar{V}_C$ is the partial equivalent volume of the free cation. The latter quantity was obtained from published ionic partial molal volume data,[18] using as reference point −5.4 ml/mol for the partial molal volume of hydrogen ion.[19] Several methods are available for estimat-

TABLE III: Dialysis Equilibria with Divalent Metal Ions and Tetramethylammonium Ion

C_1^{2+}	$(C_1^{2+})_0$	$(C_2^{+})_0 = (TMA^+)_0$	(PVS^-)	β_1'	β_2'	$\beta_1'/(C_1^{2+})_0$
Mg^{2+}	0.0167	0.1277	0.0894	0.573	0.330	34.3
	0.0402	0.1143	0.0970	0.690	0.243	17.2
	0.0800	0.1158	0.1110	0.780	0.250	9.8
Ba^{2+}	0.0021	0.1813	0.0959	0.380	0.512	181
	0.0038	0.1892	0.0936	0.451	0.523	119
	0.0058	0.1534	0.1250	0.488	0.463	84
	0.0074	0.1735	0.1195	0.571	0.370	77

TABLE IV: Volume Changes Due to Interaction of Metal Ions with Poly(vinylsulfonate)

C_1^{n+}	(PVS^-)	(C_1^{n+})	(TMA^+)	ΔV_P, ml/equiv of PVS	β_1	Δv, ml/equiv	Δv_{max}, ml/equiv	θ_v
Li^+	0.064	0.066	0.187	2.05	0.213	9.62	18.3 ± 0.7	0.53 ± 0.02
	0.065	0.099	0.156	2.44	0.296	8.24		0.45 ± 0.02
	0.066	0.132	0.124	2.78	0.375	7.41		0.40 ± 0.02
Na^+	0.063	0.069	0.182	2.99	0.288	10.38	20.8 ± 1.1	0.50 ± 0.02
	0.063	0.100	0.153	3.87	0.396	9.77		0.47 ± 0.02
	0.070	0.133	0.133	4.14	0.463	8.94		0.43 ± 0.02
K^+	0.063	0.081	0.139	3.86	0.392	9.85	17.9 ± 0.5	0.55 ± 0.02
	0.061	0.112	0.147	4.31	0.506	8.52		0.48 ± 0.02
	0.064	0.144	0.127	4.88	0.553	8.82		0.49 ± 0.02
	0.062	0.203	0.055	5.23	0.617	8.48		0.47 ± 0.02
H^+	0.076	0.133	0.136	2.63	0.395	6.66	16.3 ± 0.3	0.41 ± 0.01
Ag^+	0.074	0.170	0.093	9.19	0.680	13.51	19.6 ± 2.4	0.69 ± 0.08
Mg^{2+}	0.089	0.068	0.157	4.74	0.573	8.27	26.4 ± 0.8	0.31 ± 0.01
	0.097	0.107	0.134	5.69	0.690	8.25		0.31 ± 0.01
	0.111	0.167	0.143	5.26	0.780	6.74		0.26 ± 0.01
Ba^{2+}	0.096	0.038	0.230	5.74	0.380	15.11	24.1 ± 1.6	0.63 ± 0.04
	0.094	0.046	0.238	7.19	0.451	15.94		0.66 ± 0.04
	0.125	0.067	0.211	7.64	0.488	15.66		0.65 ± 0.04
	0.120	0.076	0.218	9.18	0.571	16.08		0.67 ± 0.04

ing V_C.[16,19-22] The uncertainty estimates of Δv_{max} and θ_v, given in the last two columns of Table IV, reflect the range of values of V_C obtained by these methods.

We are now in a position to compare the desolvation effects of the cations by means of the parameter θ_v. In comparing the univalent with the divalent ions, we find, somewhat surprisingly, that the divalent ions do not generally give higher values of θ_v than do the univalent cations. In fact, the values for magnesium are lower than those of any of the univalent ions studied. A comparison of the effects of the univalent ions with one another is obtained conveniently by considering the θ_v values obtained with solutions known to be in dialysis equilibrium with approximately equimolar solutions of TMA^+ and metal or hydrogen ion. These θ_v values which are underlined in Table IV are seen to follow the order $Ag^+ > K^+ > Na^+ \approx H^+ \approx Li^+$, which is consistent with the order derived in the dialysis equilibrium results. The observable rough correlation between the underlines θ_v values and the corresponding values of β_1 is not unexpected since θ_v is a measure of the *tightness* of binding and β_1 is a measure of the *number* of cations bound in competition with the common TMA^+ reference ion. Similarly, for the divalent cations, the preference of PVS for Ba^{2+} over Mg^{2+}, which was deduced from the dialysis equilibrium results, is also reflected in the θ_v values.

These results may be interpreted in terms of a competition between the cation–sulfonate coulomb interactions and the attractions of each of these species for water molecules.[23,24] For cations of high charge density, such as Mg^{2+}, Li^+, and H^+, the attraction for water molecules competes effectively with that for the large, weak-field sulfonate groups. For cations of lower charge density, such as K^+ and Ag^+, the water molecules are attracted less strongly and are more easily displaced by the sulfonate groups. An additional factor which may affect the value of θ_v is the possibility of multiple-site binding. If a cation were bound to more than one sulfonate group the extent of desolvation would be enhanced. This effect would be more likely with large than with small cations, and if the sulfonate groups involved are widely separated along the polymer contour, the effect should be reflected in a contraction of the polymer coil. The results of intrinsic viscosity determination which have a bearing on this question are given below.

Intrinsic Viscosity. Intrinsic viscosities were determined in C_1^{n+}–TMA^+ salt solutions corresponding in composition to those studied by dialysis equilibrium and dilatometry as described in the Experimental Section. The results are given in Table V expressed in units of deciliter per monomole of polyacid. All the cations are seen to depress the intrinsic viscosity from that measured in TMACl alone. Compared at corresponding C_1^{n+} to TMA^+ ratios the orders of depressing effectiveness for the univalent and divalent ions are $Ag^+ > K^+ > Na^- > Li^+ > H^+$ and $Ba^{2+} > Mg^{2+}$, respectively, which closely resembles the orders found in the dialysis equilibrium and dilatometry experiments. A revealing comparison with the dialysis equilibrium results is presented in Figure 1 where the intrinsic viscosity, $[\eta]$, is shown as a function of β_1. It is noteworthy that the data for all the univalent cations except hydrogen ion can be represented quite closely by a single curve. One might conclude from this that the intrinsic viscosity is governed solely by the effects of the cation binding on the repulsion between the charged polyion groups. However, one cannot overlook the fact that the hydrogen ion point lies a significant distance above the curve. Thus while both the dialysis equilibrium and

TABLE V: Specific Effects of Cations on the Intrinsic Viscosity of Poly(vinylsulfonate)

C_1^{n+}	$(C_1^{n+})_0$	$(TMA^+)_0$	$[\eta]$, dl/equiv
None		0.200	35.5
Li^+	0.0488	0.1495	28.5
	0.0740	0.1239	25.7
	0.1005	0.0993	24.6
Na^+	0.0480	0.1495	27.1
	0.0693	0.1281	25.2
	0.0940	0.1124	21.4
K^+	0.0509	0.1115	25.1
	0.0756	0.1290	22.4
	0.1018	0.1138	19.8
	0.1512	0.0496	15.2
H^+	0.0962	0.1110	32.8
Ag^+	0.1062	0.0822	12.0
Mg^{2+}	0.0167	0.1277	14.4
	0.0402	0.1143	7.9
	0.0800	0.1158	5.5
Ba^{2+}	0.0021	0.1813	8.3
	0.0038	0.1892	6.0
	0.0058	0.1534	2.9
	0.0074	0.1735	2.0

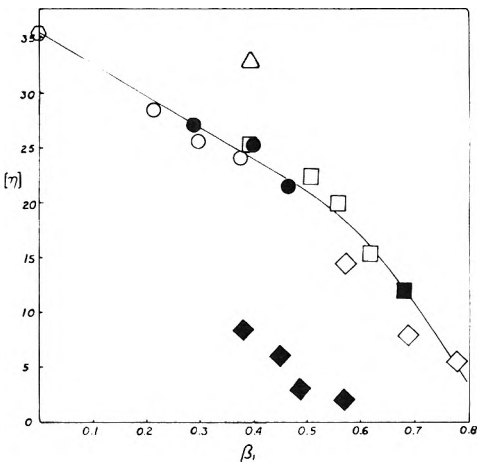

Figure 1. Intrinsic viscosity as a function of the degree of binding of hydrogen and metal ions in the presence of TMA^+: △, H^+; ○, Li^+; ●, Na^+; □, K^+; ■, Ag^+; ◇, Mg^{2+}; ◆, Ba^{2+}; ⬡, reference 0.2 *N* TMACl solution in the absence of other cations.

dilatometry results indicate a specific interaction of PVS^- with H^+, of strength about equal to that with Li^+, the H^+ clearly has an exceptionally small effect on the molecular dimensions compared to Li^+ and the other metal ions. This result can be interpreted to indicate that the bound univalent metal ions exhibit some specific depressing effect on the excluded volume through short-range interactions such as dipole-dipole attractions between metal sulfonate complexes or the multiple-site binding mentioned above. Such interactions would be expected to increase uniformly with increasing overall binding, which would result in the single curve. The small hydrogen ion can produce little or no such short-range interactions, and its effect on being bound may be mainly that of a reduction of the long-range charge repulsions.

In examining the effects of the divalent ions we note that the magnesium points lie only slightly below the curve defined by the univalent ions. This result is not too surprising in the light of the weakness of the interactions as indicated by the low values of θ_V. This weakness partly compensates for the greater tendency toward multiple site binding which would be expected for the increased cation charge. The same tendency very likely accounts for the results obtained with barium ion which produces a very much larger contracting effect on the PVS^- than do any of the univalent cations.

Conclusion

The three experimental methods which have been used here to study the interactions of several cations with poly(vinylsulfonate) indicate a high degree of correlation between the solvation changes, the selectivity, and the changes in molecular dimensions associated with these interactions. In both the alkali metal and alkaline earth metal series the effects appear to become stronger with increasing size of the *unhydrated* ions. The findings are in contrast to results obtained with polyphosphates,[3,4,6,7] polyphosphonates,[7] and polycarboxylates[25] where inversions from this order have been reported and where also, in some instances, deviations from a simple correlation between the degree of binding and the molecular dimensions have been observed.[4,6] In the case of polyphosphates the inversions in the binding order have been ascribed to very strong interactions accompanied by high degrees of desolvation which cause the ions with the smaller dehydrated size to be bound preferentially. However, the latter have less tendency for multiple site binding and hence produce a relatively smaller contracting effect on the molecular dimensions, thus accounting for the deviations from the correlation between the extent of binding and the molecular dimensions. In the case of poly(vinylsulfonate) the interactions are weaker and generally the larger unhydrated metal ions which are bound more strongly to one site are also more susceptible to binding to multiple sites.

References and Notes

(1) The support of this research by a grant from the United States Public Health Service (Grant No. GM 12307) is gratefully acknowledged.
(2) R. W. Armstrong and U. P. Strauss, "Polyelectrolytes," in "Encyclopedia of Polymer Science and Technology," Vol. 10, H. F. Mark, N. G. Gaylord, and N. M. Bikales, Ed., Wiley-Interscience, New York, N. Y., 1969, pp 781-861.
(3) U. P. Strauss and P. D. Ross, *J. Amer. Chem. Soc.*, **81**, 5299 (1959).
(4) U. P. Strauss, D. Woodside, and P. Wineman, *J. Phys. Chem.*, **61**, 1353 (1957).
(5) H. Eisenberg and G. R. Mohan, *J. Phys. Chem.*, **63**, 671 (1959).
(6) P. D. Ross and U. P. Strauss, *J. Amer. Chem. Soc.*, **82**, 1311 (1960).
(7) U. P. Strauss and Y. P. Leung, *J. Amer. Chem. Soc.*, **87**, 1476 (1965).
(8) D. S. Breslow and G. E. Hulse, *J. Amer. Chem. Soc.*, **76**, 5361, 6399 (1954).
(9) H. Eisenberg and D. Woodside, *J. Chem. Phys.*, **36**, 1844 (1962).
(10) A.O.A.C. Official Methods of Analysis, 8th ed, 1955, Method 2.28, pp 43, 574.
(11) J. Rasper and W. Kauzmann, *J. Amer. Chem. Soc.*, **84**, 1771 (1962).
(12) G. Manning, *J. Chem. Phys.*, **51**, 924 (1969).
(13) F. Helfferich, "Ion Exchange," McGraw-Hill, New York, N. Y., 1962, p 174.
(14) In these and all other experiments involving silver ion, nitrate was used instead of chloride.
(15) C. Tondre and R. Zana, *J. Phys. Chem.*, **75**, 3367 (1971).
(16) C. Tondre and R. Zana, *J. Phys. Chem.*, **76**, 3451 (1972).
(17) A. J. Begala and U. P. Strauss, *J. Phys. Chem.*, **76**, 254 (1972).
(18) F. J. Millero, *Chem. Rev.*, **71**, 147 (1971).
(19) R. Zana and E. Yeager, *J. Phys. Chem.*, **70**, 954 (1966); **71**, 521, 4241 (1967).
(20) J. Padova, *J. Chem. Phys.*, **40**, 691 (1964).
(21) P. Mukerjee, *J. Phys. Chem.*, **65**, 740, 744 (1961).
(22) B. E. Conway, R. E. Verrall, and J. E. Desnoyers, *Z. Phys. Chem.*, **230**, 157 (1965).
(23) G. Eisenman in "Symposium on Membrane Transport and Metabolism," Academic Press, New York, N. Y., 1961, pp 163-179.
(24) G. N. Ling, "A Physical Theory of the Living State," Blaisdell, New York, N. Y., 1962.
(25) H. P. Gregor and M. Frederick, *J. Polym. Sci.*, **23**, 451 (1957).

Physical Properties and Electrochemical Stability of the Thio Solvents Dimethylthioformamide and Hexamethylphosphorothioic Triamide

John W. Diggle* and D. Bogsányi

The Research School of Chemistry, Australian National University, Canberra, A.C.T. Australia *(Received October 29, 1973)*

The thio solvents dimethylthioformamide (SDMF) and hexamethylphosphorothioic triamide (SHMPT) have recently been identified as two powerful solvators of soft cations (each being a stronger soft cation solvator than the corresponding oxygen analog). For this reason the physical properties useful in correlating ion-solvent behavior have been determined for each solvent. The electrochemical stability of SDMF and SHMPT has also been determined and found to be inadequate anodically presumably due to the oxidation of the sulfur moiety. The available voltage range for SDMF and SHMPT containing 0.1 *M* tetraethylammonium perchlorate is +0.15 to −2.5 V and +0.4 to −1.3 V, respectively, *vs.* the Pleskov electrode in acetonitrile as reference. The high dielectric constants of 47.5 and 39.5 for SDMF and SHMPT, respectively, suggest that they would make good solvents for strong electrolyte solutions, and the dipole moments, being 4.37 and 4.83 D for SDMF and SHMPT, respectively, indicate these solvents to be highly polarizable. From the dipole moment it is also concluded that both HMPT and SHMPT are slightly associated in the pure form, whereas DMF and SDMF are not associated. In contrast to HMPT, sodium or potassium metal when added to SHMPT does not liberate the blue coloration supposedly characteristic of the solvated electron.

Introduction

Dimethylthioformamide (SDMF) and hexamethylphosphorothioic triamide (SHMPT) and their respective oxygen analogs DMF and HMPT permit a convenient comparison of ion-solvent interactions in terms of the Pearson[1] hard-soft classification. For example,[2,3] SDMF and SHMPT, both being classified as soft solvents, interact strongly with soft cations (Ag^+, Cu^+) resulting in these thio solvents being stronger solvators for soft cations than the oxygen analogs. Conversely, hard cations (Li^+, Na^+ and K^+) interact much more weakly with the soft solvents SDMF and SHMPT than they do with the harder oxygen analogs DMF and HMPT, thus the oxygen analogs are stronger solvators of the hard cations. Since data on the physical properties of these two thio solvents appeared sparse, these data were generated in the present work. It was also considered to be of interest to ascertain the electrochemical stability of SDMF and SHMPT, this was done using tetraethylammonium perchlorate and sodium tetrafluoroborate as solutes.

Experimental Section

Dimethylthioformamide was prepared from dimethylformamide and phosphorus pentasulfide, according to the method of Willstatter and Wirth,[4] and then twice fractionally distilled after drying with activated 4A molecular sieves.

Hexamethylphosphorothioic triamide was prepared by the reaction between phosphorus trichloride and dimethylamine in an ether medium, according to Burg and Slota,[5] and then allowing the product $(Me_2N)_3P$ to react with sulfur according to Vetter and Noeth.[6] The product SHMPT was finally twice fractionally distilled after drying with activated 4A molecular sieves.

SDMF and SHMPT prepared in the manner described above contained 45 and 19 ppm of H_2O, respectively, as determined by Karl Fischer titration.

Boiling point, melting point, and density (weighing bottle technique) were determined in the conventional manner.[7] Refractive indices (n_D) were determined using an Abbé 60 refractometer; specific conductivity was determined using a Type B221 Wayne Kerr bridge and conductivity cell of cell constant 1.93 cm^{-1}; surface tension was determined using a Cambridge Du Nuoy tensiometer and viscosity was determined by employing a No. 6 Viscometer tube for SHMPT and a Kimax A53 Size 50 viscometer tube for SDMF.

The dielectric constants (ϵ) of SDMF and SHMPT were determined using a capacitance meter and probe,[8] described in ref 9 in conjunction with a capacitance cell comprising of a 22 gauge platinum wire 25 mm in length axially disposed in a copper cylinder of 5 mm diameter and 25 mm length. The frequency of the capacitance measurement (2 MHz) is sufficiently high to permit accurate measurement, in the picofarad range, without significant error being introduced by dc conduction in the capacitance cell.

This capacitance meter, cell, and probe was calibrated with nine solvents of known dielectric constant (ranging from 7.5 to 80) and a direct capacitance reading (in pF) *vs.* dielectric constant calibration graph constructed. The dc resistance of all solvents studied in this work was >100 Kilohms when in the capacitance cell.

The dipole moment (μ) of SDMF and SHMPT was obtained by the following methods: (i) Onsager calculation[10] using the physical properties as measured in this work; (ii) the Halverstadt and Kumler method[11] in which the values of ϵ, n_D, and density are determined for a series of solutions of the thio solvent in both benzene and carbon tetrachloride.

The electrochemical stability of SDMF and SHMPT containing either 0.1 *M* tetraethylammonium perchlorate or 0.1 *M* $NaBF_4$ (saturated solutions containing >0.1 *M* were used in some cases) was determined using a conventional three-compartment double H cell, each compartment being separated from the other by a porosity 4 sin-

TABLE I: Physical Properties of SDMF, SHMPT, DMF, and HMPT[a]

Property	Solvent			
	SDMF	DMF[b]	SHMPT	HMPT[b]
Bp, °C	67–70 (1 mm)	153.0 (760 mm)	94 (1.5 mm)[c]	233 (760 mm)
Mp, °C	−8.5	−60.4	29.0	7.2
Density, d, g/cm^3	1.0237 (27°)	0.9440	1.043	1.0270 (20°)
n_D	1.5741 (27°)	1.4282	1.5070	1.4570
Specific conductivity, Mhos/cm	1.9×10^{-7}	6×10^{-8}	3.1×10^{-7}	1.9×10^{-7} (23°)[d]
Surface tension, dyn/cm	45.4	35.2	28.7	33.8 (20°)
Viscosity, cP	1.98	0.802	5.55	3.47 (20°)
ϵ	47.5	36.7	39.5	28.3[e]
μ, Onsager calcd[f]	4.44	4.07	6.25	5.38
μ, in stated solvent	4.37 (CCl_4)[g]	3.86 (C_6H_6)	4.83 (CCl_4)[g]	4.48 (C_6H_6)[g,h]
Basicity, $SbCl_5$[i]	37.3[j]	26.6[k]		38.8[k]
Basicity, $CHCl_3$[l]		0.78[m]	0.90[n]	1.83[n]
Basicity,[o] ΔG_{tr}, Na^+	+11.7	−4.5	+5.9	−5.5
Basicity,[o] ΔG_{tr}, Ag^+	−22.6	−5.2	−18.8	−9.6
Molar polarizability,[p] cm^3	75.4	71.3	177.7	158.0
Molecular polarizability,[q] Å^3	14.7	7.91	22.5	18.8

[a] For SHMPT all measurements were at 30°; all other measurements were at 25° except where stated otherwise. [b] Reference 25. [c] This value agrees quite closely with that reported by Keat and Shaw[29] but does not agree with that value reported by Vetter and Noeth.[6] [d] Reference 26. [e] Reference 20. [f] Reference 10. [g] See text for discussion of these values. [h] Reference 21. [i] Basicity expressed as the negative of the enthalpy of interaction between $SbCl_5$ and the stated solvent in high dilution in 1,2-dichloroethane.[16] [j] Reference 2. [k] Reference 16. [l] Basicity expressed as nmr chemical shifts of $CHCl_3$ at infinite dilution in the stated solvent.[27,28] [m] Reference 27. [n] Reference 28. [o] Basicity expressed as the free energy of transfer (kcal/mol) of either Na^+ or Ag^+ from water to the stated solvent taken from ref 2 and 3. [p] $[(\epsilon - 1)/(\epsilon + 2)](M/d)$. [q] $[(n_D^2 - 1)/(n_D^2 + 2)][3/4\pi N]$.

ter. The working electrode[12] (a platinum disk of area 25 mm^2) was situated in the center compartment, and the counter electrode (a large surface area platinum spiral) in the right compartment. Into the left compartment which contained the working electrolyte was dipped the reference electrode of Ag|10^{-2} M $AgClO_4$, 10^{-1} M TEAP, acetonitrile, contained within its own compartment and separated from the thio solvent in the left compartment by an additional porosity 4 sinter. The voltage range of each solvent containing Et_4NClO_4 or $NaBF_4$ was obtained using a Princeton Applied Research Model 170 electrochemistry system in the cyclic voltammetry mode at 100 mV/sec and employing iR compensation. The voltage range is recorded as those anodic and cathodic voltages at which the total current exceeds 50 μA.

The measured physical properties of SDMF and SHMPT along with solvent basicity values and molar and molecular polarizabilities are shown in Table I. The electrochemical data from SDMF and SHMPT are shown in Table II. In both tables the respective data for DMF and HMPT are shown for the purposes of comparison.

TABLE II: Electrochemical Voltage Range of DMF, HMPT, SDMF, and SHMPT Containing Either Et_4NClO_4 or $NaBF_4$ of 0.1 M Concentration Except Where Otherwise Noted[a]

Solvent	Solute	
	0.1 M Et_4NClO_4, V	0.1 M $NaBF_4$, V
DMF	+1.2 to −2.7	+1.2 to −3.4
SDMF	+0.15 to −2.5	+0.2 to −3.5[b]
HMPT	+0.6 to −1.3	+0.5 to −2.5[c,d]
SHMPT	+0.4 to −1.3[b]	+0.5 to −3.1[b]

[a] The reference electrode in each case being Ag|10^{-2} M $AgClO_4$, 0.1 M Et_4NClO_4, acetonitrile. [b] Saturated solution of the solute in this solvent was less than 0.1 M. Appropriate iR compensation in the experimentation was however still possible. [c] This cathodic limit is equivalent to −2.2 V *vs.* aqueous sce, the electrode Ag|10^{-2} M $AgClO_4$, CH_3CN being +0.300 V *vs.* aqueous sce. This value of −2.2 V does however include junction potentials due to HMPT|CH_3CN and CH_3CN|H_2O junctions; however, these are considered to introduce only a ±50 mV error.[30] [d] This cathodic limit is suspected to be low due to low level water contamination which, for HMPT, is known[31] to produce a positive potential shift in the cathodic limit. Previously reported values[31-33] range from −3.0 to −3.2 V (aqueous sce).

Discussion

The electrochemical stability of the thio solvents to oxidation is expectedly inferior to that of the oxygen analogs, this being presumably due to the oxidation of the sulfur moiety and thus being independent of the anion present. The electrochemical stability toward reduction is dependent upon the cation, and essentially identical for each pair of thio and oxygen solvents.

The liberation of the blue coloration, supposedly indicative of solvated electrons,[13] was observed in HMPT + $NaBF_4$ at high cathodic potentials but was not observed for SHMPT + $NaBF_4$. Both sodium and potassium metal were essentially insoluble in SHMPT with no blue coloration being observed (this is in contrast to the well-known moderately stable blue solutions of Na or K in HMPT[14,15]). If the electron may be classified as a hard acid then greater stabilization, *i.e.*, solvation, will occur with the harder of the two solvents, *i.e.*, HMPT.[2,3]

As mentioned in the Introduction, SDMF and SHMPT are strong solvators, *i.e.*, strong bases, of soft cations, *e.g.*, Ag^+, while they are weak bases in their interactions with hard cations, *e.g.*, Na^+ (see Table I). On these principles the greater donor number for SDMF on the Gutman scale of basicities[16] shows SDMF to be a stronger base than DMF; therefore, $SbCl_5$:SDMF adduct formation must typify a soft–soft interaction. The basicities expressed as $CHCl_3$ chemical shifts would seem to represent, at least in the case of SHMPT and HMPT, a hard–hard interaction since SHMPT has the lower shift of the two solvents.

The thio solvent molecules are more covalent and more polarizable than their oxygen analogs.[17] The dipole mo-

ments of both thio solvents are higher than their respective oxygen analogs (see Table I), the value for SDMF of 4.37 D being in good agreement with the previous literature[18] value of 4.54 D obtained in CCl_4 solvent. The dipole moment results in Table I would seem to indicate that the greater polarizability of the thio solvent molecule more than compensates for the decreased ionicity of the P=S bond; thus, the dipole moments of thio solvents are greater than their respective oxygen analogs.

Dipole moment results in benzene, at weight fractions of thio solvent up to 0.20, were substantially lower than those reported in Table I using CCl_4 as solvent, *i.e.*, in benzene, dipole moments of 3.91 and 3.37 D were obtained for SHMPT and SDMF, respectively. This would seem to be in accord with the interactions previously observed by Keat and Shaw[19] between HMPT and benzene; interactions between benzene and the solute being studied are known to produce a significant lowering of the dipole moment.[18,20]

The choice of μ = 4.48 D for HMPT requires some comment. The five literature values reported for the dipole moment of HMPT, being obtained by various methods in benzene solution, are 4.31,[21] 4.48,[21] 5.54,[22] 4.30,[23] and 4.31.[24] It is to be noted that these values, with the exception of 5.54 where no experimental procedures were stated, were obtained at weight fractions of HMPT in benzene much less than 0.020. Since the majority of results seem to favor a dipole moment of HMPT around 4.3–4.4, the most recent value[21] of 4.48 D is accepted and taken in Table I. This value for HMPT is significantly lower than the calculated Onsager value[10] of 5.38 D, *i.e.*, the Kirkwood correlation factor[10] $g > 1$; this could perhaps indicate that HMPT is somewhat associated in the pure state, a conclusion in agreement reported by Gal and Molitor-Bouchetout.[21] A similar conclusion may be made concerning SHMPT, whereas SDMF is apparently not associated since the Onsager value of 4.44 D is close to the measured value of 4.37 D.

The high dielectric constants of these two thio solvents, in conjunction with their high polarizabilities, should make SDMF and SHMPT excellent solvents for electrolyte studies and as a media for inorganic and organic reactions.

Acknowledgments. The authors gratefully acknowledge the cooperation extended to them by Dr. J. S. Dryden of the National Standards Laboratory, Sydney, for the accurate measurements of ϵ required in the Halverstadt and Kumler method for determining the dipole moments reported in this work.

The authors are indebted to Dr. A. J. Parker for his encouragement and discussion during the course of this work.

References and Notes

(1) R. G. Pearson, *Surv. Progr. Chem.*, **5**, 1 (1969).
(2) W. E. Waghorne, Ph.D. Dissertation, Australian National University, 1972.
(3) R. Alexander, D. A. Owensby, A. J. Parker, and W. E. Waghorne, *Aust. J. Chem.*, in press.
(4) R. Willstatter and T. Wirth, *Berichte*, **42**, 1908 (1909).
(5) A. B. Burg and P. J. Slota, Jr., *J. Amer. Chem. Soc.*, **80**, 1107 (1958).
(6) H. J. Vetter and H. Noeth, *Berichte*, **96**, 1308 (1963).
(7) A. Finlay, "Practical Physical Chemistry," Longmans, Green and Co., London, 1955.
(8) The capacitance meter and probe used in this work differs from that described by Pik[9] in that the capacitance range was expanded from 50 to 150 pF. The circuit diagram as given by Pik[9] is incorrect in that diode OA 91 should be located at the 100K resistor end to the 100-pF capacitor, and not after the 100-pF capacitor as shown.
(9) P. Pik, *Electron. Aust.*, 42 (March 1971).
(10) C. P. Smyth, "Dielectric Behaviour and Structure," McGraw-Hill, New York, N. Y., 1955, p 226.
(11) I. F. Halverstadt and W. D. Kumler, *J. Amer. Chem. Soc.*, **64**, 2988 (1942).
(12) The platinum working electrode surface was pretreated by etching in hot concentrated nitric acid for 2 min followed by a 5-min immersion in a saturated aqueous solution of ferrous sulfate. The electrode was then washed in water and acetone, dried, and then finally rinsed in the electrolyte to be studied.
(13) (a) J. M. Brooks and R. R. Dewald, *J. Phys. Chem.*, **72**, 2655 (1968); (b) R. Catterall, L. P. Stodulski, and M. C. R. Symons, *J. Chem. Soc. A*, 437 (1968).
(14) T. Cuvigny, J. Normant, and H. Normant, *C. R. Acad. Sci., Ser. C*, 3503 (1964).
(15) H. Normant, T. Cuvigny, J. Normant, and B. Angelo, *Bull. Soc. Chim. Fr.*, 1561 (1965).
(16) V. Gutmann, *Chem. Brit.*, 7, 102 (1971).
(17) W. Walter and J. Voss, "The Chemistry of the Amides," J. Zabicky, Ed., Interscience, New York, N. Y., 1970, Chapter 8, p 385.
(18) W. Walter and H. Hühnerfuss, *J. Mol. Struct.*, **4**, 435 (1969).
(19) R. Keat and R. A. Shaw, *J. Chem. Soc. A*, 703 (1968).
(20) I. Suzuki, *Spectrochim. Acta*, **16**, 471 (1960).
(21) J.-Y. Gal and C. Moliton-Bouchetout, *Bull. Soc. Chim. Fr.*, 464 (1973).
(22) J. E. Dubois and H. Viellard, *J. Chim. Phys.*, **62**, 699 (1965).
(23) J. P. Fayet, *C. R. Acad. Sci., Ser. C*, **270**, 9 (1970).
(24) Sr. M. Schafer and C. Curran, *Inorg. Chem.*, **4**, 623 (1965).
(25) J. A. Riddick and W. B. Burger, "Techniques of Chemistry," Vol. II, "Organic Solvents," 3rd ed, Wiley, New York, N. Y., 1970.
(26) D. A. Owensby, A. J. Parker, and J. W. Diggle, *J. Amer. Chem. Soc.*, in press.
(27) J. J. Delpuech, *Tetrahedron Lett.*, 2111 (1965).
(28) G. Martin and A. Besnard, *C. R. Acad. Sci., Ser. C*, **257**, 2463 (1963).
(29) R. Keat and R. A. Shaw, *J. Chem. Soc. A*, 4802 (1965).
(30) J. W. Diggle and A. J. Parker, *Aust. J. Chem.*, submitted for publication.
(31) J. E. Dubois, P. C. Lacaze, and A. M. de Ficquelmont, *C. R. Acad. Sci., Ser. C*, **262**, 249 (1966).
(32) J. E. Dubois, P. C. Lacaze, and A. M. de Ficquelmont, *C. R. Acad. Sci., Ser. C*, **262**, 181 (1966).
(33) Y. Kanzaki and S. Aoyague, *J. Electroanal. Chem.*, **36**, 297 (1972).

Solvent Isotope Effects for Sulfonephthalein Indicator Dianion–H^+ Recombination Kinetics

David J. Lentz, J. E. C. Hutchins, and Edward M. Eyring*

Department of Chemistry, University of Utah, Salt Lake City, Utah 84112 *(Received March 29, 1973; Revised Manuscript Received January 2, 1974)*

Publication costs assisted by the Air Force Office of Scientific Research, Chemical Directorate

Acid-base recombination rates for Bromocresol Green (BCG), Bromocresol Purple (BCP), and Chlorophenol Red (CPR) have been determined in H_2O and D_2O at 25° ($I \approx 0$) by the spectrophotometric electric field jump relaxation technique. For the reaction $H^+ + In^{2-} \rightarrow HIn^-$ in water the specific rates (in units of 10^{10} M^{-1} sec^{-1}) are 7.71 ± 0.97, 7.77 ± 0.43, and 9.44 ± 0.48 for BCG, BCP, and CPR, respectively. The corresponding specific rates in deuterium oxide for the reaction $D^+ + In^{2-} \rightarrow DIn^-$ are 5.16 ± 0.50, 6.36 ± 1.48, and 6.14 ± 0.81, respectively. The average solvent deuterium oxide kinetic isotope effect on this reaction is therefore ~1.4 in good agreement with a theoretical value of ~1.3 derivable from Debye's phenomenological equation for the specific rate of a diffusion-controlled ion recombination.

Introduction

The Debye equation[1] (eq 1) successfully predicts

$$k_{diff} = \frac{4\pi N_A Z_A Z_B e_0^2 (D_A + D_B)}{1000\epsilon kT(\exp[Z_A Z_B e_0^2/\sigma\epsilon kT] - 1)} \quad (1)$$

the maximum rates with which protons and small anions or molecules having high symmetries can diffuse together and react. (The significance of the symbols in eq 1 and their numerical values are given below.) Reactions for which recombination rate constants fall close to values predicted by eq 1 are[2-8] $H^+ + OH^-$, $D^+ + OD^-$, $H^+ + F^-$, $H^+ + HS^-$, $H^+ + NH_3$, $H^+ + (CH_3)_3N$, and $H^+ + SO_4^{2-}$. There exists, however, a far larger group of acid-base reactions whose recombination rates fall short of the values predicted by a factor of 2 or more.[9] Included in this group are the reactions of a number of sulfonephthalein indicators whose recombination rates have been measured by the spectrophotometric electric field jump technique.[10-13] Steric factors are usually invoked to account for such discrepancies.

In a recent kinetic study of Bromocresol Green (BCG) dianion recombination with H^+ in glycerol-H_2O mixtures in which solution viscosity was varied 20-fold there were indications that some process other than diffusion was rate limiting in water, whereas diffusion predominated in 70% glycerol. In the present study the recombination reactions of three sulfonephthalein indicator anions have been examined in H_2O and D_2O to determine whether rate changes are in agreement with those predicted for a diffusion controlled reaction, or not. The ratio of specific rates for the reactions $H^+ + OH^- \rightarrow H_2O$ and $D^+ + OD^- \rightarrow D_2O$ in water[2] and deuterium oxide[3] respectively is $k_r(H)/k_r(D) = 1.67 \pm 0.15$ in good agreement with the value 1.54 estimated[4] from eq 1. In the same vein, the agreement between ratios of equivalent conductances in water and in D_2O of a number of univalent electrolytes determined experimentally and estimated from the Stokes equation[14] is within 2%. Thus we have good reason to expect that the ratio of experimental specific rates for the reactions $H^+ + In^{2-} \rightarrow HIn^-$ and $D^+ + In^{2-} \rightarrow DIn^-$ in water and D_2O, respectively, where In^{2-} represents a sulfonephthalein dianion, will agree well with a value $k_r(H)/k_r(D) = 1.3$ estimated from eq 1 if these reactions involving sulfonephthalein dianions are diffusion controlled. Implicit in this expectation is the reasonable assumption that the so-called steric factor P, where $0 < P < 1$, in the equation

$$k_{obsd} = Pk_{diff} \quad (2)$$

will be unaffected by the substitution of D_2O for water as solvent in these reactions of sulfonephthalein dianions. The topics of steric factors and angular constraints in diffusion-controlled reactions have been discussed rather thoroughly by Eigen,[5,9] Grunwald,[15] and Schurr.[16]

Experimental Section

The spectrophotometric E-jump apparatus used for the kinetic measurements and its mode of operation have been previously described.[10-12] A new sample cell was constructed from Kel-F having circular quartz windows of 4 mm diameter. Unwanted electrical discharges were found to be greatly reduced by the use of Kel-F, and the cell opacity prevented spectrophotometric errors from any coronal glow at the H.V. electrode-pulse generator connection. The in-liquid light path length of the cell was 15 mm. An air-cooled 2000-W tungsten lamp (Sylvania-FEY) was used as the light source in conjunction with a Bausch & Lomb 1200 line/mm grating monochromator with slits fully open. The indicator dianion was monitored in all cases at its λ_{max}: BCG, 617 nm; BCP, 588 nm; CPR, 575 nm.

Bromocresol Green (3′,3″,5′,5″-tetrabromo-*m*-cresol sulfonephthalein, BCG) and Chlorophenol Red (3′,3″-dichlorophenol sulfonephthalein, CPR) were recrystallized from glacial acetic acid; Bromocresol Purple (5′,5″-dibromo-o-cresol sulfonephthalein, BCP) was recrystallized from benzene. Stock solutions were made by using a Mettler H16 analytical balance and diluted as required. Distilled water was deionized and redistilled from glass. Deuterium oxide (Stohler isotope chemicals 99.8% D) was redistilled before use. Analysis[17] of reaction solutions after use showed a deuterium content not less than 99.7%.

pH measurements were made with a Beckman 1019 pH meter equipped with a Broadley-James 9008 microcombination electrode. All measurements were made in the

TABLE I: Electric Field Jump Relaxation Method Experimental Data for Three Sulfonephthalein Indicators in Water at 25°

C_0,[a] 10^{-5} M	pH[b]	τ^{-1},[c] 10^6 sec^{-1}	($[H^-]$ + $[In^{2-}])\gamma_{In^{2-}}$,[d] 10^{-5} M
	Bromocresol Green in Water		
8.27	4.09	6.10	8.51
4.14	4.33	4.63	5.32
4.14	4.47	3.84	4.33
1.65	4.68	2.76	2.62
1.65	4.94	2.80	1.76
11.2	4.00	9.40	10.6
1.12	5.20	2.67	1.35
1.12	5.59	1.57	1.16
0.56	5.41	1.48	0.803
8.27	3.91	12.52	12.4
	Bromocresol Purple in Water		
11.8	4.20	4.77	6.14
11.8	4.41	2.89	3.76
11.8	4.65	1.82	2.33
11.8	4.94	1.21	1.42
11.8	5.15	0.913	1.19
	Chlorophenol Red in Water		
10.0	4.54	2.89	2.97
10.0	4.71	1.88	2.16
10.0	4.99	1.41	1.48
10.0	5.21	1.37	1.39
5.0	5.48	1.03	1.02
1.0	5.82	0.480	0.415
1.0	6.02	0.498	0.457

[a] Total sulfonephthalein concentration in moles per liter. [b] Average glass electrode pH of sample solution in the electric field jump cell before and after high voltage pulses. [c] Reciprocal of the chemical relaxation time corrected for the instrumental time constant as explained in ref 19 of the text. [d] Sum of calculated molar concentrations of hydrogen ion and sulfonephthalein dianion multiplied by the Debye–Hückel limiting law activity coefficient for a dianion.

TABLE II: Electric Field Jump Relaxation Method Experimental Data for Three Sulfonephthalein Indicators in Deuterium Oxide at 25°

C_0,[a] 10^{-5} M	pD[b]	τ^{-1},[c] 10^6 sec^{-1}	($[D^-]$ + $[In^{2-}])\gamma_{In^{2-}}$,[d] 10^{-5} M
	Bromocresol Green in D_2O		
8.74	4.77	1.83	3.24
8.74	4.61	1.82	3.54
8.74	4.41	2.76	4.49
8.74	4.21	3.84	6.47
8.74	4.00	4.28	9.82
0.874	5.57	0.778	0.784
0.874	5.04	0.772	1.16
0.874	5.21	0.667	0.950
8.46	4.38	2.88	4.72
8.46	4.17	4.28	6.94
8.46	3.96	5.77	10.9
2.54	4.67	1.56	2.48
2.54	5.06	1.07	1.64
2.54	5.38	0.896	1.62
	Bromocresol Purple in D_2O		
12.8	4.44	2.30	3.49
12.8	4.51	2.23	2.97
12.8	4.64	1.61	2.22
12.8	4.79	1.36	1.64
12.8	4.95	0.803	1.19
12.8	5.08	0.593	0.953
12.8	5.26	0.379	0.816
12.8	5.37	0.356	0.728
	Chlorophenol Red in D_2O		
7.80	4.70	1.18	1.97
7.80	5.25	0.490	0.783
7.80	5.82	0.420	0.972
7.80	5.58	0.649	1.26
7.80	5.03	0.855	1.19
7.80	4.69	1.54	2.11
1.75	6.14	0.265	0.427
1.75	5.73	0.276	0.341
1.75	5.18	0.637	0.696
1.75	5.25	0.351	0.608
1.75	5.54	0.251	0.388
1.75	5.69	0.188	0.347

[a] Total molar concentration of sulfonephthalein. [b] Glass electrode pH + 0.4 pH units. [c] Reciprocal of chemical relaxation time corrected for instrumental time constant (see footnote 19.) [d] Sum of calculated molarities of deuterium ion and sulfonephthalein dianion multiplied by the Debye–Hückel limiting law activity coefficient for a dianion.

sample cell immediately before and directly after the kinetic determination. Agreement to within ±0.01 pH units was generally obtained and the average value was used to calculate $[H^+]$, assuming pH = $-\log [H^+]$. pD was taken as pH reading plus 0.40.[18] pH or pD in the cell was adjusted by the addition by microsyringe of small amounts of acid or base made up in the appropriate indicator solution. At least four relaxation curves were obtained for each solution using photographic recording. Values of τ, the relaxation time, were determined by semilog graphing of the exponential photographic trace. The standard deviation of τ was found to average about 8% of the mean value.

Experimental kinetic data for the three sulfonephthalein indicators in water and D_2O are given in Tables I and II.

A Beckmann DB spectrophotometer with 1-cm cells thermostatted at 25 ± 0.1° was used to determine pK_a values shown in Table III. pH measurements were again made directly in the cell.

Results

Indicator reactions for BCG, BCP, and CPR are of the type

$$H^+ + In^{2-} \underset{k_d}{\overset{k_r}{\rightleftharpoons}} HIn^- \qquad (3)$$

Changes in ionic strength accompanying the relaxation of this equilibrium when the electric field is removed are neglected, and activity coefficients, γ, are found from the Debye–Hückel limiting law and the known initial ionic strength ($I < 1.5 \times 10^{-4}$ M). After cancellation of equal activity coefficients, the relaxation time,[19] τ, for the reaction in eq 3 is given by[20]

$$\tau^{-1} = \gamma_{In^{2-}}([H^+] + [In^{2-}])k_r + k_d \qquad (4)$$

Since numerical values of $K_a = k_d/k_r$ are known with much greater precision than values of τ and since the reaction being observed kinetically is unquestionably that shown in eq 3, it is more appropriate to interpret the data of Tables I and II using the equation

$$\tau^{-1} = k_r\{([H^+] + [In^{2-}])\gamma_{In^{2-}} + K_a\} \qquad (5)$$

In effect, we wish to deduce a value of k_r from a best fit of the experimental data to the equation $y = k_r\chi$ where imprecision in y is approximately a constant per cent of the magnitude of y and liability of error is essentially limited to y. In such a case[21] the least-squares straight line

$$\ln k_r = \frac{1}{N}\sum_{i=1}^{N} \ln\left(\frac{y_i}{\chi_i}\right) \qquad (6)$$

TABLE III: Spectrophotometrically Determined pK_a Values for Sulfonephthalein Dyes in H_2O and D_2O (25°, $I \approx 0$)[a]

	$pK_a(H)$	$pK_a(D)$
Bromocresol Green	4.91[b]	5.38
Bromocresol Purple	6.47	6.93
Chlorophenol Red	6.25	6.73

[a] Data given in D. J. Lentz, Ph.D. Thesis, University of Utah, 1973. [b] Value determined previously.[10]

TABLE IV: Rate Constants for Sulfonephthalein Dianion–H^+ Recombination Reactions in H_2O and D_2O at 25° ($I \approx 0$)

	$k_r(H)$,[a] 10^{10} M^{-1} sec^{-1}	$k_r(D)$,[a] 10^{10} M^{-1} sec^{-1}	$k_r(H)/k_r(D)$[b]
Bromocresol Green	7.71 ± 0.97	5.16 ± 0.50	1.49 ± 0.33
Bromocresol Purple	7.77 ± 0.43	6.36 ± 1.48	1.22 ± 0.35
Chlorophenol Red	9.44 ± 0.48	6.14 ± 0.81	1.53 ± 0.28

[a] Error limits are 95% confidence limits, $\pm ts/n^{1/2}$, where t denotes the "Student t," s is the sample standard deviation, and n is the number of observations. [b] Error limits of a quotient are the sum of the absolute values of the relative uncertainties in the factors. (F. Daniels, *et al.*, "Experimental Physical Chemistry," 7th ed, McGraw-Hill, New York, N. Y., 1970, p 437.)

most appropriately represents the observed data and was used to calculate the specific rates shown in Table IV.

Auborn, *et al.*,[10] previously reported in the case of BCG at 25° that $k_r = 5.4 \times 10^{10}$ M^{-1} sec^{-1}; for BCP, Ilgenfritz[13] found $k_r = 8.0 \times 10^{10}$ M^{-1} sec^{-1} at 15°. These workers used essentially the same techniques as in the present paper. The discrepancies between these specific rates and those of Table IV are probably attributable to slight differences in the handling of the data.[22] For CPR, Eigen[23] reported a value of $k_r = 2.3 \times 10^{10}$ M^{-1} sec^{-1} (I = 0.1 M, 15°) using T-jump. Lowering the ionic strength and raising the temperature both increase k_r.

Discussion

The Debye equation (eq 1) may be used to predict values for diffusion-controlled ion recombination rate constants in H_2O or D_2O, if a reasonable value for the reaction distance σ is assumed. Symbols in eq 1 have the following significance: N_A is Avogadro's number, Z_A and Z_B are the ionic charges, ϵ is the dielectric constant of the medium, and k is Boltzmann's constant. Substituting the following values: $D_{H^+} = 9.33 \times 10^{-5}$ cm^2 sec^{-1} (calculated from $\lambda_0 = 349.9$ Ω^{-1} cm^2/mol),[24] $D_{In^{2-}} = 2 \times 10^{-5}$ cm^2 sec^{-1},[11] $\epsilon = 78.54$,[25] and $\sigma = 7.5$ Å,[9] then $k_{diff}^{H} = 1.44 \times 10^{11}$ M^{-1} sec^{-1}. Similarly if for D_2O we use $D_{D^+} = 6.45 \times 10^{-5}$ cm^2 sec^{-1} (from $\lambda_0 = 242.4$ Ω^{-1} cm^2/mol),[14] $\epsilon = 77.94$,[25] $\sigma = 7.5$ Å, then $k_{diff}^{D} = 1.07 \times 10^{11}$ M^{-1} sec^{-1}. If the reactions are truly diffusion controlled and limited by only a steric constant P (eq 2) then

$$k_r(H)/k_r(D) = k_{diff}^{H}/k_{diff}^{D} = 1.34 \quad (7)$$

From the results in Table IV it appears that for all three sulfonephthaleins the observed ion recombination kinetic isotope effect falls close to this calculated value. The 95% confidence limits for the three kinetic isotope effects overlap, indicating that differences between the three values may not be significant. Thus these solvent isotope experiments do not lend any support to the earlier suggestion[11] that some process other than diffusion could be rate determining in the recombination of a proton with Bromocresol Green dianion in aqueous solution.

We also note in Table IV that $k_r(H)$ for BCG or BCP is probably significantly smaller than that for CPR. Thus one might be tempted to invoke steric or inductive effects, based on slight differences in the structures of the respective dianions, to account for these differences in $k_r(H)$. However, the fact that the same trend implausibly fails to emerge from the values of $k_r(D)$ prohibits such speculative arguments for the time being.

Acknowledgments. This work was supported by Grant No. AFOSR 73-2444 from the Directorate of Chemical Sciences, Air Force Office of Scientific Research.

References and Notes

(1) P. Debye, *Trans. Amer. Electrochem. Soc.*, **82**, 265 (1942).
(2) M. Eigen and L. De Maeyer, *Z. Elektrochem.*, **59**, 986 (1955).
(3) G. Ertl and H. Gerischer, *Z. Elektrochem.*, **65**, 629 (1961).
(4) G. Ertl and H. Gerischer, *Z. Elektrochem.*, **66**, 560 (1962).
(5) M. Eigen and K. Kustin, *J. Amer. Chem. Soc.*, **82**, 5952 (1960).
(6) M. T. Emerson, E. Grunwald, and R. A. Kromhaut, *J. Chem. Phys.*, **33**, 547 (1960).
(7) E. Grunwald, *J. Phys. Chem.*, **67**, 2208 (1963).
(8) M. Eigen, G. Kurtze, and K. Tamm, *Z. Elektrochem.*, **57**, 103 (1953).
(9) M. Eigen, W. Kruse, G. Maass, and L. De Maeyer, *Progr. React. Kinet.*, **2**, 306 (1964).
(10) J. J. Auborn, P. Warrick, Jr., and E. M. Eyring, *J. Phys. Chem.*, **75**, 2488 (1971).
(11) P. Warrick, Jr., J. J. Auborn, and E. M. Eyring, *J. Phys. Chem.*, **76**, 1184 (1972).
(12) S. L. Olsen, *et al.*, *Rev. Sci. Instrum.*, **42**, 1247 (1971); A. D. Maughan, M.S. Thesis, University of Utah, 1971.
(13) G. Ilgenfritz, Ph.D. Thesis, University of Goettingen, 1966.
(14) W. N. Baker and V. K. La Mer, *J. Chem. Phys.*, **3**, 408 (1935); R. W. Gurney, "Ionic Processes in Solution," Dover, New York, N. Y., 1962, p 79.
(15) E. Grunwald, *Progr. Phys. Org. Chem.*, **3**, 317 (1965).
(16) K. S. Schmitz and J. M. Schurr, *J. Phys. Chem.*, **76**, 534 (1972).
(17) M. M. Kreevoy and T. S. Straub, *Anal. Chem.*, **41**, 214 (1969).
(18) P. K. Glasoe and F. A. Long, *J. Phys. Chem.*, **64**, 188 (1960).
(19) Values of the relaxation time, τ, were corrected according to the relation: $\tau_{obsd}^2 = \tau_{chem}^2 + \tau_{elect}^2$ (D. M. Hunter, "Introduction to Electronics," Holt, Rinehart and Winston, New York, N. Y., 1964, p 102). τ_{elect} was found to be approximately 100 nsec when the photomultiplier was terminated by 1000 Ω and 60 nsec when a 220-Ω resistor was used.
(20) M. Eigen and L. De Maeyer, *Tech. Org. Chem.*, **8**, 904 (1963).
(21) A. G. Worthing and J. Geffner, "Treatment of Experimental Data," Wiley, New York, N. Y., 1943, pp 246, 247.
(22) Values of τ in ref 10 were uncorrected for electronic response time τ_{elect} (ref 19). Also no activity corrections were made. A least-squares plot of the data in ref 13 yields a value $k_r = 7.3 \times 10^{10}$ M^{-1} sec^{-1}.
(23) M. Eigen and G. G. Hammes, *J. Amer. Chem. Soc.*, **82**, 5951 (1960).
(24) B. B. Owen and F. H. Sweeton, *J. Amer. Chem. Soc.*, **63**, 2811 (1941).
(25) R. C. Weast, Ed., "Handbook of Chemistry and Physics," 50th ed, Chemical Rubber Publishing Co., Cleveland, Ohio, 1969, p E-67.

On the Kinetics of Step-Wise Micelle Association

E. A. G. Aniansson* and S. N. Wall

Department of Physical Chemistry, University of Gothenburg, S-402 20 Gothenburg, Sweden *(Received June 29, 1973; Revised Manuscript Received October 8, 1973)*

Kinetic equations have been given a form which suggest an analogy with heat conduction and identifies the rate limiting quantities. Relaxation times have been deduced for the net disintegration of and the rearrangement among the micelles. The agreement with existing experimental results is satisfactory.

During the last few years the kinetics of micelle association and dissociation in surfactant solutions have been studied experimentally with various techniques.[1-17] The degree of association is typically of the order of 100, which requires either that drastically simplified assumptions be made in treating the kinetics,[1,12,18,19] or, that a perspicuous method be found for its handling. The following treatment is a move in the latter direction.

First we shall put the kinetic equation into a form which suggests an analogy with heat conduction (diffusion, etc.) and identifies the proper rate-limiting quantities. A treatment of the relaxation process at very small deviations from equilibrium will be given and the result compared with existing experimental results. The treatment will then be extended to larger deviations from equilibrium and a plausible explanation given of the apparent linearity still exhibited by the process. Finally, the process of rearrangement among the abundant micelles will be treated by approximating the kinetic equations by a partial differential equation. This treatment is limited to a somewhat idealized case, but an extension to more realistic ones is indicated.

Equations and Their Interpretation

Fortunately, it is very plausible to assume that the association (and dissociation) proceeds in unitary steps giving the set of reactions

$$\begin{aligned} A_1 + A_1 &\underset{k_2^-}{\overset{k_2^+}{\rightleftharpoons}} A_2 \\ A_1 + A_2 &\underset{k_3^-}{\overset{k_3^+}{\rightleftharpoons}} A_3 \\ &\vdots \\ A_1 + A_{s-1} &\underset{k_s^-}{\overset{k_s^+}{\rightleftharpoons}} A_s \end{aligned} \qquad (1)$$

where A_1 represents the surfactant monomer, A_2 the dimer, etc. For ionic surfactants, A_1 denotes the surfactant ion, and the treatment is limited to cases where the counterions are more easily movable than the surfactant ions, so that they can be assumed to adjust almost immediately to the association of the latter. It is probable that this applies to the vast majority of cases.

Letting A_s also denote the concentration of the species and $\bar{A}_s$ its equilibrium value, we introduce the relative deviation from the equilibrium

$$\xi_s = (A_s - \bar{A}_s)/\bar{A}_s \qquad (2)$$

Using the fact that

$$k_s^+ \bar{A}_1 \bar{A}_{s-1} = k_s^- \bar{A}_s \qquad (3)$$

one finds

$$\bar{A}_s \frac{d\xi_s}{dt} = k_{s+1}^- \bar{A}_{s+1}[\xi_{s+1} - \xi_s(1+\xi_1) - \xi_1] - k_s^- \bar{A}_s[\xi_s - \xi_{s-1}(1+\xi_1) - \xi_1] \quad s = 2,3,\ldots \qquad (4a)$$

and particularly for $s = 1$

$$\bar{A}_1 \frac{d\xi_1}{dt} = 2k_2^- \bar{A}_2(\xi_2 - 2\xi_1 - \xi_1^2) + \sum_{s=3}^{\infty} k_s^- \bar{A}_s[\xi_s - \xi_{s-1}(1+\xi_1) - \xi_1] \qquad (4b)$$

The second term on the right side of (4a) is the net increase in unit time of the number of aggregates of size s and larger. It is thus a reaction flow in aggregation space $\{s\}$ and we shall therefore denote it by J_s

$$J_s = -k_s^- \bar{A}_s[\xi_s - \xi_{s-1}(1+\xi_1) - \xi_1] \qquad (5a)$$

Equation 4a is then the equivalent of the continuity equation, as seen more easily when written on the form

$$dA_s/dt = J_s - J_{s+1} \qquad (4c)$$

When ξ is so small that it can be neglected in the inner bracket of (5a), which is the case toward the end of jump relaxation experiments, this equation takes the form

$$J_s = -k_s^- \bar{A}_s[\xi_s - \xi_{s-1} - \xi_1] \qquad (5b)$$

There is a close analogy between this equation and the equation for heat conduction in one dimension;[20] s corresponds to the space coordinate, ξ_s to the temperature, $\bar{A}_s$ to the mass per unit length (the specific heat capacity = 1), and k_s^- to the conductivity per unit of mass per unit length. ξ_1 here plays the role of a space-independent driving force acting in the negative s direction in addition to the "derivative" of ξ_s with respect to s. *The rate-limiting quantities in the process are thus the products* $k_s^- \bar{A}_s$ and not k_s^-, as one might be inclined to think at the outset.

Dissociation of Micelles at Small Deviations from Equilibrium

In a low-disperse micellar solution the dependence of $\ln \bar{A}_s$ on s is something similar to that illustrated in Figure 1.[23-25] Also given in this figure is

$$\ln \frac{k_s^-}{k_s^+ \bar{A}_1} = -\ln \frac{\bar{A}_s}{\bar{A}_{s-1}} \cong -\frac{d \ln \bar{A}_s}{ds}$$

obtained from (3), and for comparison, $\ln s$. The micelle population is more or less sharply peaked around a most probable s value, in this example 100, and orders of magnitude below and above this region. Although the micelle

distribution n for this example is not very broad, about 20% of the average aggregation number (see Further Comments and Conclusions), the ratio $k_s^-/k_s^+\bar{A}_1$ changes very little over most of the range. It is then plausible to assume that the variations of k_s^- and k_s^+ themselves are not very much larger. That large changes of $\bar{A}_s$ can be built up from ratios of $k_s^-/k_s^+\bar{A}_1$ only slightly different from unity is due to the large number of steps.

It might then well be that the "conductivity" $k_s^-\bar{A}_s$ is very much lower in the intermediate micellar region than in the region of abundant micelles. Returning to the analogy with heat conduction, the situation is, at least in part, reminiscent of two large metal blocks connected by a thin wire, one block corresponding to the monomers and the oligomers, the other to the abundant micelles, and the wire corresponding to the region in between. After an initial, short period of adjustment the main process would be a pseudo-stationary flow from one "block" to the other through the "wire."

To pursue a calculation of the time development of this process we shall make the following more explicit assumptions.

The s space is split into three parts, $1 \leq s \leq s_1$, $s_1 + 1 \leq s \leq s_2$, and $s_2 + 1 \leq s$. The conductivities $k_s^-\bar{A}_s$ are assumed to be much larger in the first and the third part than at least some of the conductivities in the second, and the amount of material in the second part, $\sum_{s>s1}^{s2} s(1 + \xi_s)\bar{A}_s$, is assumed to be negligible compared to the material in the other two parts. We shall also assume that the deviation from equilibrium is so small that (5b) is applicable for all s. Then in parts one and three

$$\xi_s - \xi_{s-1} - \xi_1 = -\frac{J_s}{k_s^-\bar{A}_s} \cong 0 \tag{6a}$$

whereas in part two

$$\xi_s - \xi_{s-1} - \xi_1 = -\frac{J}{k_s^-\bar{A}_s} \tag{6b}$$

where J is the practically s-independent value of J_s during the pseudo-stationary phase considered. This s independence follows directly from the analogy with the blocks and wire. Due to the low "mass per unit length" of the wire even small differences between J_s and J_{s+1} would lead to large and rapid temperature variations, characteristic of the initial adjustment but not of the pseudo-stationary phase.

Summing eq 6a from $s = 2$ to $s = s_1$, eq 6b from $s = s_1 + 1$ to s_2, and eq 6b from $s = s_2 + 1$ to s'', one obtains

$$\xi_{s''} = s''\xi_1 - RJ \tag{7}$$

where

$$R = \sum_{s>s_1}^{s_2} \frac{1}{k_s^-\bar{A}_s} \tag{8}$$

R being a resistance formed by series connection of the individual resistances $1/k_s^-\bar{A}_s$. For $s' \leq s_1$ one finds similarily that

$$\xi_{s'} = s'\xi_1 \tag{9}$$

Using the requirement of material balance

$$\sum_{s=1}^{\infty} s\xi_s\bar{A}_s = 0 \tag{10}$$

and the assumption that the amount of material in the second region is negligible, one finds a relation between J and m_3, the excess amount of material in the third region

$$J = -\frac{\overline{n_1^2}c_1 + \overline{n_3^2}c_3}{R\overline{n_1^2}c_1\bar{n}_3c_3} m_3 \tag{11}$$

where

$$m_3 = \sum_{s>s_2} s\xi_s\bar{A}_s \tag{12a}$$

$$c_1 = \sum_{s=1}^{s_1} \bar{A}_s \qquad c_3 = \sum_{s>s_2} \bar{A}_s \tag{12b}$$

$$\overline{n_1^2} = \frac{1}{c_1}\sum_{s=1}^{s_1} s^2\bar{A}_s \qquad \bar{n}_3 = \frac{1}{c_3}\sum_{s>s_2} s\bar{A}_s \qquad \overline{n_3^2} = \frac{1}{c_3}\sum_{s>s_2} s^2\bar{A}_s \tag{12c}$$

To derive a differential equation for the process we note that, on the average, each micelle added to the third region increase the excess amount of material in that region with the amount $\partial m_3/\partial\sum_{s>s_2}\xi_2\bar{A}_s$ so that

$$\frac{dm_3}{dt} = \frac{\partial m_3}{\partial\sum_{s>s_2}\xi_s\bar{A}_s} J \tag{13}$$

A short calculation gives

$$\sum_{s>s_2}\xi_s\bar{A}_s = \frac{\sigma^2c_3 + \overline{n_1^2}c_1}{\bar{n}_3\overline{n_1^2}c_1} m_3 \tag{14}$$

where $\sigma^2 = \overline{n_3^2} - \bar{n}_3^2$, the variance of the distribution.

Using (11) one obtains

$$\frac{dm_3}{dt} = -\frac{1}{\tau} m_3 \tag{15a}$$

where

$$\frac{1}{\tau} = \frac{1}{RC_3}\frac{\overline{n_1^2}c_1 + \overline{n_3^2}c_3}{\overline{n_1^2}c_1 + \sigma^2c_3} \tag{15b}$$

The solution of (15a) is of the common relaxation form

$$m_3(t) = m_3(0)e^{-t/\tau} \tag{15c}$$

τ being the relaxation time.[26]

To bring out the essential features of (15b) we shall approximate it in the following way, simulating an approximately Gaussian micelle distribution.[27] The variance of this distribution, σ^2, will be assumed independent of total concentration and small compared to $\bar{n}_3^2$ so that the dependence of $\bar{n}_3$ on total concentration can then be neglected (see Appendix) and so that one can also set $\overline{n_3^2} \cong \bar{n}_3^2$. The variance of the oligomer distribution will be neglected, *i.e.*, $\overline{n_1^2} \cong 1$ and $c_1 \cong \bar{A}_1$. Then c_3 can be expressed in the total content of surfactant molecules, $\bar{A}_{tot}$, and $\bar{A}_1$.

$$c_3 \cong \frac{1}{\bar{n}_3}(\bar{A}_{tot} - \bar{A}_1) \equiv \frac{\bar{A}_{exc}}{\bar{n}_3} \tag{16}$$

We shall also assume that an r and an n_r can be found so that

$$R = \sum_{s>s_1}^{s_2} \frac{1}{k_s^-\bar{A}_s} \cong \frac{n_r}{k_r^-\bar{A}_r} \tag{17}$$

with $\bar{A}_r$ carrying the concentration dependence of R, n_r being the average "length," and $k_r^-\bar{A}_r$ the average "width" of the "narrow passage."

To express $\bar{A}_r$ in $\bar{A}_{exc}$ we assume that approximately

$$c_3 \propto \bar{A}_{\bar{n}_3} \text{ and } \bar{A}_s \propto \bar{A}_1^{\beta s} \tag{18}$$

where $\beta = 1$ for ideal nonionic surfactants.[28] This gives

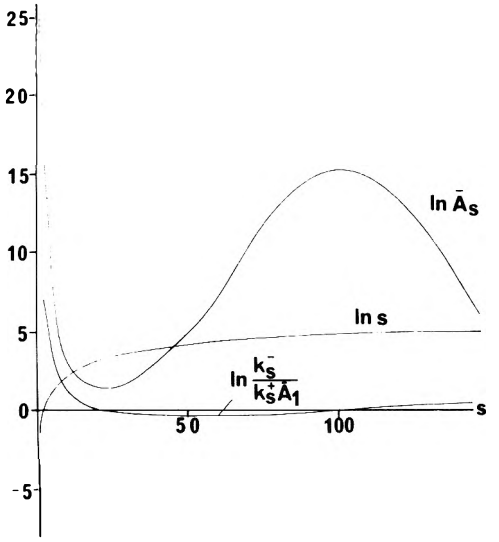

Figure 1.

$$\bar{A}_r \cong \bar{A}_{r,0}\left(\frac{c_3}{c_{3,0}}\right)^{r/\bar{n}_3} \cong \bar{A}_{r,0}\left(\frac{\bar{A}_{exc}}{\bar{A}_{exc,0}}\right)^{r/\bar{n}_3} \quad (19)$$

with the index 0 denoting a reference concentration, *e.g.*, such that $\bar{A}_{1,0}$ = cmc.

Equation 15b now takes the approximate form

$$\frac{1}{\tau} \cong \frac{k_r^- \bar{A}_{r,0}}{n_r c_{3,0}}\left(\frac{\bar{A}_{exc,0}}{\bar{A}_{exc}}\right)^{(\bar{n}_3 - r)/\bar{n}} \frac{1 + \bar{n}_3 \dfrac{\bar{A}_{exc}}{\bar{A}_1}}{1 + \dfrac{\sigma^2 \bar{A}_{exc}}{\bar{n}_3 \bar{A}_1}} \quad (20)$$

Above the critical micelle concentration region $\bar{A}_1$ may be considered approximately constant and equal to the cmc if n_3 is not too small. Then $\bar{A}_{exc} = \bar{A}_{tot}$ − cmc is a linear function of $\bar{A}_{tot}$ and the only concentration dependent variable on the right side of (20).

Equation 20 takes the simplest form, a linear one, when $\sigma = 0$ and $(\bar{n}_3 - r)/\bar{n}_3 \cong 0$, *i.e.*, when the micelles are monodisperse and the "narrow passage" is very short and close to $\bar{n}_3$. When $\sigma^2/n_3 \cong 0$, a downward trend in (20) is noticeable at values of $\bar{A}_{exc} = O(n_3/\sigma^2)$. On the other hand, when r is not very close to $\bar{n}_3$ the next to the last factor in (20) introduces an upward curvature in the region of very low $\bar{A}_{exc}$ values, *i.e.*, just above the cmc, and with the last factor, an increased downward curvature at larger values.

These two deviations from a linear dependence of $1/\tau$ on $\bar{A}_{tot}$ have both been observed in experimental results.[1,2] In Figure 2 are given the results of the best fits of (15b) to experimental results of $1/\tau$ *vs.* total concentration using Gaussian approximations of the micelle distribution for $s > s_2$ and of $1/(k_s^-\bar{A}_s)$ for $s_1 < s \leq s_2$. It is seen that there are considerable latitudes in the values of σ, r, and cmc, which are compatible with existing experimental results. The results thus far available seem to indicate low values of $(\bar{n}_3 - r)/\bar{n}_3$ and σ. The accuracy of the measurements and the ranges of concentration covered are, however, too small for detailed conclusions to be drawn. In two cases, ref 1 and 3, though, it has been explicitly stated that at larger concentrations the experimental points tended to fall below the straight line extrapolated from low concentrations, which indicates more sizable values of σ and/or $(\bar{n}_3 - r)/\bar{n}_3$. The comparatively low value of σ found from the present results are in agreement with the findings[29a,30] from light scattering and other measurements on the same or similar substances at low concentrations. (See also Further Comments and Conclusions.)

Equation 15b contains the expression resulting from the simple model proposed by Kresheck, *et al.*,[1] who assumed the micelles to be monodisperse, $\bar{A}_s = \bar{A}_n\delta_{sn}$, $s > 1$, and a single slow step, namely, the first one in the decay of the proper micelles; in our description $k_n^-\bar{A}_n \ll k_s^-\bar{A}_s$, $s < n$. In this case $\sigma = 0$ and $r = \bar{n}_3$ and (15b) and (20) take the simple form

$$\frac{1}{\tau} = k_n^-\left(1 + n\frac{\bar{A}_{exc}}{\bar{A}_1}\right) \quad (21)$$

In our model the numerical value of k_n^- obtained from (21) would be assigned to the quantity $k_r^-\bar{A}_{r,0}/n_r c_{3,0} = (1/Rc_3)_0$. Since $\bar{A}_{r,0}$ may be orders of magnitude smaller than $c_{3,0}$ and further, n_r may be considerably larger than 1, the k_r^- from this model may be many orders of magnitude larger than k_n^- from the model of Kresheck, *et al.*

In fact, estimates of k_{n3}^- from magnetic measurements[15-19] invariably indicate values that are orders of magnitude larger than those obtained from temperature-jump measurements using (21). Also, according to the present treatment, the activation energy deduced from (21) would be a more complicated quantity affected by the temperature dependence of $\bar{A}_{r,0}$, n_r, and $c_{3,0}$.

Large Deviations from Equilibrium

Due to the very large number of steps, a rather stringent requirement is placed on the smallness of ξ_1 in order for the linearization of the equations to be valid. Using (5a) instead of (5b) in deriving an expression for $\xi_{s''}$ similar to (7) under the same pseudo-stationary assumptions as used previously one finds

$$\xi_{s''} = (1+\xi_1)^{s''} - 1 - J\sum_{s>s_1}^{s_2} \frac{(1+\xi_1)^{s''-s}}{k_s^-\bar{A}_s} \quad (22a)$$

which we approximate by

$$\xi_{s''} = (1+\xi_1)^{\bar{n}_3} - 1 - J\sum_{s>s_1}^{s_2} \frac{(1+\xi_1)^{\bar{n}_3-s}}{k_s^-\bar{A}_s} + (s'' - \bar{n}_3)\xi_1 \quad (22b)$$

Unless $n_3|\xi_1| \ll 1$, $(1+\xi_1)^{n_3} - 1$ cannot be approximated by $\bar{n}_3\xi_1$, and $(1+\xi_1)^{n_3-s}$ under the summation sign cannot be approximated by 1. When, for example, n_3 is of the order of 100, $|\xi_1|$ has to be much smaller than 10^{-2} in order for (5b) to hold. In typical temperature-jump experiments[1] $|\xi_1|$ is often as large as 5×10^{-2}. Still, the relaxation curves are very nearly exponential,[1,29a] *i.e.*, $-(1/m_3)(dm_3/dt)$ is found to be practically constant.

Using (22), but otherwise the same approximations as before, one arrives at the following expression for $1/\tau_{(\xi_1)} = -(1/m_3)(dm_3/dt)$ to be compared with (15b)

$$\frac{1}{\tau(\xi_1)} = \frac{1}{R(\xi_1)c_3}\,\frac{\bar{n}_1^2c_1 + \bar{n}_3^2c_3 + \dfrac{1}{\xi_1}[(1+\xi_1)^{\bar{n}_3} - 1 - \bar{n}_3\xi_1]c_3}{\bar{n}_1^2c_1 + (n_3^2 - \bar{n}_3^2)c_3} \quad (23)$$

where

$$R(\xi_1) = \sum_{s>s_1}^{s_2} \frac{(1+\xi_1)^{\bar{n}_3-s}}{k_s^-\bar{A}_s} \quad (24)$$

Compared with the case when $\xi_1 = 0$, a negative (positive) ξ_1 decreases (increases) both $R(\xi_1)$ and the numera-

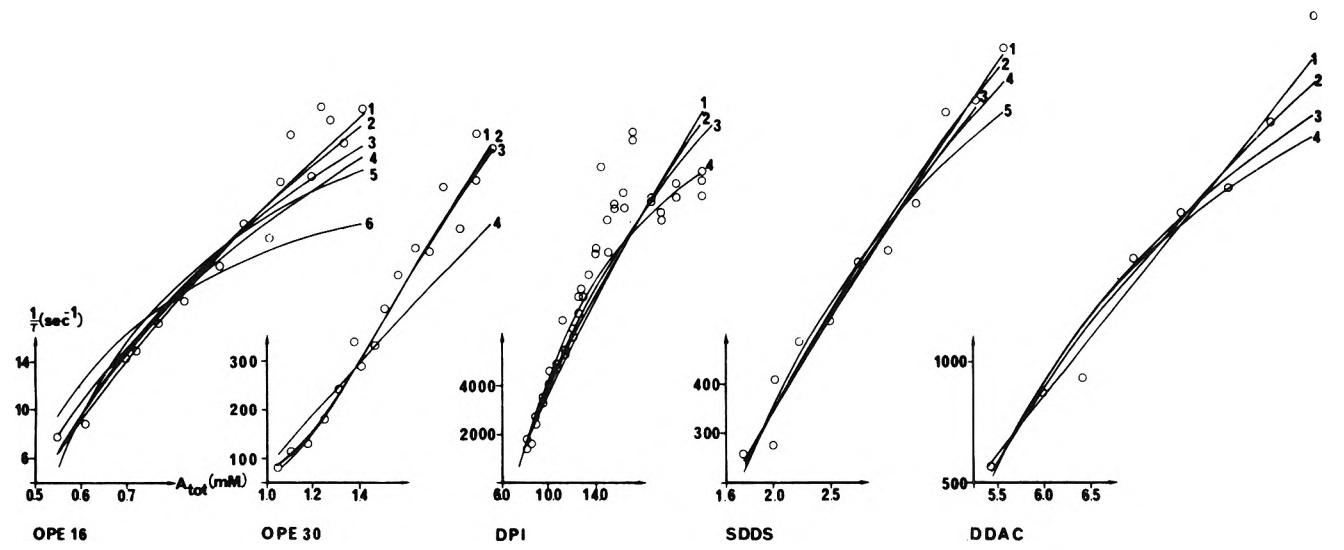

Figure 2. Experimental results (O) and calculations (lines) based on eq 15b and the following assumptions and equations. The cmc is defined as the monomer concentration $\bar{A}_1'$ where $\partial c_3/\partial \bar{A}_{tot} = 1/2\bar{n}_3'$ a prime indicating here and in the rest of the text quantities at cmc. (At larger values of $\bar{A}_{tot}$ $\partial c_3/\partial A_{tot}$ is about $1/\bar{n}_3$, and at smaller about 0.) The assumptions are $\overline{n_1}^2 = 1$, $\bar{A}_s' \propto \exp[-(s - \bar{n}_3')^2/2\sigma^2]$ for $s > s_2$, $\bar{A}_s/\bar{A}_s' = (\bar{A}_1^s/\bar{A}_1')$, $1/k_s^- \bar{A}_s' \propto \exp[-(s - s_r')^2/2\sigma_r^2]$ for $s_1 < s \leq s_2$. Replacing summations by integrations and, in case of Gaussian integrands, extending the integration limits to $\pm\infty$ one finds the following expressions: $c_3 = [A_1'/(\overline{n_3'^2} - \sigma^2)]$ $\exp[\bar{n}_3' \ln (\bar{A}_1/\bar{A}_1') + 1/2\,\sigma^2 \ln^2 (\bar{A}_1/\bar{A}_1')]$, $\bar{A}_{tot} = \bar{A}_1 + c_3[\bar{n}_3' + \sigma^2 \ln (\bar{A}_1/\bar{A}_1')]$, $\bar{n}_3^2 = [\bar{n}_3' + \sigma^2 \ln (\bar{A}_1/\bar{A}_1')] + \sigma^2$, and $1/R = (1/R')$ $\exp[s_r' \ln (\bar{A}_1/\bar{A}_1') - 1/2\,\sigma_r^2 \ln^2 (\bar{A}_1/\bar{A}_1')]$. For given values of $\bar{A}_1'$, $\bar{n}_3'$, σ, s_r', and σ_r the value of R' is sought which minimize the sum of squares of relative deviations between experimental values and calculated ones.

tor in (23), and it may well be that this compensating effect gives a practically invariant $\tau(\xi_1)$ and thus masks the nonlinearity of the process.[31] This is all the more possible since the quantity obtained in temperature-jump experiments of this kind is not proportional to m_3 (or a corresponding quantity) but to m_3 plus an unknown, additive constant, the latter being adjusted so as to make the logarithm of m_3 plus constant as linear a function of time as possible.

Incidentally, negative values of ξ_1 which are commonly met with in temperature-jump measurements tend to suppress the low $-s$ terms of $R(\xi_1)$, decreasing the effective value of $\bar{n}_3 - r$ in eq 20 in agreement with the observation that low values of this latter quantity are indicated by the experimental results. (See Figure 2).

Rearrangement among the Abundant Micelles

If $\bar{n}_3$ and/or σ change with the perturbation (temperature jump, pressure jump, etc.) in a relaxation experiment, under the given assumptions there will be an initial period of rapid adjustment of the micellar distribution to the new conditions. Although the total number of micelles with $s > s_2$ will not change during this initial period, the amount of material, m_3, in this range in general will. Although this process may be difficult to follow experimentally unless the changes in n_3 and/or σ are large, it may be of some interest to see how it could be handled theoretically.

We shall assume that for $s > s_2 + 1$ the distribution is Gaussian, *i.e.*

$$\bar{A}_s = A_0 e^{-(s-\bar{n}_3)^2/2\sigma^2} \tag{25}$$

this implies with (3) that

$$\frac{k_s^-}{k_s^+ \bar{A}_1} = \frac{\bar{A}_{s-1}}{\bar{A}_s} = e^{-1/2\sigma^2} e^{(s-\bar{n}_3)/\sigma^2} \tag{26}$$

This ratio will change with the factor $e^{2\sigma}$ when s is varied from $\bar{n}_3 - \sigma$ to $\bar{n}_3 + \sigma$, *i.e.*, essentially over the proper micelle range. If σ is not too small, *e.g.*, of the order of 10 (Figure 1), the ratio of k_s^- to k_s^+ will change very little and it would be reasonable to assume that

$$k_s^- \cong k^- \tag{27}$$

independent of s. We then note that if σ is not too small, $\bar{A}_s$, and probably also ξ_s, will change slowly with s so that they may be treated as continuous and differentiable variables. Equation 4a will then take the form

$$\bar{A}(s)\frac{\partial \xi(s,t)}{\partial t} = \frac{\partial}{\partial s} k^-(s)\bar{A}(s)\left[\frac{\partial \xi(s,t)}{\partial s} - \xi_1(1 + \xi(s,t))\right] \tag{28}$$

Assuming now that $|\xi(s,t)| \ll 1$, using (25) and (27), and looking for eigen solutions of the form

$$\xi(s,t) = \xi(s)e^{-\lambda t} \tag{29}$$

we arrive at the following equation

$$\xi'' - 2z\xi' + \mu\xi = -2\sqrt{2}\,\sigma\xi(1)z \tag{30}$$

where

$$z = (s - \bar{n}_3)/\sqrt{2}\,\sigma \tag{31a}$$

and

$$\mu = 2\sigma^2\lambda/k^- \tag{31b}$$

There is a particular solution

$$p(z) = \frac{2\sqrt{2}\,\xi(1)\sigma}{2 - \mu} z \tag{32}$$

if $\mu \neq 2$ and a homogeneous equation

$$\xi'' - 2z\xi' + \mu\xi = 0 \tag{33}$$

Unless μ is an even, nonnegative number[32]

TABLE I[a]

Parameters		OPE 16[b]						OPE 30[b]						DPI[c]						SDDS[d]						DDAC[e]					
	1	2	3	4	5	6		1	2	3	4	5	6	1	2	3	4	5	6	1	2	3	4	5	6	1	2	3	4	5	6
$\bar{A}_1' \times 10^{-3}$, M	0.42*	0.45*	0.47*	0.46	0.52*	0.46		1.11*	1.28*	1.28*	0.98	5.5*	5.6*	6.2*	6.5*	1.15*	1.25*	1.25*	1.30*	1.45*	4.3*	4.7*	5.0*	4.9*							
$\bar{n}_3'$	48	48	48	48	48	48		11	11	11	11	87	87	87	87	95	95	95	95	95	378	378	378	378							
σ'	2	2	4	0	4	4		1	1	2	0	1	2	4	4	0	3	1	3	5	0	10	10	20							
s_r'	44	40	40	30	30	30		10	8	8	9	80	80	80	60	90	90	80	85	80	360	330	250	330							
σ_r'	2	5	2	4	2	4		1	1	1	0	1	5	2	2	3	0	1	7	10	0	10	10	20							
$R' \times 10^6$	0.14	0.24	0.30	0.49	0.79	0.58		1560	3170	3250	985	38	44	66	212	0.88	1.23	1.82	1.84	3.76	0.23	0.57	0.21	0.89							

[a] An asterisk on the values for $\bar{A}_1'$ signifies that this parameter has also been varied to further minimizing the sum of squared relative deviations. OPE 16 and OPE 30 = octylphenyl polyoxyethylene ether with 16 and 30 ethoxy units, respectively; DPI = dodecylpyridinium iodide; SDDS = sodium dodecyl sulfate; DDAC = dodecylammonium chloride. The numbers in the column heading refer to the curves in Figure 2. [b] Reference 4. [c] Reference 1. [d] Reference 2. [e] Reference 3.

$$\xi \longrightarrow z^\nu e^{z^2}$$

when $z \to \infty$, *i.e.*

$$\xi(z)\bar{A}(z) \longrightarrow z^\nu e^{z^2} e^{-z^2} = z^\nu$$

which is inadmissable. Putting, then, $\mu = 2n$, where n is a positive integer or zero, we obtain a general solution of (28) in the form

$$\xi(z,t) = \sum_{n=0}^{\infty} (c_n H_n(z) \longleftarrow p_n(z)) e^{-\lambda_n t} \qquad (34)$$

where the c_n are constants, $H_n(z)$ are Hermite polynomials, $p_n(z)$ are of the form (32) except for $n = 1$ where (32) obviously fails, and

$$\lambda_n = nk^-/\sigma^2 \qquad (35)$$

We see, then, that the inverse of the relaxation time has an equally spaced, discrete spectrum, the intervals of which are k^-/σ^2. For fairly symmetric abundant micelle distributions it is practically concentration independent (see Appendix). For a given k^- the relaxation times increase with σ which is immediately understandable since the number of steps in this process increases with σ.

Using the conservation of the number of proper micelles and the orthonormality of Hermite functions, one finds that c_0 has to vanish. Similarly, the material balance, (10), implies that $p_n \equiv 0$ except for $n = 1$. For $n = 1$ the admissible particular solution is

$$p_1(z) = -2\xi(1)\sigma z \int_1^z \frac{e^{u^2}}{u^2}\,du \int_u^\infty v^2 e^{-v^2}\,dv \qquad (36)$$

except for an unspecified content of $H_1(z)$. Given $\xi(z) = \xi(z,0)$, c_n is obtained from (34)

$$c_n = \frac{1}{2^n n!\sqrt{\pi}} \int_{-\infty}^{+\infty} H_n(z) e^{-z^2} (\xi(z) - p_1(z))\,dz \qquad (37)$$

The extension of the lower limit of these integrals from $z = -(\bar{n}_3 - s_2)/\sqrt{2\sigma}$ to $-\infty$ is in accord with the previous assumptions.

A first-order correction of these results for the nonconstancy of k_s^-, the nonlinearity of the exact equation (28), and any deviation of A_s from the Gaussian form should be possible with a suitable perturbation calculation.

Further Comments and Conclusions

If the foregoing treatment is essentially correct it brings new interest to the rare, intermediate micelles and to the size distribution of the abundant micelles. Almost nothing is known experimentally about the former and only little is known about the latter. The very interesting recent treatment of micellar size distributions by Mukerjee and others[29b] depend essentially on the determination of the ratio between the mass and number averages of the molecular weights, M_w and M_n. Now, it is easily found that

$$M_w/M_n = 1 + (\sigma/\bar{n}_3)^2$$

which means that a relative dispersion $2\sigma/\bar{n}_3$ of 20% would give a value of M_w/M_n differing from 1 by only $0.1^2 = 0.01$. The errors in the experimental determinations of this ratio are certainly not smaller than this value and generally much larger. To prove a true monodispersity, a σ less than about 0.5 would have to be ascertained. For micelles containing 50 monomers it would require an experimental accuracy in M_w/M_n of 10^{-4}. Since such an accuracy is entirely out of reach today the term "low-dis-

persity" should perhaps be used at present instead of "monodispersity."[33] It seems, then, as if considerably more attention should be directed toward these two aspects of micelle formation.

The kinetics quantity obtained from (15b) is $R = \sum_{s>s1}^{s2} 1/(k_s^- \bar{A}_s)$ or, in the approximation (20), $k_r^- A_{r,0}/n_r$. In the latter form it gives some information concerning the location, length, and "width" of the narrow passage. To obtain information on k_r^-, independent measurements of $A_{r,0}$ and n_r are required.

In principle, more detailed information on the s dependence of $k_s^- \bar{A}_s$ would be obtainable from (23) and (24) at larger deviations from equilibrium. Knowing $R(\xi_2)$ as a function of ξ_1, one would be able to obtain $1/k_s^- \bar{A}_s$ as a function of s using a suitable deconvolution method. Finally, it is of interest to compare the reciprocal relaxation times expected from (20) and (35). Assuming k^- and k_r^- to be of about the same order of magnitude, and using reasonable values of σ and the other parameters entering these equations, one finds that the rearrangement among the abundant micelles tends to be faster than the overall disintegration of the same micelles. This supports the initial assumptions made in the present paper. It is not inconceivable, however, that in some cases the rate of the two processes may be of the same order of magnitude. A treatment coupling the two will then be necessary.

Acknowledgment. The authors wish to thank Dr. Mats Almgren for valuable comments on this manuscript.

Appendix

The required quantities are $\partial n_s/\partial \bar{A}_{tot}$ and $\partial \sigma^2/\partial \bar{A}_{tot}$. To derive expressions for these we shall start from eq 3 from which there follows

$$\frac{\partial \ln \bar{A}_s}{\partial \ln \bar{A}_1} - \frac{\partial \ln \bar{A}_{s-1}}{\partial \ln \bar{A}_1} = 1 \tag{A1}$$

and from this again

$$\frac{\partial \ln \bar{A}_s}{\partial \ln \bar{A}_1} = s \text{ or } \frac{\partial \bar{A}_s}{\partial \ln \bar{A}_1} = s\bar{A}_s \tag{A2}$$

Using these results we shall first obtain the derivatives with respect to $\ln \bar{A}_1$, and then $\partial \bar{A}_{tot}/\partial \ln \bar{A}_1$ from which the required derivatives are obtained.[29b,34]

From the definitions

$$c_3 = \sum_{s>s_2}^{\infty} A_s \qquad \bar{n}_3 = \frac{1}{c_3}\sum_{s>s_2}^{\infty} s\bar{A}_s$$

$$M_r = \frac{1}{c_3}\sum_{s>s_2}^{\infty} (s-\bar{n}_3)^r \bar{A}_s \quad (M_0 = 1, M_1 = 0, M_2 = \sigma^2) \tag{A4}$$

one obtains

$$\partial c_3/\partial \ln \bar{A}_1 = \bar{n}_3 c_3 \tag{A5}$$

$$\partial \bar{n}_3/\partial \ln \bar{A}_1 = \sigma^2 \tag{A6}$$

and

$$\frac{\partial M_r}{\partial \ln \bar{A}_1} = M_{r+1} - r\sigma^2 M_{r-1} \tag{A7}$$

one finds further that

$$\frac{\partial \bar{A}_{tot}}{\partial \ln \bar{A}_1} = \frac{\partial}{\partial \ln \bar{A}_1}\sum_{s=1}^{s_1} s\bar{A}_s + \frac{\partial}{\partial \ln \bar{A}_1}\sum_{s>s_2}^{\infty} s\bar{A}_s = \bar{n}_1^2 c_1 + \bar{n}_3^2 c_3 \tag{A8}$$

The expressions sought are, then

$$\frac{\partial \bar{n}_3}{\partial \bar{A}_{tot}} = \frac{\sigma^2}{\bar{n}_1^2 c_1 + \bar{n}_3^2 c_3} \tag{A9}$$

$$\frac{\partial \sigma^2}{\partial \bar{A}_{tot}} = \frac{M_3}{\bar{n}_1^2 c_1 + \bar{n}_3^2 c_3} \tag{A10}$$

and more generally

$$\frac{\partial M_r}{\partial \bar{A}_{tot}} = \frac{M_{r+1} - r\sigma^2 M_{r-1}}{\bar{n}_1^2 c_1 + \bar{n}_3^2 c_3} \tag{A11}$$

If the micelle distribution is symmetrical, as is the Gaussian distribution, $M_3 = 0$ and σ^2 is concentration independent.

To get order of magnitude expressions we set, as before, $\bar{n}_1^2 \cong 1$, $c_1 \cong A_1 \cong$ cmc, and $\bar{n}_3^2 \cong \bar{n}_3^2$. One then finds that

$$\frac{\partial \bar{n}_3}{\partial \bar{A}_{tot}} \cong \frac{\partial \bar{n}_3}{\partial \bar{A}_{exc}} \cong \frac{\sigma^2}{\bar{A}_1 + \bar{n}_3 A_{exc}} \tag{A12}$$

and

$$\frac{\partial \sigma^2}{\partial \bar{A}_{tot}} \cong \frac{\partial \sigma^2}{\partial \bar{A}_{exc}} \cong \frac{M_3}{\bar{A}_1 + \bar{n}_3 \bar{A}_{exc}} \tag{A13}$$

When $\bar{n}_3 = O(100)$ and $\bar{A}_{exc}/\bar{A}_1 = O(1)$ $\bar{A}_1$ can be neglected in the denominators and one finds that

$$\frac{1}{2}\frac{\partial \bar{n}_3^2}{\partial \ln \bar{A}_{exc}} = \sigma^2 \tag{A14}$$

and that

$$\partial \sigma^2/\partial \ln \bar{A}_{exc} = M_3/\bar{n}_3 \tag{A15}$$

When $\sigma \ll \bar{n}_3$, one finds from (A14) that $\bar{n}_3$ changes very little when $\bar{A}_{exc}$ changes by an order of magnitude from the order of cmc.

A significant relative change in σ^2 with a similar change in $\bar{A}_{exc}$ will occur only for very unsymmetrical and broad distributions. Taking as an example

$$\bar{A}_s = \begin{cases} 0 & s < s_0 \\ A_0 e^{-(s-s_0)/\alpha} & s \geq s_0 \end{cases} \tag{A16}$$

one finds $\sigma = \alpha$, $\bar{n}_3 = \sigma + s_0$, and $M_3 = 2\sigma^3$. In this case σ^2 will change by an order of magnitude with a similar relative change of $\bar{A}_{exc}$ if σ is about as large as s_0. For a moderately broad and unsymmetrical distribution such as

$$\bar{A}_s = A_0 s e^{-(s-s_0)^2/2\sigma^2}$$

one finds that

$$\frac{\partial \ln \sigma^2}{\partial \ln \bar{A}_{exc}} \cong 6\left(\frac{\sigma}{s_0}\right)^2 \left\{\left(1 + \frac{2}{3}\frac{\sigma}{s_0}\right) \Big/ \left[1 + \left(\frac{\sigma}{s_0}\right)^2_0\right]\right\} \tag{A17}$$

which again is negligible for $\sigma \ll s_0$.

References and Notes

(1) G. C. Kresheck, E. Hamori, G. Davenport, and H. A. Scheraga, *J. Amer. Chem. Soc.*, **88**, 246 (1966).
(2) B. C. Bennion, L. K. J. Tong, L. P. Holmes, and E. M. Eyring, *J. Phys. Chem.*, **73**, 3288 (1969).
(3) B. C. Bennion and E. M. Eyring, *J. Colloid Interface Sci.*, **32**, 286 (1970).
(4) J. Lang and E. M. Eyring, *J. Polym. Sci. A-2*, **10**, 89 (1972).
(5) P. F. Mijnlieff and R. Ditmarsch, *Nature (London)*, **208**, 889 (1965).
(6) K. Takeda and T. Yasunaga, *J. Colloid Interface Sci.*, **40**, 127 (1972).
(7) T. Yasunaga, H. Oguri, and M. Miura, *J. Colloid Interface Sci.*, **23**, 352 (1967).

(8) T. Yasunaga, S. Fujii, and M. Miura, *J. Colloid Interface Sci.*, **30**, 399 (1969).
(9) R. Zana and J. Lang, *C. R. Acad. Sci., Ser. C*, **266**, 893 (1968).
(10) R. Zana and J. Lang, *C. R. Acad. Sci., Ser. C*, **266**, 1347 (1968).
(11) E. Graber, J. Lang, and R. Zana, *Kolloid-Z. Z. Polym.*, **238**, 470 (1970).
(12) P. J. Sams, E. Wyn-Jones, and J. Rassing, *Chem. Phys. Lett.*, **13**, 233 (1972).
(13) J. Rassing, P. J. Sams, and E. Wyn-Jones, *J. Chem. Soc., Faraday Trans. 2*, **69**, 180 (1973).
(14) J. Oakes, *J. Chem. Soc., Faraday Trans. 2*, **68**, 1464 (1972).
(15) K. K. Fox, *Trans. Faraday Soc.*, **67**, 2802 (1971).
(16) N. M. Atherton and S. J. Strach, *J. Chem. Soc., Faraday Trans. 2*, **68**, 374 (1972).
(17) T. Nakagawa and H. Jizomoto, *Kolloid-Z. Z. Polym.*, **250**, 594 (1972).
(18) E. Graber and R. Zana, *Kolloid-Z. Z. Polym.*, **238**, 479 (1970).
(19) N. Muller, *J. Phys. Chem.*, **76**, 3017 (1972).
(20) It has come to the author's attention that a somewhat similar analogy has previously been drawn between a set of consecutive first-order reactions and a diffusion process.[21,22]
(21) J. A. Christiansen, *J. Phys. Chem.*, **15**, 445 (1932).
(22) T. A. Bak, Doctoral Dissertation, University of Copenhagen, Munksgaard, Copenhagen, 1959.
(23) C. A. J. Hoeve and G. C. Benson, *J. Phys. Chem.*, **61**, 1149 (1957).
(24) D. C. Poland and H. A. Scheraga, *J. Phys. Chem.*, **69**, 2431 (1965).
(25) D. C. Poland and H. A. Scheraga, *J. Colloid Interface Sci.*, **21**, 273 (1966).
(26) In principle different relaxation speeds would result according to the particular micellar property measured in the process. When σ and $|\xi|$ are not too large, the measured properties will be essentially proportional to m_3 and thus all give the same relaxation time.
(27) O. Lamm, *Ark. Kemi*, **18A**, no. 9 (1944).
(28) Equation 3 would give $\beta = 1$. A value of $\beta \neq 1$ reflects a concentration dependence of k_s^+ and k_s^- which should be taken into account when higher accuracy is sought.
(29) (a) S. N. Wall, W. Karlsson, and E. A. G. Aniansson, unpublished results; (b) P. Mukerjee, *J. Phys. Chem.*, **76**, 565 (1972); J. M. Corkill, J. F. Goodman, T. Walker, and J. Wyer, *Proc. Roy. Soc., Ser. A*, **312**, 243 (1969).
(30) D. Attwood, P. H. Elsworthy, and S. B. Kayne, *J. Phys. Chem.*, **74**, 3529 (1970); H. Coll, *ibid.*, **74**, 520 (1970).
(31) By expanding $R(\xi_1)$ and the numerator of (23) in powers of ξ_1 and comparing the coefficients of the two one finds that good compensation would result from a weak s dependence of $k_s^- \bar{A}_s$ in the intermediate s region. Simple numerical examples will substantiate this conclusion, at least for $\xi < 0.05$.
(32) G. Arfken, "Mathematical Methods for Physicists," Academic Press, New York, N. Y., 1966.
(33) See also forthcoming doctoral thesis of S. Wall.
(34) N. Bjerrum, *Kgl. Dan. Vidensk. Selsk. Skr.*, **12**, no. **4**, 7 (1915); *Z. Anorg. Allg. Chem.*, **119**, 179 (1921); F. J. C. Rossotti and H. Rossotti, "The Determination of Stability Constants," McGraw-Hill, New York, N. Y., 1961.

Volumetric Properties of Aqueous Solutions of Organic Compounds. III. Aliphatic Secondary Alcohols, Cyclic Alcohols, Primary, Secondary, and Tertiary Amines

S. Cabani,* G. Conti,

Istituto di Chimica Fisica, Università di Pisa, Pisa, Italy

and L. Lepori

Laboratorio di Chimica Quantistica ed Energetica Molecolare del CNR, 56100 Pisa, Italy *(Received August 6, 1973)*

Publication costs assisted by Consiglio Nazionale delle Ricerche (Rome)

Apparent molal volumes, Φ_v, in aqueous solution at 25° were determined with a differential hydrostatic balance for the following series of compounds: secondary aliphatic alcohols, cyclic alcohols, primary, secondary and tertiary *n*-aliphatic amines. The most interesting results are the following. (i) The contributions to the limiting partial molal volumes, $\bar{V}_2°$, of methylene groups in straight chain and cyclic compounds were found to be clearly different. Such a clear distinction was not observed in the case of methylene contributions to the molar volumes of the pure liquids. (ii) In the plane h-$\bar{V}_2°$ (h = slope of the straight line $\Phi_v = \bar{V}_2° + hc$, valid in dilute solutions) monofunctional compounds lie on a single correlation line; however, polyfunctional compounds are situated well below this line, the displacement increasing with larger values of $\bar{V}_2°$. (iii) The volume change in the proton ionization of the methylamines is found to be nearly constant: $\Delta V = 4.7 \pm 0.7$ ml mol^{-1}. For the higher members of the amine series the following ΔV values are instead observed: 4.6 ± 0.4 ml mol^{-1} (primary amines), 2.5 ± 0.3 ml mol^{-1} (secondary amines), 1 ± 1 ml mol^{-1} (tertiary amines).

Introduction

As part of a systematic investigation of the thermodynamic properties of organic solutes in aqueous solution, we have considered in recent papers[1,2] volumetric properties of some cyclic ethers, cyclic amines, and their corresponding hydrochlorides. Preliminary studies were made on the effects associated with the change from open chain to cyclic compounds, on the concentration dependence of apparent molal volumes, Φ_v, of mono- and bifunctional solutes, and on the volume changes in the proton ionization process of organic compounds containing nitrogen.

In order to gain a clearer picture of the nature of the volumetric behavior, we report here studies of the volumetric properties of the following series of compounds in dilute aqueous solution at 25°: aliphatic secondary alcohols (2-butanol, 3-pentanol, 3-hexanol, 4-heptanol), cyclic

alcohols (cyclopentanol, cyclohexanol, cycloheptanol), primary *n*-alkyl amines ($C_nH_{2n+1}NH_2$ with $1 \leq n \leq 7$), and also secondary [$(C_nH_{2n+1})_2NH$ with $1 \leq n \leq 4$] and tertiary amines (trimethyl-, triethyl- and diethylmethylamine).

Measurement of apparent molal volumes in aqueous solutions have been previously reported for 2-butanol[3,4] in water, and for methyl-, dimethyl-, trimethyl- and triethylamine in KOH aqueous solution.[5,6] Values of the volumes of mixing in water were also given for 2-butanol, cyclopentanol, cyclohexanol, diethyl- and triethylamine.[7]

Experimental Section

Materials. All substances employed were reagent grade commercial products. The alcohols were refluxed over calcium hydride and then fractionally distilled. The amines were rectified on metallic sodium under nitrogen. In all cases the fraction collected showed a glc purity >99.5%.

In the case of ammonia, methyl-, ethyl-, dimethyl- and trimethylamine the commercial aqueous solutions were used directly without further purification. The amine content of these solutions was determined by HCl titration.

Water used in all the experiments was deionized and further distilled from an alkaline potassium permanganate solution.

Apparatus and Measurements. The hydrostatic differential balance used for density measurements (with a precision of 1 ppm) and the experimental procedure were previously described.[1]

The apparent molal volumes of the alcohols were calculated by

$$\Phi_v = \frac{M}{d^0} - \left[\frac{d}{d^0} - 1\right]\frac{1000}{c} \qquad (1)$$

where M is the solute molecular weight, c its molar concentration, d^0 and d the density of the water and the solution, respectively.

In the case of the amines (B) apparent molal volume values, Φ_v^{obsd}, were first calculated by introducing into eq 1 the molecular weight of the hypothetical hydrate $B \cdot H_2O$. The latter were then corrected to Φ_v values of the free amines using values of the acid dissociation constants of the bases taken from Perrin[8] and values of the apparent molal volumes of the amine salts taken from Desnoyers and Arel,[9] Verrall and Conway,[10] and Laliberté and Conway.[11] The Φ_v^0 values of NaCl, NaBr, and NaOH were taken from Desnoyers, *et al.*,[12] and from Bodanszky and Kauzmann.[13] The correction procedure was described in a previous paper.[1]

As an example, Figure 1 shows the trend of the function $\Phi^*/(1-\alpha)$ *vs.* $(1-\alpha)c_B^0$ for dimethylamine, where c_B^0 is the stoichiometric concentration of the base and α is the degree of hydrolysis. Values of the function are shown corrected and uncorrected for hydrolysis. At low solute concentration marked deviations from linearity occur on changing the pK_a values used by 0.1 unit.

Results and Discussion

Table I summarizes the values at infinite dilution of the partial molal volumes, $\bar{V}_2^\circ$, and the excess molal volumes, $\bar{V}^{\circ E}$, calculated as $\bar{V}^{\circ E} = \bar{V}_2^\circ - V_2$, where V_2 is the molar volume of the pure substance. Values are also reported of the slope h of the straight line representing the concentration dependence, in dilute solution, of the functions Φ_v and $\Phi^*/(1-\alpha)$ for alcohols and amines, respectively.

As is generally noticed for all the nonelectrolytes so far considered, the excess volumes are negative and increase in magnitude with increasing size of the hydrocarbon part of the molecule and concentration.

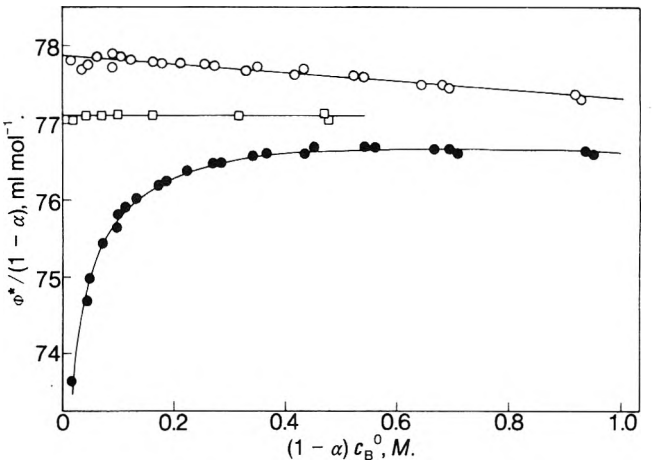

Figure 1. Apparent molar volumes of dimethylamine in aqueous solution at 25°: ●, data uncorrected for hydrolysis ($\alpha = 0$); ○, data corrected for hydrolysis; □, from measurements in 0.025 *N* KOH ($\alpha = 0$).

Though this is a well-known behavior, the large amount of data now available suggests some relationship between structure of the compounds and their volumetric properties. Particularly, these data allow one to individuate some general behavior in the dependence of Φ_v on concentration thus leading to a better understanding of solute-solute interactions in dilute aqueous solution.

Methylene Contribution in Cyclic and Open Chain Monofunctional Compounds. The linear dependence often found for many thermodynamic properties on the number of carbon atoms, n_C, in homologous series of unbranched compounds allows one to identify the slope of this function with the average contribution of a methylene group to the specific property.

In the case of volumes an average value $V(CH_2) = 16.6 \pm 0.3$ ml mol^{-1} is so obtained by applying the relationship $V = f(n_C)$ to homologous series of monofunctional open chain liquid compounds (*n*-alkanols, primary *n*-aliphatic amines, and secondary *n*-aliphatic amines). On the contrary the $V(CH_2)$ values of monofunctional cyclic compounds (secondary cyclic alcohols, secondary cyclic amines. tertiary cyclic amines, and cyclic ethers) are scattered over the large range 13.5–17.5 ml mol^{-1}. This lack of regularity in the volumetric behavior of the pure liquids precludes the use of excess volumes or the comparison of the values of $\bar{V}^\circ(CH_2)$ and $\bar{V}(CH_2)$ in different homologous series in order to interpret the volumetric properties of the solutes in aqueous solution.

It is more significant to compare the $\bar{V}(CH_2)$ values in aqueous solutions because of the clearer distinction that occurs in the volumetric properties of various molecules present in this state. For example, two separate ranges can be distinguished for monofunctional unbranched compounds: $\bar{V}^\circ(CH_2) = 15.9 \pm 0.4$ ml mol^{-1} for open chain compounds and $\bar{V}^\circ(CH_2) = 14.2 \pm 0.4$ ml mol^{-1} for cyclic compounds.[15] Such a difference can in part be due to intrinsic factors but in part may be also justified assuming that cyclic molecules are more easily introduced into the cluster cavities of the solvent. Unfortunately, the values of partial molal volumes of open chain and cyclic monofunctional compounds are not available in solvents other than water. Such data might be very useful in order to ascertain

TABLE I: Volumetric Properties of Amines and Alcohols in Water at 25°

Substance	No. of expt	Concn range, M	$\bar{V}_2°$, ml mol^{-1}	h,[a] ml l. mol^{-2}	V_2,[b] ml mol^{-1}	$\bar{V}°_E$, ml mol^{-1}	Ref
Ammonia	21	0.03–0.9	24.85 ± 0.04	−0.1 ± 0.1	28.25	−3.4	This work
			24.6				14
Methylamine	18	0.03–0.9	41.68 ± 0.04	−0.3 ± 0.1	47.33	−5.6	This work
			41.6				14
	8	0.03–0.6	41.15 ± 0.06[c]	−0.1 ± 0.1			This work
		0.07–0.14	40.0[c]				5,10
Ethylamine	21	0.03–0.8	58.37 ± 0.05	−0.9 ± 0.1	66.61	−8.2	This work
n-Propylamine	32	0.02–0.7	74.12 ± 0.04	−1.2 ± 0.1	83.15	−9.0	This work
n-Butylamine	29	0.02–0.8	89.8 ± 0.1	−1.4 ± 0.4	99.77	−10.0	This work
n-Pentylamine	31	0.01–0.5	105.7 ± 0.1	−2.0 ± 1	116.14	−10.4	This work
n-Hexylamine	30	0.01–0.1	121.6 ± 0.2	−3.0 ± 3	132.8	−11.2	This work
n-Heptylamine	18	0.005–0.025	137.6 ± 0.3	−6.5 ± 10	149.32	−11.7	This work
Dimethylamine	24	0.02–0.7	59.80 ± 0.04	−0.5 ± 0.1	69.41	−9.6	This work
			59.1				14
	8	0.02–0.5	59.0 ± 0.1[c]	0.0 ± 0.3			This work
		0.06–0.2	58.6[c]				5,10
Diethylamine	12	0.02–0.4	91.68 ± 0.10	−2.1 ± 0.5	104.56	−12.9	This work
						−15.3[d]	7
Di-*n*-propylamine	21	0.01–0.3	123.06 ± 0.10	−3.2 ± 0.5	137.93	−14.9	This work
Di-*n*-butylamine	20	0.003–0.02	155.4 ± 0.4	−25 ± 21	171.03	−15.7	This work
Trimethylamine	19	0.03–0.5	78.8 ± 0.2	−1.5 ± 0.4	94.28	−15.5	This work
			78.4				14
	14	0.02–0.5	78.6 ± 0.2[c]	−1.1 ± 0.8			This work
		0.03–0.16	77.9[c]				5,10
Diethylmethylamine[e]	9	0.03–0.6	106.77 ± 0.10	−2.3 ± 0.3			This work
Triethylamine	22	0.02–0.7	120.9 ± 0.1	−2.3 ± 0.4	139.93	−19.0	This work
			119.7[c]				10
						−21.8[d]	7
2-Butanol	15	0.02–0.5	86.66 ± 0.03	−1.7 ± 0.1	92.38	−5.7	This work
		0.003–0.1	86.53				4
						−6.8[d]	7
3-Pentanol	20	0.01–0.4	101.28 ± 0.03	−2.3 ± 0.2	108.00	−6.7	This work
3-Hexanol	16	0.01–0.15	117.14 ± 0.09	−3.2 ± 1.4	125.47	−8.3	This work
4-Heptanol	13	0.005–0.04	133.2 ± 0.2	−19 ± 7	142.60	−9.4	This work
Cyclopentanol	10	0.02–0.2	89.06 ± 0.02	−2.2 ± 0.2	91.34	−2.3	This work
						−2.9[d]	7
Cyclohexanol	7	0.02–0.3	103.54 ± 0.03	−2.5 ± 0.2	105.95	−2.4	This work
						−2.0[d]	7
Cycloheptanol	18	0.01–0.1	116.88 ± 0.04	−3.0 ± 0.6	120.26	−3.4	This work

[a] In the case of the following amines: *n*-butylamine (0.4); *n*-pentylamine (0.3); diethylmethylamine (0.45); triethylamine (0.35); the function $\Phi^*/(1-\alpha) = f[(1-\alpha)c_B°]$ was found to be linear up to the concentration value indicated in parentheses. [b] The molar volumes V_2 at 25° of pure substances were evaluated from density data reported in the literature. [c] From measurements in 0.025 *N* KOH aqueous solutions. [d] At 26.5°. [e] The $\bar{V}_{BHCl}°$ of $Et_2MeN \cdot HCl$, necessary for hydrolysis correction, was obtained from measurements on aqueous solutions of the amine neutralized with HCl. As a result of seven runs in the concentration range 0.03–0.5 *M* we found: $\Phi_{BHCl} - 1.868\sqrt{c} = (222.81 \pm 0.01) - (2.15 \pm 0.03)c$.

whether the observed difference between the $\bar{V}°(CH_2)$ of open chain and cyclic compounds is prevailingly due to effects of the solutes on the water structure or to geometric factors characteristic of the molecules.

The above interpretation assumes a two-state model for water. Such a model has already been adopted in order to interpret the differences between the methylene contribution of open chain and cyclic monofunctional compounds to the hydration entropies[16a] ($\Delta S_h(CH_2) = -3.5 \pm 1.0$ cal deg^{-1} mol^{-1} for open chain and $\Delta S_h(CH_2) = -2.6 \pm 0.3$ cal deg^{-1} mol^{-1} for cyclic compounds), to the hydration enthalpies[16a] ($\Delta H_h(CH_2) = -0.95$ kcal mol^{-1} for open chain and $\Delta H_h(CH_2) = -0.6$ kcal mol^{-1} for cyclic compounds) and to the partial molal heat capacities[16b] ($\Phi_{Cp}(CH_2) = 22 \pm 2$ cal deg^{-1} mol^{-1} for open chain and $\Phi_{Cp}(CH_2) = 18 \pm 2$ cal deg^{-1} mol^{-1} for cyclic compounds). These differences are in our opinion to be ascribed to the higher structure promoting effect exhibited by open chain compounds as a result of the larger hydrophobic surface that their alkyl chains expose to the solvent through less restricted rotation.

When intrinsic structure factors reduce this internal rotation freedom the contribution of the hydrocarbon part to the thermodynamic property (*e.g.*, partial molal volume or partial molal heat capacity) for the open chain compound approaches the value which is observed for the corresponding cyclic compound. In this respect an interesting comparison can be made between the pairs diethylamine–pyrrolidine and diethylmethylamine–*N*-methylpyrrolidine for which the values $\delta\bar{V}_2° = 13.8$ ml mol^{-1} and $\delta\Phi_{Cp} = 36.6$ cal deg^{-1} mol^{-1} and the values $\delta\bar{V}_2° = 9.5$ ml mol^{-1} and $\delta\Phi_{Cp} = 19.9$ cal deg^{-1} mol^{-1} are observed, respectively. The lower value of $\delta\Phi_{Cp}$ of cyclization for the tertiary amine was interpreted[16b] assuming that the presence of the methyl group reduces the rotational freedom of the remaining ethyl groups which are thus less effective in promoting water structure. This same effect can explain the differences now observed for $\delta\bar{V}_2°$ of cyclization of secondary with respect to tertiary amines. In other words a reduction of the degrees of internal freedom of the molecule is reflected by the partial molal thermodynamic properties primarily because of a reduced ability of the hydrophobic part of the molecule to promote structural order in the solvent.

Volume Change in Proton Ionization. Values of ΔV corresponding to the reaction $BH^+ \rightarrow B + H^+$ for a large

TABLE II: Thermodynamic Functions for Proton Ionization from Protonated Amines in Aqueous Solution at 25°

Base	$\bar{V}_B°$, ml mol^{-1}	$\bar{V}_{BHX}°$, ml mol^{-1}	X	ΔV, ml mol^{-1}	ΔH, kcal mol^{-1}	ΔS, cal deg^{-1} mol^{-1}	ΔC_p, cal deg^{-1} mol^{-1}
Ammonia	24.6[a]	36.0[a]	Cl	6.4	12.48[b]	−0.45[b]	−3.0[b]
	24.8[c]	42.6[i]	Br	7.0	12.42[e]	−0.60[e]	−0.0[e]
Methylamine	40.0[f]	53.8[f]	Cl	4.1	13.09[g]	−4.7[g]	8.0[g]
	41.6[a]	55.5[a]	Cl	3.9	13.29[h]	−4.1[h]	
	41.7[c]	60.8[i]	Br	5.6			
Ethylamine	58.4[c]	77.7[i]	Br	5.4	13.71[h]	−2.7[h]	
n-Propylamine	74.1[c]	94.1[i]	Br	4.7	13.67[e]	−2.5[e]	7.4[e]
					13.84[h]	−2.0[h]	
					13.66[j]	−2.5[j]	
					13.80[k]	−2.0[k]	
n-Butylamine	89.8[c]	110.2[i]	Br	4.3	13.88[e]	−2.1[e]	2.3[e]
					13.98[k]	−1.7[k]	
					13.88[e]	−2.1[e]	
n-Pentylamine	105.7[c]	126.1[i]	Br	4.3	13.98[h]	−1.8[h]	
n-Hexylamine	121.6[c]	142.0[i]	Br	4.3			
n-Heptylamine	137.6[c]	157.9[i]	Br	4.4			
Dimethylamine	59.8[c]	72.5[f]	Cl	5.1			18.5[l]
	59.1[a]	73.1[a]	Cl	3.8	11.86[g]	−9.5[g]	23.1[g]
	58.6[f]	72.5[f]	Cl	3.9	12.04[h]	−8.7[h]	
Diethylamine	91.7[c]	106.7[d]	Cl	2.8	12.73[h]	−7.3[h]	19.1[l]
Di-*n*-propylamine	123.1[c]	138.7[d]	Cl	2.2	13.17[h]	−6.2[h]	20.9[l]
Di-*n*-butylamine	155.4[c]	170.7[d]	Cl	2.5	13.66[h]	−5.7[h]	
Trimethylamine	78.8[c]	90.6[f]	Cl	6.0	8.81[g]	−15.2[g]	43.8[g]
	78.4[a]	91.7[a]	Cl	4.5			
	77.9[f]	90.6[f]	Cl	5.0			
Diethylmethylamine	106.8[c]	122.8[c]	Cl	1.8			33.6[l]
Triethylamine	120.9[c]	138.6[f]	Cl	0.1	10.58[e]	−13.5[e]	44.7[e]
Tripropylamine		186.8[f]	Cl				

[a] Reference 14. [b] Reference 17. [c] This work. [d] Reference 11. [e] Reference 18. [f] Reference 10. [g] Reference 19. [h] Reference 20. [i] Reference 9. [j] Reference 21. [k] Reference 22. [l] Reference 16.

number of amines are reported in Table II[17-22] as well as the values of enthalpy, entropy, and heat capacity changes associated with this process. In the calculation of ΔV the values $\bar{V}_{HCl}° = 17.83$ ml mol^{-1} and $\bar{V}_{HBr}° = 24.71$ ml mol^{-1} were assumed.[23]

Examination of these data shows the following. (a) For the first terms of the various series (*i.e.*, CH_3NH_2, $(CH_3)_2NH$, $(CH_3)_3N$) the ionization volume has an almost constant value: $\Delta V = 4.7 \pm 0.7$ ml mol^{-1} whereas the ΔH, ΔS, and ΔC_p values vary markedly as the number of methyl groups bonded to nitrogen is varied. (b) As the alkyl chain length is increased the ΔV rapidly reaches a constant value 4.6 ± 0.4 ml mol^{-1} for primary amines, 2.5 ± 0.3 ml mol^{-1} for secondary amines and 1 ± 1 ml mol^{-1} for tertiary amines. Analogously the changes of other thermodynamic functions associated with the process rapidly reach constant values: $\Delta H = 13.8 \pm 0.1$, 13.2 ± 0.4, 10.6 kcal mol^{-1}; $\Delta S = -2.2 \pm 0.4$, -6.4 ± 0.8, -13.5 cal deg^{-1} mol^{-1}; $\Delta C_p = 4.9 \pm 2.5$, 20 ± 1, 38 ± 5 cal deg^{-1} mol^{-1} for proton ionization of primary, secondary and tertiary protonated amines respectively. (c) When going from the first to the higher members within each series the ΔV and ΔC_p values decrease while the ΔS and ΔH values increase. Finally, the data in (b) indicate that in going from primary → secondary → tertiary amines, the values of ΔV, ΔH, and ΔS decrease whereas the values of ΔC_p increase.

Observation (b) allows one to deduce for intramolecular distances greater than two bonds removed from the nitrogen center that the water–hydrocarbon part and water–hydrophilic center interactions may be considered, as a first approximation, independent. Therefore the thermodynamics of the proton ionization process of charged nitrogen centers is better characterized by ΔX values (X = V, H, S, and C_p) of amines containing alkyl groups other than methyl. It would be very useful to know the separate value of partial molal properties of the free and protonated bases, but difficulties arise, for ionic species, owing to the ambiguity of assigning individual ionic contributions. However an analysis of Φ_{Cp} values of a number of primary, secondary, and tertiary amines and their hydrochlorides established that the trend in ΔC_p of the ionization process is mainly due to the fact that the contribution to the partial molal heat capacity by the charged nitrogen center decreases significantly as the number of alkyl radicals bonded to nitrogen is increased.[16b] This is in agreement with the interpretation given by Evans and Hamann[24] to the trend of the ionization entropies. According to these authors the ammonium ion is surrounded by a zone of ordered water; on substituting the hydrogen atoms bonded to nitrogen with alkyl groups the entropy loss of the solvent is lowered, thus causing the partial molar entropy of the acid cation to increase relative to that of the neutral base. There are good reasons to believe[25] also that the progressive lowering of the values of ΔV of ionization as more and more alkyl groups are bonded to nitrogen is virtually determined by interactions of water with the charged nitrogen centers; *i.e.*, the larger the number of bonded alkyl groups, the weaker is the electrostriction effect and the smaller the volume increment associated with proton ionization.

It is not readily understood why the values of ΔV of ionization in the series of methylamines are almost independent of the number of methyl groups bonded to nitrogen, whereas the ΔH, ΔS, and ΔC_p values vary markedly with this number, more so than in the case of bulkier substituents.

Dependence of Φ_v on Concentration. As already ob-

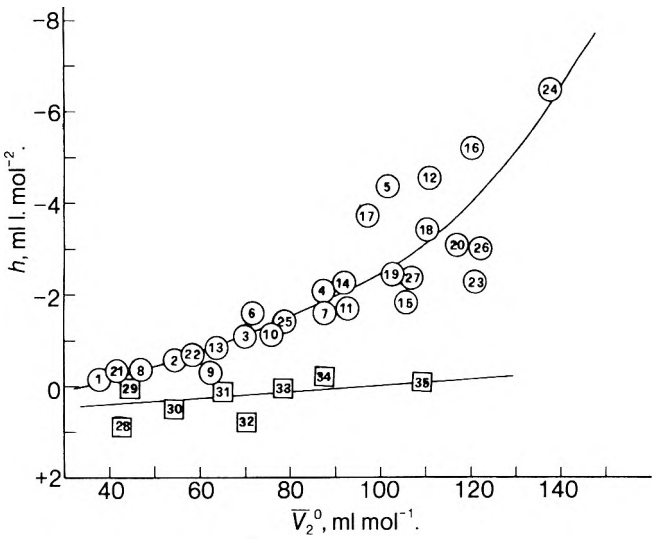

Figure 2. Plot of h *vs.* $\bar{V}_2^0$ for organic solutes in aqueous solution at 25°. Monofunctional compounds (○): 1, methanol at 20° (ref 3, 26); 2, ethanol at 20° (ref 3, 26); 3, 1-propanol at 20° (ref 3, 26); 4, 1-butanol (ref 4), 2-methyl-2-propanol (ref 4), cyclopentanol; 5, 1-pentanol at 20° (ref 3, 26); 6, 2-propanol at 20° (ref 3, 26); 7, 2-methyl-1-propanol (ref 4), 2-butanol, *n*-buthylamine; 8, ethylene oxide at 10° (ref 27), ethyleneimine (ref 1); 9, propylene oxide and trimethylene oxide (ref 28); 10, tetrahydrofuran and pyrrolidine (ref 1), *n*-propylamine; 11, tetrahydropyran and 2-methyltetrahydrofuran (ref 1); 12, 2,5-dimethyltetrahydrofuran (ref 1); 13, azetidine (ref 1); 14, piperidine (ref 1), diethylamine; 15, hexamethylenimine (ref 1), *n*-pentylamine; 16, heptamethylenimine (ref 1); 17, 1-methylpyrrolidine (ref 1); 18, 1-methylpiperidine (ref 1); 19, 3-pentanol, cyclohexanol; 20, cycloheptanol, 3-hexanol; 21, methylamine; 22, ethylamine, dimethylamine; 23, triethylamine; 24, *n*-heptylamine; 25, trimethylamine; 26, *n*-hexylamine, di-*n*-propylamine; 27, diethylmethylamine. Polifunctional compounds (□): 28, glycine (ref 29); 29, urea (ref 29); 30, thiourea (ref 29); 31, 1,3-dioxolane (ref 1); 32, glycerol (ref 30); 33, 1,4-dioxane (ref 1), 1,3-dioxane (ref 28), urethane (ref 29); 34, pyrocatechol (ref 29), resorcinol (ref 29), hydroquinone (ref 29); 35, hexamethylenetetraamine (ref 31).

served[1] in dilute solution the Φ_v values decrease with concentration according to the relationship $\Phi_v = \bar{V}_2^\circ + hc$. The value of the slope h varies consistently when going from monofunctional to bifunctional compounds of the same molecular dimensions. Among monofunctional compounds it depends on the extension of the alkyl chain. Examination of a plot of h *vs.* $\bar{V}_2^\circ$ (Figure 2)[26-31] indicates that all saturated monofunctional compounds lie on a single curve which shows an exponential increase of the absolute value of h with increasing $\bar{V}_2^\circ$ values.

Polyfunctional compounds having similar limiting partial molal volumes as the monofunctional compounds have less negative values of h. Moreover, in the latter case the h value only changes slightly with $\bar{V}_2^\circ$.

The fact that on the plane $h - \bar{V}_2^\circ$ a single correlation line represents the volumetric behavior of different types of monofunctional compounds, suggests the solute-solute interactions occurring *via* the functional groups to be probably negligible in dilute solution. The progressive volume lowering as the solute concentration is increased is thus mainly to be ascribed to a prolongation of the average life of water clusters which are included between the hydrocarbon region of two or more solute molecules. This would cause the lifetime of solutes in the cluster cavities to be enlarged with the consequent macroscopic effect of a volume decrease.

The exponential trend of the plot finally suggests that this effect of stabilization of water clusters by solute-solute interactions is probably cooperative.

Acknowledgment. This work has been supported through financial assistance from the Consiglio Nazionale delle Ricerche (C.N.R.).

References and Notes

(1) S. Cabani, G. Conti, and L. Lepori, *J. Phys. Chem.*, **76**, 1338 (1972).
(2) S. Cabani, G. Conti, L. Lepori, and G. Leva, *J. Phys. Chem.*, **76**, 1343 (1972).
(3) M. E. Friedman and H. A. Scheraga, *J. Phys. Chem.*, **69**, 3795 (1965).
(4) F. Franks and H. T. Smith, *J. Chem. Eng. Data*, **13**, 538 (1968); *Trans. Faraday Soc.*, **64**, 2962 (1968).
(5) B. E. Conway and R. E. Verrall, *J. Phys. Chem.*, **70**, 3952 (1966).
(6) B. E. Conway, R. E. Verrall, and J. E. Desnoyers, *Trans. Faraday Soc.*, **62**, 2738 (1966).
(7) K. R. Brower, J. Peslak, and J. Elrod, *J. Phys. Chem.*, **73**, 207 (1969).
(8) D. D. Perrin, "Dissociation Constants of Organic Bases in Aqueous Solution," Butterworths, London, 1965.
(9) J. E. Desnoyers and M. Arel, *Can. J. Chem.*, **45**, 359 (1967).
(10) R. E. Verrall and B. E. Conway, *J. Phys. Chem.*, **70**, 3961 (1966).
(11) L. H. Laliberté and B. E. Conway, *J. Phys. Chem.*, **74**, 4116 (1970).
(12) J. E. Desnoyers, M. Arel, G. Perron, and C. Jolicoeur, *J. Phys. Chem.*, **73**, 3346 (1969).
(13) A. Bodanszky and W. Kauzmann, *J. Phys. Chem.*, **66**, 177 (1962).
(14) S. D. Hamann and S. C. Lim, *Aust. J. Chem.*, **7**, 329 (1954).
(15) These data were obtained considering: (i) for open chain compounds 28 molecules belonging to the series of *n*-alkanols, secondary alkanols, primary and secondary *n*-aliphatic amines, primary and secondary *n*-aliphatic protonated amines; (ii) for cyclic compounds 21 molecules belonging to the series of secondary and tertiary cyclic amines, cyclic alcohols, cyclic ethers, secondary and tertiary protonated cyclic amines. The first term of each series was not taken into consideration.
(16) (a) S. Cabani, G. Conti, and L. Lepori, *Trans. Faraday Soc.*, **67**, 1943 (1971); (b) S. Cabani, G. Conti, A. Martinelli, and E. Matteoli, *J. Chem. Soc., Faraday Trans. I*, **69**, 2112 (1973).
(17) R. G. Bates and H. B. Hetzer, *J. Res. Nat. Bur. Stand.*, **42**, 419 (1949).
(18) M. C. Cox, D. H. Everett, D. A. Landsman, and R. J. Munn, *J. Chem. Soc., B*, 1373 (1968).
(19) D. H. Everett and W. F. K. Wynne-Jones, *Proc. Roy. Soc., Ser. A*, **177**, 499 (1941).
(20) J. J. Christensen, R. M. Izatt, D. P. Wrathall, and L. D. Hansen, *J. Chem. Soc., Ser. A*, 1212 (1969).
(21) R. G. Bates and H. B. Hetzer, *J. Phys. Chem.*, **65**, 667 (1961).
(22) G. Ojelund and I. Wadso, *Acta Chem. Scand.*, **22**, 2691 (1968).
(23) F. J. Millero, *Chem. Rev.*, **71**, 147 (1971).
(24) A. G. Evans and S. D. Hamann, *Trans. Faraday Soc.*, **47**, 34 (1951).
(25) Let us assume for the methylene and methyl contribution to $\bar{V}_2^\circ$ the values of 16 ml mol^{-1} and 18 ml mol^{-1}, respectively. Considering the primary amines from *n*-propyl- up to *n*-heptylamine and the secondary amines from diethyl- up to di-*n*-butylamine the following $\bar{V}_2^\circ$ contributions are obtained for $-NH_2$ and $>NH$ groups, respectively: 23.85 ± 0.15 and 23.4 ± 0.2 ml mol^{-1}. Considering, instead, the hydrobromides of the above amines the $\bar{V}_2^\circ$ contributions of the groups $-NH_3^+Br^-$ and $>NH_2^+Br^-$ are 44.1 ± 0.1 and 45.65 ± 0.1 ml mol^{-1}, respectively. These data show that the difference between the ionization volumes of primary and secondary amines [(23.85 − 23.4) − (44.1 − 45.6) = 2 ml mol^{-1}] is mainly to be ascribed to the charged nitrogen centers.
(26) D. M. Alexander, *J. Chem. Eng. Data*, **4**, 252 (1959).
(27) D. N. Glew, H. D. Mak, and N. S. Rath, *Can. J. Chem.*, **45**, 3059 (1967).
(28) K. W. Morcom and R. W. Smith, *Trans. Faraday Soc.*, **66**, 1073 (1970); *J. Chem. Eng. Data*, **16**, 197 (1971).
(29) A. Indelli, *Ann. Chim. (Rome)*, **53**, 605 (1963).
(30) J. L. Neal and D. A. I. Goring, *J. Phys. Chem.*, **74**, 658 (1970).
(31) V. Crescenzi, F. Quadrifoglio, and V. Vitagliano, *J. Phys. Chem.*, **71**, 2313 (1967).

A Modified Semi-Ion-Pair Model for the Evaluation of Activation Energies of Four-Center Addition Reactions of Hydrogen Halides to Olefins[1]

K. R. Maltman, E. Tschuikow-Roux,* and K. -H. Jung

Department of Chemistry, The University of Calgary, Calgary, Alberta, Canada T2N 1N4 *(Received September 11, 1973)*

The Benson–Bose–Haugen method for the calculation of the activation energies of four-center reactions has been modified in an attempt to remedy the failure encountered with a number of polar systems and to allow simpler treatment of the orientation effects of alkyl groups in addition reactions involving olefins. In calculating the activation energies of these reactions, a semiionic model is used, and all parameters required are determinable from ground-state properties of reactants and products. Dipole–dipole interactions are evaluated using the model of point dipoles, while energy contributions arising from breaking and forming bonds are evaluated using Johnston's bond-energy–bond-order correlation. The orientation of the transition state is fixed using a criterion related to the Kihara potential. Calculated activation energies agree with a large number of experimentally determined values to within an average of ±1.7 kcal mol^{-1}. Calculated values are presented for the addition reactions of HF, HCl, HBr, and HI to olefins, including polar olefins.

Introduction

A number of investigators have previously attempted to calculate the activation energies of four-center reactions by semiempirical means. These calculations have involved two basically different models for the transition state of such reactions. In the first, originally utilized by Noyes,[2,3] it is assumed that bond order is conserved between the four centers taking part in the reaction, and that no separation of charge occurs during the process of activation. As developed by Noyes[2,3] the actual method of calculation is suited only to treat reactions of the form AB + CD = AC + BD, and does not yield very good results. Using the same basic model for the transition state, Pahari and Basu[4,5] have developed a calculational technique using a different method of evaluation of the energy of partial bonds than that used by Noyes. This method is also applicable to addition reactions involving olefins, although one system must be used for each olefin to determine the effective bond energy of the π bond in that olefin. The agreement obtained is much better than that of Noyes, however, some of the bond energies used for small molecules differ significantly from those tabulated by Darwent.[6] The second model, originally proposed by Benson and Bose,[7] allows for the polarization of the breaking bonds in the transition state, and has essentially no bonding interaction between the centers of forming bonds. The four interacting centers are assumed to lie in one plane, and the resulting quadrilateral is assumed to be fairly rigid. The polar nature of the transition state seems relatively well established.[7] In the case of hydrogen halide elimination from haloalkanes, the work of Tsang and Rowland[8] indicates that eliminations occur almost entirely *via* the α, β reaction channel, thus supporting the contention of Benson, *et al.*,[7,9] that such reactions proceed in a concerted manner through a cyclic transition state. The assumption that the forming bonds have only van der Waal's interaction would seem to be less well substantiated; indeed, Haugen and Benson[10] calculate the orders of forming bonds to be as high as 0.18. Pahari and Basu[4] have noted that the method of Benson and Haugen fails drastically in the case of reactions of the type AB + CD = AC + BD, and Tschuikow-Roux and coworkers[11] have noted the failure of the method for fluoro-substituted polar olefins.

It is the purpose of this paper to modify the detailed model of Benson, Bose, and Haugen, and, while retaining its basic features, to present a method of evaluating energy contributions to the process of activation which is dependent only on ground-state properties of reactants and products.

Modified Semi-Ion-Pair Model

The Transition State. The transition state of the reactions under consideration is characterized by six parameters. The first four are the bond orders of the four bonds involved in the reaction. The fifth is the partial formal charge separation along the breaking bonds, and the sixth is any of the interior angles of the quadrilateral formed by the interacting bonds (four sides and one interior angle determine uniquely a convex quadrilateral). Following Benson and Bose,[7] the transition state bond orders of the breaking bonds are taken to be 0.5 less than their bond orders in the reactants. The relative orientation of the two breaking bonds and hence the value of the chosen interior angle, ϕ_1, is determined as follows: it is assumed that if the approach of the reactants is relatively unhindered, then their interaction (intermolecular) can be roughly described by the Kihara potential for the interaction of linear core systems. It was found that the bonds in the transition states for the reactions in question were sufficiently small that the typical separations of cores were much less than the value of ρ_0 (the core separation at which the potential energy of interaction is zero) for any known systems. This implies that the interaction between the breaking bonds is always of a repulsive nature. Thus, the most favorable orientation is that in which the shortest distance between the two breaking bonds is maximized. Maltman and Tschuikow-Roux[12] have shown how to obtain an analytic expression for the shortest distance between arbitrarily oriented line segments. Using this formulation, it is possible to numerically vary the value of the interior angle and choose that value which corresponds to the maximum of the intercore distance. The

value of the partial formal charge separation, δ, was taken to be the same for both of the breaking bonds, as suggested by Benson and Bose,[7] but its value was allowed to vary. The exact value for a given system was determined from parameters for the reactants and products as described below. Once the value of δ was determined, the values of the bond orders for the forming bonds (assumed equal) were calculated using the assumption of generalized bond order conservation,[7] *i.e.*, the sum of the transition state bond orders plus the partial formal charge separations equals the sum of the initial bond orders

$$n_1^0 + n_3^0 = \sum_{i=1}^{4} n_i + 2\delta \tag{1}$$

The description of the geometry of the transition state was then completed by using Pauling's rule[13] to calculate the bond lengths of the partial bonds

$$r(n) = r_s - 0.26 \ln (n) \tag{2}$$

where r_s is the length of a single bond, and n is the order of the bond.

Energy Contributions to Activation. The evaluation of the activation energy of a given reaction is greatly simplified by the assumption that the bonds of any groups attached to centers undergoing change of bonding during the course of the reaction are unchanged in energy. This assumption, which was justified by Haugen and Benson,[10] means that only terms involving the interaction between the four reaction centers contribute to the activation energy. These contributions arise from the energy required to change each of the four bonds from its reactant state to its activated complex state, and from the interaction between the two induced dipoles.

We now obtain expressions for the above energy contributions. With reference to Figure 1, we denote the breaking bonds by the subscripts 1 and 3, and those forming by the subscripts 2 and 4. The interior angle which has been calculated as described above is denoted by ϕ_1. The energies of the forming and breaking bonds are calculated using Johnston's method for the evaluation of the energy of partial bonds.[14] According to this method the energy of a bond of order n is given by

$$D(n) = D(1)n^p \tag{3}$$

where $D(1)$ is the energy of a single bond between the two atoms of interest (the zero of energy is taken here at infinite separation of the two atoms) and p is an empirical factor. For bonds of order less than unity, p is given by[14]

$$p = \frac{0.26 \ln [D(1)/\epsilon_x]}{R_x - r_s} \tag{4}$$

where r_s is the bond length of a single bond between the two atoms of interest, ϵ_x is the Lennard-Jones potential well depth of the noble gas diatom cluster formed by the noble gases in the same rows of the periodic table as the atoms in question, and R_x is the corresponding bond length (distance at which the potential minimum in the interaction occurs). For the addition of HX to olefins, we are concerned with the energy of bonds with orders between 1 and 2. To evaluate p in this case it was assumed that the bond energies for single and double bonds were given by eq 3. Then p is given by

$$p = \ln [D(2)/D(1)]/\ln 2 \tag{5}$$

where $D(2)$ is the energy of the C-C double bond in the reactant and $D(1)$ the C-C single bond energy in the product molecule. If n_i^0 is the initial order of the ith bond, the total contribution to the activation energy arising from the formation of the four bonds is given by

$$E(\text{bonds}) = \Sigma E_i = \sum_{i=1}^{4} D_i(1)(n_i^{p_i} - n_i^{0p_i}) \tag{6}$$

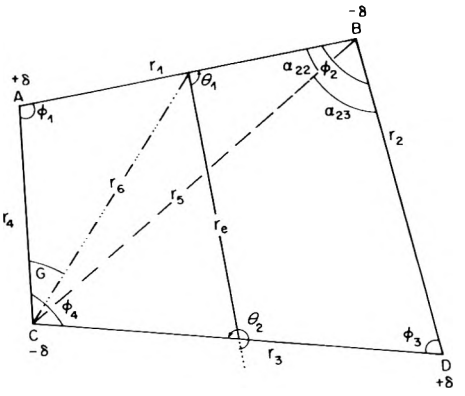

Figure 1. The geometry of the four-center transition state.

In order to calculate the interaction of the two induced dipoles, it was assumed that an adequate description is provided by the interaction of two point dipoles of the same magnitude and orientation situated at the center of the two breaking bonds. If the partial formal charge separation, δ, is given in electronic units and the distances are given in Angstrom units, the dipole-dipole interaction in kcal mol^{-1} is[15]

$$E_d = 332 r_1 r_3 \delta^2 [\cos (\theta_1 - \theta_2) - 3 \cos \theta_1 \cos \theta_2]/r_e^3 \tag{7}$$

where θ_1 is the angle between the dipole formed by the first bond and the line between the centers of the breaking bonds, θ_2 is the angle between the line of centers and the third bond, and r_e is the separation of centers (Figure 1). These angles of orientation are given in terms of the interior angles of the quadrilateral by

$$\theta_1 = \tfrac{1}{2}(\pi - \phi_2 + \phi_1) \tag{8}$$

$$\theta_2 = \tfrac{1}{2}(3\pi + \phi_3 - \phi_4) \tag{9}$$

It is possible, in turn, to express ϕ_i ($i \neq 1$) in terms of ϕ_1

$$r_5 = (r_1^2 + r_4^2 - 2r_1 r_4 \cos \phi_1)^{1/2} = (r_2^2 + r_3^2 - 2r_2 r_3 \cos \phi_3)^{1/2}$$

$$\phi_3 = \cos^{-1} [(r_2^2 + r_3^2 - r_1^2 - r_4^2 + 2r_1 r_4 \cos \phi_1)/2r_2 r_3] \tag{10}$$

$$\alpha_{22} = \cos^{-1} [(r_1^2 + r_5^2 - r_4^2)/2r_1 r_5]$$

$$\alpha_{23} = \cos^{-1} [(r_2^2 + r_5^2 - r_3^2)/2r_2 r_5]$$

$$\phi_2 = \alpha_{22} + \alpha_{23} \tag{11}$$

$$\phi_4 = 2\pi - \phi_1 - \phi_2 - \phi_3 \tag{12}$$

Similarily, r_e may be expressed in terms of the sides of the quadrilateral and the interior angles

$$r_e = [r_6^2 + \tfrac{1}{4}r_3^2 - r_3 r_6 \cos (\theta_4 - G)]^{1/2} \tag{13}$$

where

$$G = \cos^{-1} [(r_1^2 + r_6^2 - \tfrac{1}{4}r_1^2)/2r_4 r_6]$$

and

$$r_6 = (r_4^2 + \tfrac{1}{4}r_1^2 - r_1 r_4 \cos \phi_1)^{1/2}$$

Substituting (8) and (9) into (7) yields

$$E_d = 332 r_1 r_3 \delta^2 \{3 \sin [\tfrac{1}{2}(\phi_2 - \phi_1)] \sin [\tfrac{1}{2}(\phi_4 - \phi_3)] - \cos [\tfrac{1}{2}(\phi_1 + \phi_4 - \phi_3 - \phi_2)]\} / r_e^3 \quad (14)$$

in which all the quantities are known in terms of r_i (i = 1, ... 4) and ϕ_1.

The activation energy is then given by

$$E_a = E(\text{bonds}) + E_d \quad (15)$$

and can thus be evaluated from (6) and (14).

The Value of the Partial Formal Charge Separation. One of the unusual features of the method proposed by Benson and Bose[7] was that it assumed the same charge separation along the breaking bonds for all reactions. In view of the large differences in the polarizabilities of the reactants treated, this seems somewhat unlikely. Thus, although many features of this earlier treatment are retained in the present method, there is a major departure in this particular aspect. Consider the homologous series

$$\text{olefin} + \text{HX} \longrightarrow \text{alkyl halide}$$

for a given X. We suppose that the double bond energies in the olefins are known or can be derived. If polarization of the reactants is important in the reaction process then the energy required to achieve this polarization should have a bearing on the value of the parameter δ. The higher the energy required to achieve the polarization of the reactants, the greater should be the orders of the forming bonds to compensate for this, *i.e.*, δ should be lower (*viz.* eq 1). Now, for a specified X in the homologous series above, the energy required to reach the $n_3 = 0.5$ state is fixed within the series, and hence the value of δ depends only on the properties of the olefinic bond. The expression for the polarization energy of this bond is given by the first term in eq 6. Thus with $n_1 = 1.5$ and $n_1^0 = 2$ we have

$$E_1 = D_1(1)[1.5^{p_1} - 2^{p_1}] = D_d(2) - D_d(1)[1.5^{p_1}] \quad (16)$$

where, for convenience, the thermodynamic bond dissociation energies (a positive quantity) are used; *i.e.*, $D_d(1) \equiv -D(1)$ for a single bond, and $D_d(2) \equiv -D(2) = -D(1)[2^{p_1}]$ for a double bond. Using these definitions and substituting for p_1 from eq 5 in eq 16 gives

$$E_1 = D_d(2) - D_d(1) \exp\{[\ln (1.5) \ln [D_d(2)/D_d(1)]]/\ln 2\} \quad (17)$$

Differentiation of E_1 with respect to $D_d(1)$ yields

$$dE_1/dD_d(1) = f[(\ln 1.5/\ln 2) - 1] < 0 \quad (18)$$

where

$$f = \exp\{[\ln (1.5) \ln [D_d(2)/D_d(1)]]/\ln 2\} \quad (19)$$

From eq 18 it follows that as $D_d(1)$ increases, E_1 decreases and hence, according to the argument above, δ should increase. But from eq 3 as $D_d(1)$ increases for a fixed double bond dissociation energy, the corresponding p factor must decrease. The p factor for the carbon-carbon bond thus acts as an internal indicator for the system, reflecting the relative ease of the heterolytic polarization in the transition state. For this reason the following correlation was proposed between this p factor, p_X^{0l}, and the parameter, δ_X^{0l} of the reaction above

$$\delta_X^{0l} = \delta_X^{e} - \beta(p_X^{0l} - p_X^{e}) \quad (20)$$

where δ_X^e is the value of the partial formal charge separation for the reaction ethylene + HX and p_X^e is the value of the p factor for the carbon-carbon bond in this reaction. The value of δ_X^e was determined by trial and error fitting to experimental data. The constant, β, was determined by fitting the activation energy of the reaction HCl + propene = *n*-propyl chloride and then solving eq 20 for β. The value thus obtained was $\beta = 0.415$. However, this value does not take into account the effect of steric hindrance. In the addition of the X species to secondary or tertiary carbon positions, the onset of sp^3 hybridization would lead to greater separation of X and the attached groups. Thus, one expects the transition state to lie closer to the product side for these cases, *i.e.*, the bond orders of the forming bonds should be greater than otherwise expected, or, conversely, δ_X^{0l} should be smaller (*viz.* eq 1). For this reason a larger value of β is expected, eq 20. One further expects this factor to depend on the size of the X group. To account quantitatively for these expectations the following procedure was adopted. The appropriate values of the slope factor were determined for X = F,Cl (by trial and error fitting of experimental data for the addition of X to propene to give isopropyl X). A plot of this slope (β) *vs.* covalent radii of X was then made, assuming the relation to be linear. The β_s factors for sterically hindered additions of other species (X = Br,I) were then determined from this plot. The basic data for the four halogens are listed in Table I.

TABLE I: Parameters for HX Addition to Olefins

X	p_X[c]	δ_X[c]	r_c[a]	β[b]	β_s[c]	β_i[d]	$S(X)$[c]
F	0.9212	0.2174	0.72	0.415	0.447	0.265	5.3
Cl	0.9470	0.2570	0.99	0.415	0.695	0.344	3.7
Br	0.9470	0.2445	1.14	0.415	0.833	0.360	3.7
I	0.9584	0.2505	1.33	0.415	1.008	0.391	3.0

[a] Covalent radii, Angstrom units. [b] β factor for any nonpolar olefin where X adds to terminal carbon. [c] β corrected for steric effect for addition of X to nonterminal carbon atom of a nonpolar olefin. [d] β corrected for inductive effect for addition of X to halogenated carbon in a polar olefin. [e] In units of kcal mol^{-1}.

TABLE II: Carbon–Carbon Double Bond Energies

Olefin	D_d(C=C), kcal mol^{-1}	Source
C_2H_4	171	*a*
C_2H_3F	163	*a*
CH_2CF_2	131	*a*
C_2H_3Cl	157	*a*
CH_2CCl_2	159	*a*
CHCl·CHCl	146	*a*
C_3H_6	164	*b*
1-C_4H_8	164	*c*
2-C_4H_8	168	*c*
i-C_4H_8	159	*c*

[a] Derived from thermochemical calculations. [b] From bond-energy–bond-length plot (see text). [c] From double bond energy *vs.* single bond energy plot (see text).

A number of reactions were treated in which the olefin was a halogenated olefin. In these cases it is clearly unfavorable to set up a positive partial formal charge on the carbon with the excess of the electron-withdrawing halogen species. This should manifest itself in a lowering of the value of δ_X^{0l} over the predicted value, and should depend on the electronegativity E_n of the olefin substituents. It was found that $\beta_i = 0.344$ provided satisfactory results for three chloro systems for which experimental data are available. Assuming that there exists a linear relationship between the factor β and the electrone-

TABLE III: Results of Activation Energy Calculations[a]

Olefin	$\Delta H_f°_{,Ol}$	Ref	HX	$\Delta H_f°$, C-Prod	Ref	E_{ad}(calcd)	E_{elim}(calcd)	E_{elim}(exptl)	Ref
Ethene*	12.5	*b*	HF	−62.5	*c*	50.3	60.2	58.2; 59.9 ± 1.0	*d, e*
C_2H_3F[f]	−33.5	*g*		−118.0	*h*	45.7	65.1	65 ± 0.9; 61.9 ± 1.8	*i, j*
C_2H_3F[k]	−33.5	*g*		−104.8	*g*	50.1	56.3	62.9 ± 0.9	*l*
CH_2CF_2[k]	−82.5	*h*		−158.9	*h*	55.6	66.9	65.4 ± 2.6	*m*
CH_2CF_2[f]	−82.5	*h*		−178.2	*h*	37.2	67.8	73.6 ± 4.1; 68.7 ± 2.4	*i, n*
propene[k]	4.9	*c*		−67.2	*c*	51.8	58.8	58.3	*o*
propene[f]*	4.9	*c*		−69.0	*c*	44.8	53.6	53.9	*o*
Isobutene[k]	−4.0	*b*		−74.5	*g*	50.8	56.2	58.6	*o*
Isobutene[f]*	−4.0	*b*		−78.5	*p*	41.7	51.7	51.5	*o*
Ethene*	12.5	*b*	HCl	−26.3	*b*	40.3	57.0	56.5	*q*
C_2H_3Cl[f]	8.6	*r*		−30.7	*r*	38.7	55.9	53.5	*q*
C_2H_3Cl[k]	8.6	*r*		−30.7	*r*	39.9	57.5	54.0 ± 3.5	*s*
CH_2CCl_2[k]	0.6	*r*		−35.5	*r*	39.4	51.0		
CH_2CCl_2[f]	0.6	*r*		−34.4	*h*	38.8	51.7	54.2	*q*
CHClCHCl	1.1	*r*		−35.5	*r*	37.5	49.6		
Propene[k]	4.9	*c*		−31.3	*b*	40.9	55.0	55.0	*q*
Propene[f]*	4.9	*c*		−33.0	*b*	35.4	51.2	51.1	*q*
Isobutene[k]	−4.0	*b*		−37.5	*b*	39.8	51.2	53.2	*q*
Isobutene[f]	−4.0	*b*		−43.1	*b*	31.4	48.4	45.0	*q*
Ethene*	12.5	*b*	HBr	−16.1	*b*	34.4	54.3	53.9	*q*
Propene[k]	4.9	*c*		−21.1	*b*	34.5	51.8	50.7	*q*
Propene[f]	4.9	*c*		−23.7	*b*	27.9	47.8	47.8	*q*
Isobutene[f]	−4.0	*b*		−30.5	*b*	24.5	42.3	41.8	*q*
$(CH_3)_2C{=}C(CH_3)_2$	−15.9	*b*		−39.5	*b*	24.1	39.0	38.4	*q*
Ethene*	12.5	*b*	HI	−2.2	*b*	28.4	49.4	50.0	*q*
Propene[f]	4.9	*c*		−9.5	*b*	23.4	44.1	45.0	*q*
1-Butene[f]	0	*b*		−14.4	*b*	23.4	44.1	45.0	*q*
2-Butene	−2.2 (av)	*b*		−14.4	*b*	25.0	43.5	43.0	*q*
Isobutene[f]	−4.0	*b*		−17.3	*b*	19.1	38.7	38.1	*q*

[a] All energy values in kcal mol^{-1}. Systems used to fix constants are marked by an asterisk. [b] Reference 24. [c] D. R. Stull, E. F. Westrum, and G. C. Sinke, "The Chemical Thermodynamics of Organic Compounds," Wiley, New York, N. Y., 1969. [d] M. Day and A. F. Trotman-Dickenson, *J. Chem. Soc. A*, 233 (1969). [e] P. Cadman, M. Day, and A. F. Trotman-Dickenson, *ibid.*, 2498 (1970). [f] Markovnikov addition. [g] Estimated by group additivity. [h] J. R. Lacher and H. A. Skinner, *J. Chem. Soc. A*, 1034 (1968). [i] P. Cadman, M. Day, and A. F. Trotman-Dickenson, *ibid.*, 1356 (1971). [j] Reference 11a. [k] Anti-Markovnikov addition. [l] J. A. Kerr and D. M. Timlin, *Int. J. Chem. Kin.*, **3**, 427 (1971). [m] M. V. C. Sekhar and E. Tschuikow-Roux, *J. Phys. Chem.*, **78**, 472 (1974). [n] Reference 11b. [o] P. Cadman, M. Day, A. W. Kirk, and A. F. Trotman-Dickenson, *Chem. Commun.*, 203 (1970). [p] $\Delta H_f°$(*t*-C_4H_9F) estimated to be −78.5 kcal mol^{-1} by extension of observed trend in the homologous series, *i*-C_3H_7X to the series *t*-C_4H_9X. [q] Recommended value from ref 24. [r] J. D. Cox and G. Pilcher, "Thermochemistry of Organic and Organometallic Compounds," Academic Press, New York, N. Y., [s] K. A. Holbrook, R. W. Walker, and W. R. Watson, *J. Chem. Soc. B*, 577 (1971).

gativity[13] of the substituent atom on the olefin and using the fact that $\beta = 0.415$ for the addition of HX to ethylene, it was then possible to obtain β_I for the inductive effect in fluoro-substituted ethenes from the equation $\beta_I(X) = 0.5807 - 0.07889E_n(X)$.

Input Data

As indicated above, the only information required for the calculation of the activation energies are the values of the bond energies of the participating bonds, and their single-bond bond lengths. The single bond lengths are all fairly well known[16] and the value of the activation energy is, in any case, virtually insensitive to small variations in these quantities. For this reason, standard, averaged values are sufficient for calculational purposes. On the other hand, the bond energies in question are not well known except for a very limited number of the bonds of interest, and it was therefore necessary to find some means of estimating these values.

Since the bond energies of most of the simple diatomics and other small molecules are relatively well known,[6] the major problem in obtaining usable input data was then to estimate the bond energies of carbon–carbon single and double bonds. The procedure adopted was as follows. For HX addition to ethene, the carbon–carbon bond dissociation energy of the product, C_2H_5X, was either known or could be estimated from thermochemical data. This value was then compared to the value of the C–C bond dissociation energy of propane[17] [$D_d(C_2H_5\text{-}CH_3) = 85$ kcal mol^{-1}]. It was found that the bond dissociation energies were invariably higher than those of propane. The difference between the two quantities was denoted by $S(X)$. It was assumed that the presence of the X group in a terminal position on a carbon chain would always increase the energy of the adjacent carbon–carbon bond by $S(X)$ relative to its strength in the species in which the X was replaced by a CH_3

$$D_d(R\text{-}CH_2X) = D_d(R\text{-}CH_2CH_3) + S(X) \qquad (21)$$

Next it was noted that the C–C bond dissociation energy in isobutane[17] was less than that in *n*-butane despite the fact that the former is the thermodynamically more stable compound. This suggested that this might also be the case with compounds in which the X group was in a primary or secondary position. From thermochemistry and the value of the C–H bond energy in $CHCl_3$[17] the bond energy of the C–C bond in *i*-C_3H_7Cl was estimated to be approximately 81 kcal/mol[18] which is almost the same as the difference between the C–C bond dissociation energy in propane and the value of $S(Cl)$ (3.7 kcal/mol). Therefore, the general procedure adopted to calculate the bond energy of the carbon–carbon single bond in a species with a

group X in the secondary position was to substitute H for X, note the bond dissociation energy, and subtract $S(X)$

$$D_d(RCHX\text{-}CH_2R') = D_d(RCH_2\text{-}CH_2R') - S(X) \quad (22)$$

For the cases in which the X group was in a tertiary position, not enough data could be found to estimate readily any of the relevant bond energies. For this reason, the system HF + isobutene was used to fix an optimum bond dissociation energy for the C-C bond in *tert*-butyl fluoride of 74.7 kcal mol^{-1}. This was found to be $S(F)$ = 5.3 kcal mol^{-1} less than the bond dissociation energy of the compound in which a CH_3 group replaced the fluorine atom, *i.e.*, neopentane,[19] $D_d[(CH_3)_3C\text{-}CH_3]$ = 80 kcal mol^{-1}. This was also used as a general rule, *i.e.*

$$D_d[(RR')CX\text{-}R''] = D_d[(RR')C(CH_3) - R''] - S(X) \quad (23)$$

$S(X)$ values for the four halogens are listed in Table I. For polyfluoroethanes the carbon-carbon single bond energies were calculated from known thermochemistry, while for polychloroethanes the values were obtained from ref 20 and from thermochemistry.

The determination of double bond energies was more difficult. Those for the various ethylenic species were obtained from thermochemistry, but for olefins with three or more carbons the thermochemical data were not available. A plot of bond length *vs.* the logarithm of bond dissociation energy was drawn for carbon-carbon bonds using the following values for the dissociation energies of acetylene, ethylene, and ethane: 230.0,[17] 171.1 (thermochemical), and 88.0.[17] Since the carbon-carbon bond length in propylene is known[16] this plot could then be used to obtain an estimate of the double bond energy in propylene. The double bond energies of other olefins were obtained from the values for ethylene and propylene by a linear plot of single bond energy of the hydrogenated olefin *vs.* the corresponding double bond energy. This extrapolation was used only for nonhalogenated olefins. Carbon-carbon double bond dissociation energies discussed in this paper are listed in Table II.

Results and Conclusions

The calculated results for 29 systems are presented in Table III. It is evident that the present method is highly successful in predicting the activation energies of a large number of HX addition reactions. These include polar olefins for which the model of Benson, Bose, and Haugen was unsuccessful. Thus, while providing support for the semiionic model, the present work represents a quantitative improvement on previous methods. It should be noted that the agreement obtained in the case of the HF eliminations from polyfluorinated species is subject to a certain degree of uncertainty since the heats of formation of reactants and products are not well established. It is felt, however, that the success of the method when applied to other systems for which heats of formation are better known justifies a high degree of confidence in the activation energies for the addition reactions. It has been noted by Setser and coworkers[21,22] that the Benson-Bose-Haugen model is geometrically too loose to account quantitatively for the observed A factors of some HX eliminations from haloalkanes. The present transition state model is considerably smaller and hence qualitatively answers this objection.

Acknowledgment. We wish to thank Dr. M. V. C. Sekhar of this laboratory for helpful discussions.

Appendix

Example. Consider the reaction HBr + isobutene = *tert*-butyl bromide. The basic input data are the relevant bond lengths and bond dissociation energies of product and reactants. Thus from ref 13 we first obtain the single-bond bond lengths of the C-C, C-H, H-Br, and C-Br bonds: 1.54, 1.09, 1.41, and 1.94 Å, respectively. Next, using the method discussed in the text, the C-C bond dissociation energy in the product is estimated from eq 23 to be 76.3 kcal mol^{-1}. Since the C-H bond formed in the product is to a CH_2 group giving rise to a methyl group, the C-H bond dissociation energy is taken to be the same as in ethane,[17] 98.0 kcal mol^{-1}. The dissociation energy of HBr, D_d(H-Br) = 87.5 kcal mol^{-1} is taken from the literature[6] as is the value $D_d(t\text{-}C_4H_9\text{-}Br)$ = 63.0 kcal mol^{-1}.[17] The C-C double bond energy in isobutene is estimated to be 159.2 kcal mol^{-1} by the graphical method described in the text. Then, using the relevant bond length and bond energy values above, the p factors for the C-H, H-Br, and C-Br bonds are calculated from eq 4 to be 1.0812, 0.8871, and 0.9582, respectively, where the values of ϵ_x and R_x were obtained from ref 14. The p factor for the carbon-carbon bond is found from eq 5. Thus using $D_d(C{=}C)_{t\text{-}Bu}$ = 159.2 kcal mol^{-1} and $D_d(C\text{-}C)_{t\text{-}BuBr}$ = 76.3 kcal mol^{-1}, $p_{Br}^{t\text{-}Bu}$ = 1.0611. From Table I we also have p_{Br}^{e} = 0.9470, δ_{Br}^{e} = 0.2445, and β_s = 0.833 which have been obtained as described in the text. Substitution of these quantities and $p_{Br}^{t\text{-}Bu}$ in eq 20 yields $\delta_{Br}^{t\text{-}Bu}$ = 0.1494. Then using the conservation equation, eq 1, and the assumed values for the transition state bond orders for the C-C and the H-Br bonds (n_1 = 1.5 and n_3 = 0.5, respectively), we obtain $n_2 = n_4 = (1 - 2\delta_{Br}^{t\text{-}Bu})/2$ = 0.3506. With the bond orders thus specified, eq 2 gives the following values for the transition state bond lengths of the C-C, C-H, H-Br, and C-Br bonds: 1.43, 1.36, 1.59, and 2.21 Å, respectively. The computer subroutine[23] calculates the value of the angle ϕ_1 = 88°. These values for r_i (i = 1, ... 4) and ϕ_1 specify the structure of the transition state, and together with $\delta_{Br}^{t\text{-}Bu}$ lead to E_d = −2.6 kcal mol^{-1} *via* eq 14. The individual energy contributions, E_i, from the four bonds (i = 1, ... 4) as given by eq 6 are 41.9, −31.6, 40.2, and −23.1 kcal mol^{-1}, respectively. Thus from eq 15, E_{ad} = 24.8 kcal mol^{-1}. Benson and O'Neal[24] give $\Delta H°$ = 17.8 kcal mol^{-1} for the reverse, elimination reaction, hence $E_{elim} = E_{ad} + \Delta H°$ = 42.6 kcal mol^{-1} as compared to the preferred experimental value[24] of 41.8 kcal mol^{-1}.

References and Notes

(1) Work supported by the National Research Council of Canada. Abstracted, in part, from M.Sc. Thesis of K. R. Maltman, University of Calgary, Calgary, 1973.
(2) R. M. Noyes, *J. Amer. Chem. Soc.*, **88**, 4311 (1966).
(3) R. M. Noyes, *J. Amer. Chem. Soc.*, **88**, 4318 (1966).
(4) M. B. Pahari and R. Basu, *J. Chim. Physicochim. Biol.*, **68**, 753 (1971).
(5) M. B. Pahari and R. Basu, *J. Chim. Physicochim. Biol.*, **68**, 1356 (1971).
(6) B. deB. Darwent, *Nat. Ref. Data Ser., Nat. Bur. Stand.*, **No. 31**, (1970).
(7) S. W. Benson and A. N. Bose, *J. Chem. Phys.*, **39**, 3463 (1963).
(8) Y. Tsang and F. S. Rowland, *J. Amer. Chem. Soc.*, **90**, 570 (1968).
(9) S. W. Benson and G. R. Haugen, *J. Amer. Chem. Soc.*, **87**, 4036 (1965).
(10) G. R. Haugen and S. W. Benson, *Int. J. Chem. Kinet.*, **2**, 235 (1970).
(11) (a) E. Tschuikow-Roux, W. J. Quiring, and J. M. Simmie, *J. Phys. Chem.*, **74**, 2449 (1970); (b) E. Tschuikow-Roux and W. J. Quiring, *ibid.*, **75**, 295 (1971).
(12) K. Maltman and E. Tschukow-Roux, to be submitted for publication.
(13) L. Pauling, "The Nature of the Chemical Bond," 3rd ed, Cornell University Press, Ithaca, N. Y., 1960.

(14) H. S. Johnston, "Gas Phase Reaction Rate Theory," Ronald Press, New York, N. Y., 1966.
(15) E. M. Purcell, "Electricity and Magnetism," McGraw-Hill, New York, N. Y., 1963, p 439.
(16) (a) L. E. Sutton, *Chem. Soc., Spec. Publ.*, **No. 11** (1958); (b) *ibid.*, **No. 18** (1965).
(17) J. A. Kerr, *Chem. Rev.*, **66**, 465 (1966).
(18) From the enthalpy change of the reaction

$$(CH_3)_2CHCl + H_2 \rightarrow CH_4 + C_2H_5Cl \quad \Delta H^\circ = -11.2 \text{ kcal mol}^{-1}$$

and the known bond dissociation energies for H_2 and CH_4 we obtain

$$D_d(CH_3\text{-}CHClCH_3) = -11.2 + D_d(CH_3CHCl\text{-}H)$$

where the last term may be estimated from an assumed proportionality relationship

$$D_d(CH_3CHCl\text{-}H) - D_d(CH_2Cl\text{-}H) \simeq D_d(CH_3CH_2\text{-}H) - D_d(CH_3\text{-}H)$$

since the quantities on the right-hand side are known[17] and $D_d(CH_2Cl\text{-}H) \simeq 98.3$ kcal mol^{-1} is estimated in relation to $D_d(CCl_3\text{-}H) = 95.7$ kcal mol^{-1} [17] and the general trend of chloro substitution in methane. Thus $D_d(CH_3CHCl\text{-}H) \simeq -6.0 + 98.3 = 92.3$ kcal mol^{-1} and hence $D_d(CH_3\text{-}CHClCH_3) \simeq 81.1$ kcal mol^{-1}.
(19) S. W. Benson, *J. Chem. Educ.*, **42**, 502 (1965).
(20) J. A. Franklin and G. H. Huybrechts, *Int. J. Chem. Kinet.*, **1**, 3 (1969).
(21) J. C. Hassler and D. W. Setser, *J. Chem. Phys.*, **45**, 3246 (1966).
(22) K. Dees and D. W. Setser, *J. Chem. Phys.*, **49**, 1193 (1968).
(23) Available on request from the authors.
(24) S. W. Benson and H. E. O'Neal, *Nat. Ref. Data Ser., Nat. Bur. Stand.*, **No. 21** (1970).

COMMUNICATIONS TO THE EDITOR

Diffuse Reflectance Spectra of Metachromatic Dyes. Existence of a Long Wavelength Band in Solid States[1]

Sir: The visible spectrum of a metachromatic dye solution is known to show a shift of the principal absorption maximum toward *shorter wavelength* and occasionally a "metachromasy" band in this region at high concentrations or in the presence of polyelectrolytes. In many previous studies of metachromatic behavior, the *longer wavelength* feature of the observed spectrum has mostly been ignored, although suggestions have been made on the existence of a new absorption band in the long wavelength side of the principal maximum.[2,3] Meanwhile, computational analyses of experimental data have cumulatively revealed a weak component band in that region.[4-9] We present here for the first time unambiguous experimental evidence that such a new long wavelength band (designated as L band) indeed exists in some spectra of metachromatic dyes, describe conditions responsible for it, and briefly discuss observed optical properties.

The diffuse reflectance method was employed for measuring the spectrum of a pure dye in a solid which was regarded as an extreme of concentrated solutions.[10] An anhydrous crystalline dye was ground finely with an anhydrous white solid used as a diluent. For each dye the molar mixing ratio of diluent to dye, R, was varied from *ca.* 10^2 to 10^4. Diluents with various surface properties (sucrose, SiO_2, MgO, NaCl, and polyphosphate) were used to ascertain the authenticity of the L band. The typical diffuse reflectance spectra of six solid triphenylmethane and acridine dyes are shown in Figure 1, where the ordinate is expressed in terms of the Kubelka-Munk function, $F(r_\infty)$,[11] to compare with the absorption spectra in dilute solutions. As indicated by an arrow, each ground solid dye-diluent system clearly exhibits the L band in the wavelength region longer than the principal maximum which broadens but remains in solid. The L band appears for each dye in every combined case of R and diluent, while none is observed in the solution spectrum.

The L band may thus be associated with an intermolecular dye-dye or dye-diluent interaction in crystalline state, and/or with the new conformation of undissociated individual dye molecules in crystal lattice. To discriminate these possibilities, the crystal structure of solid dye was destroyed by dissolving each dye-diluent mixture in water. This sample was then frozen in Dry Ice-acetone, lyophilized, vacuum dried, and finally powdered. Although weaker and less defined, the L band was always observed in the reflectance spectrum of each sample thus prepared in a low R range regardless of diluent species (high coverage). As the R of the sample was increased, however, the L band gradually disappeared (low coverage). These results can be interpreted as indicating that in the high coverage mixture the dye molecules partly exist in clusters, in which some may be aggregated as in the crystalline state to show the L band, while in the low coverage sample they exist mostly in the molecularly dispersed state in which the electronic configuration of the dye may remain as in dilute solution not to show the L band.

The L band of those dyes, which commonly possess a quaternary nitrogen atom and free or substituted amino groups, can therefore be concluded to be authentic and primarily result from dye-dye interaction. The metachromatic behavior of dyes studied is inconspicuous in the

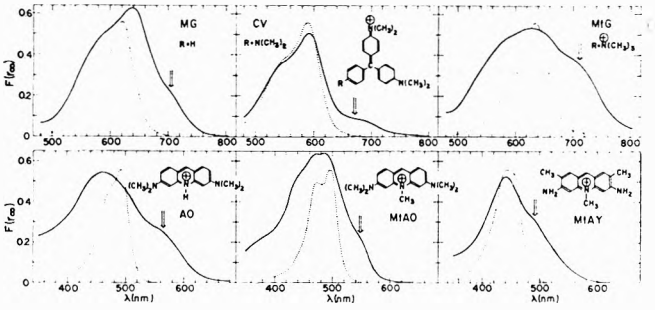

Figure 1. Diffuse reflectance spectra (solid line) of crystalline dye-sucrose systems and the corresponding absorption spectra (dotted line) in dilute aqueous solutions (*ca.* 10^{-5} *M*, absorbance on an arbitrary scale) at 25°: MG, Malachite Green; CV, Crystal Violet; MtG, Methyl Green; AO, Acridine Orange; MtAO, 10-Methylacridinium Orange; MtAY, 10-Methylacridinium Yellow. These dyes are in the chloride form. Spectra of the dye-diluent sample were recorded against the same nonabsorbing diluent on a Hitachi EPS-3T spectrophotometer with an integral sphere reflectance attachment.

solid, which suggests that solvent water is involved in metachromasy. Detailed work will be published together with comparison of the L band of AO and CV with computed results.[5-9] The esr triplet excitation spectrum of AO was recently reported to show a maximum at 570 nm but no absorption maximum.[12] We believe the L band of solid AO at 550–570 nm in sucrose or SiO_2 corresponds to the missing maximum.

References and Notes

(1) This paper is Spectral Studies of Organic Dyes. III. For part II of this series see ref 10.
(2) V. Zanker, *Z. Phys. Chem.*, **199**, 225 (1952).
(3) K. Yamaoka and R. A. Resnik, *J. Phys. Chem.*, **70**, 4051 (1966).
(4) K. Bergmann and C. T. O'Konski, *J. Phys. Chem.*, **67**, 2169 (1963).
(5) M. E. Lamm and D. M. Neville, Jr., *J. Phys. Chem.*, **69**, 3872 (1965).
(6) W. West and S. Pearce, *J. Phys. Chem.*, **69**, 1894 (1965).
(7) K. K. Rohatgi and G. S. Singhal, *J. Phys. Chem.*, **70**, 1695 (1966).
(8) E. Braswell, *J. Phys. Chem.*, **72**, 2477 (1968).
(9) W. H. J. Stork, G. J. M. Lippits, and M. Mandel, *J. Phys. Chem.*, **76**, 1772 (1972).
(10) K. Yamaoka, J. Demoto, and M. Miura, *J. Sci. Hiroshima Univ.*, in press.
(11) W. Wm. Wendlandt and H. G. Hecht, "Reflectance Spectroscopy," Interscience, New York, N. Y., 1966, p 55.
(12) H. Schmidt, *Z. Phys. Chem. (Frankfurt am Main)*, **80**, 44 (1972).

Faculty of Science
Hiroshima University
Hiroshima 730, Japan

Kiwamu Yamaoka*
Yukio Matsuoka
Masaji Miura

Received December 27, 1973

Partial Molal Expansibilities from the Temperature of Maximum Density of Aqueous Solutions

Publication costs assisted by the National Science Foundation

Sir: Measurements of the effect of solutes upon the temperature of maximum density of aqueous solutions have been used for interpreting solvent structure in dilute solutions.[1-4] Although the experimental technique is convenient, the results have been presented in terms of the excess volume of mixing, $\partial \Delta V^M/\partial T$, and a set of parameters consisting of the molar volumes and thermal expansibilities of the pure components. Accurate measurement of the solute parameters may be troublesome, but still more perplexing is quantitative application of $\partial \Delta V^M/\partial T$ values to problems of solution structure, especially if the pure solute is not a liquid phase. I suggest a method for obviating some of these difficulties.

The equation developed by Wada and Umeda[1] expresses the shift in the temperature of maximum density, relative to that of water, as

$$\Delta\theta = -1/(1 - x)2\beta V_1^*[x\alpha V_2^0 + \partial \Delta V^M/\partial T] \quad (1)$$

where x is the mole fraction of solute, α is the thermal coefficient of expansion of pure solute, β is the coefficient in the parabolic relation to temperature of the molar volume of water in the vicinity of 3.98°, V_2^0 is the molar volume of pure solute at 0°, and V_1^* is the molar volume of water at 3.98°.

Since one may express the molar volume of water at a particular temperature as $V = (1 - x)V_1 + x\phi = (1 - x)V_1 + xV_2 + \Delta V^M$, where ϕ is the apparent molal volume of the solute, it follows that

$$\partial \Delta V^M/\partial T = x(\partial \phi/\partial T - \partial V_2/\partial T) \quad (2)$$

Setting $\partial V_2/\partial T = \alpha V_2^0$ involves an assumption already included in (1), *i.e.*, that α is constant in the temperature range considered. Then, substituting (2) into (1) gives

$$\Delta\theta = -x/(1 - x)2\beta V_1^*[\partial \phi/\partial T] \quad (3)$$

Note that $\partial \phi/\partial T$ is the apparent molal expansibility as defined by Gucker.[5] The fact that $\Delta\theta$ is a linear function of x over a wide concentration range of many electrolytes facilitates the determination of the limiting slope of $\Delta\theta$ *vs.* x, the Despretz[6] constant, which will be designated $(\Delta\theta/x)_1$. Furthermore, as x approaches zero, then $(1 - x)$ approaches unity, and $\partial \phi/\partial T$ approaches $\partial \bar{V}_2^*/\partial T$, the partial molal expansibility at infinite dilution and 3.98°. Then one may write

$$\partial \bar{V}_2^*/\partial T = -2\beta V_1^*(\Delta\theta/x)_1 \quad (4)$$

Equation 4 may be converted into an expression for the thermal coefficient of partial molal expansion of the solute at infinite dilution and 3.98°

$$\bar{\alpha}^* = 1/\bar{V}_2^*[\partial \bar{V}_2^*/\partial T] = -2\beta V_1^*/\bar{V}_2^*[\Delta\theta/x]_1 \quad (5)$$

As an illustration of a possible application of eq 5, Despretz constants for a selection of 1:1 electrolytes were assembled from the literature, including some for which solvolysis is a dominant interaction between solute and solvent, some for which a quasi-clathrate of the solvent may be a factor, but, without exception, ones for which electrostriction of solvent must be considered. A value of $\beta V_1^* = 1.44 \times 10^{-4}$ was computed from density tables,[7] and values of $\bar{V}_2^*$ were interpolated from tables of conventional partial molal volume of ions compiled by Millero.[8]

Detailed interpretation of trends in $\bar{\alpha}^*$ values (Table I) with relation to a specific model of solution structure is beyond the scope of this communication. Nevertheless, a few observations may be appropriate at this point. The peaking of values with sodium chloride seems consistent with the concept that, among this set of electrolytes, this salt might be expected to come closest to affecting an uncomplicated electrostricturing of the solvent. Trends toward lower values correlate with lower charge densities

TABLE I: Thermal Coefficients of Partial Molal Expansion at Infinite Dilution and 3.98° for Some 1:1 Electrolytes in Aqueous Solution[a]

	Chloride	Bromide	Iodide
Lithium	5.94[b]	5.02[b]	3.75[b]
Sodium	15.45[b]	11.49[b]	8.84[b]
Potassium	7.71[b]	6.61[b]	5.98[b]
Rubidium	6.36[b]	5.90[b]	5.39[b]
Cesium	5.24[b]		
Ammonium	3.27[b]	3.28[d]	
Tetramethylammonium	1.35[c]	1.42[d]	
Tetraethylammonium	1.00[c]	1.01[d]	1.16[d]
Tetra-*n*-propyl-ammonium	0.88[c]		0.88[d]
Tetra-*n*-butyl-ammonium	0.96[c]	1.06[d]	
Tetra-*n*-amyl-ammonium	1.26[c]		

[a] Entries in the table are $\bar{\alpha}^* \times 10^3$, deg^{-1}. [b] Reference 7. [c] Reference 4. [d] Reference 2.

of ions or with specific solvolysis. Among the quaternary ammonium salts, where quasi-clathrate solvent structure is a possibility, smaller and more uniform values are found, with ammonium halides intermediate between the alkali halides and the quaternary ammonium halides. Illustrations of a reversal of the sign of $\bar{\alpha}^*$ can be found with certain nonionic solutes such as low molecular weight alcohols.[1,3]

Temperature of maximum density measurements can provide, with relative ease and precision, the partial molal expansibility of solutes at infinite dilution and 3.98° (the negative of the partial derivative of partial molal entropy with respect to pressure) and, therefore, may become more useful in the search for an understanding of the structure of aqueous solutions.

References and Notes

(1) G. Wada and S. Umeda, *Bull. Chem. Soc. Jap.*, **35**, 646 (1962); **35**, 1797 (1962).
(2) G. Wada and M. Miura, *Bull. Chem. Soc. Jap.*, **42**, 2498 (1969).
(3) F. Franks and B. Watson, *Trans. Faraday Soc.*, **63**, 329 (1967).
(4) A. J. Darnell and J. Grayson, *J. Phys. Chem.*, **72**, 3021 (1968).
(5) F. T. Gucker, Jr., *J. Amer. Chem. Soc.*, **56**, 1017 (1934).
(6) N. C. Despretz, *Ann. Chem. Phys.*, **70**, 49 (1839).
(7) E. W. Washburn, Ed., "International Critical Tables," Vol. III, McGraw-Hill, New York, N. Y., 1933.
(8) F. J. Millero, "Water and Aqueous Solutions: Structure, Thermodynamics, and Transport Processes," R. A. Horne, Ed., Wiley-Interscience, New York, N. Y., 1972, Chapter 13, pp 532–534.

Department of Chemistry
The University of North Carolina at Charlotte
Charlotte, North Carolina 28213

James R. Kuppers

Received January 18, 1974

Journal of Chemical and Engineering Data

APRIL 1974, Vol. 19, No. 2

TABLE OF CONTENTS

■ Supplementary material for this paper is available separately, in photocopy or microfiche form. Ordering information is given in the paper.

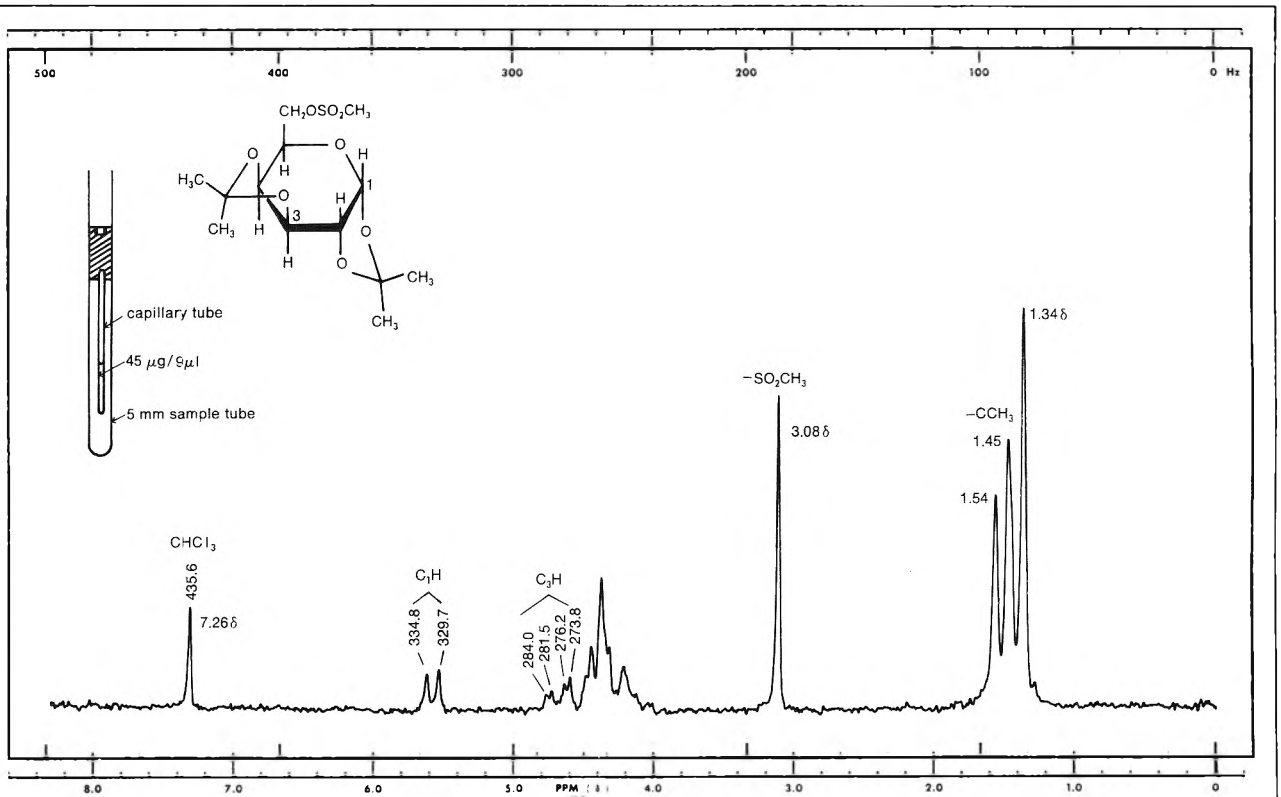

MANUAL AUTO

SWEEP OFFSET (Hz):
SPECTRUM AMPLITUDE:
INTEGRAL AMPLITUDE:
SPINNING RATE (RPS):
SWEEP TIME (SEC): (250)
SWEEP WIDTH (Hz): (500)
FILTER: (2)
RF POWER LEVEL: (.05)

SAMPLE: 1,2:3,4 -di-O-isopropylidine-6-O-methane-sulfanyl-α-D-galactopyranose
Sample courtesy of Stanley Opella, Dept. of Pharmacology, Stanford University.
SOLVENT: $CDCl_3$

REMARKS: 285 blocks of 50 acquisitions
total time = 14.4 hours
SW = 700 Hz, 4K f.i.d.
PW = 50 μsec., LB = 0.2 Hz
plot = 500 Hz

TRANSFORM TECHNOLOGY INC.

DATE: Nov. 6-7, 1973 OPERATOR: ZJ

60 MHz NMR
SPECTRUM NO.

Analysis of very small samples is best done using a microcell approach. Here, 45 micrograms of a compound with molecular weight 338 was contained in a capillary tube of 1.0 mm I.D. The peak at 3.08δ, although weak after one block of acquisitions, served adequately for the peak register method, which effectively cancels long-term field drift. Signal frequencies and chemical shifts were copied from an oscilloscope display of peak positions using an assigned value of 435.6 Hz for the chloroform peak. The spectrum is very well defined, and demonstrates that overnight FT operation with a T-60A/TT-7 system is quite feasible and very useful for microsample analysis.

MICROSAMPLE ANALYSIS with a TT-7/T-60A System

The TT-7 pulsed RF Fourier transform accessory benefits NMR operation by dramatically increasing sensitivity over that obtained in the normal CW mode of operation. Typically, samples five to ten times smaller than those now being handled can be run in the same amount of analysis time. Signal input, accumulated free induction decay, or transformed spectra can be displayed on the TT-7's cathode ray tube for visual monitoring. The spectra can be plotted using the T-60 recorder. Digital integrations of spectra can be viewed or plotted as well.

Not only will the TT-7 enhance the sensitivity and increase sample throughput of your T-60 but it will also provide an excellent Fourier transform training facility. Its ease of use is incomparable. In addition, spin-lattice relaxation times can be determined from a series of runs using the progressive saturation technique. Optional automatic T_1 measurements are available using the inversion-recovery technique as well as other multi-pulse experiments. In addition to sensitivity improvement and T_1 measurement applications, the basic TT-7 system will provide computer calculations of theoretical NMR spectra of up to six spins (seven spins with 12K core memory and disk memory system).

Phone or write for more details.

NICOLET INSTRUMENT CORPORATION

5225 Verona Road, Madison, Wisconsin 53711
Phone: 608/271-3333